COO-2185-13

LAMONT-DOHERTY GEOLOGICAL OBSERVATORY

OF

COLUMBIA UNIVERSITY

PALISADES, NEW YORK 10964

REPORT SUBMITTED TO

DIVISION OF ENVIRONMENTAL AND BIOMEDICAL RESEARCH

DEPARTMENT OF ENERGY

TRANSPORT AND TRANSFER RATES IN THE WATERS OF THE CONTINENTAL SHELF

Annual Report

September 1980

Principal Investigator: Pierre E. Biscaye

Co-Investigators: Hugh Ducklow
Arnold L. Gordon
Yuan-Hui Li

DISCLAIMER

CONTENTS

		Pages From	To
I.0	INTRODUCTION		
	1.1 Objectives	1.1/1	1.1/6
	1.2 Accomplishment of DOE Goals	1.2/1	1.2/3
2.0	PROCESSES ASSOCIATED WITH SUSPENDED SOLIDS	2.0/1	2.0/1
	2.1 The Production and Fate of Phytoplankton Biomass	2.1/1	2.1/24
	2.1.1 Phytoplankton	2.1/2	2.1/13
	2.1.2 Zooplankton	2.1/14	2.1/24
	2.2 Natural and Man-Made Radionuclides in the Water Column	2.2/1	2.2/9
	2.3 Concentrations, Size Frequency Distributions and Sediment Trap Collections of SPM	2.3/1	2.3/15
	2.3.1 SPM Concentrations; RACACA Cruise	2.3/3	2.3/7
	2.3.2 Size Frequency Distributions; RACACA Cruise	2.3/7	2.3/10
	2.3.3 Sediment Trap Samples; Low Radon Zone	2.3/10	2.3/15
3.0	PROCESSES ASSOCIATED WITH SEDIMENTS AS SINKS FOR RADIONUCLIDES AND OTHER POLLUTANTS	3.0/1	3.0/3
4.0	SPREADING OF WATER CHARACTERISTICS AND SPECIES IN SOLUTION		
	4.1 Hydrographic and Physical Mixing Processes	4.1/1	4.1/117
	4.1.1 Introduction	4.1/1	4.1/2
	4.1.2 The Data Set	4.1/3	4.1/6
	4.1.3 Data Analysis	4.1/6	4.1/110
	A. N.Y. Bight Stratification	4.1/6	4.1/8
	B. Seasonal evolution of T/S relation	4.1/8	4.1/37
	C. Frontal Structure, Cold Pool, & Cross-Shelf Mixing	4.1/37	4.1/59
	D. Pycnocline Salinity Maximum	4.1/59	4.1/62
	E. Warm Core Eddies	4.1/62	4.1/72
	F. Temperature-Oxygen Relation	4.1/72	4.1/78
	G. Estimates of K_z	4.1/78	4.1/85
	H. Importance of River Runoff in Pycnocline development	4.1/85	4.1/89
	I. RACACA Cruise	4.1/89	4.1/110
	Introduction	4.1/89	4.1/90
	Observations	4.1/90	4.1/110
	I. Warm Core Eddy	4.1/92	4.1/96
	II. Calving	4.1/96	4.1/96
	III. Longshore Variations	4.1/96	4.1/107
	IV. Low Radon Zone	4.1/107	4.1/110
	4.1.4 Field Work - 1980	4.1/111	4.1/117

4.2 Oxygen Isotopes as Tracers of Water Mass Origins and Mixing on the Continental Shelf	4.2/1	4.2/8
4.2.1 Recent Results	4.2/1	4.2/3
4.2.2 Discussion	4.2/3	4.2/8
4.3 Tritium as a Tracer of Water Mass Origins on the Continental Shelf	4.3/1	4.3/2
4.4 Radon-222 as a Tracer of Water Motions and Mixing	4.4/1	4.4/48
4.4.1 Introduction	4.4/1	4.4/3
4.4.2 Source Function of Radon-222 from Sediments	4.4/3	4.4/8
4.4.2.2 Radon Source Function on the Slope	4.4/8	4.4/18
4.4.3 Horizontal Distribution of Dissolved ^{222}Rn on the Shelf	4.4/18	4.4/34
4.4.3.1 Modeling of Horizontal Distributions	4.4/25	4.4/34
4.4.4 Vertical Distribution of ^{222}Rn	4.4/35	4.4/40
4.4.4.1 Seasonal Description of Vertical Thermocline	4.4/35	4.4/38
4.4.4.2 Modeling of Vertical Distributions	4.4/38	4.4/40
4.4.5 The Low-Radon Zone	4.4/41	4.4/47
4.4.6 Summary of Utility of Radon in Continental Shelf-Slope Studies	4.4/47	4.4/48
5.0 FIELD WORK	5.0/1	5.0/2

APPENDICES

The Appendices, while part of this Annual Report, are bound separately from the report and only a limited quantity have been made. Requests for copies of any of the individual appendices (papers published, in press and submitted for publication) should be made directly to the authors or to the Principal Investigator.

1. Y.-H. Li, P.H. Santschi, A. Kaufman, L.R. Benninger and H.W. Feely, Natural radionuclides in waters of the New York Bight, submitted to EPSL.

2. P.H. Santschi, Y.-H. Li and J. Bell, Natural radionuclides in the water of Narragansett Bay, EPSL 45, 201, 1980.

3. P.H. Santschi, D. Adler, M. Amdurer, Y.-H. Li, and J. Bell. Thorium isotopes as analogues for "particle-reactive" pollutants in coastal marine environments. EPSL 47, 327, 1980.

4. P.H. Santschi, Y.-H. Li, J. Bell, R. Trier and K. Kawtaluk, Pu in coastal marine environments, EPSL, in press, 1980.

5. Y.-H. Li, Geochemical cycles of "biophile" elements and manganese in the ocean, submitted to GCA.

6. Y.-H. Li, Interelement relationships in oceanic pelagic clays and manganese nodules, submitted to Science.

7. Y.-H. Li, Ultimate removal mechanisms of elements from the Ocean, submitted to Science.

8. C.R. Olsen, P.E. Biscaye, H.J. Simpson, R.M. Trier, N. Kostyk, R.F. Bopp, Y.-H. Li and H.W. Feely, Reactor-released radionuclides and fine-grained sediment transport and accumulation patterns in Barnegat Bay, New Jersey and adjacent shelf waters, Estuarine and Coastal Marine Science 10, 119, 1980.

9. T.C. Malone, and M.B. Chervin, The production and fate of phytoplankton size fractions in the plume of the Hudson River, New York Bight, Limno. Oceanogr. 24, 683, 1979.

10. T.C. Malone, R. Houghton and A.L. Gordon, Vertical exchange of properties under stratified conditions in the New York Bight, submitted to Limnology and Oceanography.

11. A.L. Gordon and F. Aikman III, Middle Atlantic Bight pycnocline salinity maximum, Limno. Oceanogr. in press, 1980.

1.0 INTRODUCTION

1.1 Objectives

The long-term goal of our work on the continental shelf and slope is to understand and to quantify the processes that govern the transport and dispersal of energy-related pollutants introduced to those waters by man's activities. To this end we have attempted to integrate the efforts of the Lamont-Doherty Geochemistry, Physical Oceanography and Biological Oceanography groups since most of the processes under study involve aspects related to the particular concern and expertise of each of these disciplines. Each of these disciplines brings to the program a data set to be integrated with and to complement the others, as well as an ability to focus on one or more of the processes affecting the fate of pollutants more effectively than the other disciplines. It is therefore useful to briefly summarize the processes affecting the introduction and fate of energy-related pollutants, and to indicate both those processes, to the understanding and quantification of which we are making a contribution by one or more techniques, as well as those for which we at present have no applicable technique in any of the disciplines.

Figure 1.0-1 is a schematic cross section of the Bight from the Hudson River to the lower continental slope which we have used in previous reports but which still represents the processes we are trying to understand. In the lower left hand corner is a plan view of the New York Bight as defined by the shoreline and by the 50 and 200m isobaths. A number of production, removal, mixing and regeneration processes are schematically portrayed primarily by arrows and figures which are numbered. In Table 1.0-1 are listed the processes represented and a brief identifi-

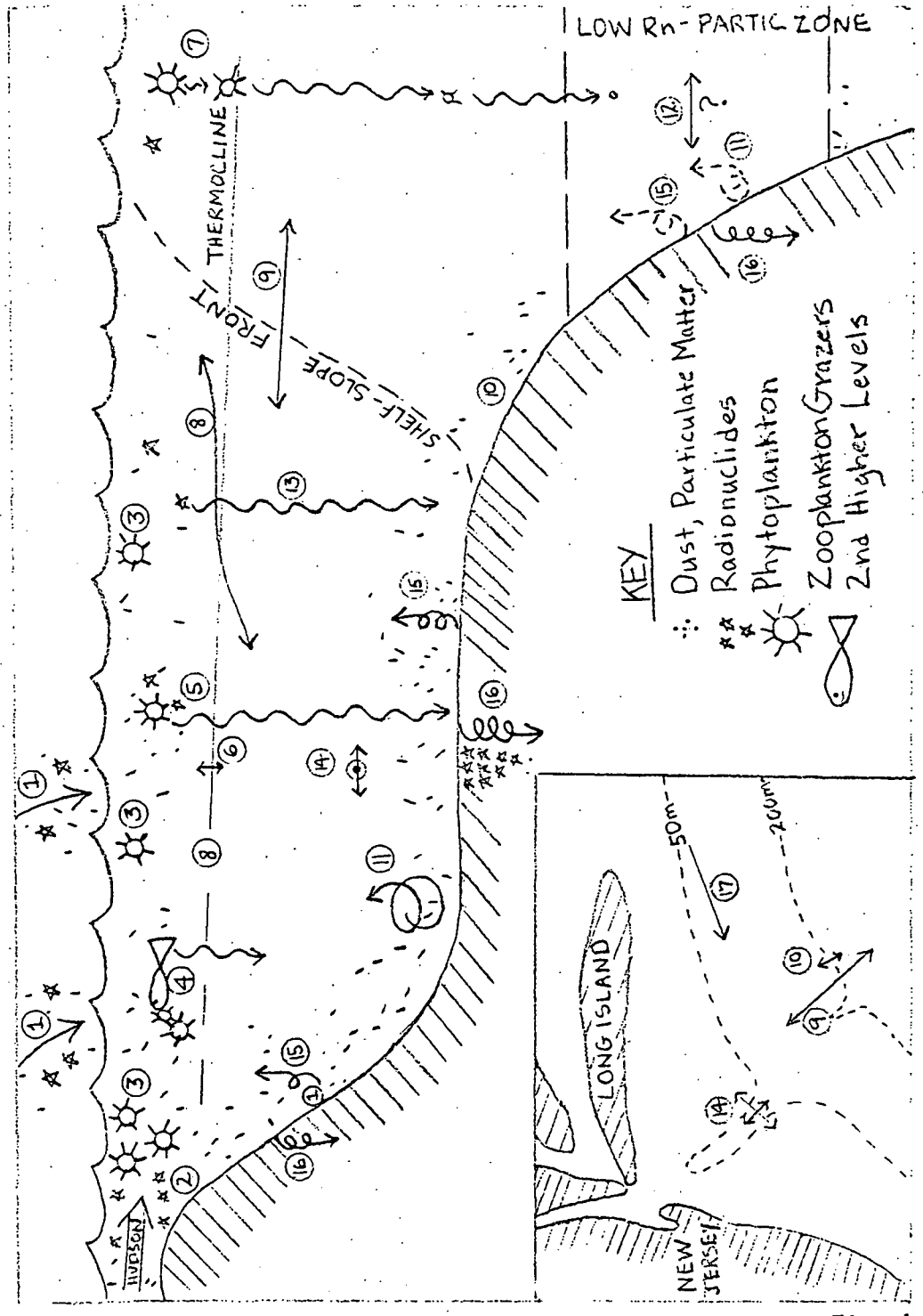
LOW Rn - PARTIC ZONE
THERMOCLINE
FRONT
SHELF - SLOPE
KEY
Dust, Particulate Matter
Radionuclides
Phytoplankton
Zooplankton Grazers
2nd Higher Levels
HUDSON
LONG ISLAND
NEW JERSEY
50m
200m

Fig. 1.0-1

Table 1.0-1

No.	Process	Observational or Analytical Techniques
1	Atmospheric infall of dust and radionuclides	Literature
2	Input of radionuclides and nutrients from the Hudson River and Barnegat Bay	Work of Simpson, et al., at Lamont; nutrient chemistry, α, β, γ-counting
3	Phytoplankton production biomass	Fluorescence (chlorophyll a), C-14 techniques for productivity
4	Grazing and fecal pellets	Zooplankton tows and microscopic analyhsis; incubation experiments
5	Transport of radionuclides from surface waters on sinking particulates	^{234}Th, ^{228}Th ^{210}Po, $^{239,240}Pu$ in the water column
6	Vertical mixing across the thermocline	^{222}Rn, oxygen and nutrient budgets
7	Decomposition of sinking dead phytoplankton and resultant nutrient regeneration (or cycling)	Bacteriological analysis; nutrient chemistry including O_2 analysis; microscopic examination of filtered particulate matter
8	Isopycnal mixing through the thermocline	Hydrography
9	Cross front exchange	Hydrography, ^{3}H, $^{18}O/^{16}O$
10	Benthic layer exchange (Slope water intrusions)	Hydrography, ^{3}H, $^{18}O/^{16}O$
11	Near Bottom Vertical Mixing	^{222}Rn
12	Mixing regime on slope producing low Rn zone (possibility of rapid horizontal or isopycnal mixing)	^{222}Rn, ^{228}Ra, ^{3}H, thermistor chain measurements of ΔT
13	Fluxes of particles and radionuclides to the sediments	Sediment Traps on Slope; sedimentation rate determination by ^{210}Pb integrated total ^{137}Cs, $^{239,240}Pu$ activities in the sediment column
14	Horizontal mixing or eddy diffusion cross shelf and long shelf	^{222}Rn

(Cont.)

Table 1.0-1 (Cont.)

No.	Process	Observational or Analytical Techniques
15	Particulate resuspension and chemical regeneration	Suspended particulate measurements ^{234}Th, ^{228}Th, ^{228}Ra, ^{210}Pb, $^{239,240}Pu$ in water column; bacteriological analysis
16	Sediment mixing and accumulation	^{234}Th, ^{210}Pb, ^{14}C, ^{137}Cs $^{239,249}Pu$ profiles in sediment columns
17	Long shelf advection	$^{18}O/^{16}O$, ^{3}H

cation of the observational and analytical techniques available to the Lamont Geochemical, Physical and Biological groups which will aid in understanding how pollutants are dispersed throughout and removed from the New York Bight in particular and the shelf in general.

Although the project must necessarily reflect some of the administrative and budgetary organization along classical disciplinary lines (geochemistry, physical-and biological oceanography), conceptually the scientific approach to understanding the fate of energy-related pollutants in continental shelf waters is organized according to processes. This is reflected in the division of this report (as well as the renewal proposal) into three scientific sections dealing with; 1) Processes Associated with Suspended Solids; 2) Processes Associated with Sediments as Sinks for Radionuclides and other Pollutants; and 3) Spreading of Water Characteristics and Species in Solution. Within these sections there is a mixture of geochemical, biological and physical aspects to almost every subsection. Nor can one ignore cross-disciplinary aspects of the major sections with each other. Finally a short section on Field Work (none was funded this year) emphasizes the interdisciplinary nature of our work in that all groups participate in each cruise and make measurements on the same casts and samples.

Although this is an Annual Report, since this is a review year we have emphasized the work of the past contract year, but also tried to incorporate as summary statements or background work that has been reported previously. The primary output of our efforts is reflected in the Appendix in which eleven papers (either published, in press or submitted since the last report) are reproduced. These are just the start

of an output that is increasing as data and samples acquired during the begining years of the project comes to fruitiion. Where papers have been produced which describe our work on that process or data set, the discussion in the report is often abbreviated to some sort of introduction or background followed by short statements of the important results with references to the appropriate appendix or appendices. For work that is still in progress or has not gotten to the point of a paper being written, the report given here is more lengthy. The section following this one gives in brief form some of the important results over the last year or so which specifically represent accomplishments related to DOE goals.

1.2 Accomplishment of DOE Goals

The following statements and conclusions represent accomplishments during the past year toward our long-term goal of understanding by what processes and at what rates pollutants are dispersed and transported through and removed from the New York Bight. We believe these accomplishments are particularly pertinent to the mandate and goals of DOE in the marine environment.

- During much of the year the waters of the continental shelf are divided into two relatively well-mixed reservoirs which are separated vertically by strong gradients in physical, chemical and biological characteristics. The rate of a number of processes affecting the fate of pollutants within the reservoirs depend on the rate at which mixing occurs between the two reservoirs. From field data we have made estimates of this important mixing rate using three different approaches — radioactive tracer (^{222}Rn), nutrient demand by phytoplankton and rate of oxygen production by phytoplankton, and vertical heat flux.

- Two processes control the rate of removal of reactive pollutants from the water column — adsorption on resuspended sediment particles and incorporation into living organisms and sinking of organic debris (dead organisms, fecal matter). We have found that different parts of the shelf and slope regime are characterized by varying rates and degrees of effectiveness of these processes. For example, in the shelf the former process is dominating.

- Measurements of plutonium on sediment cores and on suspended particulate material suggest that this very toxic element may not be removed from the system once it is accumulated in the sediments, but may be remobilized into the water column as dissolvable Pu (V+VI) or colloidal

particles. Evidence by coworkers at Lamont suggests that plutonium may even be transported back into the Hudson Estuary from the shelf.

- The microcosms experiments and the interelement relationship in oceanic pelagic clays prove that thorium isotopes are good proxy for other reactive elements with regard to their removal behaviors. The reactive elements include tri-and tetra-valent cations (e.g., Fe, Ti, Ge, Zr, Hf, Th, Y, rare earths, In, Cr, Pu, Am, etc.) and Pb and Hg, etc.

- Measurements of radioactive tracers in sediment cores from a large area of fine-grained sediment on the shelf (the "mud hole") indicates that the area is a zone of net accumulation of sediments and reactive pollutants. However, the net accumulation of reactive pollutants is mainly controlled by the mixing and resuspension of surface sediments by bioturbation. We also always observe a plume of resuspended sediment being carried away from this area, and it must also be an intermediate source of reactive pollutants. Similar measurements on sediment cores from the adjacent slope indicate that, although those sediments are a sink for reactive pollutants, slumping of sediments distorts the record making measurement of a steady-state rate of accumulation difficult.

- During the summer the predominant exchange of shelf water with relatively pollutant-free open ocean (slope) water occurs on isopycnal surfaces, though at rates considerably slower than previously estimated. A sharp boundary between the two distinct water types persists throughout the summer. The cross-shelf exchange occurs primarily in two layers: near the surface at 30 m depth (in the pycnocline) and on the shelf floor (benthic layer). During the rest of the year cross-shelf exchange is driven by storms and warm core Gulf Stream rings. We have observed the

exchange of heat and salt between shelf and slope waters as they flow southwest along the coast from the Hudson Canyon to Cape Hatteras. From there these waters presumably are entrained by the Gulf Stream and mix into the deep ocean as they flow to the northeast.

- From measurements of excess ^{222}Rn, we have determined that a zone of near-bottom water adjacent to the continental slope and rise, in which rapid mixing apparently takes place, extends from the Hudson Canyon as far south as Cape Hatteras. This zone is important because it represents a potential locus of dispersion of pollutants from the continental boundary out into the interior ocean.

- Oxygen isotope ratios and salinity measurements indicate that the "cold pool" water (or the winter shelf water) on the Middle Atlantic Bight shelf is an admixture of 3.7% local meteoric water with pure Labrador Sea water. The surface slope waters fall on a mixing line between Gulf Stream water and the "cold pool" water. Oxygen isotope ratios and salinity measurements offer the first conservative tracer-pair suitable for detailed study of the water mass mixing in the coastal environment.

2.0 PROCESSES ASSOCIATED WITH SUSPENDED SOLIDS

A field within oceanography which has burgeoned greatly within the past decade is that which deals with the measurement of suspended particulate matter (SPM) in the oceans from any of a number of viewpoints. One of the disciplines in which this increase has been most important is marine geochemistry in which there has been a realization that a large proportion of the chemical gradients which exist in the ocean is maintained by the flux of SPM. This is particularly true of the highly reactive elements and chemical species which are rapidly adsorbed onto or incorporated within particles. The question of the generation, pathways and fate of the many kinds of particulate matter is of primary concern to our understanding what happens (and at what rate it happens) to energy related pollutants in the marine environment adjacent to the continents. The three subsections which follow treat the question of particulate matter from primarily (but not exclusively) the biological, geochemical and physical viewpoints in that order.

2.1 THE PRODUCTION AND FATE OF PHYTOPLANKTON BIOMASS

INTRODUCTION

Suspended particles play a major role in the transport of heavy metals, radionuclides and chlorinated hydrocarbons within and through the continental shelf. Since populations of phytoplankton and zooplankton influence the production, distribution and fate of particulate organic matter, research has been conducted to determine the extent to which these populations affect time- and space-dependent distributions of radionuclides and other contaminants in the continental shelf ecosystem. The main mechanisms by which phytoplankton and zooplankton influence the distribution of particulate matter is through growth, sinking, resuspension, fecal pellet production and vertical migrations.

The following conclusions have been formulated from the research to date (Malone, 1976, 1977; Walsh et al., 1978; Malone and Chervin, 1979; Malone et al., submitted). (1) Phytoplankton productivity is the major source of organic matter on the shelf, and phytoplankton biomass is a major component of total suspended solids, particularly during phytoplankton blooms prior to the onset of thermal stratification and in zones of high production associated with the plume of the Hudson River and the shelf-break. (2) Prior to stratification, during February to April, blooms of netplankton (>20u) occur. Since zooplankton populations are small and grazing pressure is low, most of the phytoplankton biomass remains unconsumed and eventually sinks out of the water column into the sediments. (3) During the summer when the seasonal thermocline is established, phytoplankton biomass is low and composed largely of nanoplankton (<20u). Phytoplankton

productivity is closely coupled with zooplankton grazing and concomittant nutrient regeneration as well as nutrient fluxes into the euphotic zone. Thus, most of the phytoplankton production enters pelagic food chains or sinks from the water column as fecal material.

Research during the last year was designed to extend our observations during the summer stratification regime into waters of the outer continental shelf and slope from the Hudson Canyon to Cape Hatteras. Our major objectives were to compare the abundance, distribution and productivity of plankton between shelf and shelf-break waters and slope waters, to correlate phytoplankton levels and rate of production with zooplankton abundance and to evaluate spatial and temporal variations in rates of fecal pellet production and radionuclide content of fecal pellets.

2.1.1 PHYTOPLANKTON

METHODS

During the D.O.E. sponsored cruise on the R/V Conrad (C22-08) from 11 June to 2 July 1979, stations were occupied from the Hudson Canyon to Cape Hatteras along transects across the slope from approximately the 80 M contour to the base of the slope as well as one transect across the shelf of the New York Bight to a water depth of 25 M (Fig. 2.1.1-1). Water was collected in conjunction with the physical oceanography and geochemical sampling programs. Using methods as previously described (D.O.E. 1978 and 1979 Annual Reports) measurements of chlorophyll a, particulate organic carbon and nitrogen, dissolved inorganic nutrients (ammonia, nitrate, phosphate and silicate phytoplankton enumeration and identification, and phytoplankton production estimates were made. In addition, vertical profiles and sur-

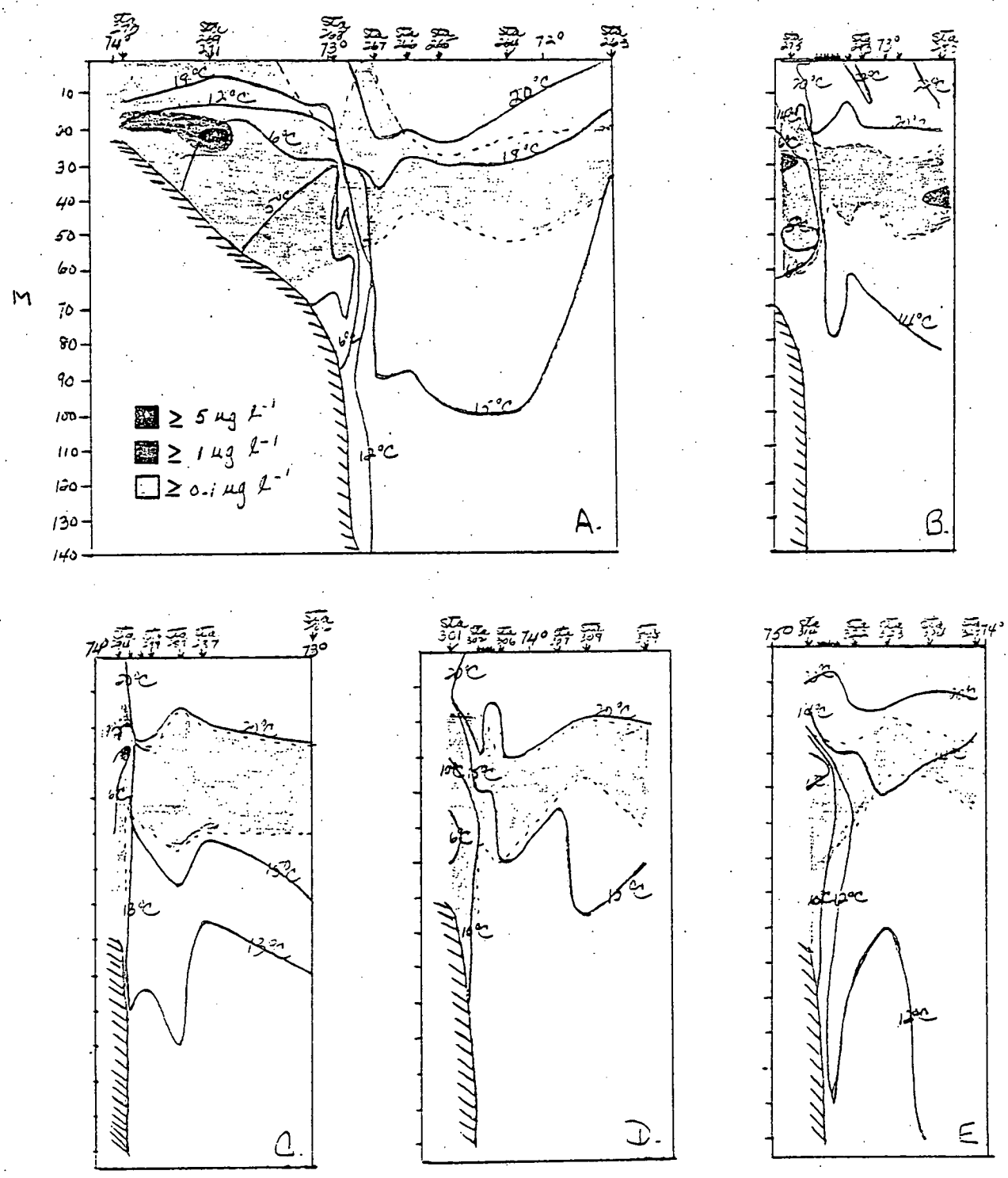

Figure 2.1.1-1. Distribution of temperature (°C) and chlorophyll a (ug l^{-1}) with depth (meters) along five transects across shelf-break area from Hudson Canyon south to Cape Hatteras area, 11 June to 2 July, 1979; A. Transect I B. Transect II C. Transect III D. Transect IV E. Transect V.

face mapping of *in vivo* chlorophyll *a* fluorescence were obtained using a submersible pump and the ship's seawater system. Primary production estimates were made using a simulated *in situ* incubator and standard methods of ^{14}C uptake.

RESULTS

Chlorophyll *a* concentrations were generally low (Fig. 2.1.1-1) with surface values less than 0.1 ug l^{-1} in both shelf and slope waters. In slope waters maximum concentrations of 0.1 - 0.5 ug chl *a* l^{-1} were found in the thermocline. At the shelf-break and along the one shelf transect maximum concentrations were 1.2 and 5.5 ug l^{-1}, respectively, and were associated with the top of a cold pool of water (<6°C). The chlorophyll maximum was dominated by net-plankton (>20u) on the shelf and at the shelf-break, and by nano-plankton (<20u) in slope waters.

Nanoplankton were characterized by small naked flagellates, whereas dinoflagellates and diatoms composed the netplankton fraction (Table 2.1.1-1). *Ceratium tripos* was present in numbers up to 10,000 l^{-1} in the chlorophyll maximum and in the cold pool of water on the shelf and at the shelf-break. Netplankton diatoms were dominated by *Rhizosolenia stolterfothii* (numbers up to 25,000 l^{-1}) on the shelf, *Leptocylindrus danicus* in surface waters at the shelf-break and *Dactyliosolen mediterraneus* in association with an epiphytic flagellate in deep euphotic waters at the shelf-break and on the slope. Large numbers of ciliates were observed in the phytoplankton samples from all stations sampled, reaching concentrations up to 11,000 l^{-1} on the shelf (Table 2.1.1-1).

Table 2.1.1-1. Abundance of major phytoplankton groups and ciliates for stations occupied from Hudson Canyon to Cape Hatteras during the cruise of R/V Conrad (C22-08), 11 June to 2 July, 1979.

			NETPLANKTON (>20u)						NANOPLANKTON (<20u)						CILIATES
Sta.	Area	Depth	Diatoms		Dino-flagellates		Other Flagellates		Flagellates		Diatoms		Other		
		M	#/l	% tot.	#/l	% tot.	#/l	% tot.	#/l	% tot.	#/l	% tot.	#/l	% tot.	#/l
271	Shelf	5	26,320	97.9	560	2.1			308,718	65.2	35,897	7.6	129,231	27.3	9,240
		13	7,375	28.1	18,875	71.9			589,744	83.6			115,385	16.4	11,625
		22	9,660	23.5	31,395	76.5			41,282	46.7	23,590	26.7	23,590	26.7	460
		28	26,390	59.7	17,810	40.3			53,333	88.1	6,667	11.1			1,560
314	Shelf	0	30,030	97.8	660	2.2			92,928	100					0
	break	45	2,970	57.4	2,200	42.6			59,136	100					770
284	Slope	0			840	53.8	720	46.1	107,690	97.2			3,080	2.8	600
		45	16,120	95.4	650	3.8	130	0.8	42,900	48.1	39,600	44.4	6,600	7.4	520
310	Slope	0			2,672	64.7	1,461	35.3	151,173	96.9			4,774	3.1	1,181
		43	363	13.4	2,356	86.6			178,225	94.1			11,139	5.9	3,772

Major inorganic nutrients were low at all stations sampled (Table 2.1.1-2). Nitrate and phosphate were depleted from surface waters and reached concentrations of $\geq$ 1 ug-at l^{-1} only within or below the thermocline. However, at the shelf station nitrate was virtually undetectable throughout the water column. Silicate concentrations were lowest in surface waters - 1 ug-at l^{-1} and increased with depth, reaching concentrations of - 8 ug-at l^{-1} on the shelf. Ammonia measurements at the shelf station indicated a close correspondence between the depth of the chlorophyll maximum and a dramatic increase in ammonia at the base of the thermocline (Fig. 2.1.1-2).

Primary production estimates were highest on the shelf, approximately 1 g C m^{-2} day^{-1} for both the nanoplankton and netplankton fractions (Table 2.1.1-3). At the shelf-break and in slope waters primary production was substantially lower in both fractions. Calculations of production per unit biomass, however, indicated that variations in production were more related to variations in biomass rather than growth rate. Except for netplankton at the shelf-break, production per unit biomass was generally high everywhere ranging from 92-225 mg C $(chl)^{-1}$ day^{-1} and 54-202 mg C $(chl)^{-1}$ day^{-1} for nanoplankton and netplankton, respectively. At the shelf-break netplankton chlorophyll *a* was maximal at the bottom of the euphotic zone and production per unit biomass was reduced to 5 mg C $(chl)^{-1}$ day^{-1}.

Thus, phytoplankton populations in the areas sampled were turning over rapidly. Doubling times on the order of less than a day were calculated for all euphotic areas (assuming a C:Chl = 47) except for the netplankton at the shelf-break where the estimate of turnover time was approximately 6.5 days.

Table 2.1.1-2. Concentration of major dissolved inorganic nutrients for stations occupied from Hudson Canyon to Cape Hatteras during the cruise of R/V Conrad (C22-08), 11 June to 2 July, 1979.

Date	Sta.	Area	Depth M	Nitrate ug-at/l	Phosphate ug-at/l	Silicate ug-at/l	Ammon ug-at
6/15/79	269	Shelf	1	0.0	0.0	1.1	1.4
			8	0.1	0.0	1.5	0.1
			13	0.2	0.3	3.7	2.0
			18	0.0	0.7	3.1	0.1
			20	0.0	0.6	4.6	0.4
			22	0.0	0.3	3.0	-
			24	0.5	0.8	3.4	5.6
			26	0.0	1.0	3.5	4.6
			34	0.0	0.9	8.7	5.7
			40	0.0	0.8	4.8	4.5
	271	Shelf	0	0.0	0.0	1.2	
			5	7.1	0.0	2.2	
			13	0.0	0.2	1.0	
			20	0.1	0.4	5.8	
			22	0.1	0.9	5.0	
			24	0.0	1.3	5.8	
			26	0.0	1.0	3.2	
			28	0.1	1.0	3.3	
			31	0.0	0.9	3.1	
			36	0.1	1.1	2.4	
			40	0.1	1.0	4.5	
			43	0.4	0.9	4.3	
6/18/79	284	Slope	0	0.0	0.0	1.2	
			15	0.0	0.0	2.2	
			25	0.0	0.0	2.6	
			35	0.0	0.0	3.9	
			41	0.1	0.5	2.2	
			55	9.4	1.1	4.6	
6/22/79	307	Slope	0	0.0	0.0	1.9	
			17	0.0	0.0	1.7	
			32	0.0	0.0	1.7	
			38	0.0	0.0	2.4	
			46	0.3	0.9	5.9	
			55	11.5	1.3	3.4	
6/24/79	314	Shelf break	0	0.0	0.0	4.6	
			14	3.1	0.0	1.1	
			30	0.1	0.3	0.5	
			45	3.2	1.9	3.2	
			60	3.2	1.1	3.0	

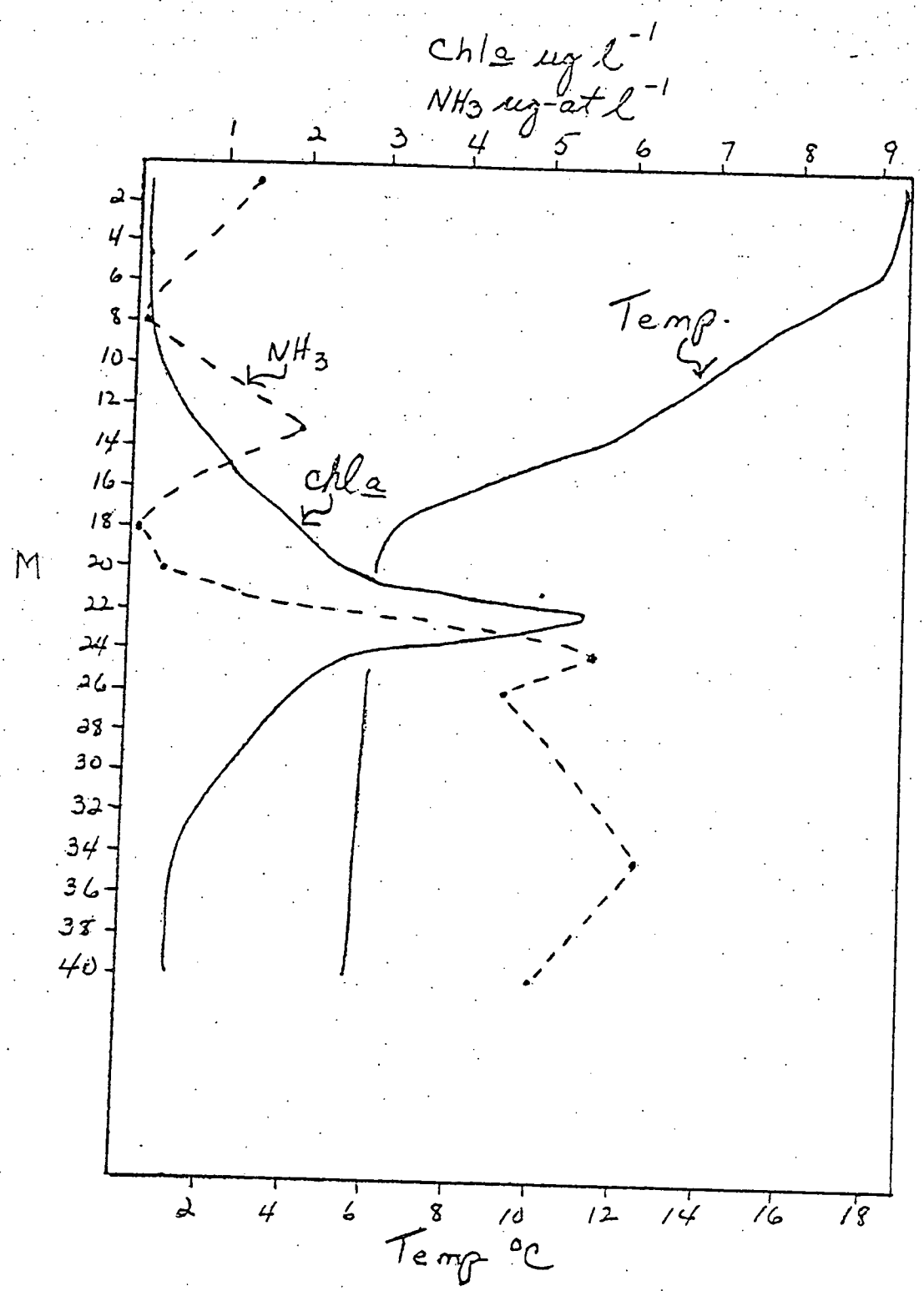

Figure 2.1.1-2. Distribution of temperature (°C), chlorophyll a (ug l^{-1}) and ammonia (ug-at l^{-1}) with depth (meters) at station 269 on shelf along transect I.

Table 2.1.1-3. Primary production (PP), chlorophyll *a* (chl *a*) and doubling time for nano- and netplankton sampled from Hudson Canyon to Cape Hatteras during the cruise of R/V Conrad (C22-08), 11 June to 2 July, 1979; depth of euphotic zone determined from 1% light depth.

Sta.	Area	Euphotic Zone M	Fraction	Chl *a* mgm^{-2}	PP gm^{-2}	PP/Chl *a* day^{-1}	Doubling Time days
271	Shelf	33	nano	10.93	1.25	114.7	0.6
			net	16.82	1.02	61.0	0.8
			total	27.8	2.28		
314	Shelf break	46	nano	1.65	0.37	225.3	0.4
			net	10.69	0.57	5.3	6.5
			total	12.34	0.43		
284	Slope	51	nano	8.36	0.78	92.8	0.6
			net	2.60	0.14	54.8	0.9
			total	10.96	0.92		
310	Slope	51	nano	5.22	0.48	92.4	0.6
			net	0.22	0.44	201.8	0.4
			total	5.44	0.53		

A preliminary assessment of the presence of phytoplankton in sediments and the importance of their resuspension was made on surface sediments of a box core collected from 800 M at station 279 on the slope. A small subsample of the sediment, much less than a gram, was inoculated into several tubes of culture media and placed in a constant temperature (16°C) light incubator. Within one week a very diverse and dense group of large celled diatoms were present. Ditylum brightwelli and several chain-forming Chaetoceros spp. were particularly dominant, as were Skeletonema costatum, Thalassiosira spp. and numerous pennate forms. Microscopic observations of the sediment sample did not reveal obvious concentrations of any of these diatoms suggesting that they grew at extremely fast rates during the first week in response to being introduced into conditions conducive for growth.

DISCUSSION

The low phytoplankton biomass observed in surface waters both on the shelf and in slope waters from the Hudson Canyon to Cape Hatteras is typical of summer conditions when strong water column stratification exists (Walsh et al., 1978). The association of chlorophyll maxima with the bottom of the photic zone within the pycnocline and nutricline has previously been documented (D.O.E. 1979 Annual Report; Walsh et al., 1978; Malone et al., submitted). The generally motile nature of the phytoplankton at this time of year denotes a selection for species which can in part control their position in the water column so as to attain conditions favorable for growth. The presence of vertical isotherms at the shelf-break could indicate mixing of

deep nutrient rich water into the photic zone. The fact that nutrient concentrations and phytoplankton biomass remained low in surface waters at the shelf-break further implies that steady state conditions existed. A close coupling between nutrient supply, phytoplankton production and heterotrophic grazing is inferred. Since turnover rates of phytoplankton were generally fast and variations in primary production were primarily related to variations in phytoplankton biomass, the importance of environmental factors other than those which directly affect growth rate, i.e. grazing, sinking and resuspension of seed populations, is signified.

The importance of the coupling of heterotrophic grazing to primary productivity and nutrient recycling under conditions of nutrient depletion in surface waters has recently been emphasized by several groups (Sheldon and Sutcliffe, 1978; McCarthy and Goldman, 1979; Gieskes et al., 1979). Such studies have also indicated the problems associated with such a close coupling between the autotrophic and heterotrophic components and a possible underestimate of primary production. Similarly, the results of this study appear to reflect such a close coupling. The presence of large numbers of ciliates in the phytoplankton samples and presumably also in the ^{14}C incubation bottles helps to explain two aspects of the results. Release of ammonia during ciliate grazing probably supplied part of the nitrogen necessary to account for the high growth rates observed even in surface waters depleted of nitrate. At shelf station 271 both the highest rates of biomass specific production and the largest populations of ciliates were observed in surface waters. Nitrate was depleted throughout the water column and ammonia concentrations were low in surface waters and increased only below the chlorophyll maximum. Pre-

sumably, the ammonia generated by ciliate grazing was quickly removed from the water by the phytoplankton. Also, the netplankton production measured was excessively high (>700 ug C $(chl)^{-1}$ day^{-1}) for the biomass levels present. The ciliates were most likely grazing on the nanoplankton and yet were caught on the 20 u mesh net and included in the estimate of netplankton productivity.

The presence of Ceratium tripos in the cold pool of water on the shelf and at the shelf-break is of interest since this species of dinoflagellate was associated with massive fish kills along the New Jersey coast during the summer of 1976 (Malone, 1978). The moderate population levels observed during the summer of 1979 are in sharp contrast to the bloom concentrations (>10^5 cells l^{-1}) which occurred from April to July, 1976. However, these large populations originated from similar offshore areas and moved onshore only after stratification developed.

Malone and Chervin (1979) have emphasized the importance of resuspension of pelagic diatoms into the photic zone by storm events during the summer and during the winter and early spring when thermal stratification breaks down. The potential for production by the resuspension of such phytoplankters has never been assessed. The preliminary observations reported above indicate that large diatoms can respond quickly to favorable growth conditions upon resuspension from sediments and aphotic conditions. Many phytoplankters have been found to survive for a long time, months to more than a year, under cold, dark conditions in the laboratory (Antia and Cheng, 1970; Umebayashi, 1972; Smayda and Mitchell-Innes, 1974), retaining an ability to rapidly photosynthesize upon re-entry into light conditions (Anderson, 1975; French and Hargraves, 1980; Davis et al., 1980).

An assessment of phytoplankton populations in sediments and the potential for growth upon resuspension will be addressed further and more quantitatively using samples from box cores obtained during the summer 1980 cruise.

CONCLUSIONS

Two main mechanisms by which phytoplankton can influence the distribution and fate of pollutants and radionuclides within the New York Bight and adjacent slope waters have emerged from the studies over the last few years: (1) When the coupling between grazing and primary production is close, as during the summer and under strongly stratified conditions, pollutants and radionuclides associated with phytoplankters will be rapidly introduced into higher trophic levels. Removal of pollutants from the water column into the sediments would be largely controlled by the sinking of fecal pellets (see zooplankton section). (2) During winter, early spring and storm events when the water column is well mixed, large phytoplankters, particularly diatoms, bloom and remain largely ungrazed (Malone and Chervin, 1979). Sinking of such populations into the sediments of the shelf and slope would then be the main biological mechanism for removal of pollutants from the pelagic system; re-introduction would be controlled by processes affecting sediment resuspension.

2.1.2 ZOOPLANKTON

METHODS

The zooplankton portion of this study involved assessment of macrozooplankton (>202 um) abundance at the shelf, shelf-break and slope and collection of sufficient macrozooplankton fecal pellets for radionuclide analysis. During C22-08 zooplankton was collected at selected stations from the Hudson Canyon to Cape Hatteras along transects across the slope as well as one transect along the shelf of the New York Bight (Fig. 2.1.1-1). Either oblique or discrete depth tows were made at each station in conjunction with phytoplankton collections. Oblique tows not exceeding 50 m were made with paired 1/2 m, 202 um mesh nets equipped with inner and outer TSK flow meters. Discrete depth samples were collected in the mixed layer and below the chlorophyll maximum with messenger-actuated opening-closing 3/4 m, 202 um mesh nets equipped with an inner TSK flow meter and a time-depth recorder. Once on board, samples were split with a Folsom plankton splitter. One half was preserved in 4% buffered formalin and used for taxonomic analysis. The remaining half was frozen for dry weight analysis. In the laboratory, zooplankton was identified to major groups and biomass determined by drying samples to constant weight in a 60°C oven.

The system used to collect fecal pellets for radionuclide analysis was modified from that described by LaRosa (1976). It consisted of a 200 gal tank fitted with a liner (Fig. 2.1.2-1). The bottom of the liner was constructed of 202um netting in order to retain zooplankton but still allow fecal pellets to pass through. On station the tank was filled with seawater filtered through 20 um netting. Live animals

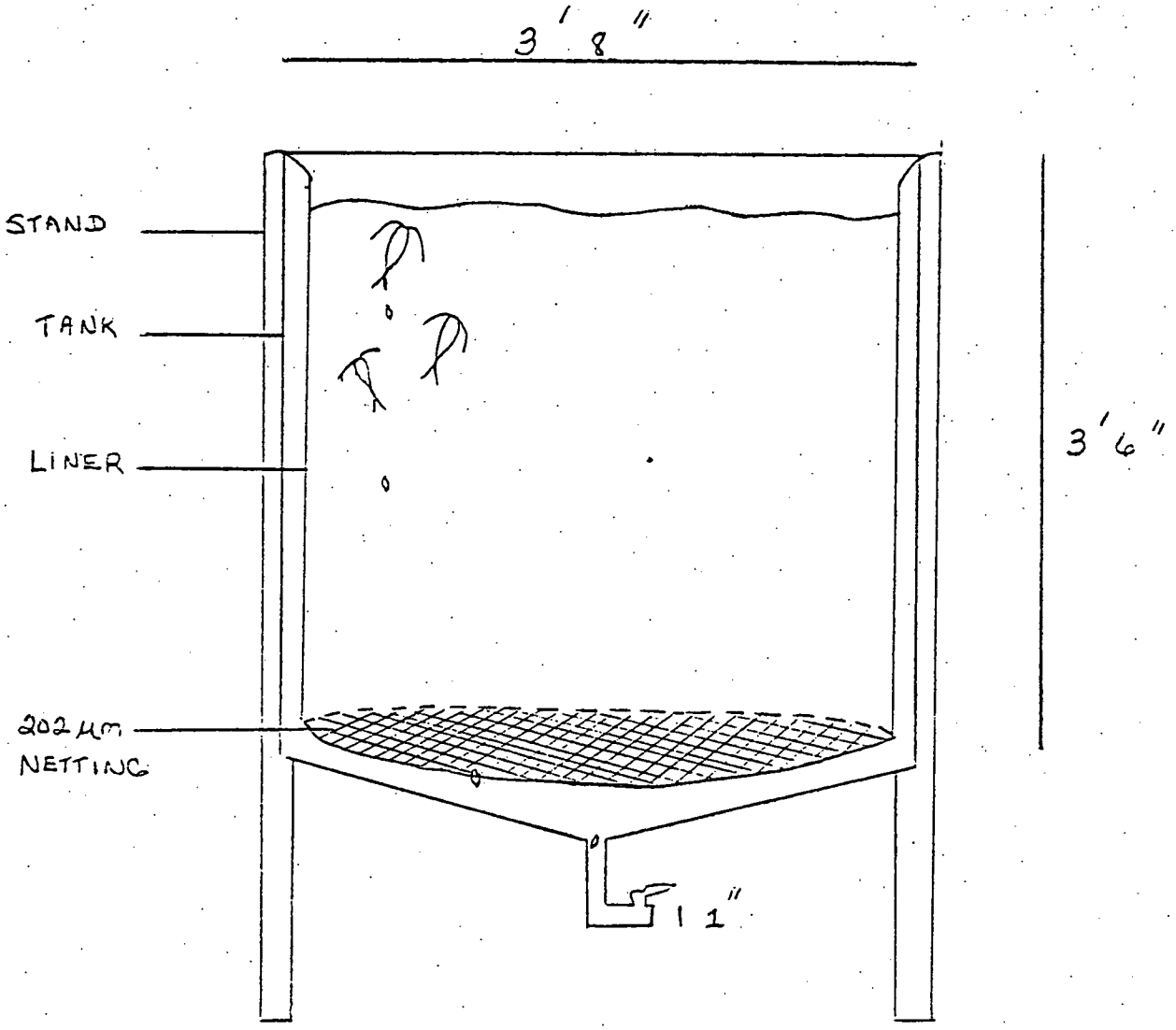

Figure 2.1.2-1. Tank used for fecal pellet collections.

were collected with 202 um nets and the tank stocked. Accumulated fecal material was collected at 2-3 hr intervals. The total number of fecal pellets collected was insufficient for radionuclide analysis which requires 0.5 - 1 g dry weight fecal pellets (Li, pers. comm.). The size of the mesh at the base of the liner and bacterial degradation accelerated by the high June temperatures apparently influenced the size of the collections. Although zooplankton was collected with a 202 um net and presieved on 202 um or 333 um netting, the 202 um mesh at the base of the liner proved too large to retain many of the copepods. Animals were able to squeeze through the netting resulting in a loss of fecal pellets through coprophagy. Honjo and Roman (1978) and Small et al. (1979) have observed that bacterial degradation of fecal pellets can be quite rapid above 15°C. Temperatures in the tank ranged from 22°-24°C during the experiments. Although collections were made at 2-3 hr intervals, it was not possible to collect large numbers of intact fecal pellets. This suggests that bacterial decomposition of fecal pellets at temperatures above 20°C may proceed at greater rates than presently indicated in the literature. On the basis of these results, plans have been made to further modify the collection system (see Proposal, Section 2.1).

RESULTS

A comparison of zooplankton abundance, primary production and water column Th-234 at the shelf, shelf-break and slope indicates that during the time sampled phytoplankton production and zooplankton grazing were closely coupled. The coupling was particularly evident at the shelf-break where zooplankton grazing and subsequent fecal pellet production and sinking appear to be a significant pathway for the removal of radionuclides from the water column.

Copepods were the dominant group at the shelf, shelf-break and slope composing >95% of total macrozooplankton at the shelf and shelf-break and 45-82% on the slope where other groups as chaetognaths, euphausiids and pelagic gastropods were more abundant (Table 2.1.2-1). Estimates of water column grazing pressure exerted by copepods at the shelf, shelf-break and upper 100 m of the slope were calculated using grazing constants reported in the literature for similar copepods (Table 2.1.2-2). Grazing pressure was highest at the shelf-break accounting for 61-275% of primary production. Close coupling between phytoplankton production and grazing is in agreement with the idea that steady state conditions prevailed at the shelf-break. Zooplankton grazing kept phytoplankton biomass low in surface waters of the shelf-break (Fig. 2.1.1-1) despite high turnover rates of phytoplankton (Table 2.1.1-3) and large inputs of nutrients (see Phytoplankton section). Grazing pressure was generally low at both the shelf and slope where it accounted for only 1-14% of primary production. This is probably an underestimate since it does not include grazing by microzooplankton (64-202 um) which were abundant as ciliates on the shelf and slope at this time and would have been consuming the nanoplankton fraction (Table 2.1.1-1).

Water column fecal pellet production was estimated using water column copepod abundance and a mean fecal pellet production rate of 2 pellets copepod^{-1} hr^{-1} (Adler et al., submitted; Honjo and Roman, 1978) (Table 2.1.2-3). Fecal pellet production was highest at the shelf-break (330 x 10^4 d^{-1}), lowest on the slope (15-18 x 10^4 d^{-1}) and intermediate between shelf-break and slope estimates on the shelf (91 x 10^4 d^{-1}). Comparison of these estimates with Th-234 measure-

Table 2.1.2-1. Abundance of copepods and other groups of macrozooplankton at representative stations occupied at the shelf, shelf-break and slope during C22-08, 11 June - 2 July, 1979. (Ob = oblique tow; Dd = discrete depth tow).

Sta.	Area	Type of Tow	Depth of tow (M)	COPEPODS		OTHERS	
				#/M^3	% Total	#/M^3	% Total
270	Shelf	Ob	0-14	793	97.7	19	2.3
314	Shelf	Dd	10	1415	95.5	66	4.5
	break	Dd	50	700	95.2	35	4.8
272	Slope	Ob	0-45	51	82.3	11	17.7
307	Slope	Ob	0-32	37	45.1	45	54.9
284	Slope	Ob	0-10	30	71.4	12	28.6
		Dd	20	74	77.9	21	22.1
		Dd	65	18	66.7	9	33.3

Table 2.1.2-2. Grazing pressure exerted by copepods at the shelf, shelf-break and slope estimated on the basis of water column abundance and biomass.

Sta.	Area	Copepods	Grazing[a]	Grazing/PP	Macro-zooplankton Biomass	C[b]	Grazing[c]	Grazing/PP
		M^{-2}	mg cop^{-1} d^{-1}	%	mg m^{-2}	mg m^{-2}	mgC mgC^{-1} d^{-1}	%
270	Shelf	18855	104 324	5 14	130	52	21	1
314	Shelf break	68750	378 1184	88 275	1631	652	261	61
284	Slope	3040[d]	17 52	2 6	106[d]	42	17	2
307	Slope	3700[d]	20 64	4 12	100[d]	40	16	3

[a]Calculated using minimum and maximum assimilation rates reported by Chervin et al (submitted) for copepods in the New York Bight during July.

[b]Zooplankton carbon, represented primarily by copepods, calculated as 40% of dry weight (Beers, 1966).

[c]Calculated using 40% as percentage of bodily carbon ingested d^{-1} (Dagg and Grill, 1980).

[d]Slope abundance and biomass estimated for upper 100 m only.

Table 2.1.2-3. Measurements of Th-234 and water column fecal pellet production estimated from copepod abundance at the shelf, shelf-break and slope.

AREA	Fecal Pellet Production d^{-1} (10^4)[a]	Sta.	Th-234 dpm $(100\ Kg)^{-1}$[b]
Shelf	91	269	60.2 ± 3.3
		270	53.3 ± 4.4
		271	83.9 ± 4.7
		329	56.8 ± 2.5
Shelf break	330	332	11.8 ± 0.3
Slope	15-18[c]	263	133.3 ± 6.7
		264	140.2 ± 6.9

[a]Calculated at a rate of 2 fecal pellets $copepod^{-1}$ hr^{-1}.

[b]Data supplied by Li.

[c]Upper 100 m only.

ments suggests an inverse relationship between fecal pellet production and radionuclide concentration (Table 2.1.2-3). High production of fecal pellets at the shelf-break where there is a close coupling between grazing and phytoplankton production corresponds to low Th-234 (11.8 dpm $100kg^{-1}$) while low grazing and fecal pellet production on the slope corresponds to high Th-234 (133.3-140.2 dpm $100kg^{-1}$). This inverse relationship suggests that sinking fecal pellets may be an important pathway for the removal of radionuclides at the shelf-break. On the shelf and slope where ciliates were abundant and macrozooplankton grazing did not correlate as well with phytoplankton production as at the shelf-break, radionuclide concentration in the water column remained high. Ciliates do not produce fecal pellets and thus although phytoplankton production and grazing are probably still well coupled, radionuclide concentration is not affected because of the lack of fecal pellet production.

CONCLUSIONS

The relationship between zooplankton, phytoplankton production, fecal pellet production and Th-234 suggests that during the summer, when there is a close coupling between phytoplankton production and macrozooplankton grazing, copepod fecal pellets are an important pathway for the removal of radionuclides. Fecal pellets of euphausiids are known to concentrate radionuclides as well as heavy metals (Heyraud et al., 1976; Fowler, 1977; Higgo et al., 1977; Beasley et al., 1978). The results reported here indicate this is also true of other macrozooplankton. A more quantitative assessment however is needed and is planned for next year's research (see Proposal, Section 2.1).

The results also suggest that the nature of the heterotrophic community, micro- vs. macrozooplankton, affects the water column concentrations of radionuclides. This too will be assessed to a greater extent next year.

Literature Cited (Section 2.1)

Adler, D.M., P.H. Santschi, M. Chervin, K.R. Hinga and M. Andurer. (submitted). The importance of zooplankton grazing to the removal of metals from shallow estuaries. Nature.

Anderson, O.R. 1975. A possible origin of some olive-green cells in aphotic marine environments. Limnol Oceanogr. 20: 1000-1004.

Antia, N.J. and J.Y. Cheng. 1970. The survival of axenic cultures of marine planktonic algae from prolonged exposure to darkness at 20°C. Phycologia 9: 179-183.

Beasley, T.M., M. Heyraud, J.J.W. Higgo, R.D. Cherry and S.W. Fowler. 1978. ^{210}Po and ^{210}Pb in zooplankton fecal pellets. Mar. Biol. 44: 325-328.

Beers, J.R. 1966. Studies on the chemical composition of the major zooplankton groups in the Sargasso Sea off Bermuda. Limnol. Oceanogr. 11: 520-528.

Chervin, M.B., T.C. Malone and P.J. Neale. (submitted). Interactions between suspended organic matter and copepod grazing in the plume of the Hudson River. Est. Coast. Mar. Sci.

Dagg, M.J. and D.W. Grill. 1980. Natural feeding rates of Centropages typicus females in the New York Bight. Limnol. Oceanogr. 25: 597-609.

Davis, C.O., J.T. Hollibaugh, D.L.R. Seibert, W.H. Thomas and P.J. Harrison. 1980. Formationof resting spores by Leptocylindrus danicus (Bacillariophyceae) in a controlled experimental ecosystem. J. Phycol 16: 296-302.

Fowler, S.W. 1977. Trace elements in zooplankton particulate products. Nature 269: 51-53.

French, F.W. and P.E. Hargraves. 1980. Physiological characteristics of plankton diatom resting spores. Mar. Biol. Lett. 1: 185-195.

Gieskes, W.W., G.W. Kraay, and M.A. Baars. 1979. Current ^{14}C methods for measuring primary production: gross underestimates in oceanic waters. Neth. J. Sea Res. 13: 58-78.

Heyraud, M., S.W. Fowler, T.M. Beasley and R.D. Cherry. 1976. Polanium-210 in euphausiids: a detailed study. Mar. Biol. 34: 127-136.

Literature Cited (Section 2.1) cont.

Higgo, J.J.W., R.D. Cherry, M. Heyraud and S.W. Fowler. 1977. Rapid removal of plutonium from the oceanic surface layer by zooplankton fecal pellets. Nature 266: 623-624.

Honjo, S. and M.R. Roman. 1978. Marine copepod fecel pellets: production, preservation and sedimentation. J. Mar. Res. 36: 45-57.

LaRosa, J. 1976. A simple system for recovering zooplanktonic fecal pellets in quantity. Deep-Sea Res. 23: 995-997.

McCarthy, J.J. andJ.C. Goldman. 1979. Nitrogenous nutrition of marine phytoplankton in nutrient depleted waters. Science 203: 670-672.

Malone, T.C. 1976. Phytoplankton productivity in the apex of the New York Bight: September 1973 - August 1974. NOAA Tech. Memo. U.S. Dept. Comm. ERL MESA-5.

_____. 1977. Light-saturated photosyntheses by phytoplankton size fractions in the New York Bight, U.S.A. Mar. Biol. 42: 281-292.

_____. 1978. The 1976 Ceratium tripos bloom in the New York Bight: causes and consequences. NOAA Tech. Rep. NMFS Circular 410. U.S. Dept. Comm.

_____ and M.B. Chervin. 1979. The production and fate of phytoplankton size fractions in the plume of the Hudson River, New York Bight. Limnol. Oceanogr. 24: 683-696.

_____, W. Houghton and A. Gordon. (submitted). Vertical exchange of properties under stratified conditions in the New York Bight. Limnol. Oceanogr.

Sheldon, R.W. and W.H. Sutcliffe. 1978. Generation times of 3 h for Sargasso Sea microplankton determined by ATP analysis. Limnol. Oceanogr. 23: 1051-1055.

Small, L.F., S.W. Fowler and M.Y. Unlu. 1979. Sinking rates of natural copepod fecal pellets. Mar. Biol. 51: 233-241.

Smayda, T.J. and B. Mitchell-Innes. 1974. Dark survival of autotrophic, planktonic marine diatoms. Mar. Biol. 25: 195-202.

Umebayashi, D. 1972. Preservation of some cultured diatoms. Bull. Tokai reg. Fish. Res. Lab. 69: 55-61.

Walsh, J.J., T.E. Whitledge, F.W. Barvinck, C.D. Wirick, S.O. Howe, W.E. Esaias, and J.T. Scott. 1978. Wind events and food chain dynamics within the New York Bight. Limnol. Oceanogr. 23: 659-683.

2.2 Natural and Man-Made Radionuclides in the Water Column

With regard to understanding the removal behavior of ^{228}Th from the New York Bight water column during the different seasons, what factors control the removal rate of ^{228}Th from the water column, and how the ^{228}Th results can be applied to other "particle-reactive" trace elements, we have made encouraging progress during the last fiscal year (see Appendix 1 to 7). Some of the highlights are:

1) During the periods of density stratification in the New York Bight water column (i.e., spring, summer and fall seasons), the half removal times of ^{228}Th from the surface waters by settling particles, t_c, are essentially the same for all three seasons, i.e., $t_c = 20\pm10$ days in the surface shelf water and $t_c = 70\pm10$ days in the surface slope water (Li et al., 1979, and Appendix 1). The general trend of decreasing t_c from the surface slope water toward the shore is strongly correlated with the general increasing trend of the suspended particle concentration toward the shore. It is not correlated with the phytoplankton production and the zooplankton grazing rates (Fig. 2.2-1 and Appendix 1). Because the general shoreward increase in suspended particle concentrations in the New York Bight is due to sediment resuspension (Biscaye and Olsen, 1976), we conclude, in coastal marine environments, that the scavenging of ^{228}Th by the resuspended sediment particles is the dominant factor on determining removal rates (Appendix 1 and 2). This is in contrast to the open ocean where removal on zooplankton fecal pellets appears to be the dominant scavenging mechanism (Li et al., 1980).

2) The removal behavior or the half removal time of ^{228}Th can be applied (to a first approximation) to the other "particle-reactive"

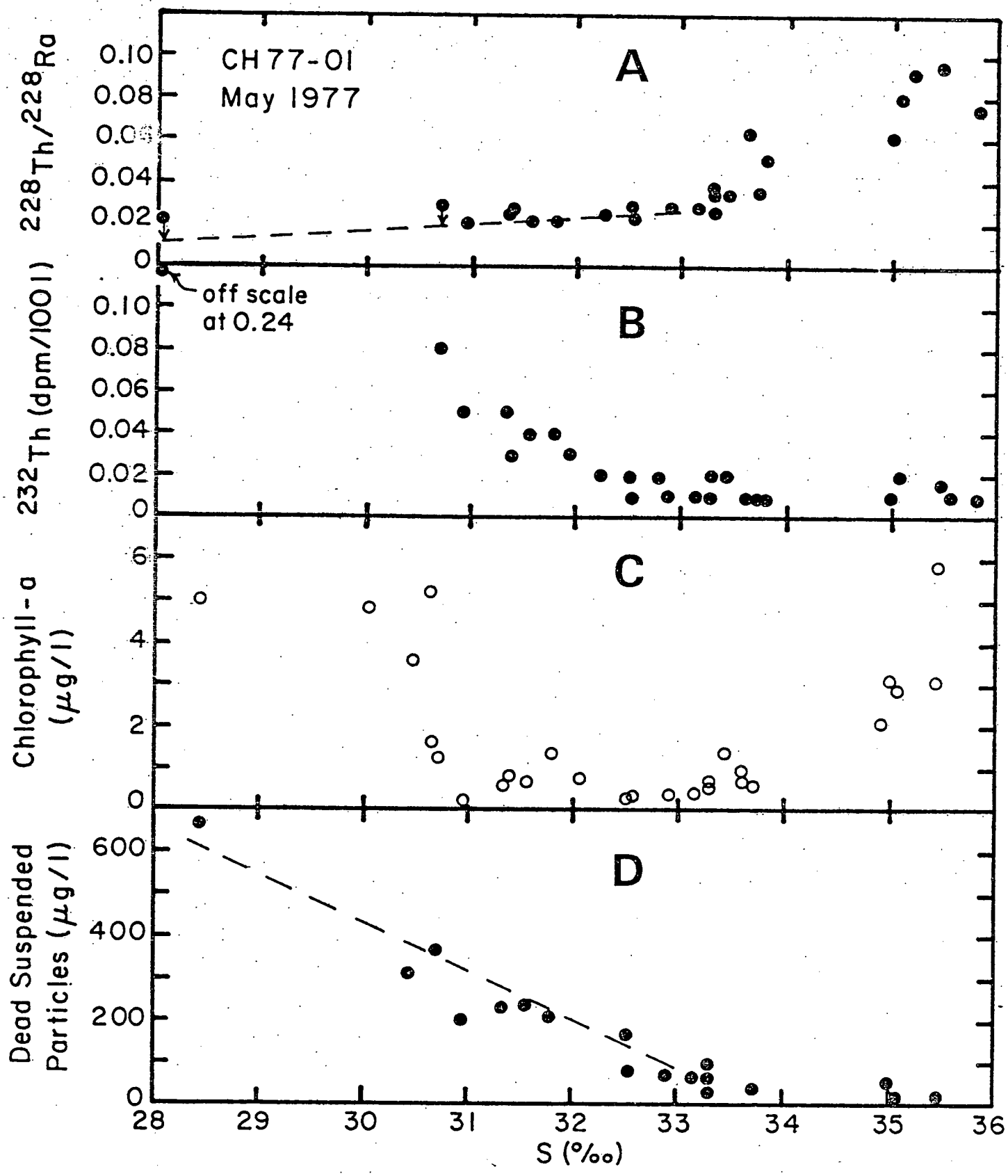

Fig. 2.2-1 The plots of salinity vs. A) $^{228}Th/^{228}Ra$ activity ratio, B) ^{232}Th concentration, C) chlorophyll-a concentration and D) non-living suspended particles during the spring cruise (May 1977, CH77-01).

elements such as Fe, Ti, Ge, Zr, Hf, Y, rare earths, In, Cr, Am, Pu, etc., which are tri- and tetra-valent cations and usually form hydroxide complexes in seawater, and to elements such as Sn, Pb and Hg (Appendix 3 and 6).

3) The geochemical behavior of $^{239,240}Pu$ in the New York Bight and Narragansett Bay is fully discussed in Appendix 4. According to Nelson and Lovett (1978), about 85% of $^{239,240}Pu$ in the Irish Sea is present as a relatively unreactive anionic Pu (V+VI) species and only about 15% as the "particle-reactive", highly-hydrolized Pu (III+IV), which is continuously removed to sediments at a rate similar to ^{228}Th (Appendix 4). The high concentration of the total $^{239,240}Pu$ in the near-shore waters of the New York Bight and Narragansett Bay during periods of high sediment resuspension (Fig. 2.2-2 and Fig. 2.2-3) can be best explained by the injection of more-soluble, less-reactive anionic Pu (V+VI) or aged-colloidal Pu (III+IV) species from the bottom sediments to the overlying water column. The possible reduction-oxidation cycle of $^{239,240}Pu$ in the coastal marine environments needs to be studied further.

We have been interested not only in the geochemical behavior of ^{228}Th, ^{228}Ra and $^{239,240}Pu$, etc., but also of other elements in the ocean. Appendices 5 to 7 summarize our attempt to synthesize various pertinent geochemical data and to find out what factors govern the cycling and deposition of various elements in the ocean. The important conclusion are:

1) The river input rates of "biophile" elements (e.g., I, Ag, Au, Sb, Hg, Cu, Zn, Cd, Pb and probably Se and Sn) are much higher than the deposition rates in oceanic sediments. The most plausible explanation is that these "biophile" elements are recycled from the surface ocean through the atmosphere to the rivers (Appendix 5).

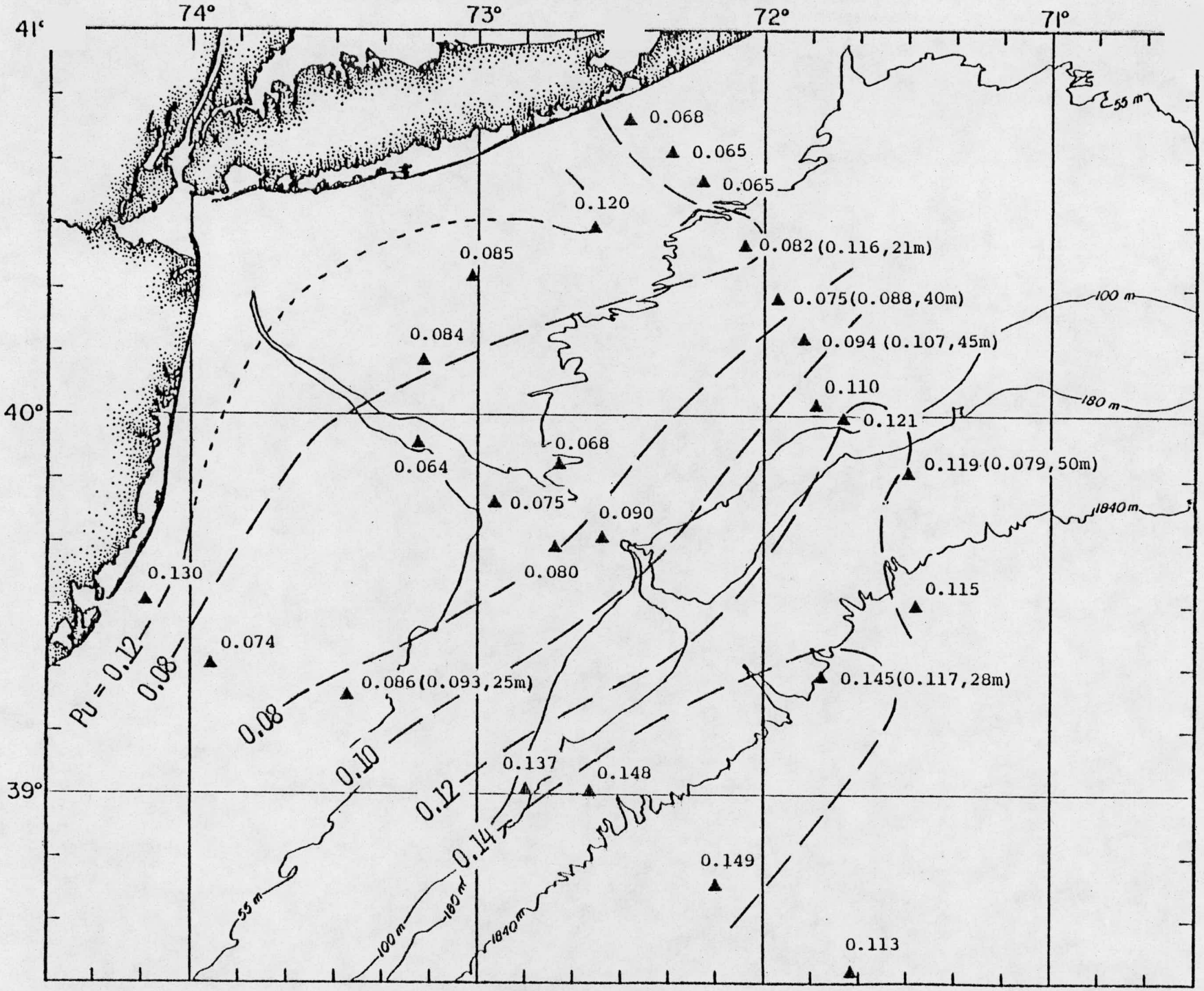

Fig. 2.2-2 Areal distribution of $^{239,240}Pu$ in the surface waters and subsurface waters (parenthesis) of the New York Bight during April 29 - May 8, 1977 (CH77-01).

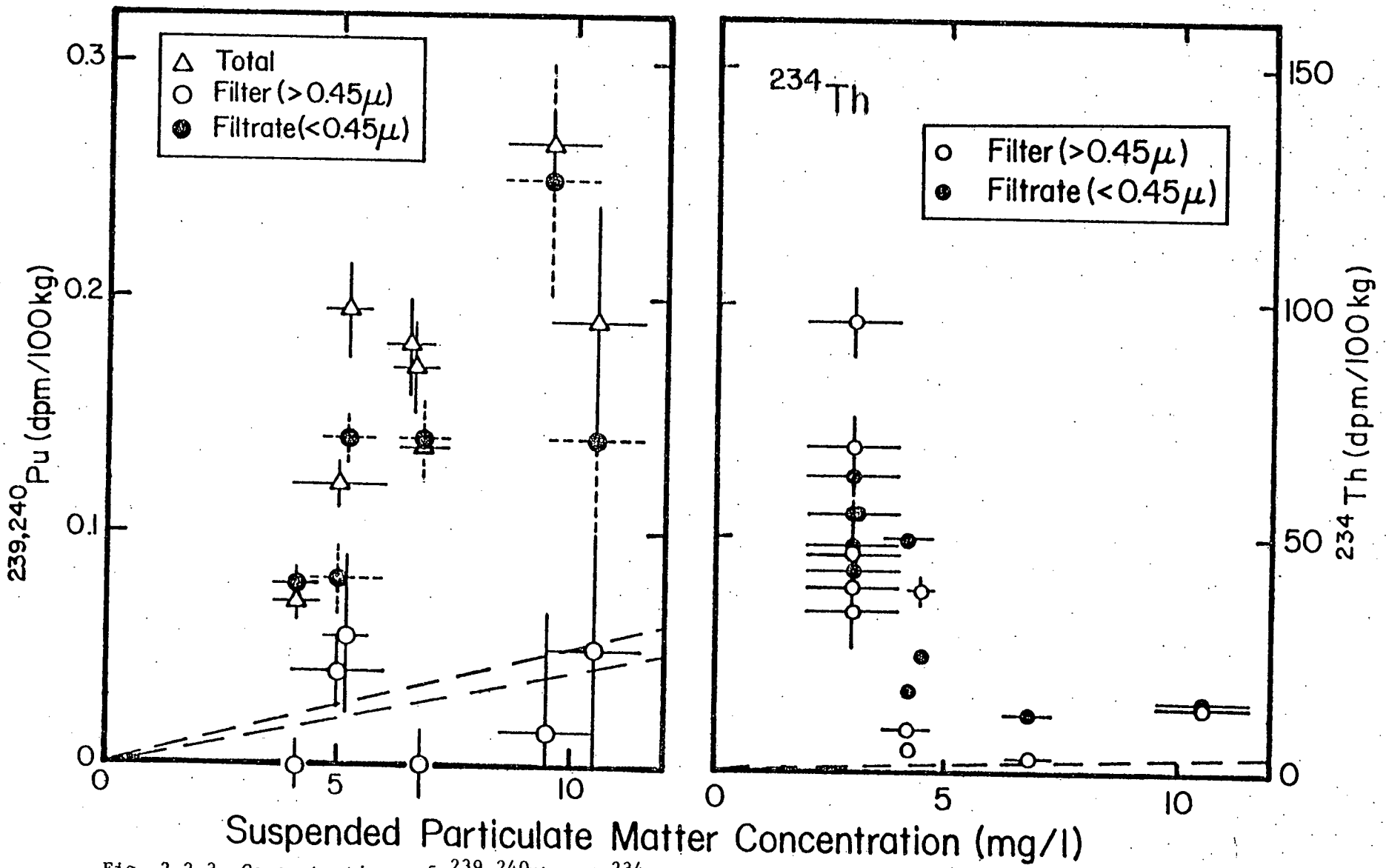

Fig. 2.2-3 Concentrations of $^{239,240}Pu$ and ^{234}Th in water samples of Narragansett Bay versus the particulate matter concentrations. Dashed lines indicate expected concentrations if the particulate matter has the same activity as the surface sediments.

2) The settling of fecal pellets and fecal aggregates is the most important mechanism for transporting most of the elements (Mn, Co and Ni are exceptions) from the surface to the deep oceans. Mn, Co and Ni are probably incorporated directly into pelagic clay at the sediment-water interface (Appendix 5).

3) Once elements are transported down to the deep ocean, a certain fraction of each element is remineralized and dissolved back to the water column and another fraction is incorporated into pelagic clays and Mn-nodules. The factor analysis (Fig. 2.2-4) and the enrichment pattern of elements in Mn-nodules relative to pelagic clays (Fig. 2.2-5) show that both in oceanic pelagic clays and in Mn-nodules, elements such as K, Rb, Cs, Be and Ga are mainly correlated with the aluminosilicate detritus phase. The elements related to or incorporated into iron oxide phases are anion or oxyanions (e.g., P, S, Se, Te, As, B, Sn, I, Br, F, U, Pb, Hg, etc.) and hydroxide complexes of tri- and tetra-valent cations (e.g., Ti, Ge, Zr, Hf, Th, Y, rare earths, In, Cr, etc.) in seawater. The elements incorporated into manganese oxide phases are mono- and di-valent cations (e.g., Tl, Mg, Ca, Ba, Co, Ni, Cu, Zn, Bi, Ag, Cd, etc.) and oxyanions with high affinity to Mn such as Mo, W. and Sb in seawater. Mg, Ca and Ba in pelagic clays are also related to other phases, such as aluminosilicates, carbonates and barite (Appendix 6).

4) The concentration of various elements in the ocean or in the average rivers is mainly controlled by the adsorption equilibria between the solution and solid phases - mainly iron oxides, manganese oxides and aluminosilicate detritus phases (Fig. 2.2-6 and Appendix 7).

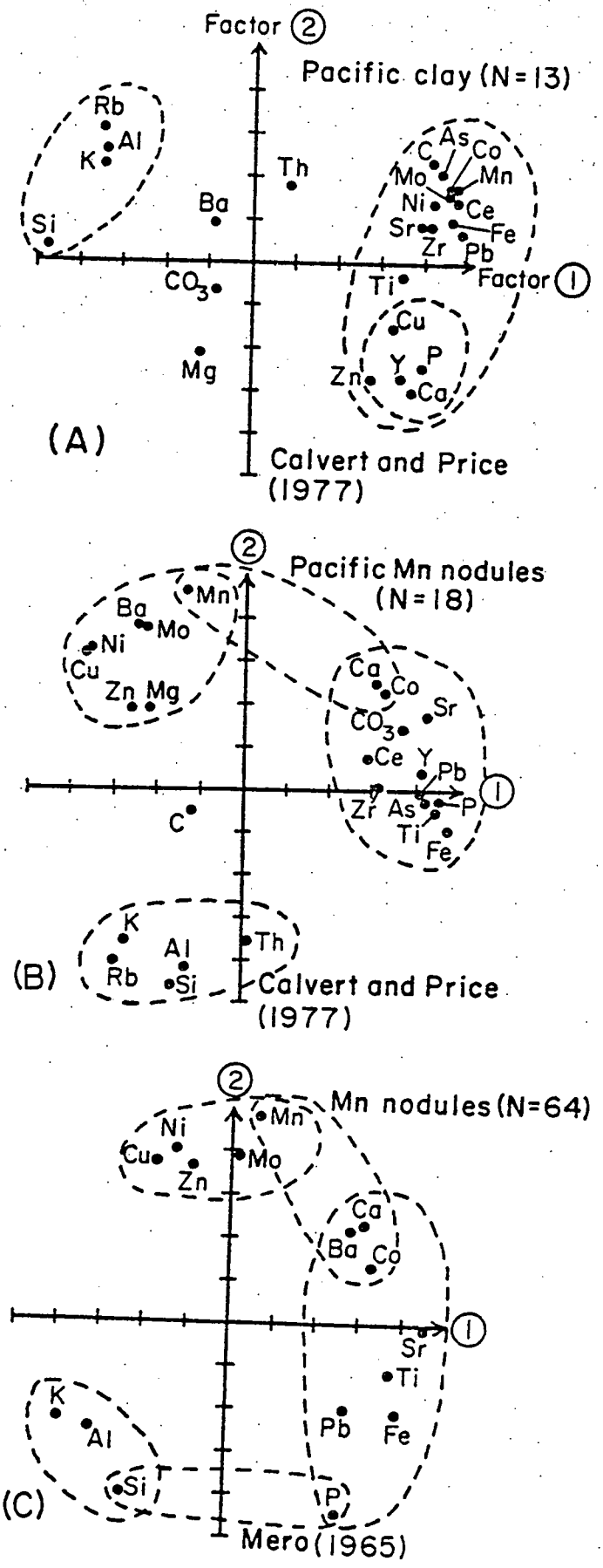

Fig. 2.2-4 The plots of the principal component factor 1 and factor 2 for A) Pacific clay by Calvert and Price, B) Pacific Mn-nodules by Calvert and Price, and C) Pacific Mn-nodules by Mero.

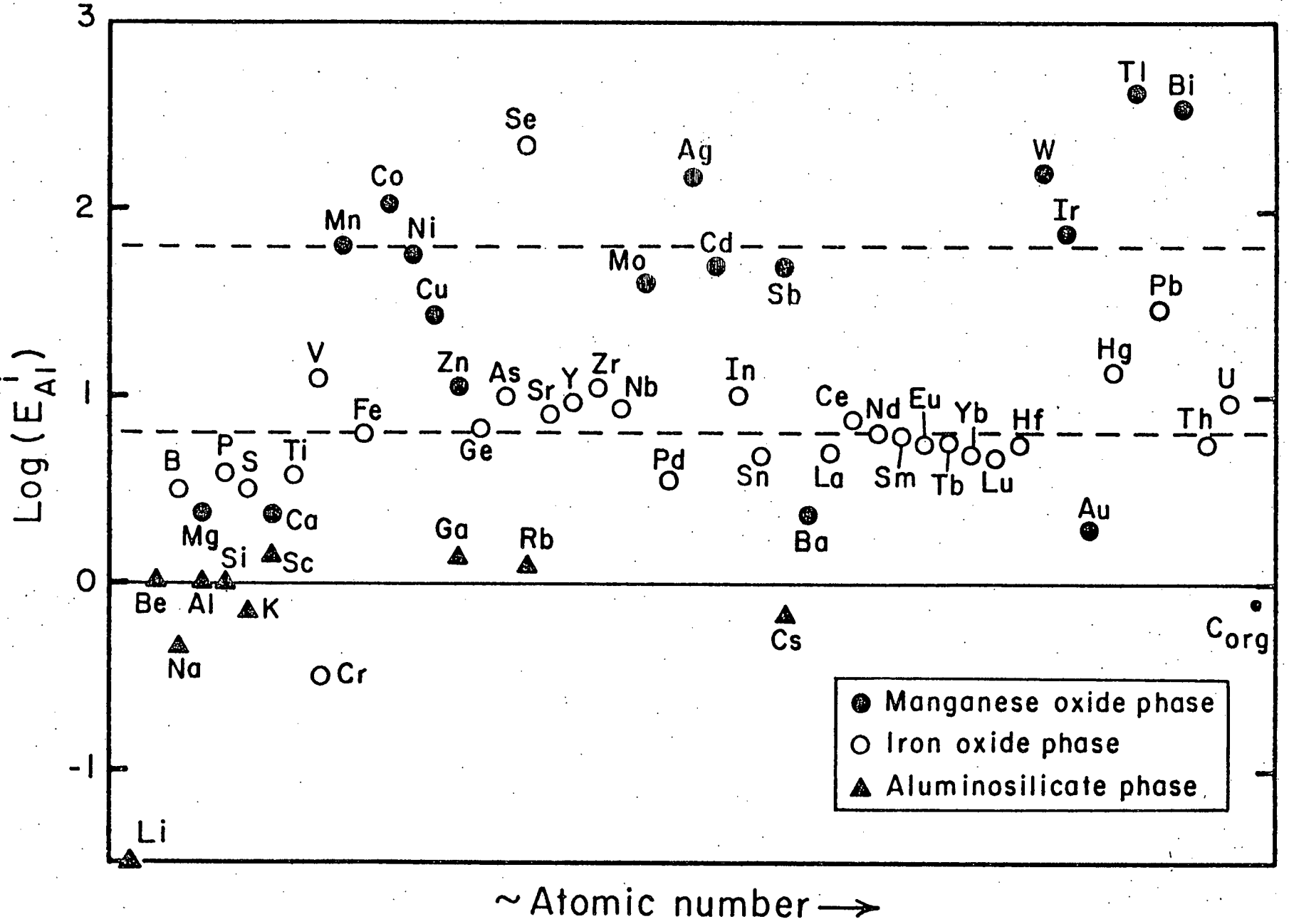

Fig. 2.2-5 The enrichment factors of various elements in Mn-nodules, as compared to oceanic pelagic clays.

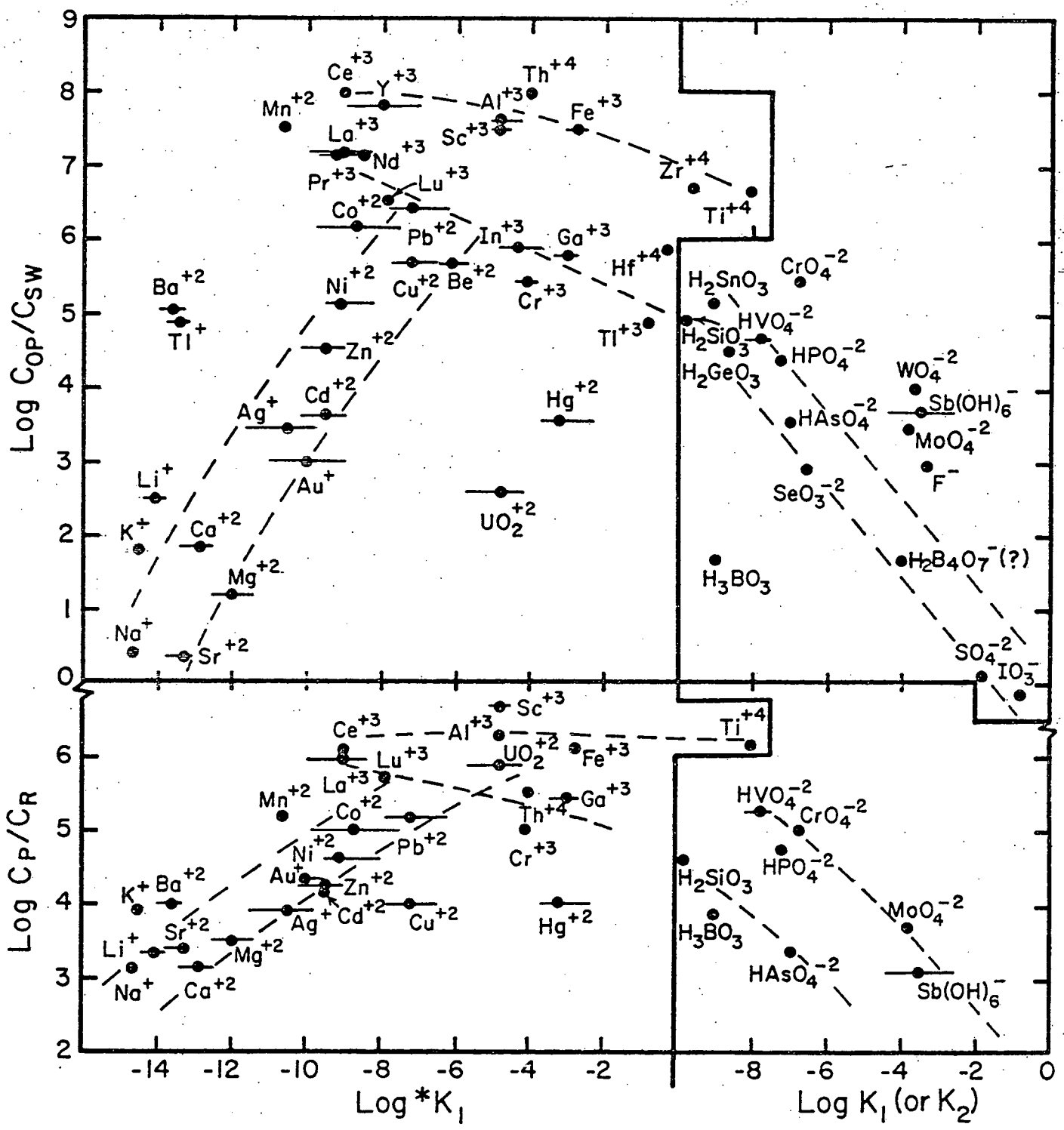

Fig. 2.2-6 The plots of log C_{op}/C_{sw} and log C_p/C_R vs. log $*K_1$ (the first hydrolysis constant) and log K_1 (the first dissociation constant of acids) or log K_2 (the second dissociation constant of acids). C_{op}, C_{sw}, C_p and C_R are concentrations (ppm/g) in oceanic pelagic clays, seawater, river-suspended particles and river water, respectively.

2.3 Concentrations, Size-Frequency Distributions and Sediment Trap Collections of SPM

In previous reports we have presented data on the distribution of suspended particulate matter (SPM) on samples taken throughout the water column. These ditributions have been interpreted in a qualitative way in near-surface samples in the context of measurements of chlorophyl a as an index of primary biological activity, and, in samples below the pycnocline, in the context of the distribution of surface sediments and of excess radon concentrations. In the relatively shallow waters of the shelf, the general relationships are that; a) there is a general decrease in SPM concentrations throughout the water column as a function of distance from shore and/or increasing water depth, but that this first-order decrease has superimposed on it a number of modifications related to biological productivity and sediment distributions; b) the positive relationship between SPM and chlorophyl a as a measure of biological productivity in surface waters is, to a first approximation, true, but patchiness in space and time primarily of productivity introduces very large scatter into the correlation; c) local pockets of fine-grained surface sediments (such as the Hudson Shelf Channel and the Mudhole) are sources of high concentrations of SPM in the water column by sediment resuspension; d) the plumes of near-bottom, high concentrations of SPM are related, to a first approximation, to the plumes of excess radon which also have as their source the local pockets of fine-grained sediment in an otherwise very sandy shelf.

We had hoped that as part of his thesis, Steve Carson would have had time to do some modeling of the near-bottom shelf water SPM distributions

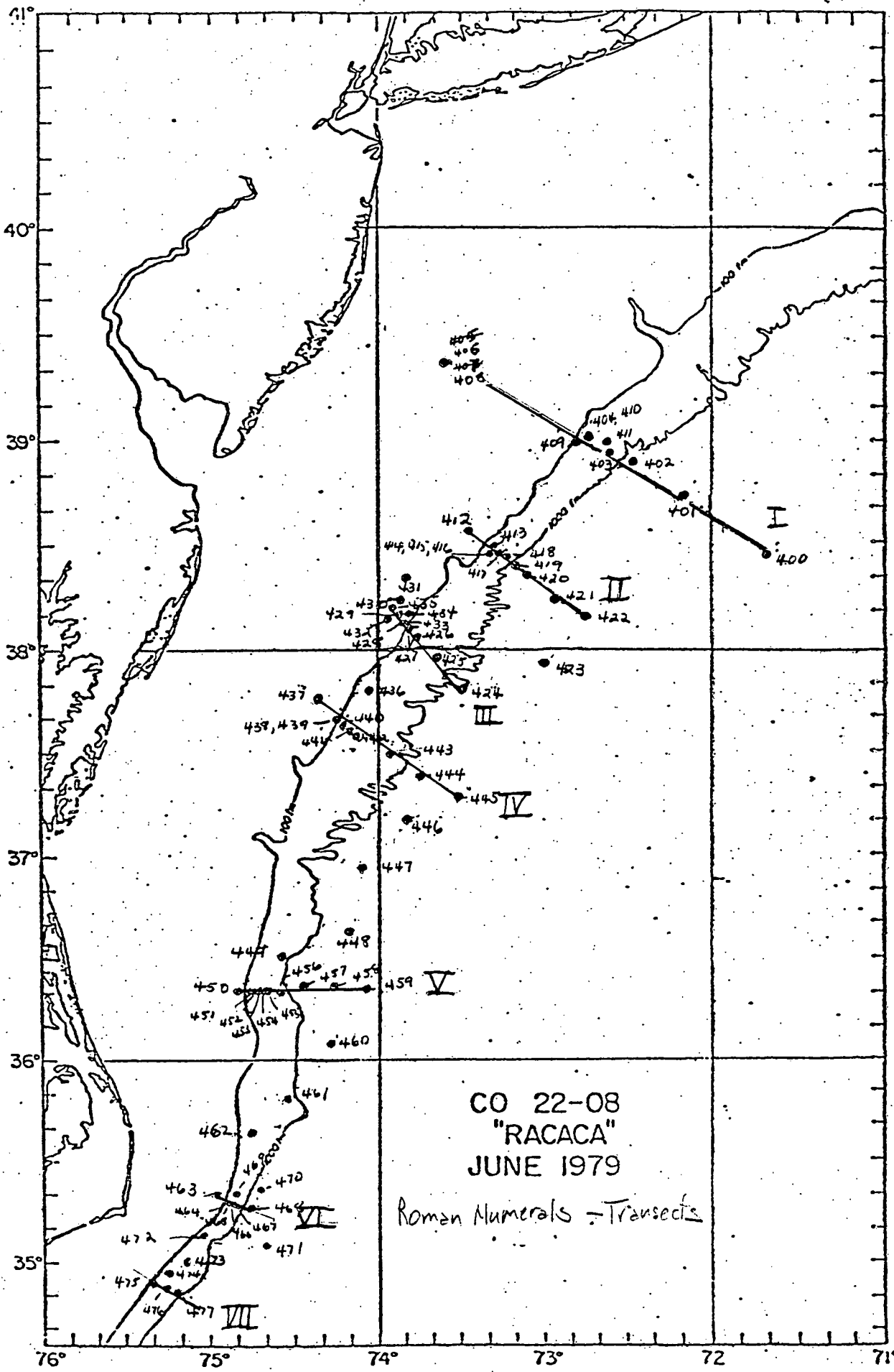

CO 22-08
"RACACA"
JUNE 1979

Roman Numerals = Transects

FC 22-08
Rx Stations

to yield model particle residence times using the radon, with its known "residence time" (half life), as an analogue. It is now apparent that this is an unrealistic hope in that Carson has more than enough to do in completing his thesis on the radon alone (see section 4.4). We hope to be able to interest a graduate student in this problem, but at present have no definite prospect.

2.3.1 SPM Concentrations; RACACA Cruise

In the slope waters beyond the shelf break most of our SPM concentrations data are on near bottom samples and the most interesting phenomenon we have reported in past was the apparent minimum in SPM concentration (and standing crop) at approximately the depth at which we found the minimum in excess radon (the low radon zone discussed in sections 4.4.5 and 4.1.3-I-IV). Admittedly we did not have a large number of data points on which to base this, but what data we had on four different cruises at different seasons suggested a decrease in SPM near-bottom concentration from the shelf break down to approximately 1000m followed by an increase in even deeper samples. We reported last year in preliminary fashion new data based on the results of the RACACA cruise in which seven transects from the shelf break to 2500-3000m water depth were made from Hudon Canyon to Hatteras. The locations of the transects are shown in figure 2.3-1 and the particle standing crops in $\mu g/cm^2$, integrated up to the top of each sample profile which was generally about 100m above bottom, are shown in figures 2.3-2 to -4. The values of the standing crop of SPM and of excess radon are plotted at the water depth of the bottom of the cast alongside a profile of the continental slope underlying the transect. It is obvious that there is no clear generalization one can make about these data in

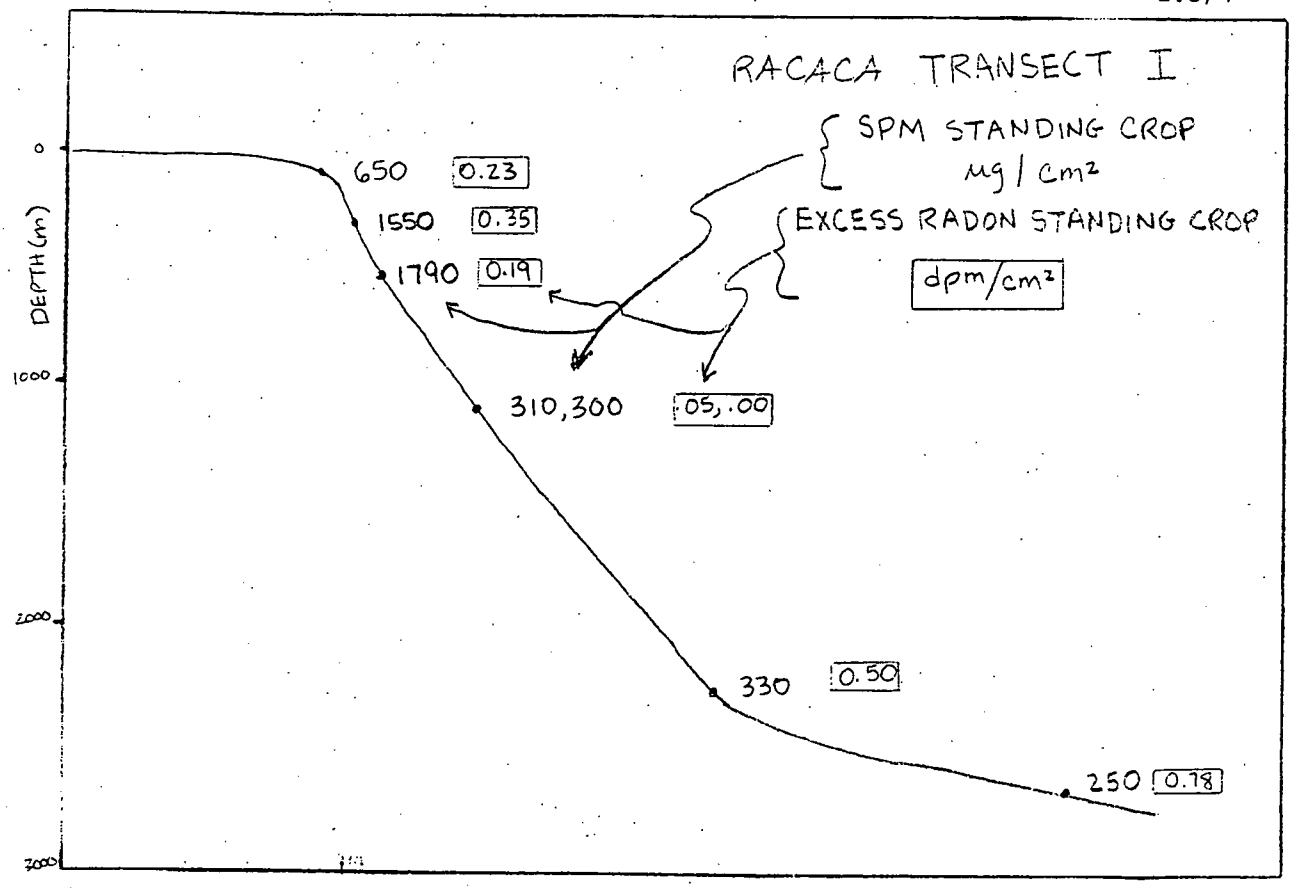
RACACA TRANSECT I
SPM STANDING CROP
µg / cm²
EXCESS RADON STANDING CROP
dpm/cm²
DEPTH (m)
0
1000
2000
3000
650 0.23
1550 0.35
1790 0.19
310,300 05, .00
330 0.50
250 0.78

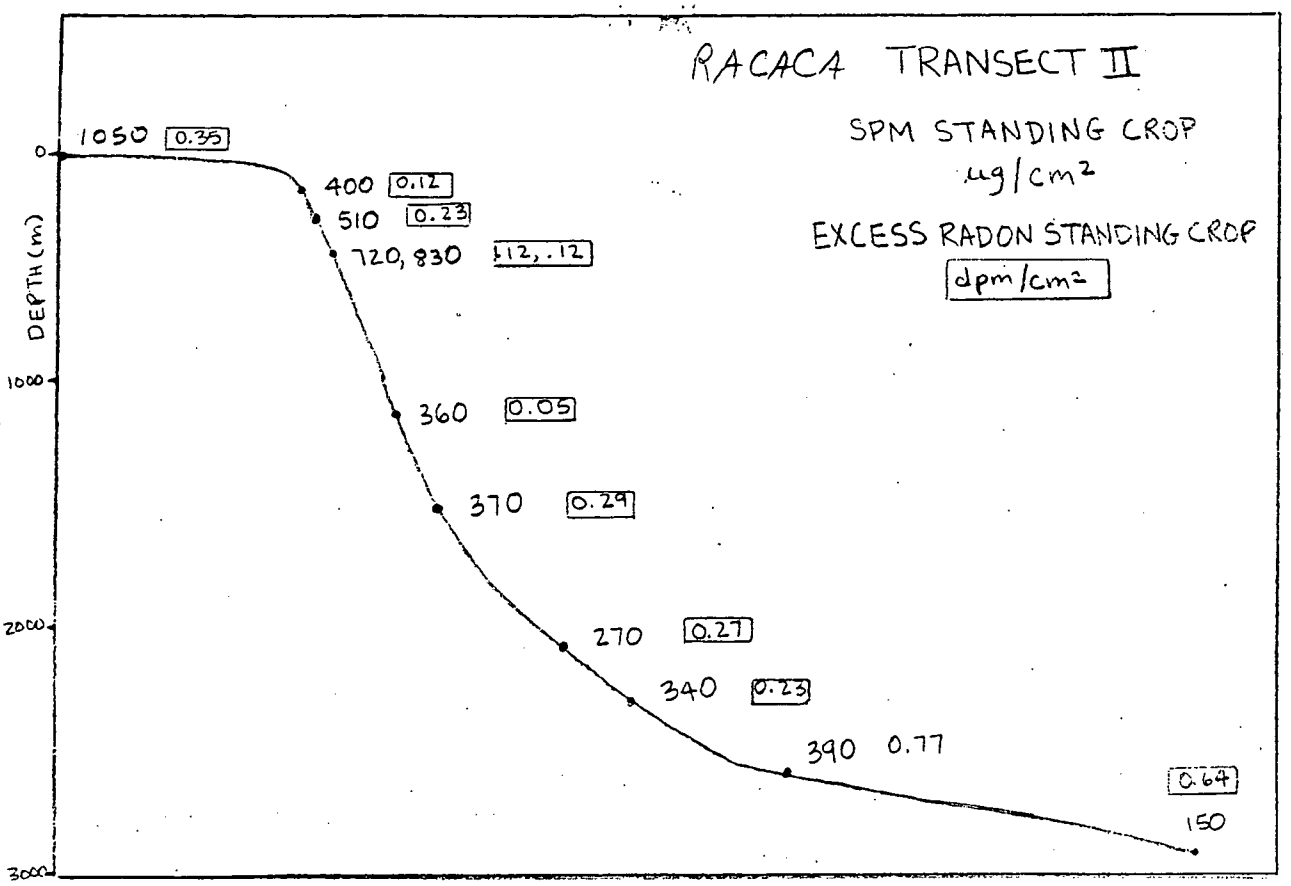
RACACA TRANSECT II
SPM STANDING CROP
µg/cm²
EXCESS RADON STANDING CROP
dpm/cm²
DEPTH (m)
0
1000
2000
3000
1050 0.35
400 0.12
510 0.23
720, 830 12, .12
360 0.05
370 0.29
270 0.27
340 0.23
390 0.77
0.64
150

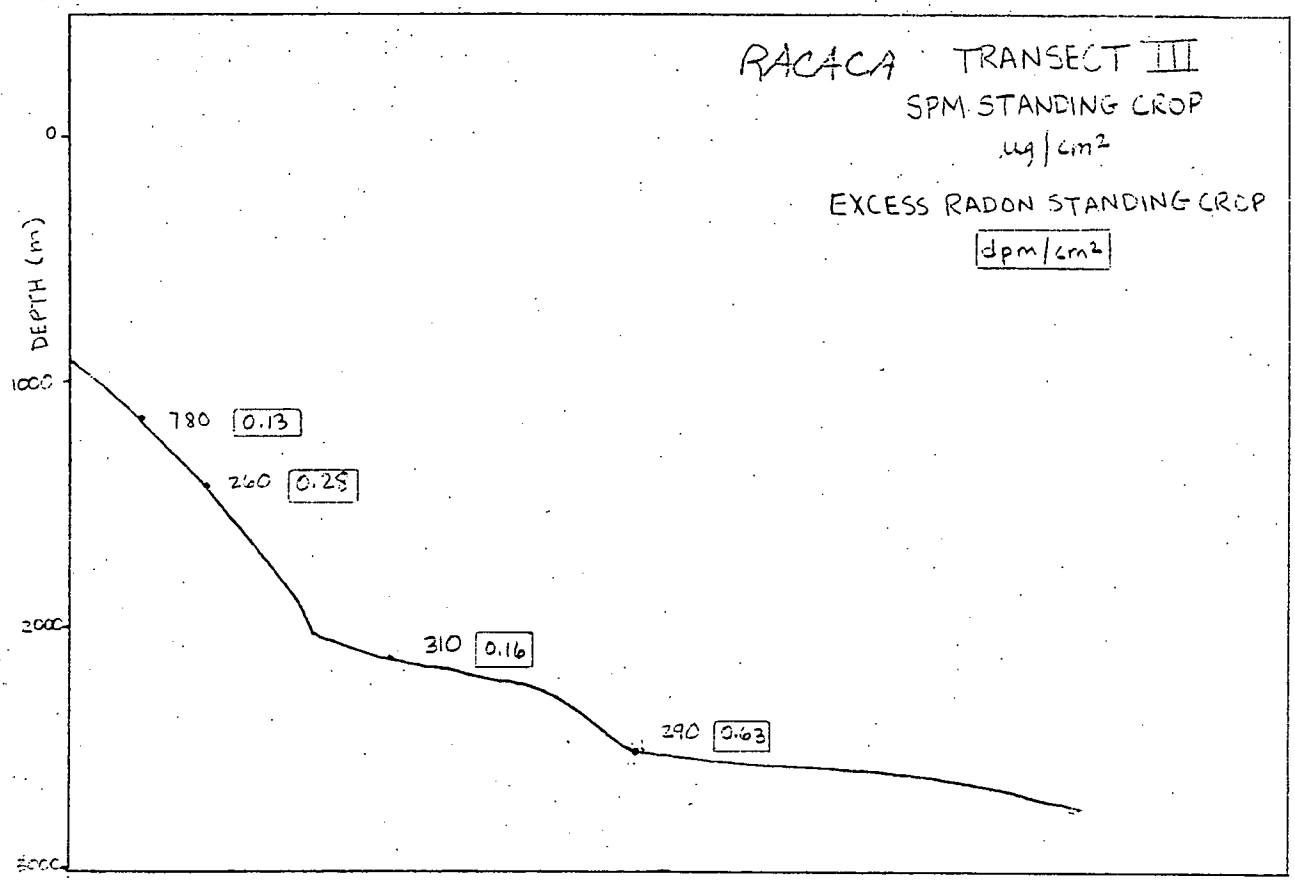
RACACA TRANSECT III
SPM STANDING CROP
μg/cm²
EXCESS RADON STANDING CROP
dpm/cm²
DEPTH (m)
0
1000
2000
780 0.13
260 0.25
310 0.16
290 0.63

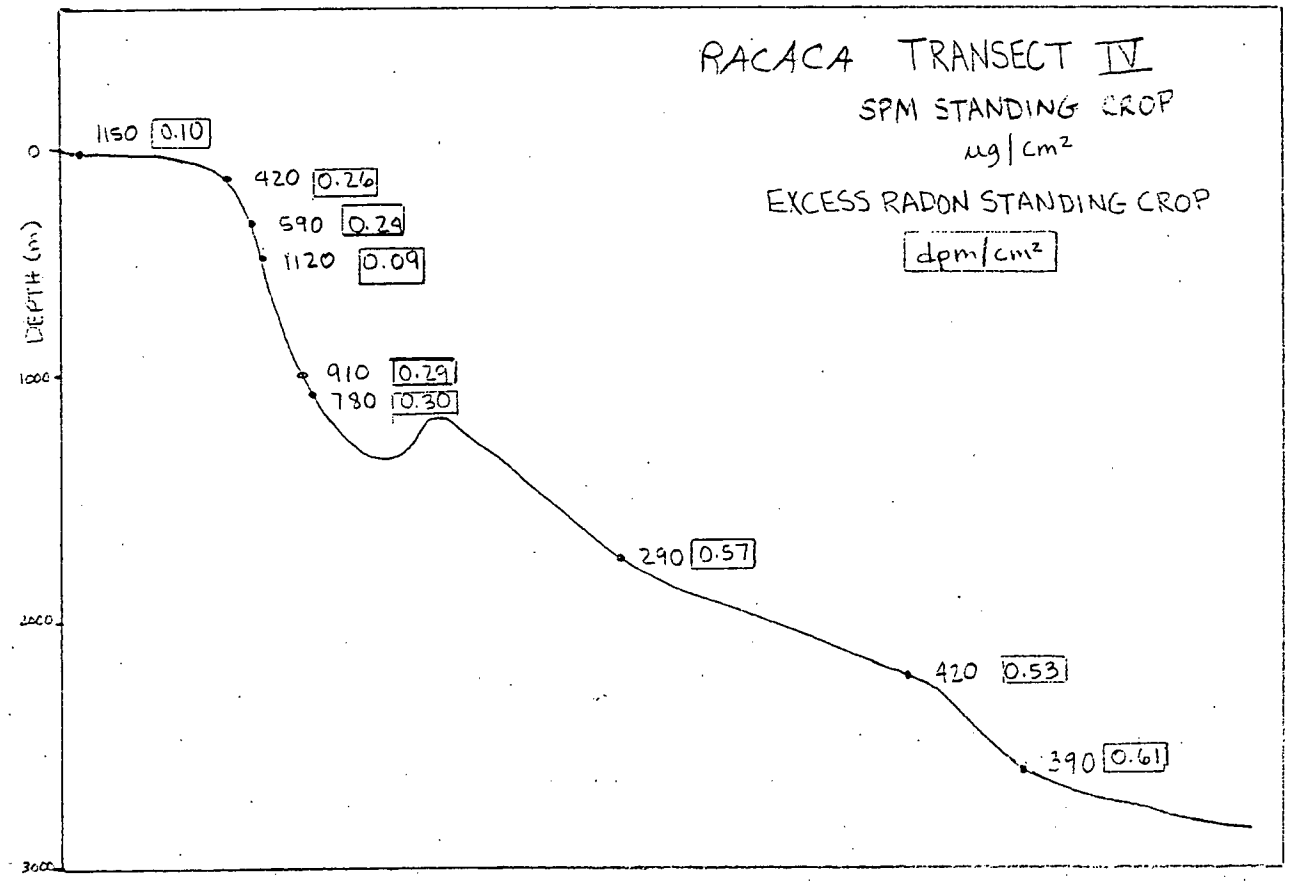
RACACA TRANSECT IV
SPM STANDING CROP
μg/cm²
EXCESS RADON STANDING CROP
dpm/cm²
DEPTH (m)
0
1000
2000
3000
1150 0.10
420 0.26
590 0.29
1120 0.09
910 0.29
780 0.30
290 0.57
420 0.53
390 0.61

terms of a particle minimum with respect to the radon or any other function of depth. There does, however, appear to be a general increase in the standing crops in deep water (say, below 2,000m) going from north (transect I near Hudson Canyon) to south (transect VI off Hatteras).

2.3.2 Size Frequency Distributions, RACACA Cruise

Each of the water samples analyzed for SPM concentration was also analyzed for size frequency distribution of SPM by Dr. Jean-Claude Brun-Cottan of the University de Pierre et Marie Curie (Paris) and of the Centre Nationale de Recherche Scientifique laboratory at Gif sur Yvette, France. Dr. Brun-Cottan spent three months in our laboratory at Lamont last year under DOE support (travel and living expenses; not salary which was paid by CNRS) during which time he also participated in the RACACA cruise. He used his own modified Coulter Counter in which the output of the basic Coulter Counter probe is divided into more than 200 channels (cf. the standard Coulter Counter's 16 channels) and stored on punched tape for subsequent reduction by computer. By the end of the cruise Dr. Brun-Cottan had accumulated size frequency distribution data on more water samples than on all the numerous previous cruises on which he had used his equipment. He brought his data back to Paris where he has been working on it under CNRS support.

Besides the characterization of SPM in the oceans, the important reason one wants size frequency distribution data is as a means of estimating the settling rate and, hence, the flux, of particulate matter through the oceans. It is the fluxes of particles which we want to know to quantify their obviously important role in the transport of pollutants in the

marine environment. Most size frequency data in the literature has been described in terms of an exponential distribution, often called a Jungian distribution after Junge (1963) who described such a function in airborne particulate matter. Recently the group led by Roger Chesselet at CFR/CNRS/CEA (Gif sur Yvette) began to investigate the size frequency distributions of individual particle types by means of scanning electron microscopy combined with electron microprobe (SEM-EMP) techniques. Based primarily on studies of suspended aluminosilicate particles from many places in the world oceans, they concluded that the distributions are best described by a log normal distribution (which yields a straight line on log vs. probability paper), rather than an exponential distribution (which yields a straight line on log vs. log paper) (Lambert et al., in press). One great advantage of this observation is that it greatly facilitates flux calculations because mean parameters can be used to describe the population of particles. And from the flux calculations can be derived mean settling velocities and residence times which may be compared with other estimates such as those based on our own radioisotope measurements (section 2.2).

After returning to Paris with the RACACA data last year, Dr. Brun-Cottan undertook their reduction using the exponential model. As the SEM-EMP data in their lab began to suggest the log-normal model as more appropriate, he had to revise his computer programs and restart the reduction of our data. He has sent several examples of the first output on samples from our RACACA ship station 263 and these are shown in Figure 2.3-5. It is premature to comment in any detail on the few data in hand,

marine environment. Most size frequency data in the literature has been described in terms of an exponential distribution, often called a Jungian distribution after Junge (1963) who described such a function in airborne particulate matter. Recently the group led by Roger Chesselet at CFR/CNRS/CEA (Gif sur Yvette) began to investigate the size frequency distributions of individual particle types by means of scanning electron microscopy combined with electron microprobe (SEM-EMP) techniques. Based primarily on studies of suspended aluminosilicate particles from many places in the world oceans, they concluded that the distributions are best described by a log normal distribution (which yields a straight line on log vs. probability paper), rather than an exponential distribution (which yields a straight line on log vs. log paper) (Lambert et al., in press). One great advantage of this observation is that it greatly facilitates flux calculations because mean parameters can be used to describe the population of particles. And from the flux calculations can be derived mean settling velocities and residence times which may be compared with other estimates such as those based on our own radioisotope measurements (section 2.2).

After returning to Paris with the RACACA data last year, Dr. Brun-Cottan undertook their reduction using the exponential model. As the SEM-EMP data in their lab began to suggest the log-normal model as more appropriate, he had to revise his computer programs and restart the reduction of our data. He has sent several examples of the first output on samples from our RACACA ship station 263 and these are shown in Figure 2.3-5. It is premature to comment in any detail on the few data in hand,

marine environment. Most size frequency data in the literature has been described in terms of an exponential distribution, often called a Jungian distribution after Junge (1963) who described such a function in airborne particulate matter. Recently the group led by Roger Chesselet at CFR/CNRS/CEA (Gif sur Yvette) began to investigate the size frequency distributions of individual particle types by means of scanning electron microscopy combined with electron microprobe (SEM-EMP) techniques. Based primarily on studies of suspended aluminosilicate particles from many places in the world oceans, they concluded that the distributions are best described by a log normal distribution (which yields a straight line on log vs. probability paper), rather than an exponential distribution (which yields a straight line on log vs. log paper) (Lambert et al., in press). One great advantage of this observation is that it greatly facilitates flux calculations because mean parameters can be used to describe the population of particles. And from the flux calculations can be derived mean settling velocities and residence times which may be compared with other estimates such as those based on our own radioisotope measurements (section 2.2).

After returning to Paris with the RACACA data last year, Dr. Brun-Cottan undertook their reduction using the exponential model. As the SEM-EMP data in their lab began to suggest the log-normal model as more appropriate, he had to revise his computer programs and restart the reduction of our data. He has sent several examples of the first output on samples from our RACACA ship station 263 and these are shown in Figure 2.3-5. It is premature to comment in any detail on the few data in hand,

marine environment. Most size frequency data in the literature has been described in terms of an exponential distribution, often called a Jungian distribution after Junge (1963) who described such a function in airborne particulate matter. Recently the group led by Roger Chesselet at CFR/CNRS/CEA (Gif sur Yvette) began to investigate the size frequency distributions of individual particle types by means of scanning electron microscopy combined with electron microprobe (SEM-EMP) techniques. Based primarily on studies of suspended aluminosilicate particles from many places in the world oceans, they concluded that the distributions are best described by a log normal distribution (which yields a straight line on log vs. probability paper), rather than an exponential distribution (which yields a straight line on log vs. log paper) (Lambert et al., in press). One great advantage of this observation is that it greatly facilitates flux calculations because mean parameters can be used to describe the population of particles. And from the flux calculations can be derived mean settling velocities and residence times which may be compared with other estimates such as those based on our own radioisotope measurements (section 2.2).

After returning to Paris with the RACACA data last year, Dr. Brun-Cottan undertook their reduction using the exponential model. As the SEM-EMP data in their lab began to suggest the log-normal model as more appropriate, he had to revise his computer programs and restart the reduction of our data. He has sent several examples of the first output on samples from our RACACA ship station 263 and these are shown in Figure 2.3-5. It is premature to comment in any detail on the few data in hand,

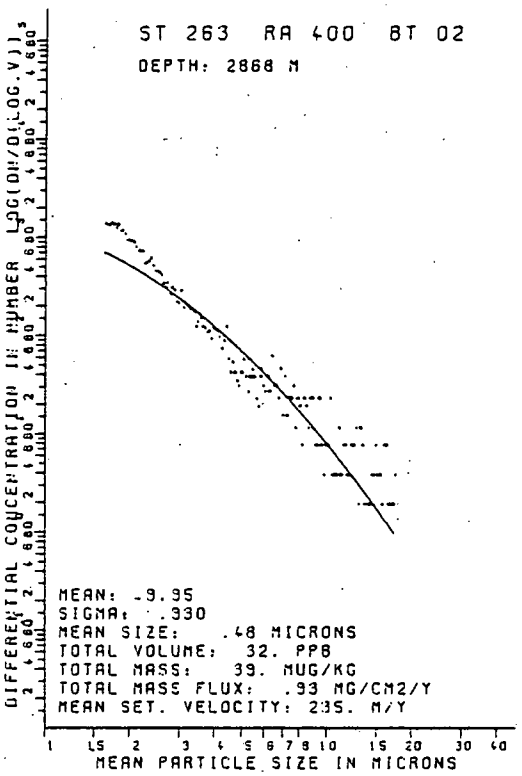

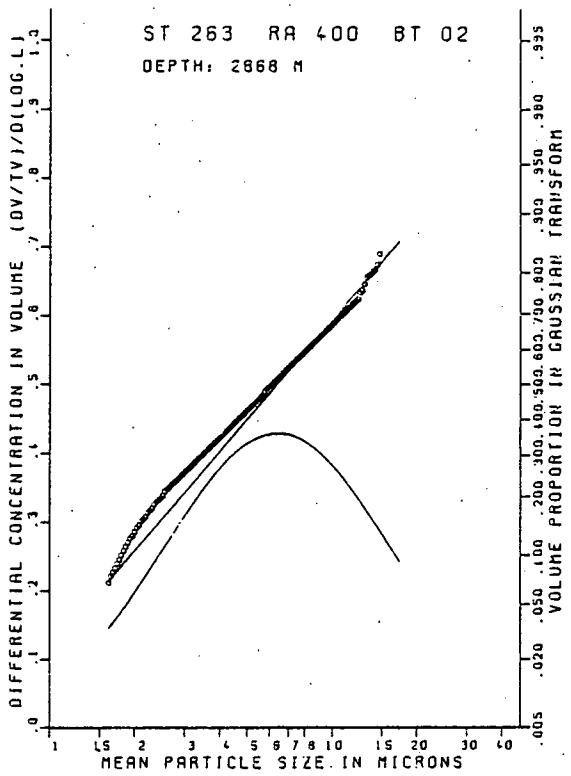

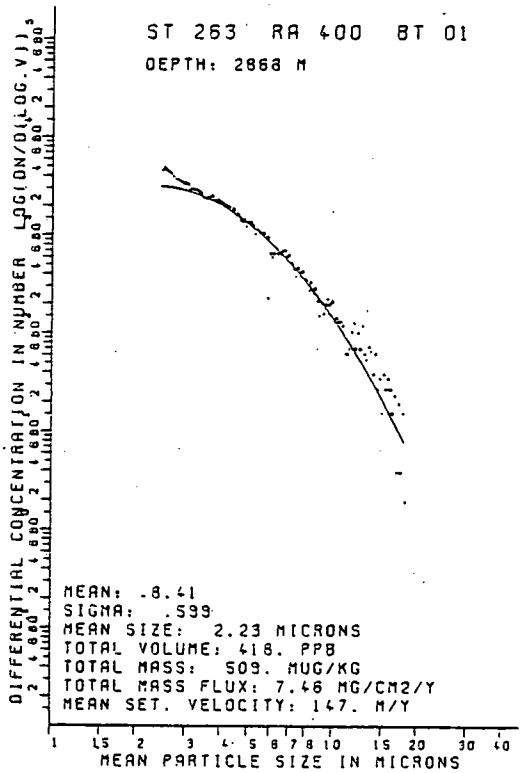

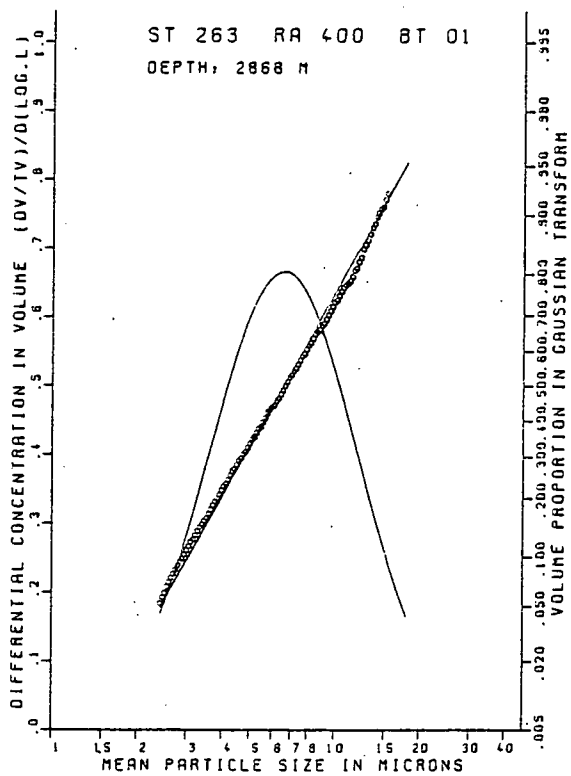

Size frequency distributions of SPM in two samples from Ship Stn 263, RACACA cruise (June 1977). Bottle 1 (BT01) was taken 7 mab and Bottle 2 (BT02) 13 mab. The distribution and mean parameters are significantly different for the two samples.

but several points can be made. First, the right-hand plot of each of the two samples shows the data points plotted in log-normal coordinates and the line through the points is the best (least squares) log-normal fit. The curved line is the log-normal curve in linear-log coordinates. In the corner of the left-hand plot are the parameters derived from the data. It is interesting that the parameters for most other samples at this station resemble those of Bottle 2 (which was tripped 13m above bottom) and they are all significantly different from those which describe Bottle 1 (7 mab). It will be interesting to see the degree to which the size frequency distributions within other profiles, stations and transects differ from each other. For example, is the apparent southward increase in deep (greater than 2000m) water SPM standing crops matched by a regional change in the size frequency distribution? These and other questions about the SPM data will be explored when Dr. Brun-Cottan spends several weeks in our laboratory this November.

2.3.3 Sediment Trap Samples; Low Radon Zone

Since it is the fluxes of SPM which are the crux of a quantitative understanding of the rates of dispersal and removal of particle-associated pollutants, we desire: a) independent methods of determining fluxes; b) methods which cover the entire range of particle sizes and hence fluxes; and c) methods which provide time averaged flux measurements as well as the instantaneous estimates provided by bottle samples. Sediment traps would appear to provide these benefits, but, like all sampling methods, there are inadequacies in trap samples. The first, and most important, of these is whether or not sediment traps accurately measure the vertical flux of particulate matter in the marine environment. The

3.0 Processes Associated with Sediments As Sinks for Radionuclides and Other Pollutants

Because many highly reactive pollutants are associated with suspended particulate matter which will eventually settle to the bottom, what subsequently happens to this material must concern us since arrival at the bottom does not necessarily mean simple burial and removal from the system. To what extent does sediment get resuspended from the bottom versus getting mixed downward with older sediments by benthic faunal activities? What are the rates of the net sediment accumulation and sediment mixing (bioturbation), and how do they vary with different geographic locations and sedimentation regimes? How do they affect the accumulation of pollutants? In seeking means to answer these questions, we have successfully developed a two-layer sedimentation-mixing model to fit simultaneously the observed $^{234}Th_{ex}$, $^{210}Pb_{ex}$ and $^{239,240}Pu$ profiles in the New York Bight sediment cores. The model yields the net sedimentation rate and the sediment-mixing coefficients in the top and bottom layers. The details of our numerical model are given in Appendix 4. The highlights of the modeling results are:

1) The fine-grained deposit on the southern New England shelf (nicknamed "mud hole" or "mud patch") represents a modern sediment accumulation, with a sedimentation rate of between 0.01 g/cm^2yr and 0.14 g/cm^2yr. The sediment mixing coefficients range from 4 to 32 cm^2/yr in the surface mixed layer (5 to 10 cm thick) and from 0.3 to 2.5 cm^2/yr in the layer below (25 to 40 cm thick). These results are very similar to those in the Long Island Sound sediments (Benninger et al., 1979).

2. The continuous resuspension of sediment particles from the bottom by benthic faunal activities (which adsorb $^{239,240}Pu$ from the water column) and sediment mixing by bioturbation (which effectively mixes and dilutes the polluted surface sediments with less contaminated sediments below) can explain the observed high sedimentary inventory and deep penetration of $^{239,240}Pu$ in the coastal marine sediments (Fig. 3.0-1). The net sediment accumulation rate alone is too low to explain the above observations.

3. Since the sandy shelf sediments outside the "mud hole" are also important sinks for ^{210}Pb (Bothner, personal communication), we expect that appreciable amounts of $^{239,240}Pu$ and other particle-reactive pollutants should have been deposited in the sandy sediments. We shall emphasize the core analysis from the sandy areas.

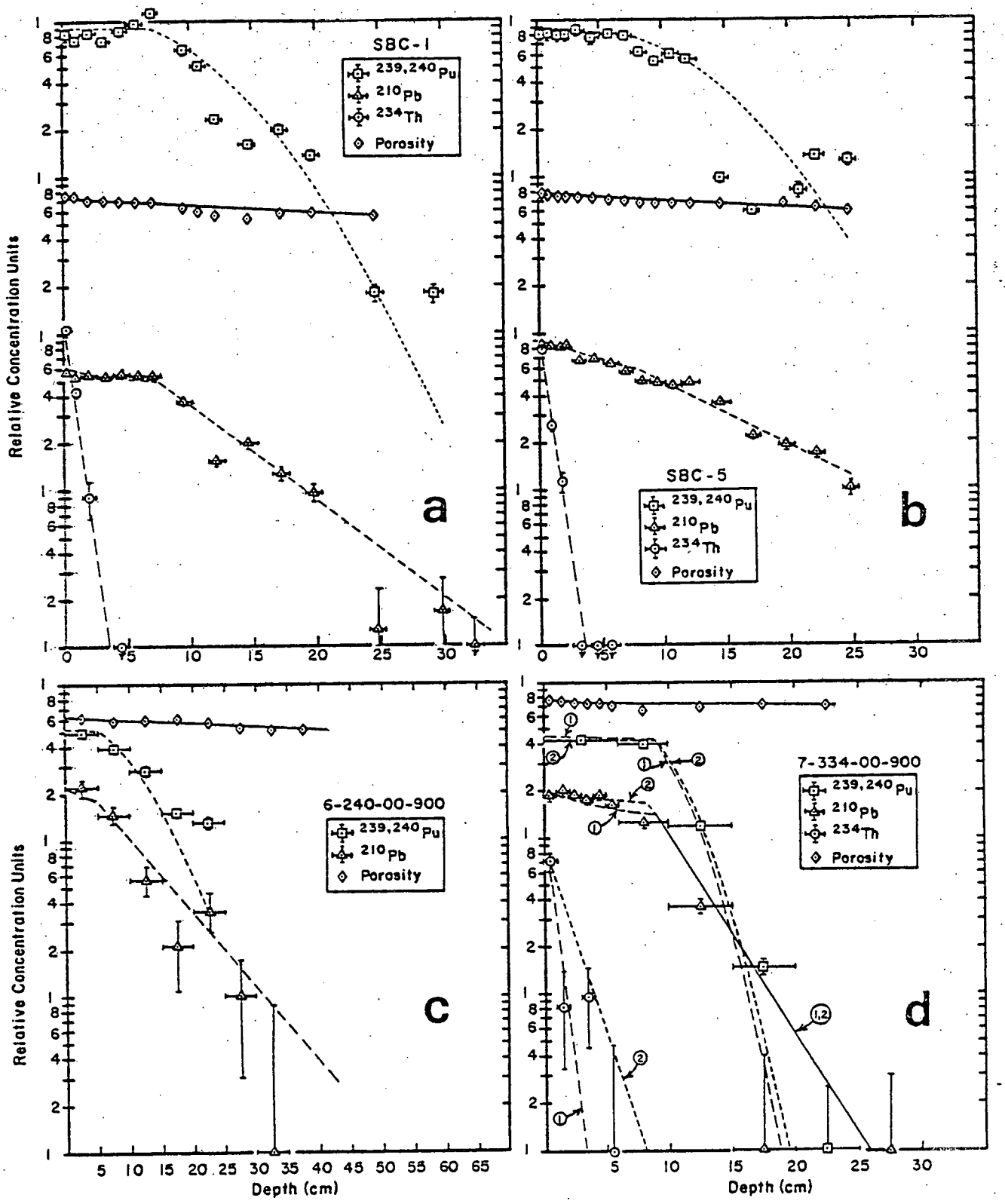

Fig. 3.0-1 Sediment analyses for $^{234}Th_{xs}$, $^{210}Pb_{xs}$, $^{239,240}Pu$ (all in dpm/g) and proosity (cm^3 water/cm^3 wet sediments). Best fits from the numerical mixing and sedimentation model are shown for comparison.

4.0 SPREADING OF WATER CHARACTERISTICS AND SPECIES IN SOLUTION

4.1 Hydrographic and Physical Mixing Processes

4.1.1 INTRODUCTION

In last year's report (August 1979) a comprehensive overview was given of the 1978-1979 data analysis being conducted with the New York Bight hydrographic data set. The focus of the research deals with the seasonal evolution of thermohaline stratification and water types of the shelf and slope region, and the role of shelf-slope exchange in this evolution. The initial work is basically descriptive in nature, though simple "conceptual" models are included. The results of the work will provide a foundation for more quantitative mixing models for the New York Bight.

Since the August 1979 Report two components of the study have been completed:

1) Gordon, A.L. and F. Aikman III, (in press). The Middle Atlantic Bight Pycnocline Salinity Maximum. Limn. and Oceanogr.

A slope to shelf water salt flux of almost 50% of that needed to balance the annual river(fresh) water input to the Middle Atlantic Bight is computed, and conveyed via an intrusive salinity maximum in the upper portion of the seasonal pycnocline.

2) Malone, T., R. Houghton and A. Gordon, (submitted). Vertical Exchange of Properties Under Stratified Conditions in the New York Bight. Limn. and Oceanogr.

Estimates of an effective vertical eddy diffusion coefficient, K_z, through the summer thermocline are based on the flux of heat from the cold pool, the diffusion of oxygen from the O_2 maximum layer, and the flux of nutrients into the euphotic zone.

In addition, progress has been made in a number of other areas:

3) Frontal structure and cross shelf mixing

Alongshore advection and structure, and intrusions detached from their source make it difficult to apply a strictly two

dimensional mixing model to the shelf/slope regime, however consistent features such as benthic intrusions, the front, the cold pool, and the pycnocline salinity maximum, and assumptions of alongshore constancy make the application of a two dimensional model viable.

4) The cold pool

The origin of this most distinctive and ubiquitous feature is still a matter of controversy (see the section on oxygen 18), yet the hydrographic data, while limited in space and time, indicates it is predominantly a locally formed remnant of the wintertime, vertically well mixed, shelf bottom water.

5) Warm core eddies

We have observations of eddies interacting with slope and shelf waters and discuss their role in the exchange of heat and salt between shelf, slope and Sargasso Sea waters.

6) The temperature-oxygen relationship

The T/O_2 relationship is used to evaluate oxygen utilization in the cold pool and a supersaturated layer in the summer thermocline.

7) River runoff and pycnocline development

A hypothesis is presented in which river runoff is thought to control the springtime haline stratification of the shelf surface water, thus determining the intensity and depth of the summer pycnocline over the shelf, and the degree to which the cold pool is isolated from surface heating. A reversal of the intermediate depth lateral density gradient, induced by the mismatch of the shelf and slope pycnoclines, may force a fold in the shelf/slope front and an intrusion of slope water into the shelf pycnocline(the pycnocline S-max).

8) RACACA cruise results

The seven transects of this June,1979 cruise provide a quasi-synoptic look at the outer shelf and slope water stratification between the Hudson Canyon and Cape Hatteras, including longshore variations of slope water thermohaline characteristics and the benthic hydrographic structure over the slope in the low radon zone.

The following is an update of the August 1979 Report using excerps from that report for background.

4.1.2 THE DATA SET

Preliminary processing of the CTD data is complete, and listings and plots have been distributed to the Lamont DOE investigators. Distribution of the CTD stations in the New York Bight from 1974-79 are shown in Fig. 4.1-1A. The complete track of the 1979 RACACA cruise is shown in Fig. 4.1-1b.

The CTD-O_2 hydrographic data has not yet been officially released. This would be done when the data is run through the full data processing system presently deing developed for handling our Antarctic data set. This system is essentially the same as the one developed at Woods Hole Oceanographic Institution. It is likely that it will be ready for our New York Bight data later in 1980. In any case, the large signals encountered in the New York Bight permit the first level of data processing and display (the distributed data reports) to meet nearly all our needs. The study of the finest scale of vertical structure (less than 1 meter) would benefit from the next level processing.

In addition to the DOE CTD data set we have been able to use the SWIG (Slope Water Intrusions Galore) data set collected south of Cape Cod in Spring and Summer 1979 on three separate cruises. This NSF supported joint Physical/Biological study of the shelf/slope frontal region and the small scale processes and structure associated with this region can often serve to complement our DOE work.

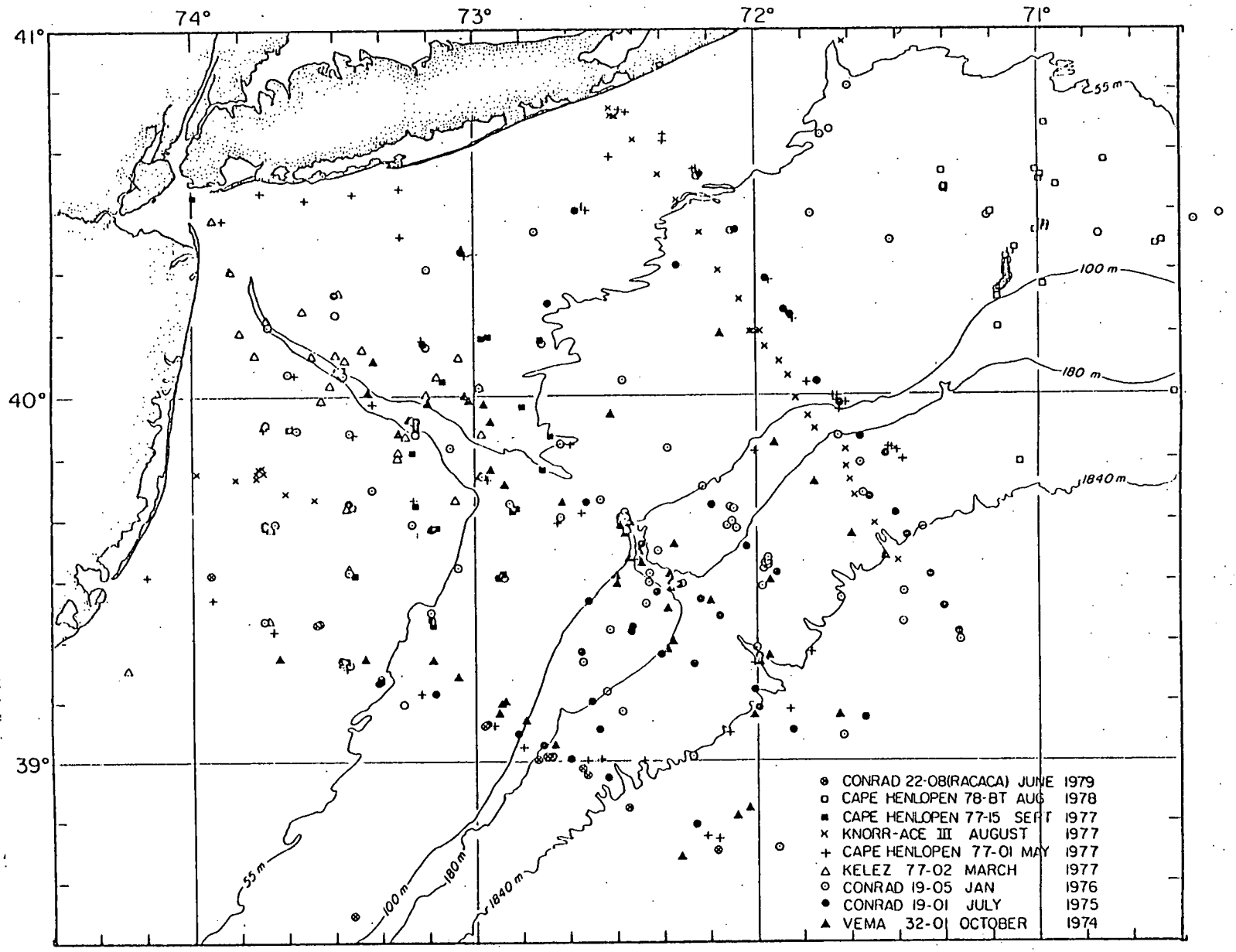
74°
73°
72°
71°
41°
40°
39°
55 m
100 m
180 m
1840 m
CONRAD 22-08(RACACA) JUNE 1979
CAPE HENLOPEN 78-BT AUG 1978
CAPE HENLOPEN 77-15 SEPT 1977
KNORR-ACE III AUGUST 1977
CAPE HENLOPEN 77-01 MAY 1977
KELEZ 77-02 MARCH 1977
CONRAD 19-05 JAN 1976
CONRAD 19-01 JULY 1975
VEMA 32-01 OCTOBER 1974

Fig. 4.1-1a

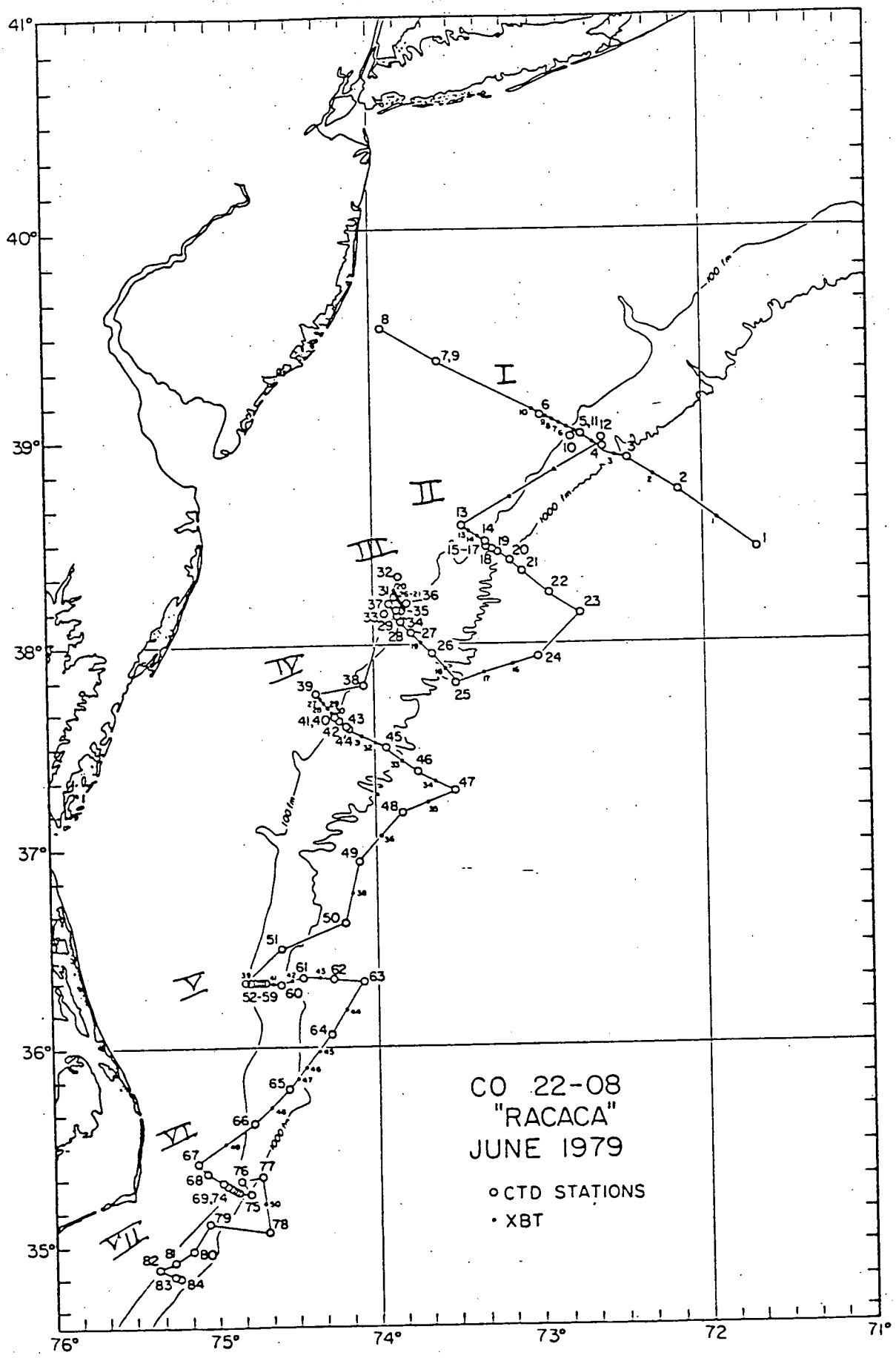
41°
40°
39°
38°
37°
36°
35°
76°
75°
74°
73°
72
71°
I
II
III
IV
V
VI
VII
100 fm
1000 fm
CO 22-08
"RACACA"
JUNE 1979
o CTD STATIONS
• XBT

Fig. 4.1-1b

The Historical NODC Hydrographic Serial Cast data for the Middle Atlantic Bight is now in hand, up to date and in such a format that it is easily used. This data goes back to the 1930's and supplemented with the USGS historical river outflow data and the National Climate Center's historical meteorologic data provides a solid background from which to view our seasonal data.

4.1.3 DATA ANALYSIS

A. New York Bight Stratification

This section discusses the progress made in the DOE supported study of New York Bight thermohaline stratification. The overall structure of the approach is to describe the seasonal evolution of the temperature-salinity relation and define the key processes responsible for this development. The extent of the seasonal variation in the water column can be quickly seen from comparison of the temperature, salinity, and

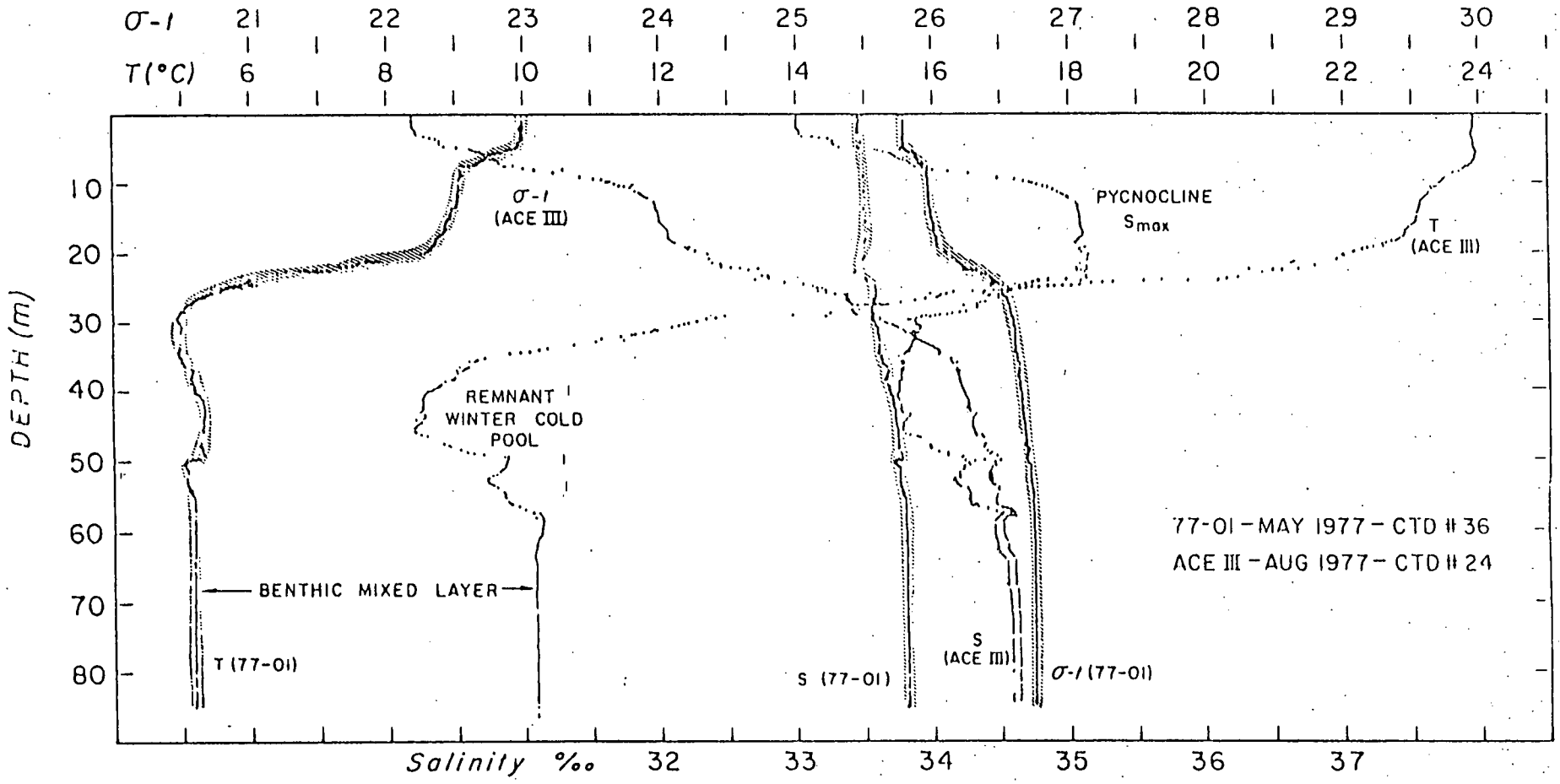

Characteristic profiles: May, weakly stratified (shaded); August, fully stratified.

Fig. 4.1-2

density profiles of May and August 1977 (Fig. 4.1-2) over the Long Island outer shelf. Since the characteristics are discussed below, as the seasonal development of the T-S relation is developed, the water column structure is not described at this point.

B. Seasonal evolution of Stratification - T/S relation

The T/S relation of the CTD and STD data clearly show the seasonal nature of the thermohaline stratification. The simple "seven" shape of the winter T/S relation is preserved to some extent in the warmer months as the cloud of T/S points migrates to warmer temperatures, establishing the summer T/S pattern. A schematic of the large scale water mass distribution is given in Figure 4.1-3 as a guide.

In recognition of the strong seasonal signal, the T/S relations will be discussed in a monthly chronological order rather than in the chronological order in which the data were obtained. Since interannual variations are large, care must be taken in not "overgeneralizing" the results. Using the historical data as a guide, that problem can be minimized.

January 1976 - (Winter Structure)

The January 1976 T/S relation (Fig. 4.1-4a) and historical January data (Fig. 4.1-4b) represents the winter situation, though on the average the full extent of the winter is expected in February. We note however that February 1976 was an anomalously warm month, which induced early stratification, and which may have been responsible for the anoxic condition developed

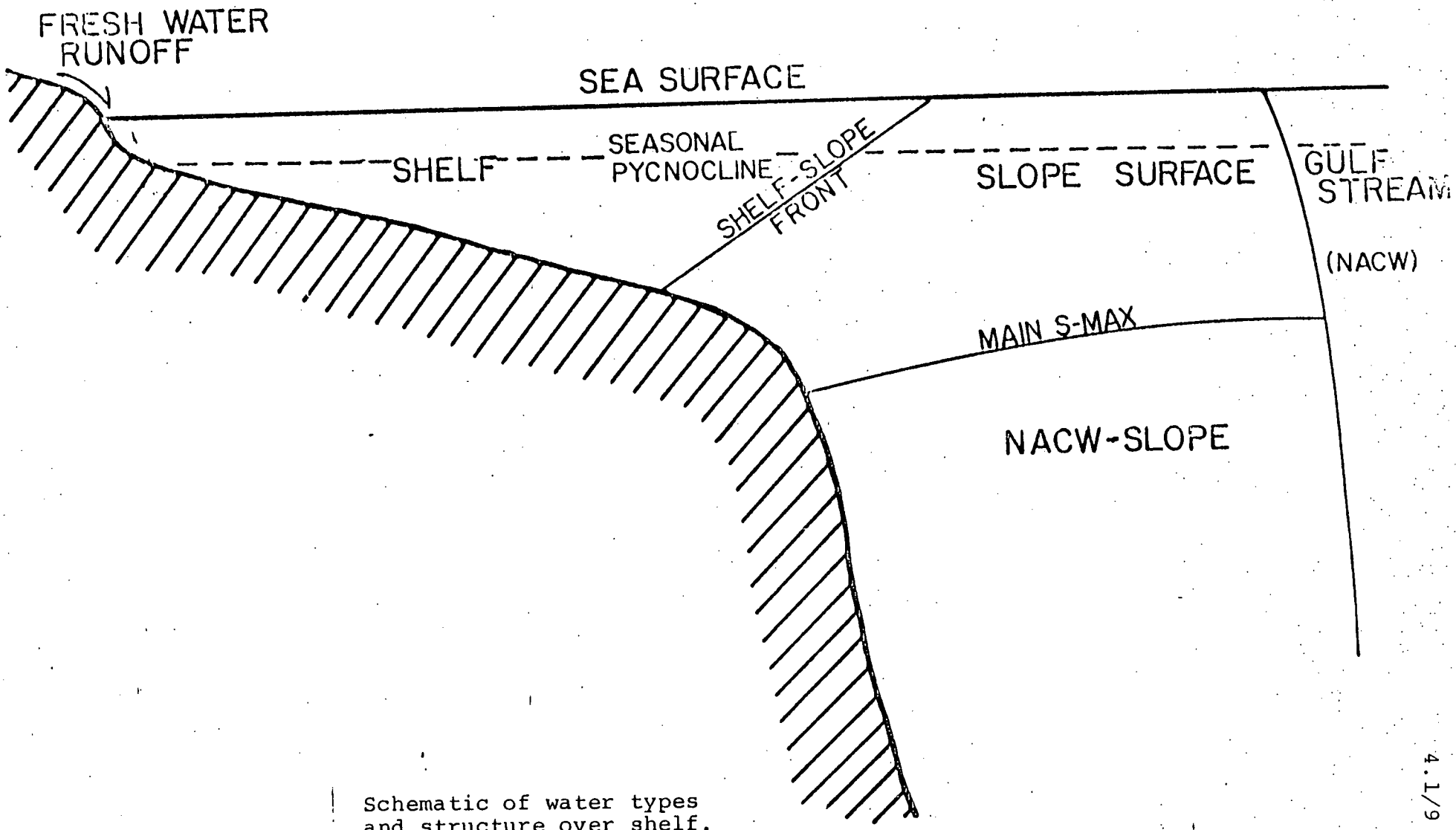

Schematic of water types and structure over shelf.

Fig. 4.1-3

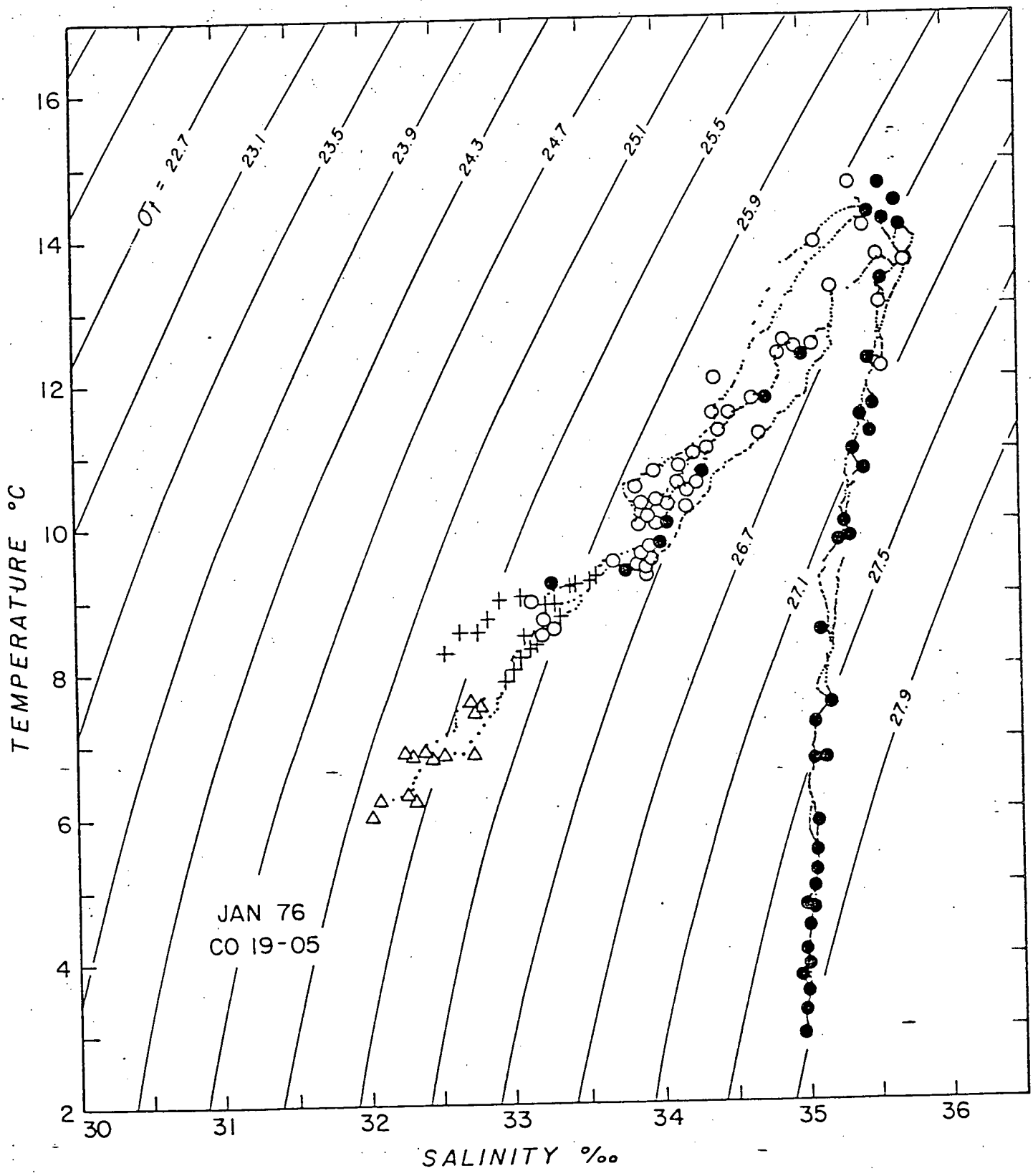
TEMPERATURE °C
SALINITY ‰
σt = 22.7
23.1
23.5
23.9
24.3
24.7
25.1
25.5
25.9
26.7
27.1
27.5
27.9
JAN 76
CO 19-05
2
4
6
8
10
12
14
16
30
31
32
33
34
35
36

Fig. 4.1-4a

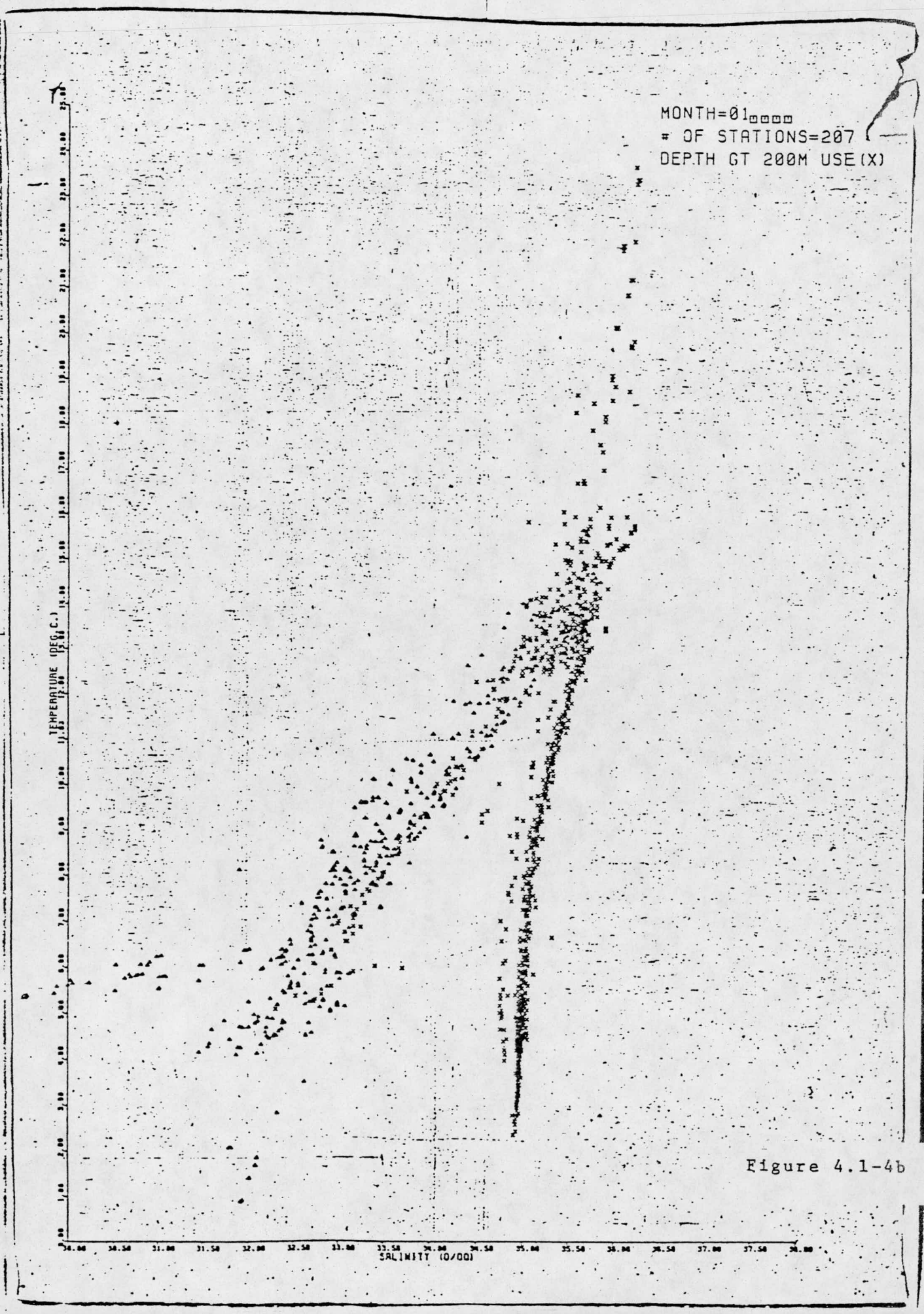
MONTH=01
# OF STATIONS=207
DEPTH GT 200M USE(X)
TEMPERATURE (DEG.C.)
SALINITY (0/00)

Figure 4.1-4b

later in 1976 in the New York Bight (Walsh et al., 1978). Therefore the January 1976 data may represent the maximum winter extreme for 1976.

The T/S relationship below the salinity maximum (S-max) in the slope regime near 13°C and 35.6 °/₀₀ defines the continental slope modification of the Islen 1936 North Atlantic Central Water (NACW) as discussed by McLellan (1957). This modification shifts the NACW curve towards lower salinity at nearly all isotherms. Gordon et al. (1976) discussed the various slope changes observed in the NACW-slope T/S relation, as evident in the October 1974 VEMA data set; this discussion is equally valid for the other data sets, since seasonal variability has an insignificant influence below the slope S-max.

The position of the T/S-max point on the NACW-slope T/S relation defines the deepest and densest water influenced directly by the continental shelf water. It is noted that an anomalous (relative to the NACW-slope T/S curve) condition occurs when volumes of more concentrated NACW water are introduced to the slope region by warm-core Gulf Stream rings in the slope region of the New York Bight (discussed below). The S-max marking the top of the NACW-slope water will be called the main S-max to differentiate it from the salinity maximum layers observed in the shelf water. Presumably, the main S-max is free to "slide" along the NACW-slope T/S curve, depending on variability in the density of the shelf component, or in the processes which mix it into the slope regime.

At depths above the main S-max the January 1976 T/S points fall along a nearly straight T/S line, suggestive of simple two-point mixing. The observed T/S relation is colder at any isohaline and/or saltier at any isotherm than would be expected were the water at the main S-max position to mix with the freezing point river water introduced at the western boundary. The sense of the displacement is expected, since the local sea to air heat loss implies that temperature is non-conservative in the active mixed layer (Fig. 4.1-5). The difference of the observed winter T/S curve from a simple conservative slope water-riverine mixing line cannot simply be a product of the non-conservative salinity effect induced by excess evaporation over precipitation. The salinity excess (difference of observed salinity to the salinity expected from the simple two-part slope-riverine mixing) at an isotherm is about 3-6°/₀₀, which requires evaporation excess over precipitation of many meters, far above any reasonable value. Bunker and Worthington (1976) show an annual evaporation of 100 cm for the New York Bight, which is close to the average annual precipitation in New York City [Climate of New York, from Climatography of the United States, No.60-30, U.S. Dept. of Commerce], which should be representative of the regional precipitation. The average E-P is near zero.

The segment of the water column for each station above the main S-max, or seafloor in the case of the stations on the continental shelf, is used to determine the heat deficiency relative to simple two-point (winter riverine water at 0°C,

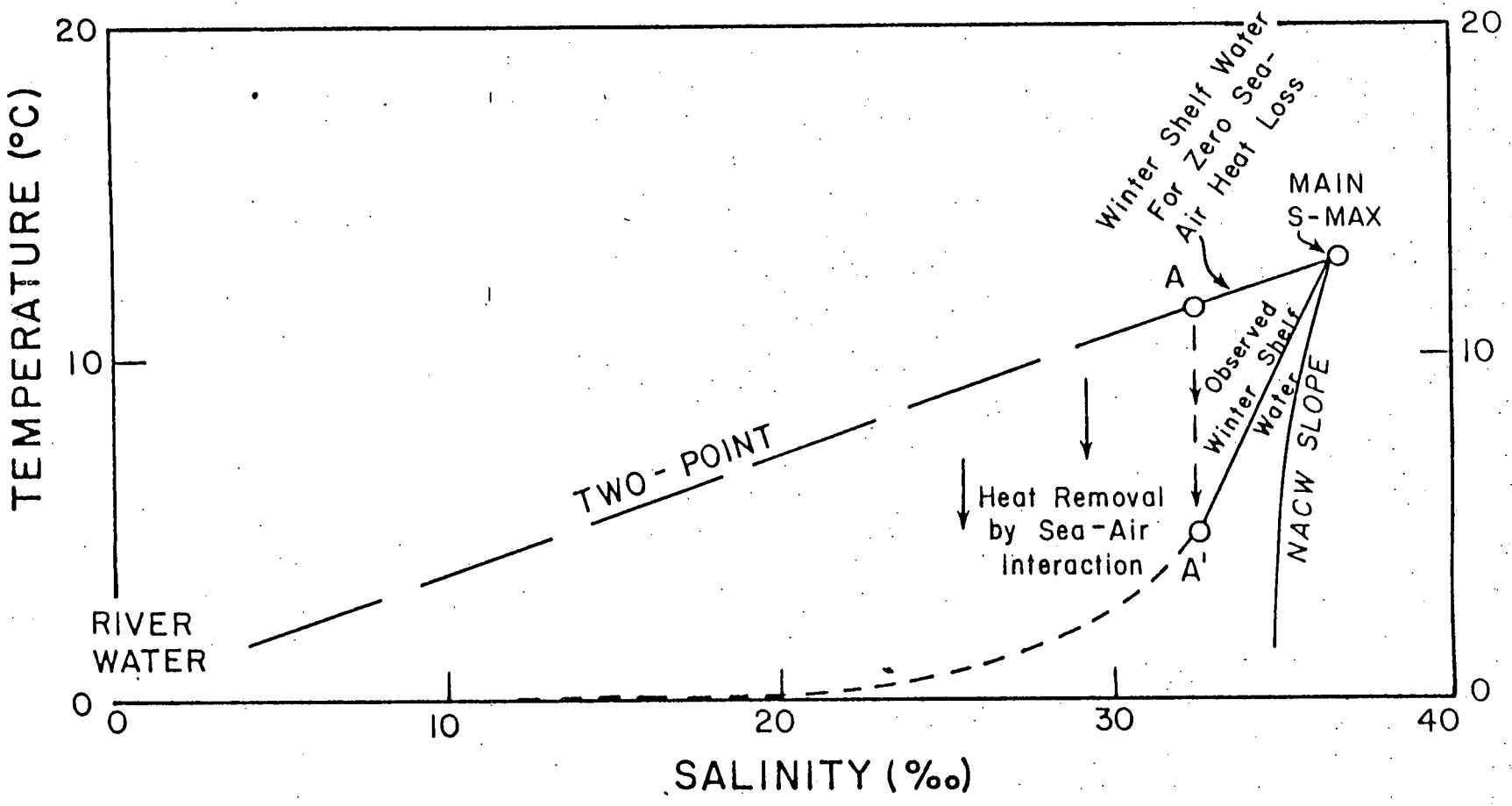
TEMPERATURE (°C)
SALINITY (‰)
20
10
0
0
10
20
30
40
TWO-POINT
RIVER WATER
Winter Shelf Water For Zero Sea-Air Heat Loss
MAIN S-MAX
A
Heat Removal by Sea-Air Interaction
A'
Observed Winter Shelf Water
NACW SLOPE

Fig. 4.1-5

0°/₀₀, and the main S-max θ/S point at 13°C, 35.6°/₀₀) conservative mixing. That is the coldest T/S relation that would develop if the sea-air heat exchange in the New York Bight were zero.

The distribution (Fig. 4.1-6) indicates maximum heat deficiency over the middle and outer shelf of between 3 to 4×10^4 cal/cm^2. The Hudson Channel and Canyon regions are particularly high. The decreased deficit landward of the inner 3.0×10^4 cal isopleth is due to the shallowness of the water column, whereas the decrease seaward of the outer 3.0×10^4 cal isopleth is most likely the result of attenuated mean sea-air temperature differences and increased air mass humidity due to air mass modification by the oceanic heat and water source.

The heat deficit can be explained by sea to air heat loss after the seasonal thermocline (this includes summer heat of the riverine water) is essentially removed. Inspection of the historical data set indicates that this occurs by the end of November. The heat deficit must be accomplished by sea-air heat loss in approximately two months. The daily average heat loss is approximately 400 to 650 cal/cm^2/day over the shelf, and 150-250 cal/cm^2/day over the slope. Hopkins and Garfield (1979) determined the total heat loss in the Gulf of Maine during the 1974-75 winter had a daily average of 200-500 cal/cm^2/day.

The above determination is carried out in an effort to conceptually address the question of gradient T°:S°/₀₀ ratio of

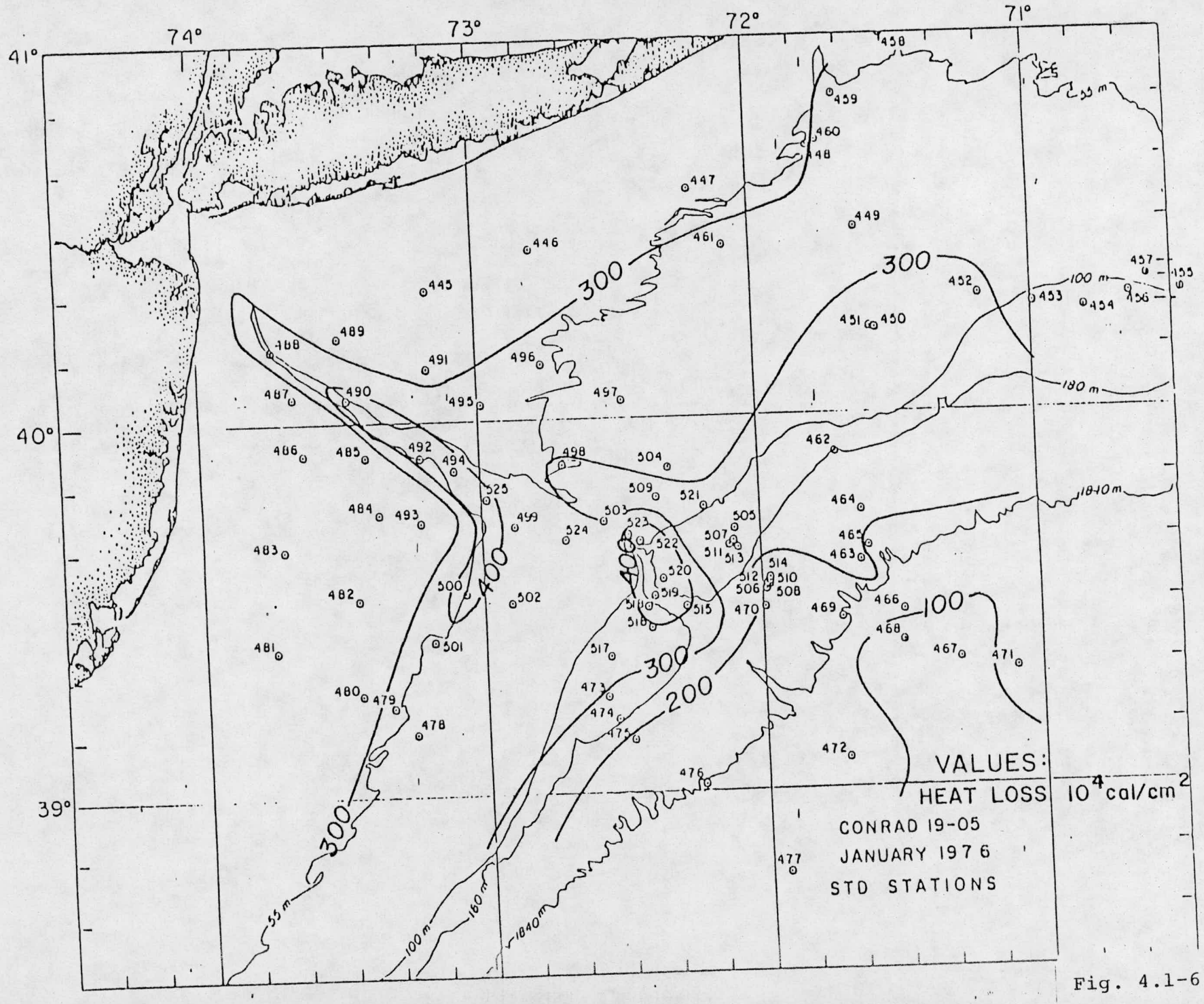
74°
73°
72°
71°
41°
40°
39°
VALUES:
HEAT LOSS 10^4 cal/cm^2
CONRAD 19-05
JANUARY 1976
STD STATIONS
55 m
100 m
160 m
180 m
1840 m
300
400
200
100

Fig. 4.1-6

the basic 'end-of-winter' T/S curve of the shelf water and slope surface water. Ocean to atmosphere heat flux steepens the T/S ratio or gradient. Naturally annual variations in the percentage of riverine and saline NACW-slope water present at the end of winter would vary the T/S length (i.e. salinity range) of the shelf and slope surface water in T/S space.

A characteristic winter shelf water salinity of 33.5°/₀₀ represents a 93% input of NACW-slope water in the shelf water volume with 7% of river water. A 10% increase in river water content (caused by increased river input or increased river water residence time) would lower the average shelf water salinity by 0.27°/₀₀. Therefore, assuming the winter sea-air heat flux has no annual variation, the winter shelf water T/S ratio would vary due to differences in river water residence time.

In summary: It is expected that the magnitude of the T/S gradient and the mean T/S characteristics of the shelf water of the end of winter shelf and slope surface water is due to a combination of: a) Sea to Air Heat Flux - colder winters would induce a steeper T/S gradient;

b) River Water Residence Time - decreased residence volume of river water due to decreased river runoff or increased onshore flux of NACW-slope water would induce a steeper T/S gradient;

c) T/S Position of Main S-Max - the saline end member T/S point may vary.

Since the mixed layer composes a large percentage of the water column at shelf depths, particularly in winter, both temperature and salinity are extremely non-conservative over the shelf and within the upper slope water above the main S-max, and it is expected that the mean T/S characteristics of these waters as well as the position and slope of the T/S baseline (mixing line) in T/S space will vary according to variations in air temperature (sea to air heat flux), precipitation, and river water outflow. The NODC historical hydrographic data, USGS historical river outflow data, and NOAA's National Climate Center's historical meteorologic data have all been examined for the New York Bight region and any relationships between their variabilities.

The interannual variability in the end of winter (February-March) shelf water characteristics are compared to the meteorological and river outflow data for the years in which we have either suitable NODC data or our own observations. In figure 4.1.7 the temperature at the 33.5 °/oo isohaline and the air temperature anomaly recorded at JFK for the six months (August-January) preceding the hydrographic observations are plotted for the years 1956-79. Similarly, in figure 4.1.8 the salinity at the 7°C isotherm, the precipitation anomaly recorded at JFK for the same preceding six month period, and the Hudson River outflow anomaly for the 12 months preceding the salinity (hydrographic) observations are plotted for the same period. In

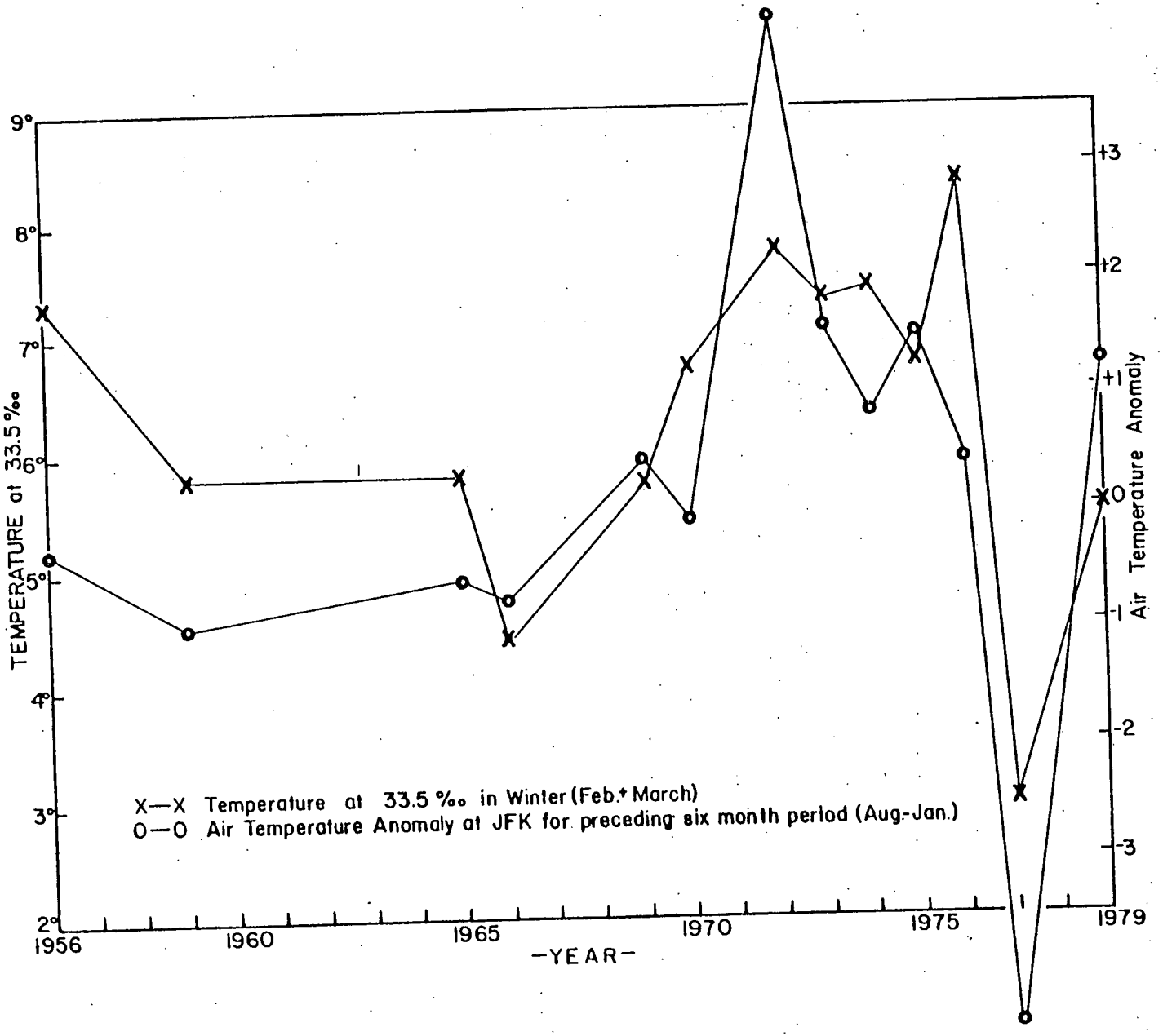
9°
8°
7°
6°
5°
4°
3°
2°
TEMPERATURE at 33.5‰
+3
+2
+1
0
-1
-2
-3
Air Temperature Anomaly
X—X Temperature at 33.5 ‰ in Winter (Feb.+ March)
O—O Air Temperature Anomaly at JFK for preceding six month period (Aug-Jan.)
1956
1960
1965
1970
1975
1979
-YEAR-

Fig. 4.1-7

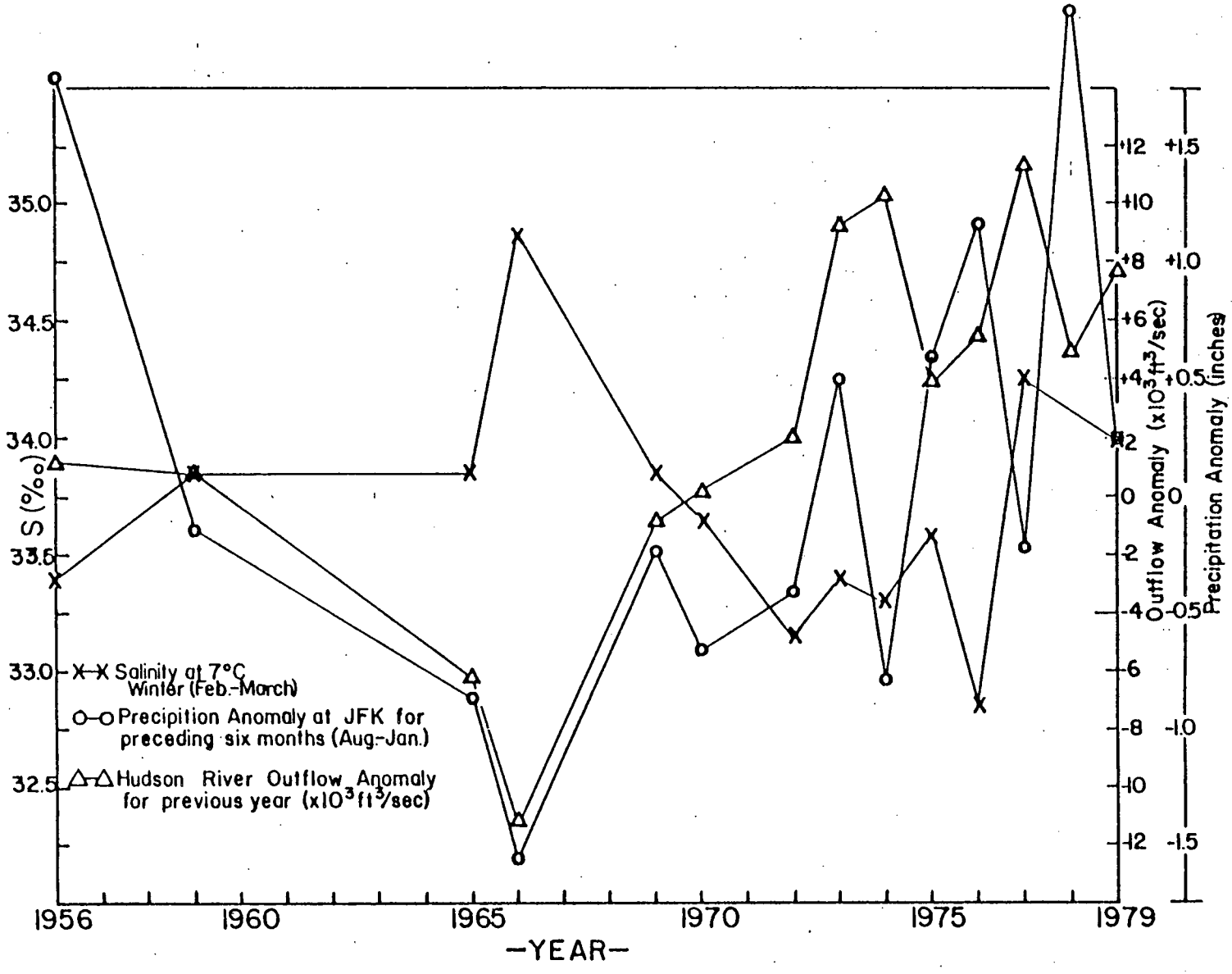
35.0
34.5
34.0
33.5
33.0
32.5
S (‰)
X–X Salinity at 7°C Winter (Feb.-March)
O–O Precipition Anomaly at JFK for preceding six months (Aug.-Jan.)
Δ–Δ Hudson River Outflow Anomaly for previous year (x10³ ft³/sec)
+12
+10
+8
+6
+4
+2
0
-2
-4
-6
-8
-10
-12
Outflow Anomaly (x10³ ft³/sec)
+1.5
+1.0
+0.5
0
-0.5
-1.0
-1.5
Precipitation Anomaly (inches)
1956
1960
1965
1970
1975
1979
–YEAR–

Fig. 4.1-8

both diagrams a very strong correlation (positive for temperature and negative for salinity versus fresh water input) makes obvious the sensitive relationship between the end of winter, usually vertically mixed, shelf water column T/S properties and both the meteorological and continental river outflow factors. Unfortunately, these correlations do not help distinguish which processes (air-sea interaction or river water outflow) are dominant. It appears that the shelf water and slope surface water T/S variability is due to a combination of these two factors, plus the possibility of a third potentially important factor not easily included in this analysis. This is the variability in the T/S character of the slope water or in slope water intrusions which must mix with the fresh, riverine input to form the shelf water. Such changes have been observed associated with the passage of warm-core Gulf Stream rings in the slope region of the New York Bight.

The historical data also allows comparison of the interannual and seasonal position of the T/S baseline on T/S diagrams. The characteristic 'seven' shape to the T/S curve is always apparent, even in summer when points over the shelf migrate upward to warmer temperatures. The year to year variations in any season appear in the change of position or slope of the T/S mixing line (see line AB-insert of Figure 4.1.9). This baseline, though always approximately linear, is not the result of simple two-point mixing between its two end members:

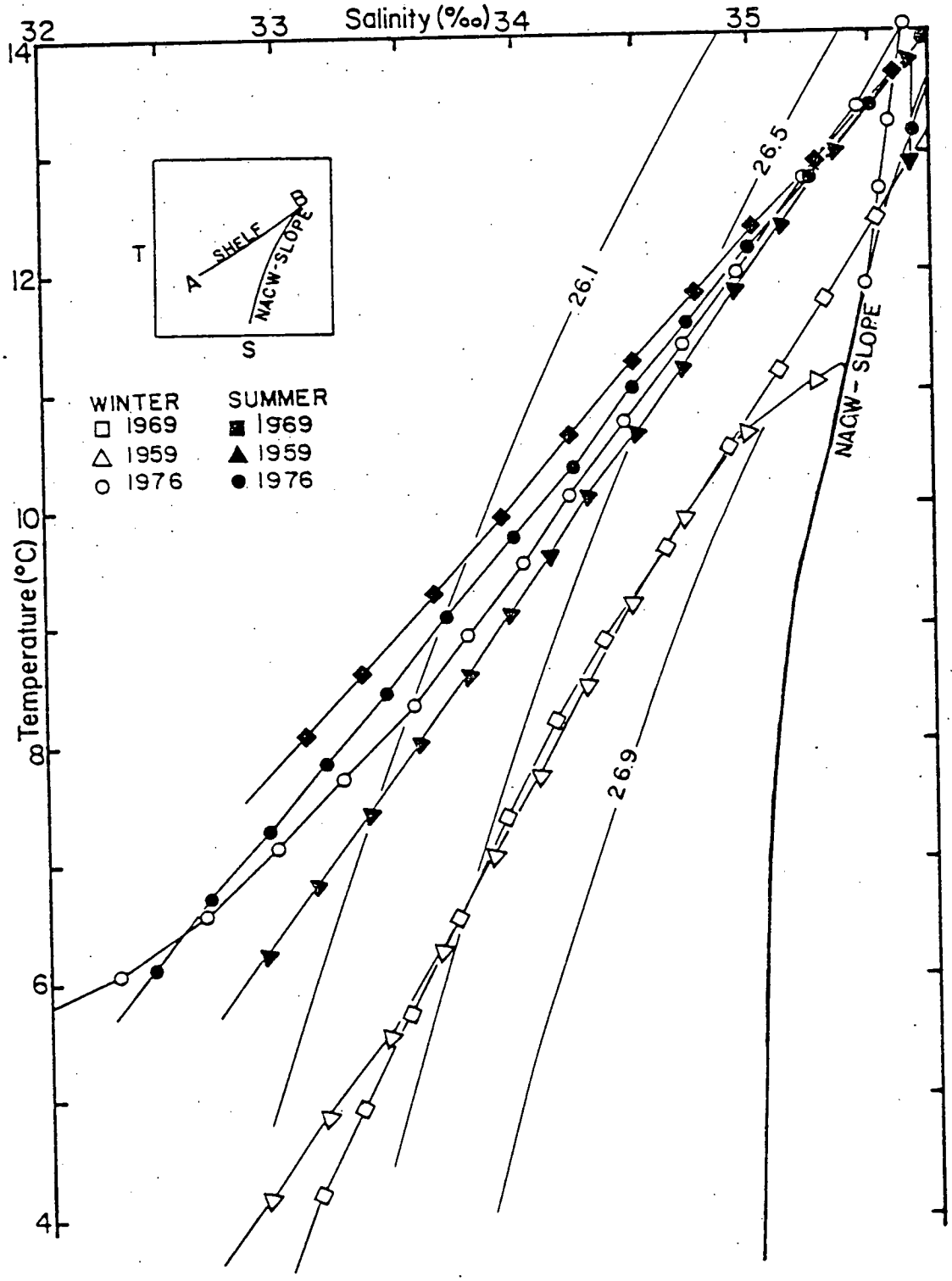
Salinity (‰)
32
33
34
35
14
12
10
8
6
4
Temperature (°C)
T
S
A
SHELF
B
NACW-SLOPE
WINTER
1969
1959
1976
SUMMER
1969
1959
1976
26.1
26.5
26.9
NACW-SLOPE

Fig. 4.1-9

(A) being fresh, cool river input and (B) being warm, salty NACW-slope water. As noted earlier, points falling on the T/S baseline are observed to be colder at any isohaline and/or saltier at any isotherm than what conservative mixing between its two end members would dictate. The position and slope of the mixing line must be dependent on the variability of its end members as well as local air-sea interaction. The historical data allows a qualitative look at this, with the exception that it doesn't provide the resolution to comment on the variability of end member (B).

We have selected three representative years from the NODC historical data (Fig. 4.1.9) and, as described below, compared the character of the seasonal T/S baseline in the New York Bight to temperature and precipitation data from JFK and to Hudson River outflow data. Both the winter 1959 and 1969 T/S baselines exhibit a steep T/S gradient and correspond to cool and dry autumns and winters. The river outflow for 1959 was anomalously high, while for 1969 it was anomalously low, thus possibly accounting for the fresher end mumber to the 1959 baseline. The summer T/S baselines for these two years diverge considerably. Spring and summer 1969 were unusually warm and wet with excessive outflow, and this could explain the high position of its baseline in T/S space. Spring and summer 1959 were typically average and the transition in T/S Space from winter to summer is less graphic. The winter

1976 curve appears to be the result of an unusually wet autumn and winter with air temperatures slightly above normal, while the spring and summer conditions were normal.

Admittedly this is a very qualitative comparison, but it points to the correlation between the T/S gradient of the baseline in the New York Bight and its sensitivity to local heating, precipitation and river water outflow. We hope to quantify this relationship on a more exhaustive examination of the historical data.

May 1977 - (Spring Structure)

Development of the seasonal pycnocline is well underway by May (Fig. 4.1.10a, with Fig. 4.1.10b showing the historical data set for May), as T/S points of the shelf and slope surface water are lifted off the winter T/S baseline. The slope and shelf waters are separated by an intense shelf break frontal zone, which now clearly shows up in T/S space. The coldest cold pool water observed was 3°C, as low as any value found in the historical data set, which may be expected from the severity of the 1976-77 winter. The temperature and salinity near the shelf floor is similar to that of March 1977 [see Fig. 4.1-15, in which the 1977 seasonal progression of the T/S baseline is exhibited], but suggestive of warming (about 1°C) and/or freshening (about a 0.3 °/oo salinity decrease).

The shelf T/S curves at temperatures above the winter base are nearly isohaline, though often the warmest section at the sea surface shows a pronounced decreasing salinity as tempera-

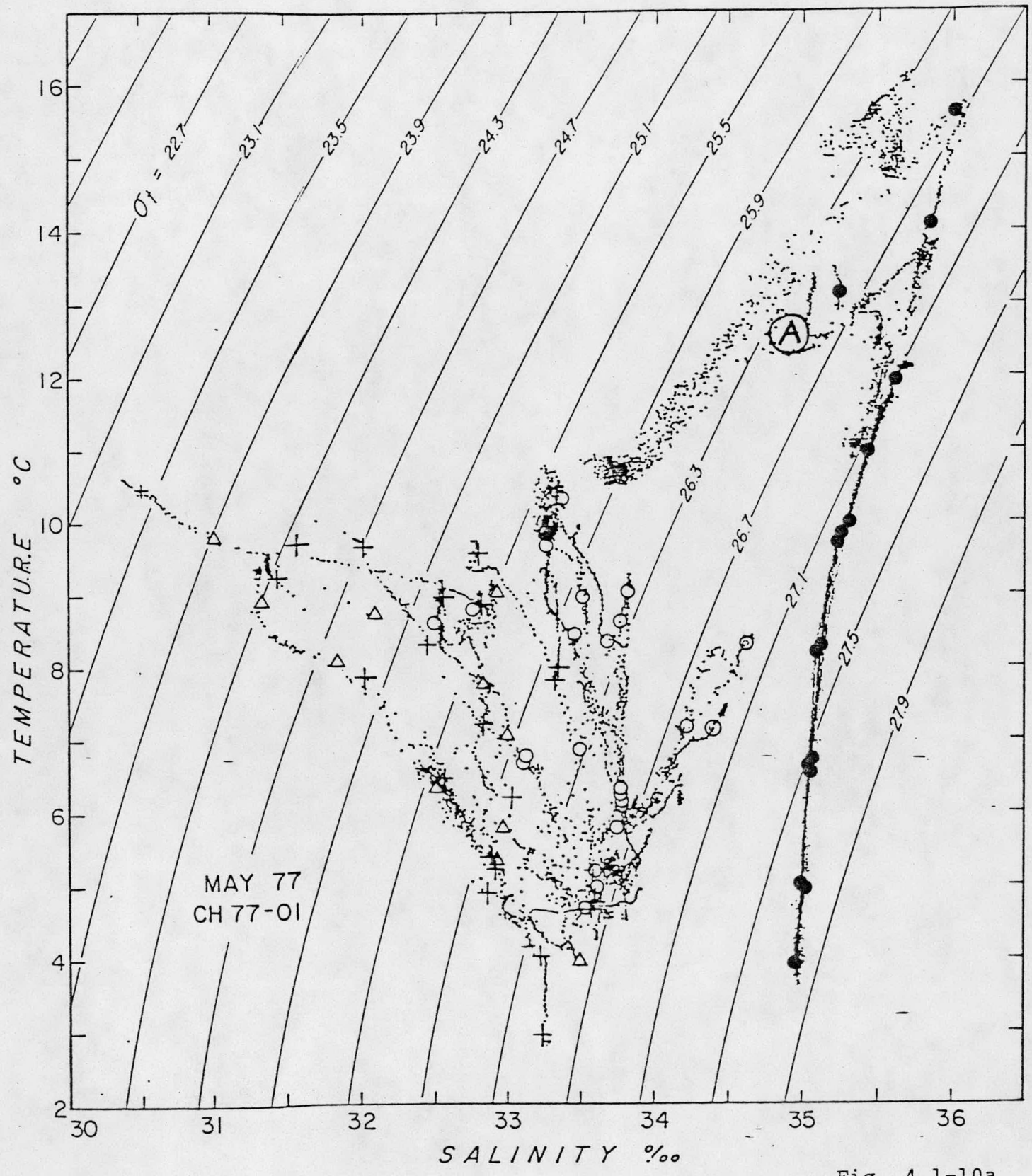
σt = 22.7
23.1
23.5
23.9
24.3
24.7
25.1
25.5
25.9
26.3
26.7
27.1
27.5
27.9
A
MAY 77
CH 77-01
TEMPERATURE °C
SALINITY ‰
2
4
6
8
10
12
14
16
30
31
32
33
34
35
36

Fig. 4.1-10a


MONTH=05
# OF STATIONS=251
DEPTH GT 200M USE(X)
TEMPERATURE (DEG.C.)
SALINITY (0/00)

Fig. 4.1-10b

ture warms. This is expected, since at these elevated temperatures the river input is concentrated into a density region in which no slope water exists, and hence there is a diminished availability of highly saline water, assuming isopycnal processes are an effective mode of exchange.

The slope water above the main S-max shows many inversions, as the lower salinity shelf water mixes with the slope water. The pronounced concavity (area A on the T/S diagram, Fig.4.1-10a) is induced by seaward mixing of the cold pool water, fed by the large reservoir situated on the sea floor at the middle continental shelf. The rapid cooling and decreased salinity at the surface is seaward spreading of the shelf surface water, unopposed by an isopycnal saline input.

The water layer below the T-min is called the benthic layer over the shelf, and subsurface water over the slope (where it is underlain by the main S-max rather than the seafloor). This layer is shown in the preceding section on thermohaline stratification (Fig. 4.1-2). The benthic layer is composed of two parts: a lower homogeneous mixed layer, and a layer of near-linear T/S characteristics between the T-min and bottom mixed layer. The T/S relation suggests that the linear T/S layer is composed of a mixture of cold pool water and the main S-max water.

July 1975 - (Summer Stratification)

The July 1975 T/S relation (figure 4.1-11a) and historical July data (figure 4.1-11b) show the fully developed seasonal stratification. The vertical thermal gradients are remarkably strong over the continental shelf, with a total temperature range of 18°C in the characteristic middle shelf depth of 50 meters.

The inner and middle shelf form the low salinity component above the cold pool water. The slope surface water forms the high salinity component. The outer shelf and some middle shelf stations show a pronounced salinity maximum near the 24.3 to 24.7 σ-t level (area B on figure 4.1-11a). Over the outer shelf this S-max is essentially slope surface water. Since it occurs in the upper section of the seasonal pycnocline, it is called the pycnocline S-max. It is obviously a layer dominated or at least significantly influenced by slope surface water.

The slope surface water above the main S-max is relatively saline, though markedly decreased surface salinity is observed, presumably as the low density river influence spreads seaward within the surface mixed layer.

Relatively low salinity is also observed in the slope region just above the main S-max, often accompanied by a T-min in the density level 26.3 σ-t. The low temperature and salinity characteristics point to an origin within the remnant cold pool and benthic layer on the continental shelf. The benthic layer over the outer shelf in July 1975 falls in the 26.3 σ-t level and hence provides the most likely isopycnal source of the slope water S-min

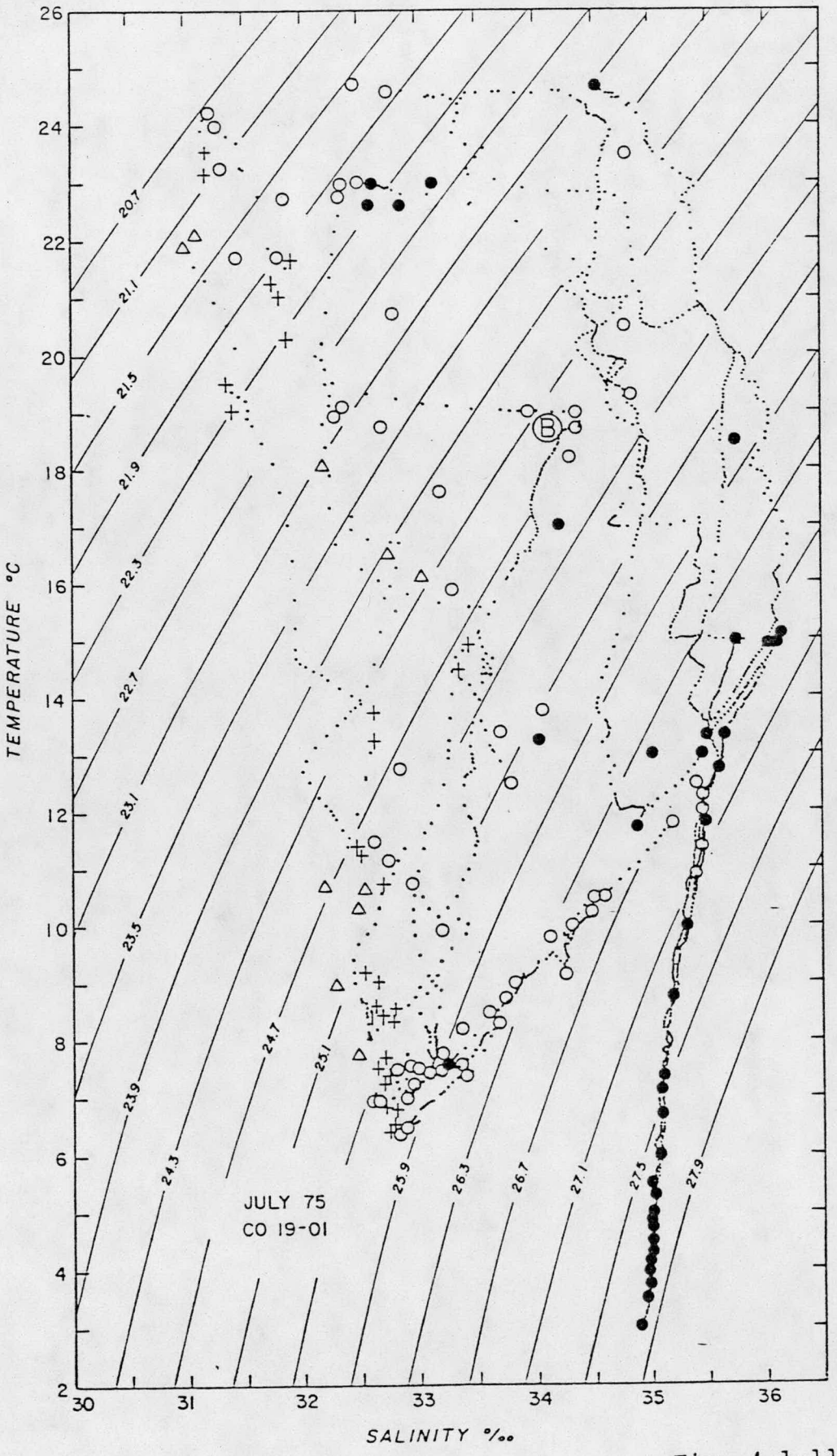
TEMPERATURE °C
SALINITY °/oo
JULY 75
CO 19-01
B
20.7
21.1
21.5
21.9
22.3
22.7
23.1
23.5
23.9
24.3
24.7
25.1
25.9
26.3
26.7
27.1
27.5
27.9

Fig. 4.1-11a

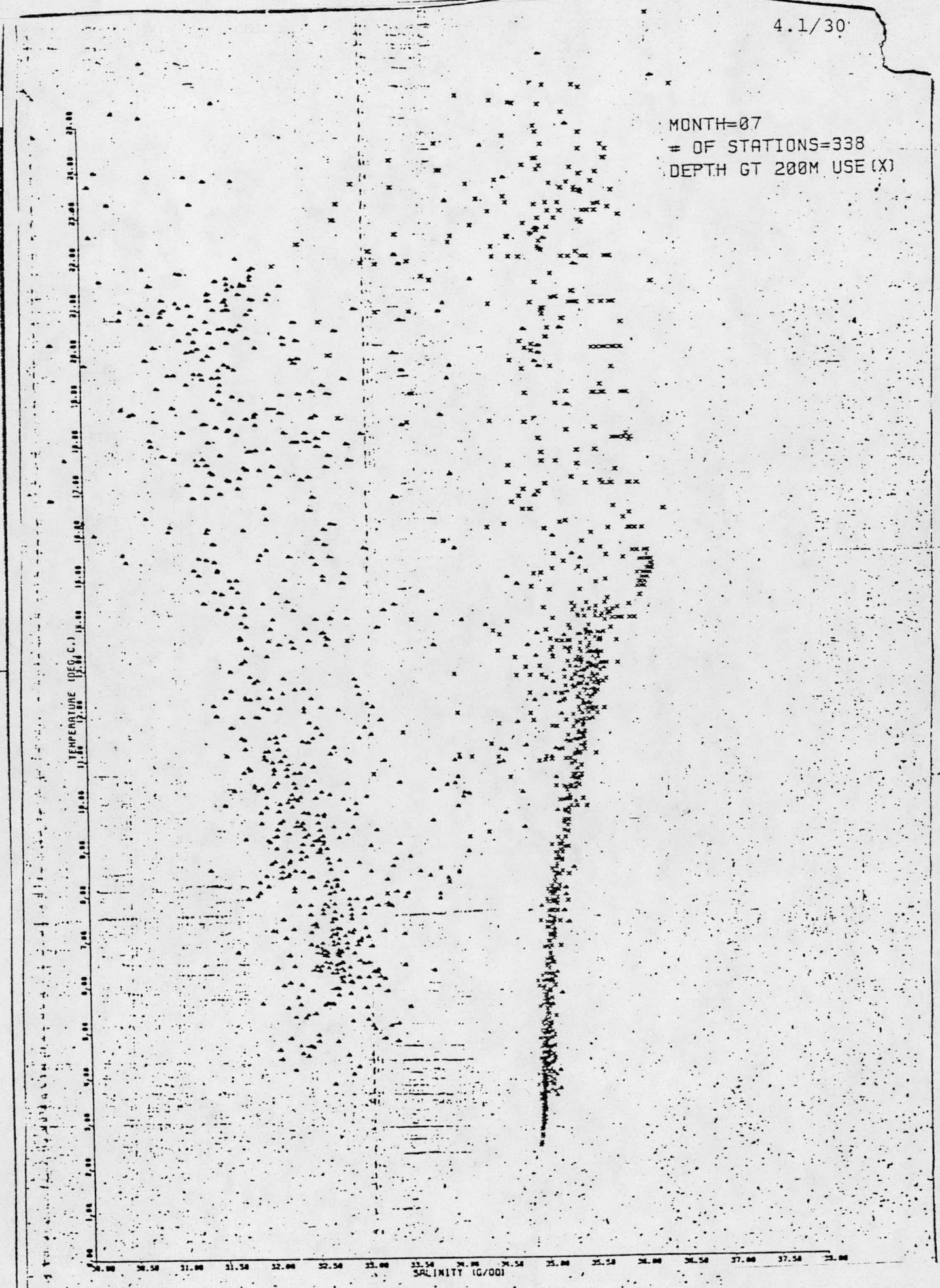
MONTH=07
# OF STATIONS=338
DEPTH GT 200M USE(X)
TEMPERATURE (DEG.C.)
SALINITY (0/00)

Fig. 4.1-11b

layer at the base of the slope pycnocline, rather than the main body of cold pool water.

In a uniform distribution of data an oceanic front is indicated by a low density of T/S points (or low volume of water in the frontal T/S area). The low density of data points in the area of Figure 4.1-11a pierced by the pycnocline S-max (area B), marks the shelf-slope frontal zone. Hence the pycnocline S-max represents significant cross-frontal exchange.

In July 1975 a volume of very saline water was observed over the slope (Fig. 4.1-11a). This is identified as a warm core eddy and is discussed in section (E).

August 1977 - (Summer Structure)

The August 1977 cruise and historical T/S relationships for August (Fig. 4.1-12 a,b) is similar to the July characteristics. The inner and middle shelf water above the seafloor T-min forms the low salinity (31.5-33.5 °/oo) component over an impressive temperature range (9° to 22°C). The slope surface water over the main S-max forms the saline (34.5-35.3 °/oo) component.

Between the two components are few data points, though cross-over between components occurs over the outer shelf and at some stations over the middle shelf. The outer and some middle shelf waters show the dominant slope water traits, marked by a S-max near 20-22°C and 23.9-24.7 σ-t levels (area B on Fig. 4.1-12a), in the upper pycnocline, with dominant shelf water characteristics

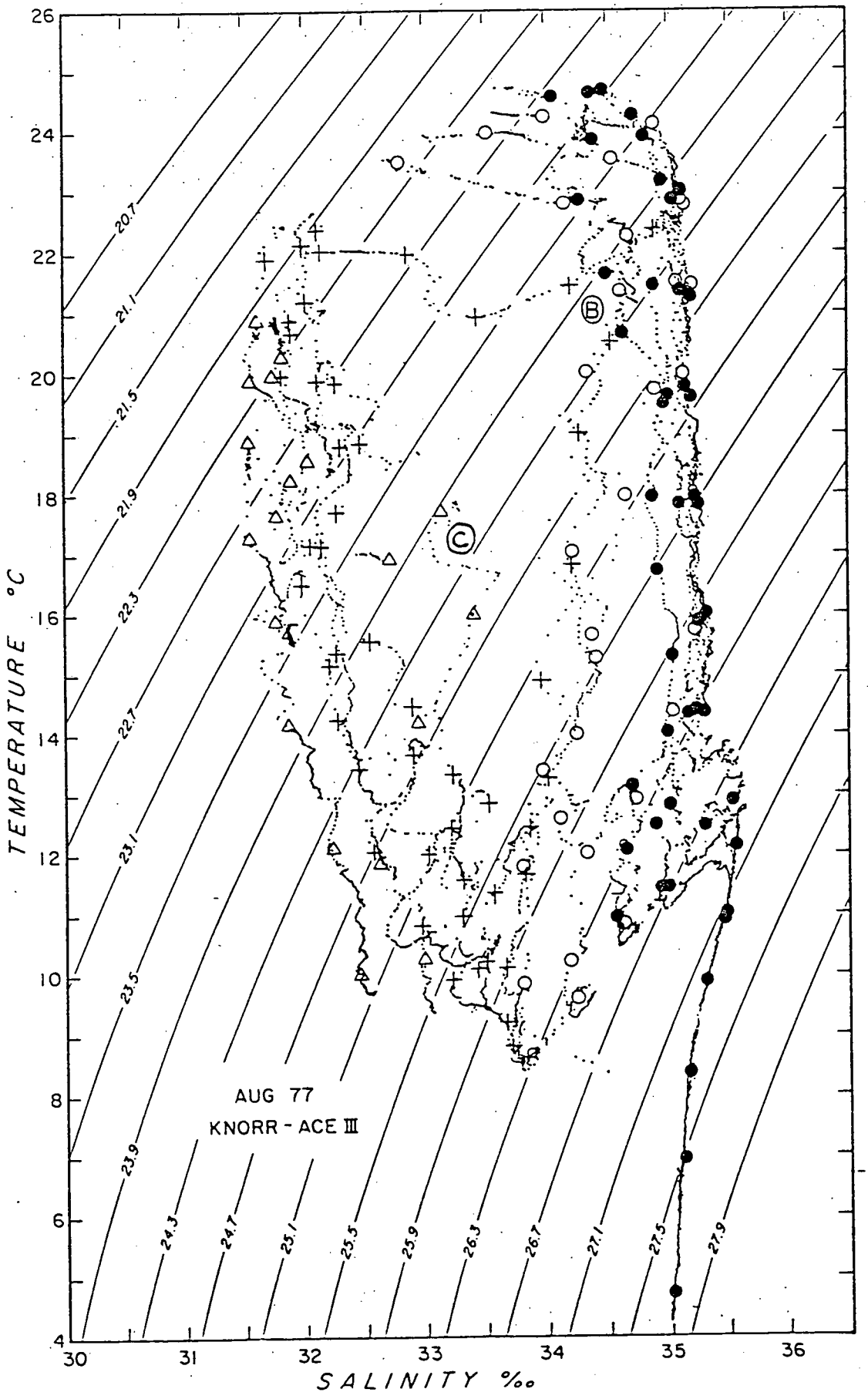
TEMPERATURE °C
SALINITY ‰
AUG 77
KNORR - ACE III
Ⓑ
Ⓒ
20.7
21.1
21.5
21.9
22.3
22.7
23.1
23.5
23.9
24.3
24.7
25.1
25.5
25.9
26.3
26.7
27.1
27.5
27.9

Fig. 4.1-12a

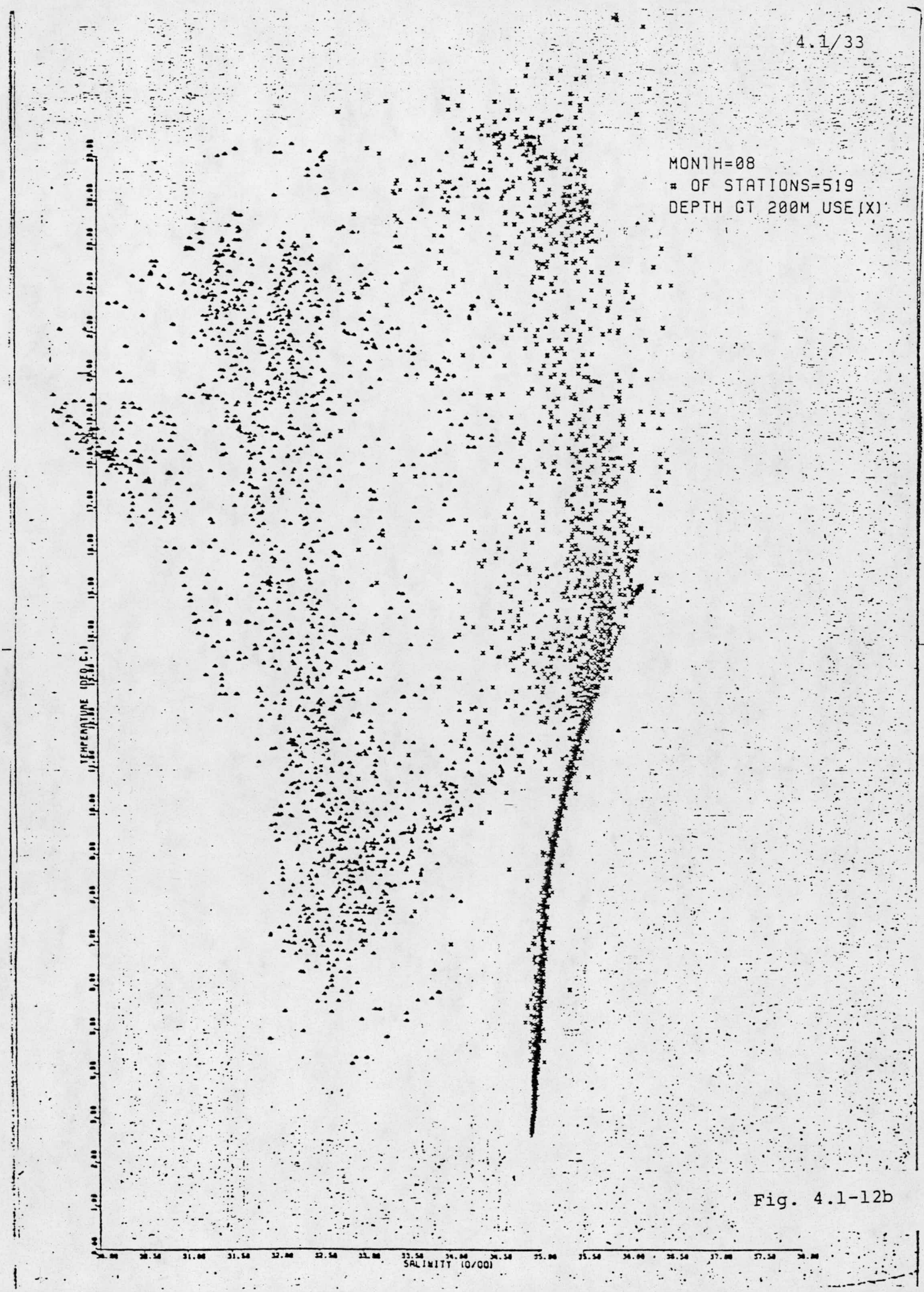
MONTH=08
# OF STATIONS=519
DEPTH GT 200M USE(X)
TEMPERATURE (DEG.C.)
SALINITY (O/OO)

Fig. 4.1-12b

at the pycnocline base marking the seaward extension of the T-min winter remnant cold pool waters near 26.3-26.7 σ-t levels.

The slope water has two T/S areas influenced by the shelf water: the surface low salinity layer, and a low salinity layer in the same σ-t levels marking the seaward T-min extension.

The inner shelf T/S relation of station 17 displays some excursions into the T/S void between the shelf and slope water. While this excursion (area marked C on fig.4.1-12a) occurs at 16-18°C, its density is 23.9-24.7 σ-t, which is identical to the density range of the slope water dominated pycnocline S-max. This is taken as evidence that shoreward isopycnal spreading of slope waters characteristic in the upper pycnocline extends to the inner shelf regions.

The August section does not show a well developed shelf-slope frontal zone, however the near void of T/S points in the region between areas C and B of the Fig. 4.1-12a is suggestive of a frontal region. As in the July 1975 situation, the pycnocline S-max represents significant cross frontal exchange.

October 1974 (Fall Structure)

The VEMA 32:01 data obtained in October 1974 is shown in T/S space on figure 4.1-13a, with the historical data shown in figure 4.1-13b. The October 1974 oceanography has been discussed by Gordon et al., 1974.

In October the surface mixed layer deepens as heat is removed by the atmosphere. The lower layers of the thermocline

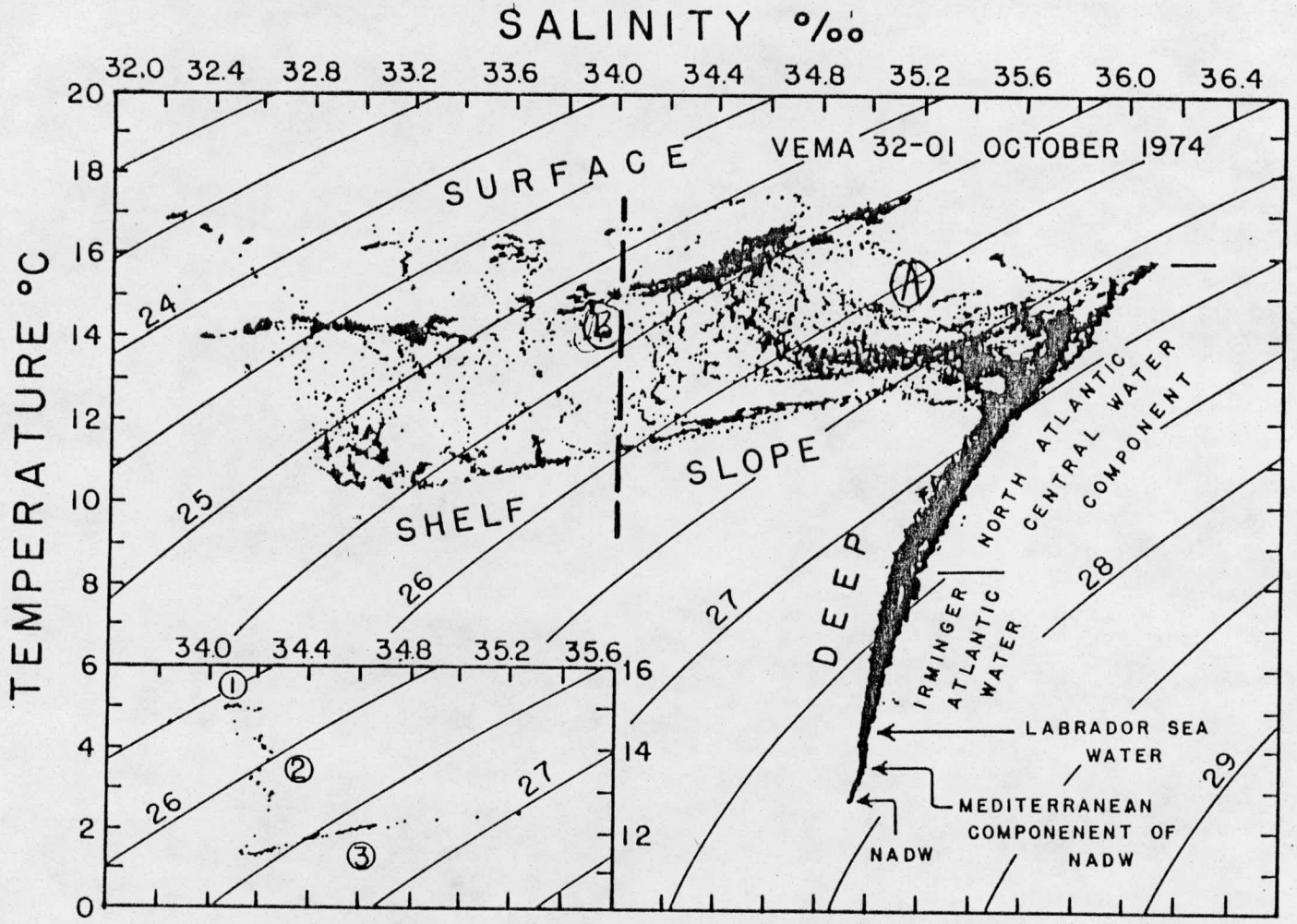
SALINITY ‰
32.0 32.4 32.8 33.2 33.6 34.0 34.4 34.8 35.2 35.6 36.0 36.4
TEMPERATURE °C
20 18 16 14 12 10 8 6 4 2 0
VEMA 32-01 OCTOBER 1974
SURFACE
SHELF
SLOPE
DEEP
24
25
26
27
28
29
A
B
NORTH ATLANTIC CENTRAL WATER COMPONENT
IRMINGER ATLANTIC WATER
LABRADOR SEA WATER
MEDITERRANEAN COMPONENENT OF NADW
NADW
340 344 348 352 356
16 14 12
1
2
3
26
27

Fig. 4.1-13a

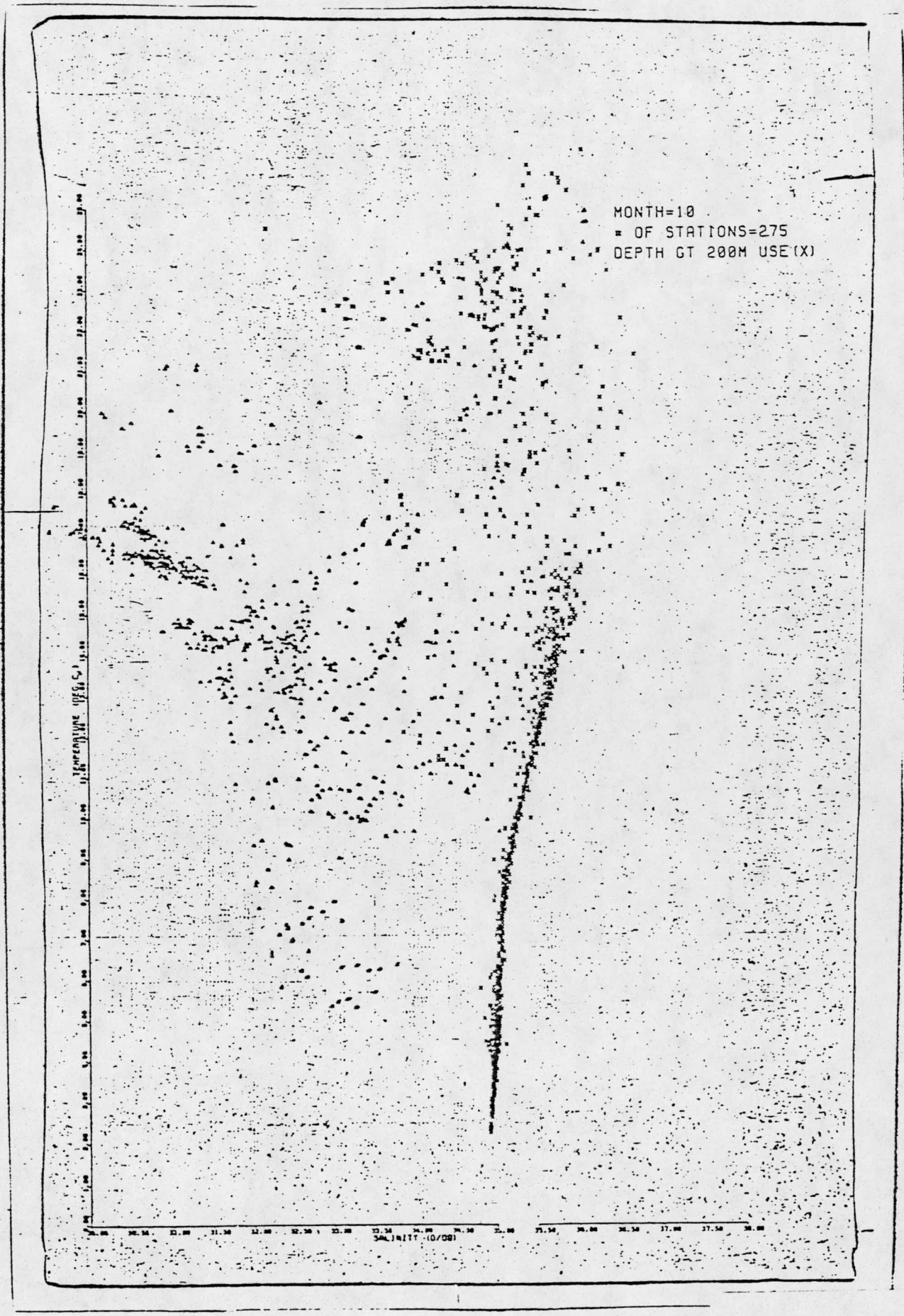

Fig. 4.1-13b

remain. Not until late in November is the summer thermocline removed.

The subsurface S-min of the slope region marking the seaward extent of shelf water into the slope pycnocline (area A of Fig. 4.1-13a) remains, as does the outer shelf remnant of the phcnocline S-max (area B of Fig. 4.1-13a). Low salinity surface water is observed throughout the area as the accumulated river water in the summer upper mixed layer is mixed downward by the autumnal convection.

C. Frontal Structure, Cold Pool, and Cross Shelf Mixing.

In this section we describe studies of the shelf/slope frontal structure from which we derive models of cross-shelf exchange. Because of the great temporal and spatial variability a large data set is required to establish the representative features. Analysis of the ever increasing cumulative hydrographic data set is providing a clearer picture of the frontal structure as well as documenting significant variations from the mean.

There are significant interannual variations of water properties in which, for instance, the average salinity on the shelf can vary by more than 0.5 $^{\circ}/_{\circ\circ}$. These variations undoubtedly reflect interannual variations in factors such as river runoff, incidence of warm core eddies on the shelf, or rate of vernal stratification over the shelf.

Schematic sketches of the mixed winter and stratified summer frontal structure are shown in Fig. 4.1-14. The winter structure, vertically mixed over the shelf with a baroclinic front at the shelf break, is well documented in the literature

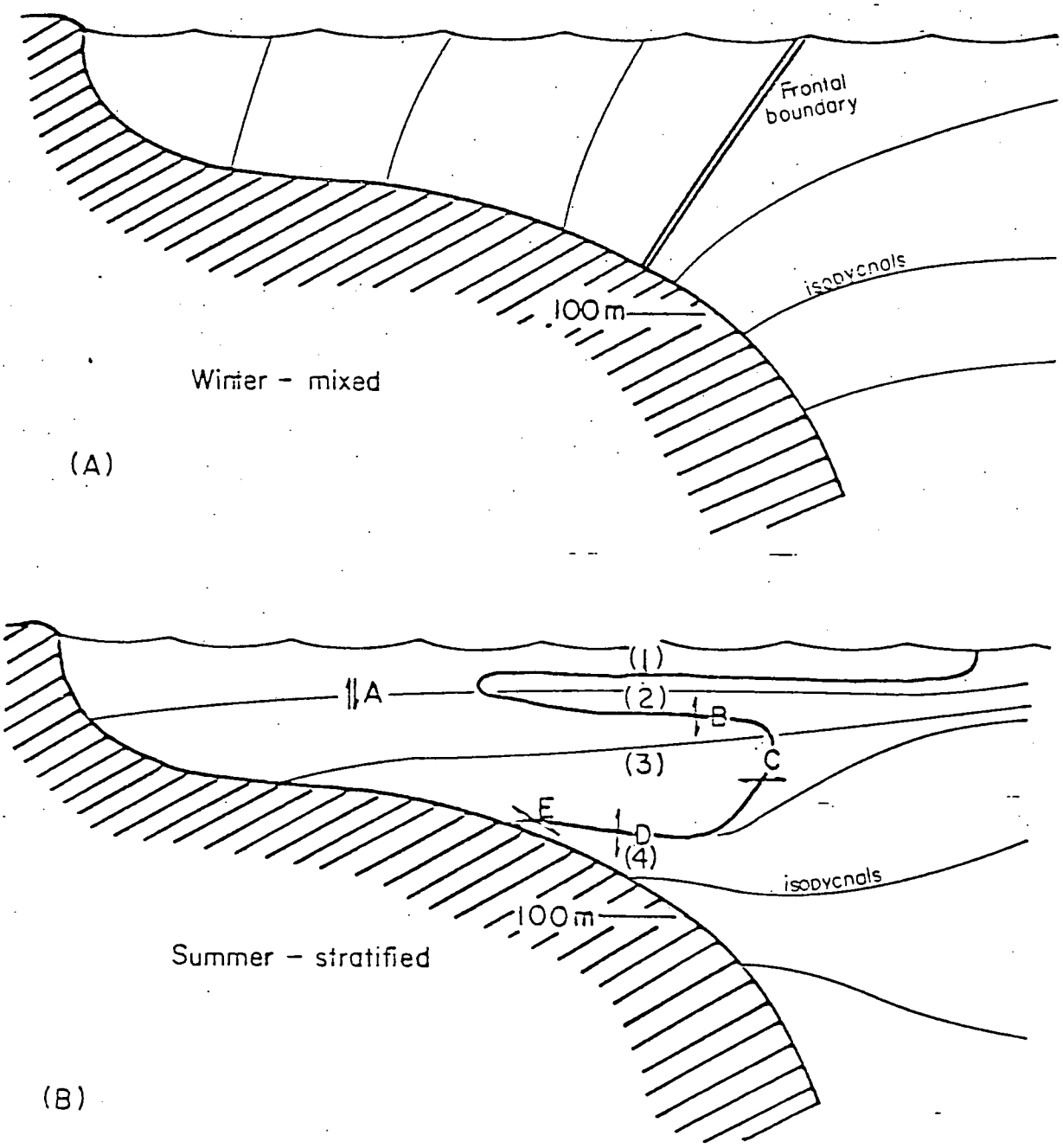

Schematic of density structure and shelf/slope water frontal boundary.

Fig. 4.1-14

(e.g. Beardsly and Flagg, 1976). Forcings by winds, Gulf Stream meanders and warm core rings result in a highly convoluted boundary. Analysis of satellite imagery (Halliwell & Moorers, 1979) give characteristic alongshore scales of 80 km and cross shelf scales less than 50 km.

By contrast during the highly stratified summer conditions the very weak surface expression of the front precludes the effective use of satellite data to examine frontal structure. Since the mixed warm surface layer extends seaward far beyond the shelf break, and there is very little temperature gradient between shelf and slope water, the structure shown in Fig. 4.1-14B is more apparent in the salinity field. There are four distinct layers in the frontal structure:

1. A surface mixed layer of fresh shelf water extending seaward of the wintertime shelf-slope front position.
2. An intrusion of slope water along the upper portion of the pycnocline.
3. The cold pool - a remnant of winter cooled shelf water.
4. The benthic intrusion of slope water.

The pycnocline over the shelf is produced primarily by the seasonal thermocline. The surface layer (1) made fresher by the river runoff intensifies the stratification especially over the mid and inner shelf. This inhibits vertical mixing into the cold pool. It also may contribute to the dynamic structure that results in the slope intrusion (see section H).

A significant fraction of the river runoff may pass through this layer directly to the slope without mixing into the shelf water.

An analysis of the pycnocline slope water intrusion (2) is given by Gordon and Aikman, 1980, (see section D). The intrusion terminates over the mid shelf and can contribute up to 50% of the cross shelf salt flux required to balance the fresh water input.

The cold pool (3) is the most distinctive hydrographic feature over the shelf during the summer. The origin of this water is still a matter of controversy. The intense stratification and weak tidal current in the New York Bight inhibit vertical mixing which would erode the cold pool during the summer. Some years the cold pool remains distinct throughout the summer into September. It is not certain whether during this period the cold pool is being renewed from some northern source such as the Gulf of Maine.

Upstream sources of cold water are limited. Stratification is reduced by the vigorous tidal mixing over Nantucket Sheals and Georges Bank. The only path for cold water from the Gulf of Maine is the Great South Channel which has a depth of 75 m.

Few data sets are sufficiently detailed and synoptic to assess the structure and seasonal evolution of the cold pool. The best abailable is that of Colton et al. (1968), which covers the Gulf of Maine and the northern New York Bight for the years 1965-66. Although the station grid is not sufficiently fine to

rule out advection of cold water from the Gulf of Maine via the Great South Channel between the Nantucket Shoals and Georges Bank, this is not likely since the coldest cold pool temperatures are persistently found in the New York Bight near the Hudson Canyon.

The mean circulation in the New York Bight has now been evaluated from the long term MESA moorings (Mayer et al., 1979). The near bottom circulation is weaker, 25-40 km/month to the southwest, and contains greater interannual variability than originally suspected (Beardsley et al., 1976). At times the bottom flow reverses direction to the northeast. These results suggest that for the months of May to September when the cold pool is such a distinct feature the bottom water near the Hudson Channel originated most likely during the previous winter within the New York Bight. The Nantucket Shoals Flux Experiment by Beardsley, Butman and Wright of WHOI, USGS and NMFS respectively will provide a continuous current meter and hydrographic record spanning at least one full year. This should provide a better picture of the conditions upstream of the New York Bight and the potential for renewing the cold pool.

We have almost always observed that the cold pool is coldest in the apex of the New York Bight. This would support the idea that the cold pool is a remnant of locally cooled winter water. However, there is longshore structure to the cold pool with pockets of colder water with alongshore dimensions of 10's of

kilometers. This structure makes interpretation of alongshore gradients very difficult.

In 1977 there were four sets of data from which the evolution of the cold pool water and of the linear T/S component of the benthic layer can be defined (Fig. 4.1-15; Fig. 4.1-1 shows the station positions). The linear T/S line slowly warms and its gradient becomes less steep (smaller T:S ratio). At 33.5 °/oo the total temperature increase amounts to over 6°C. Warming is expected, since there is no source of cold water to maintain the cold pool water, as local convection stops by April and any possible connection with Gulf of Maine Intermediate Water (which Hopkins and Garfield, 1979, suggest is the source of the New York Bight cold pool water) is apparently cut off.

The outer boundary of the cold pool remains very sharp throughout the summer. The frontal surface is often less than 1 km with temperature gradients up to 5°C. This surface is highly convoluted in the horizontal plane with cross shelf scales often comparable to alongshelf scales. For instance, during the 1978 BT cruise we observed a feature with a cross and alongshelf scale of approximately 15 km (Fig. 4.1-18).

The Benthic intrusion (4) is also a persistent feature which may be observed during the winter although it is more pronounced during the summer when it may penetrate more than 10 km onto the shelf. This benthic layer could be the result of mixing by internal tides which are generated at the shelf break or lateral shear between the shelf and slope current

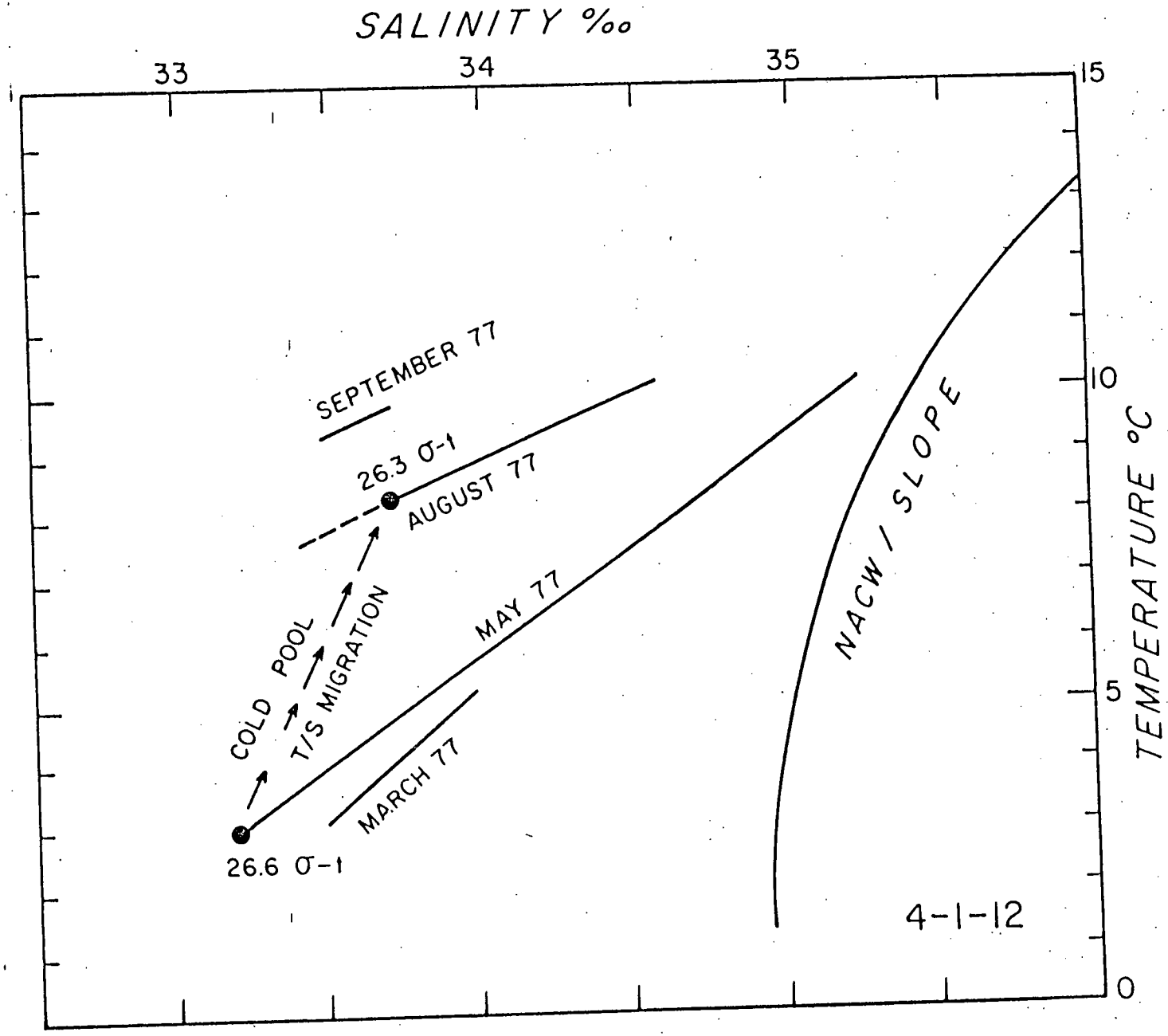
SALINITY ‰
33
34
35
15
10
5
0
TEMPERATURE °C
SEPTEMBER 77
26.3 σ-1
AUGUST 77
COLD POOL
T/S MIGRATION
MAY 77
MARCH 77
26.6 σ-1
NACW / SLOPE
4-1-12

Figure 4.1-15

regimes. Warm core eddies over the slope can be another driving mechanism for benthic layer intrusions (see section E). As the anticyclonic eddy passes along the slope the northeastward flow at the shelf break would produce an onshore flow in the benthic layer.

A fundamental objective of our work has been to understand the cross front exchange between shelf and slope water. A schematic of cross-shelf exchange processes is given in Fig. 4.1-16. The existence of alongshore advection, structure with scales of 5-20 km and intrusions that may be sheared and hence detached from their source make it difficult to apply a strictly two dimensional model. However, assuming that the cross-frontal exchange processes, the source water types and the air-sea exchange are roughly constant over the 400-500 km frontal boundary of the New York Bight and that the residence time within the bight is 2-3 months, we can assume that these small scale features average out and we can estimate mean cross-shelf fluxes in a two dimensional model.

For example, the pycnocline slope water intrusion often exhibits parcels of high salinity water in the fine structure over the mid-shelf. These may be completely detached parcels or connected to their slope source in the along-shelf dimension. This is illustrated by a section of closely spaced CTD stations across the frontal boundary (Fig. 4.1-17) during the BT cruise in August 1978. We find a complex structure with "detached" parcels of shelf

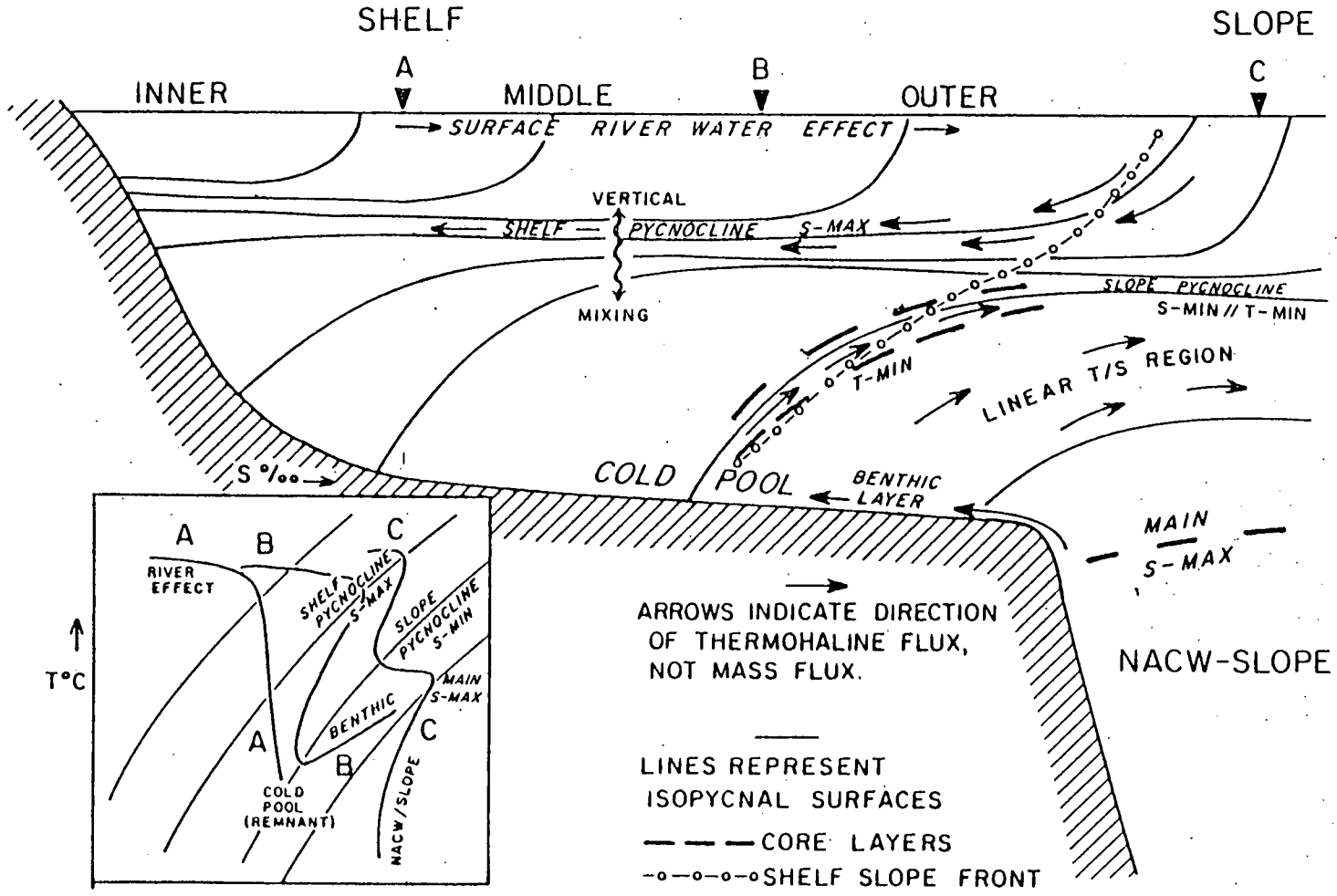
SHELF
SLOPE
A
B
C
INNER
MIDDLE
OUTER
SURFACE RIVER WATER EFFECT
VERTICAL
SHELF PYCNOCLINE S-MAX
MIXING
SLOPE PYCNOCLINE
S-MIN // T-MIN
T-MIN
LINEAR T/S REGION
S °/oo
COLD POOL
BENTHIC LAYER
MAIN S-MAX
NACW-SLOPE
ARROWS INDICATE DIRECTION OF THERMOHALINE FLUX, NOT MASS FLUX.
LINES REPRESENT ISOPYCNAL SURFACES
CORE LAYERS
SHELF SLOPE FRONT
T°C
RIVER EFFECT
SHELF PYCNOCLINE S-MAX
SLOPE PYCNOCLINE S-MIN
MAIN S-MAX
BENTHIC
COLD POOL (REMNANT)
NACW/SLOPE

Fig. 4.1-16

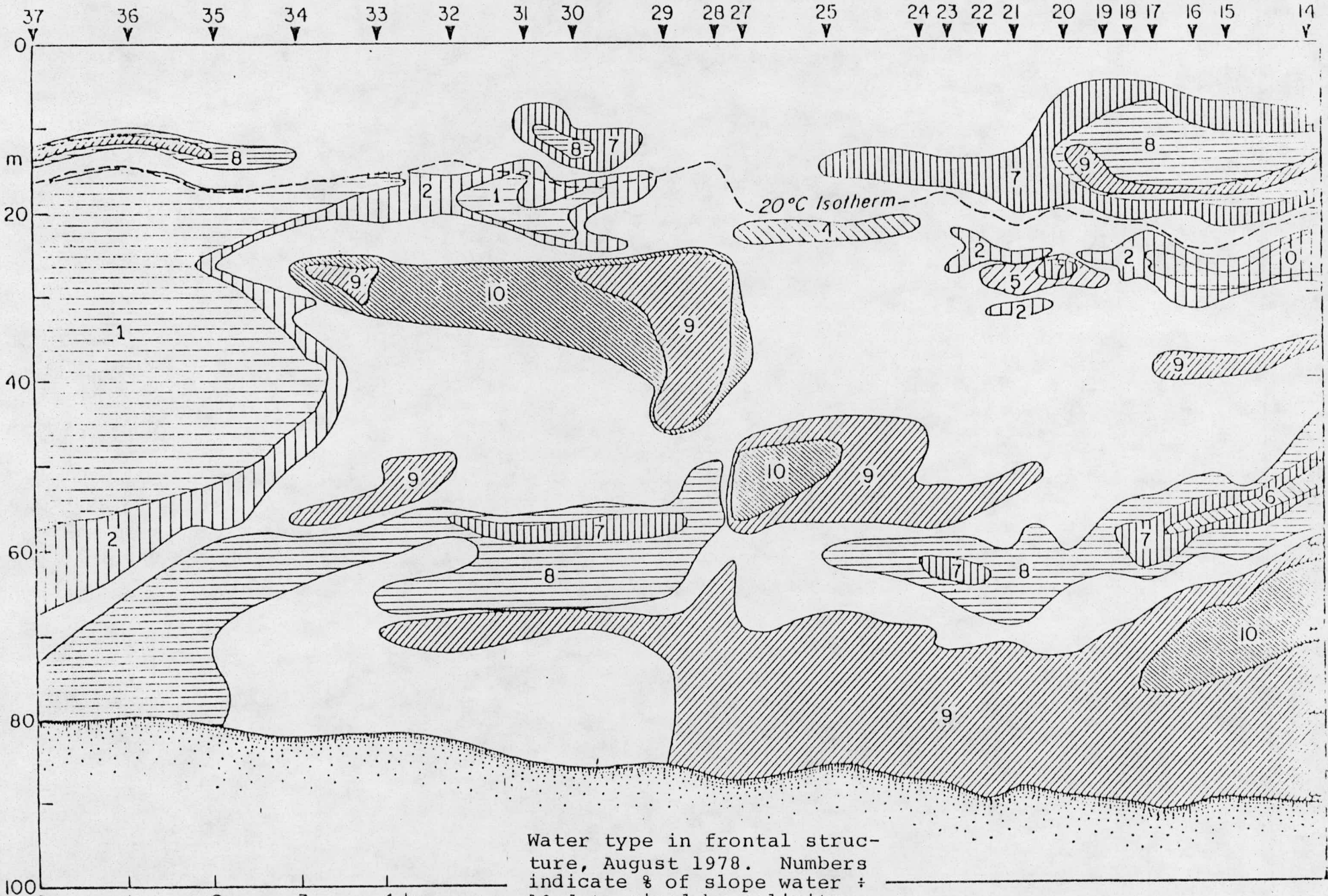

Water type in frontal structure, August 1978. Numbers indicate % of slope water ÷ 10 determined by salinity:

0= S <32.7 °/oo

10 = S >35.0 °/oo

Fig. 4.1-17

4.1/46

and slope water. These may have resulted from the narrow cross-shelf excursion of the frontal boundary shown in Fig. 4.1-18. This demonstrates that lateral advection of the frontal boundary is more rapid than the lateral mixing across the boundary. Once the advective intrusion is detached from its source by the complex current shears that characterize the frontal region, the rate at which it is mixed away does not affect the net cross-shelf flux.

The processes responsible for cross-shelf exchange of shelf and slope water vary with the season. During the winter the shelf water is vertically mixed and the shelf-slope front is baroclinic. Cross shelf exchanges are essentially across isopycnals driven by surface winds and warm core eddies. With summer stratification vertical mixing is inhibited and exchange is predominantly along isopycnal surfaces. This is especially true in layer (1) and (2) where shelf and slope water protrude far across the plane of the front.

The T-S diagrams can be used to identify frontal structures and mixing processes. A composite T-S diagram of all the CTD profiles from the BT section (Fig. 4.1-17) is shown in Fig. 4.1-19. The sharp boundaries between the distinct water parcels produces the gaps and general organization in an otherwise confusing pattern. The cold pool and near surface slope water intrusion are distinct. There are two bands where vertical mixing and lateral intrusions between shelf and slope water predominate in the lower surface of the pycnocline.

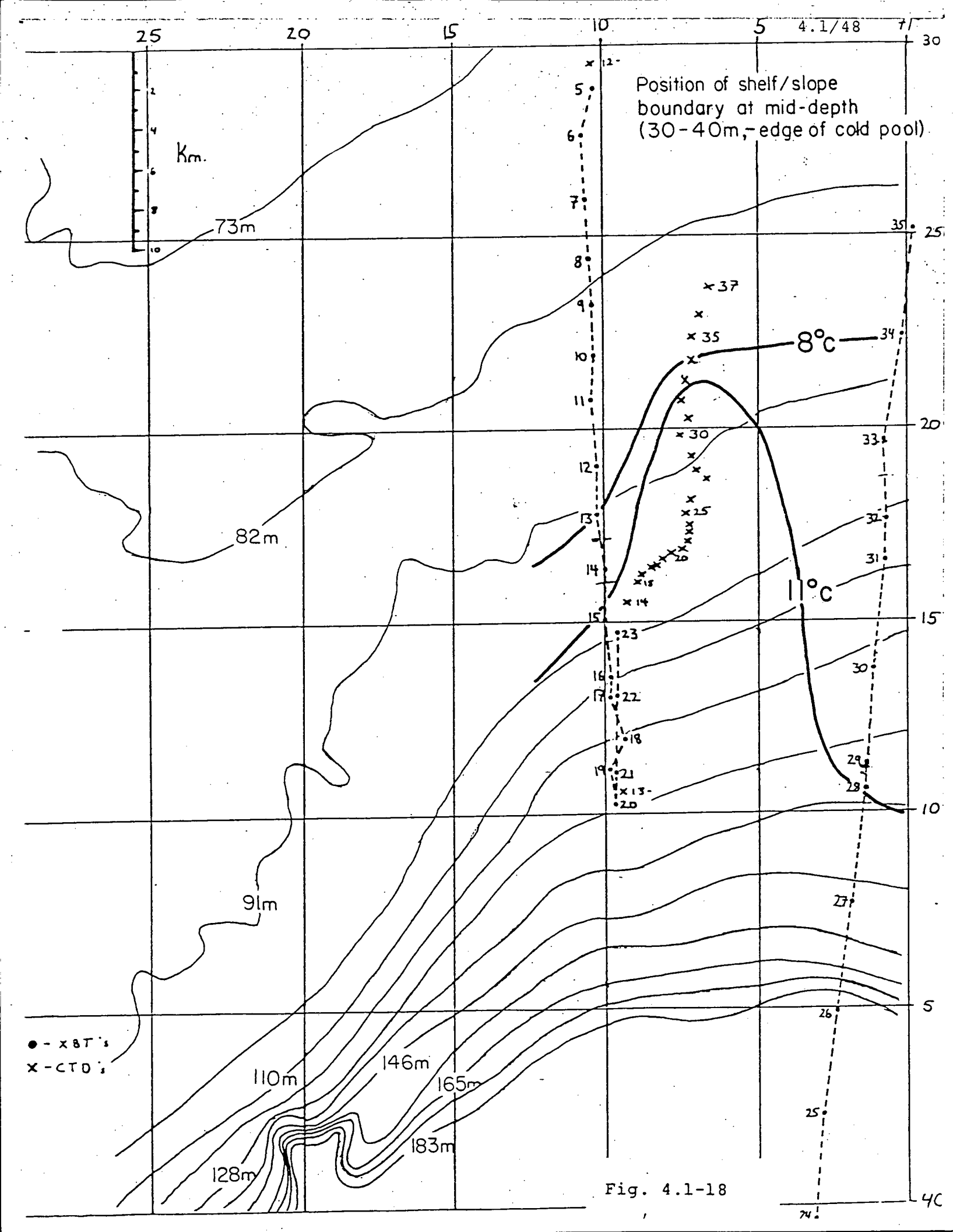
25
20
15
10
5
4.1/48
Position of shelf/slope boundary at mid-depth (30-40m, - edge of cold pool)
Km.
73m
82m
91m
110m
146m
165m
183m
128m
8°C
11°C
● - XBT's
× - CTD's

Fig. 4.1-18

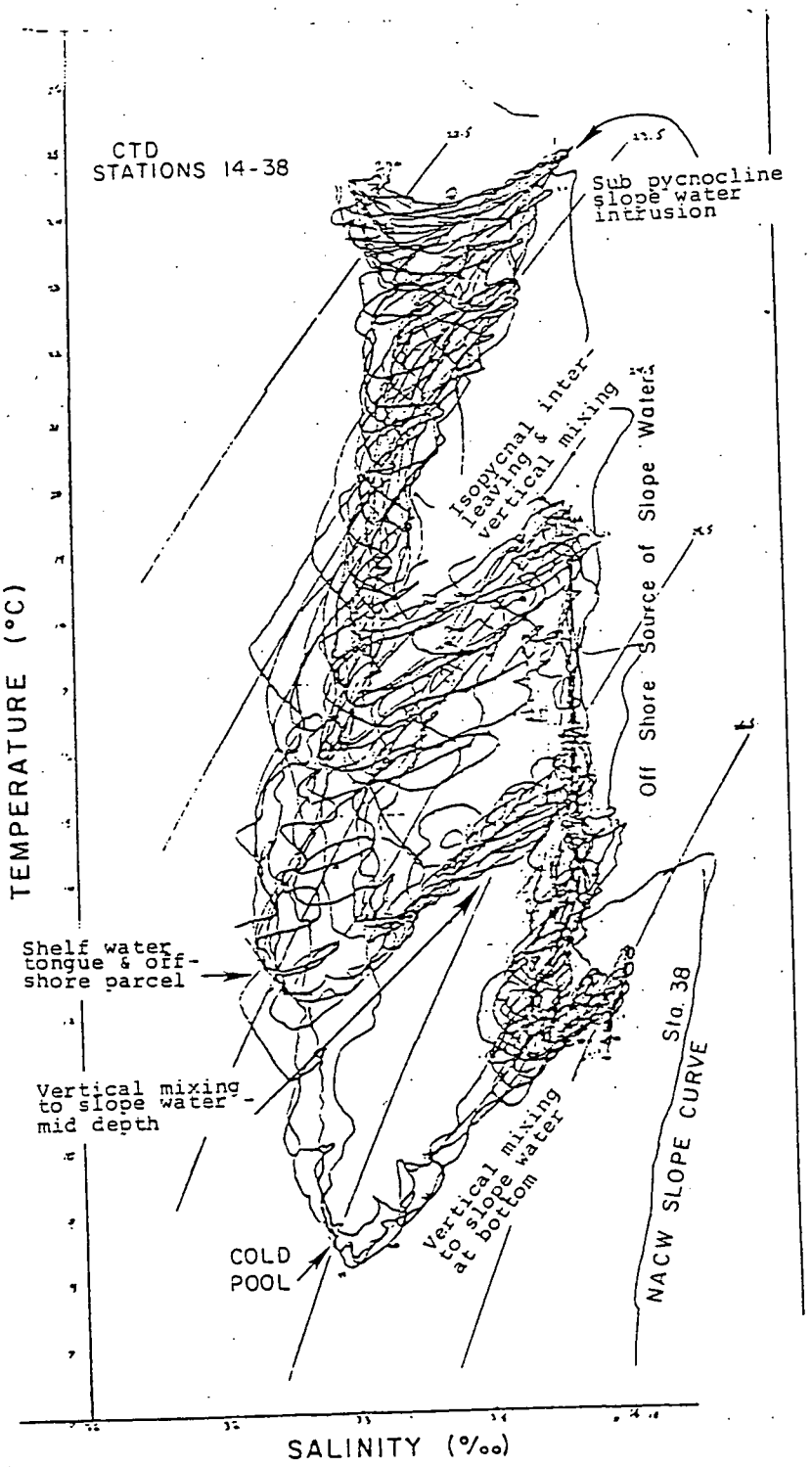
CTD
STATIONS 14-38
Sub pycnocline
slope water
intrusion
Isopycnal inter-
leaving &
vertical mixing
Off Shore Source of Slope Water
Shelf water
tongue & off-
shore parcel
Vertical mixing
to slope water -
mid depth
COLD
POOL
Vertical mixing
to slope water
at bottom
Sta. 38
NACW SLOPE CURVE
TEMPERATURE (°C)
SALINITY (‰)

Fig. 4.1-19

The dominant exchange processes with the cold pool are less obvious. Above 70 m the frontal boundary is thermohaline so there is isopycnal communication between the cold pool and slope water. The change in the position of the cold pool water in T-S space is used to evaluate the relative importance of the various exchange modes with the cold pool. In Fig. 4.1-20 a schematic of the T-S correlation of a profile at the shelf break is shown. The arrows show the evolution of the cold pool due to (A) vertical mixing with the warm fresh surface water, (B) vertical mixing with the slope water intrusion, (C) isopycnal mixing with slope water, (D) and (E) mixing with the benthic layer.

Examples of the cold pool evolution are shown in Fig. 4.1-21 where we plot the position in T-S space of the minimum temperature in the cold pool for four different years. The seasonal evolution is primarily along isopycnal surfaces. In the summer of 1966 the stratification weakened, increasing the vertical mixing while in 1979 the entire T-S correlation curve shifted vertically between March and May. Thus it appears that the dominant mixing processes are (A) and (B) and their relative importance changes seasonally and interannually.

Since the slope water intrusion (layer (2) in Fig. 4.1-14) extends to the mid-shelf, vertical mixing into the cold pool via (A) or (B) should be different. Process (A) would mix heat but not salt into the cold pool. The profiles from a

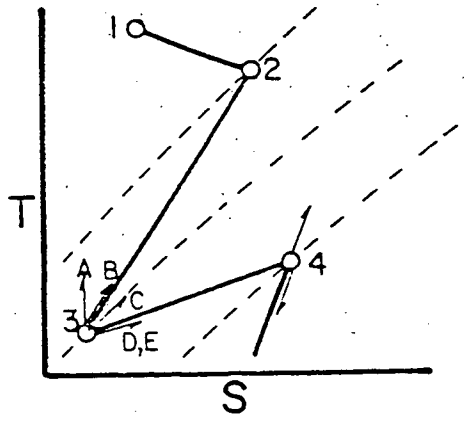

Fig. 4.1-20

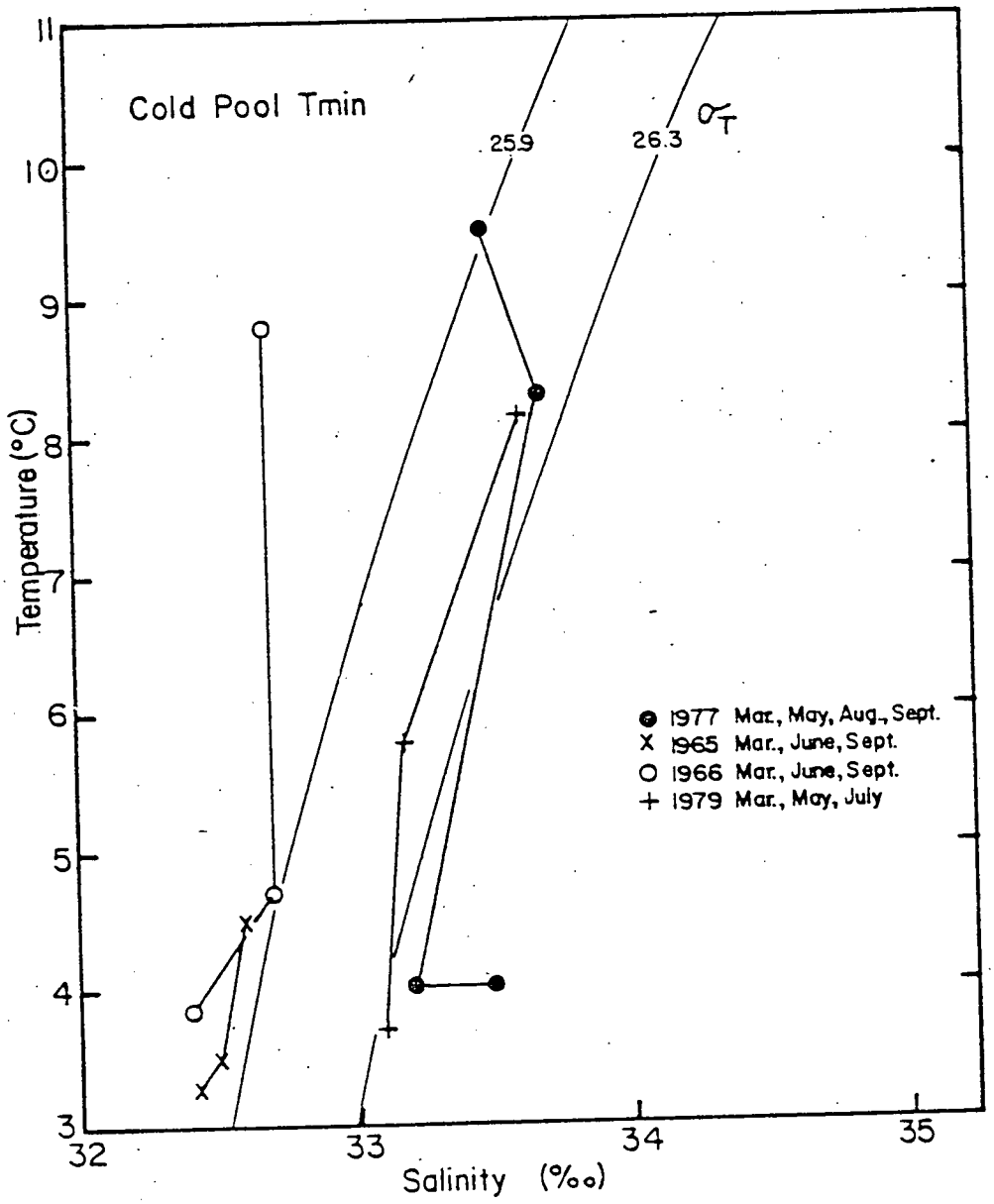
Cold Pool Tmin
25.9
26.3
σ_T
Temperature (°C)
Salinity (‰)
11
10
9
8
7
6
5
4
3
32
33
34
35
1977 Mar., May, Aug., Sept.
1965 Mar., June, Sept.
1966 Mar., June, Sept.
1979 Mar., May, July

Fig. 4.1-21

series of stations across the shelf (Fig. 4.1-22; 23) when the slope intrusion was fully developed do not show this effect. Of course the lateral mixing within the cold pool could eliminate any subtle across-shelf differences.

Across most of the shelf the cold pool is laterally well mixed with very weak horizontal gradients. The temperature minimum, which occurs above the shelf floor because of the benthic intrusion, lies on an isopycnal surface. The transition to slope water characteristics occurs rapidly across a narrow frontal boundary. If isopycnal mixing were vigorous we might expect to find in T-S space the series of curves shown in Fig. 4.1-24 as one moves across the frontal boundary. This is especially true since density surfaces enclose larger volumes of water in the cold pool than they do on the slope water side of the front. The lateral mixing along the isopycnal surfaces should extend the cold pool water influence offshore. Instead we consistently find the pattern where the locus of the cold pool T-min moves along the main mixing curve and not the isopycnal passing through the inner shelf cold pool (see Fig. 4.1-23, sta. 250 and Fig. 4.1-25, sta. 59-63). Mixing of denser water from the benthic layer could account for this.

The existence of parcels of slope water imbedded in the cold pool on the isopycnal of the T-min is additional evidence for the weakness of isopycnal mixing near the front. An example of this is station 251 in Fig. 4.1-23 and 26. The

series of stations across the shelf (Fig. 4.1-22; 23) when the slope intrusion was fully developed do not show this effect. Of course the lateral mixing within the cold pool could eliminate any subtle across-shelf differences.

Across most of the shelf the cold pool is laterally well mixed with very weak horizontal gradients. The temperature minimum, which occurs above the shelf floor because of the benthic intrusion, lies on an isopycnal surface. The transition to slope water characteristics occurs rapidly across a narrow frontal boundary. If isopycnal mixing were vigorous we might expect to find in T-S space the series of curves shown in Fig. 4.1-24 as one moves across the frontal boundary. This is especially true since density surfaces enclose larger volumes of water in the cold pool than they do on the slope water side of the front. The lateral mixing along the isopycnal surfaces should extend the cold pool water influence offshore. Instead we consistently find the pattern where the locus of the cold pool T-min moves along the main mixing curve and not the isopycnal passing through the inner shelf cold pool (see Fig. 4.1-23, sta. 250 and Fig. 4.1-25, sta. 59-63). Mixing of denser water from the benthic layer could account for this.

The existence of parcels of slope water imbedded in the cold pool on the isopycnal of the T-min is additional evidence for the weakness of isopycnal mixing near the front. An example of this is station 251 in Fig. 4.1-23 and 26. The

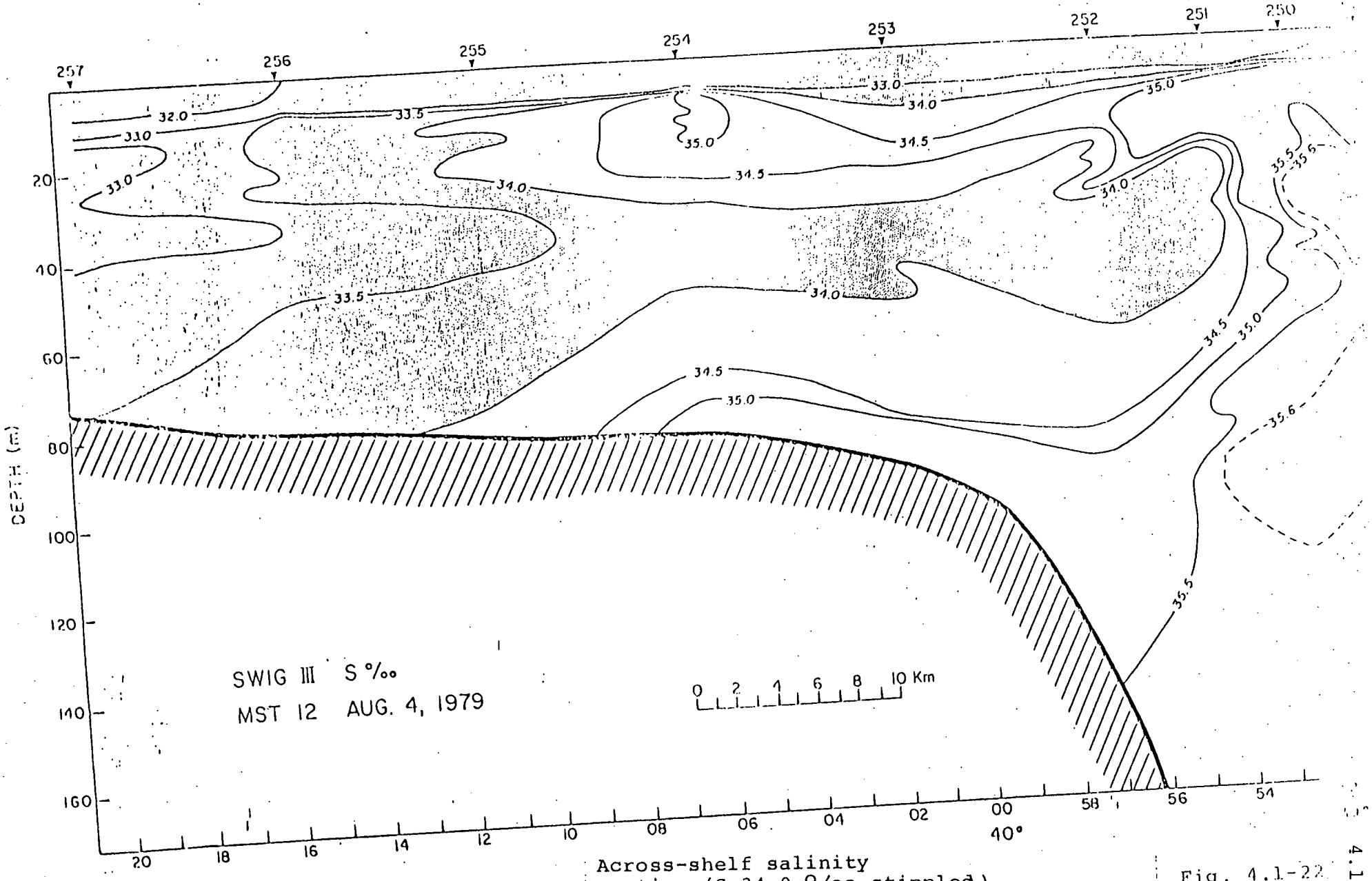

Across-shelf salinity section (S<34.0 °/oo stippled) from an NSF supported study of frontal fine structure.

Fig. 4.1-22

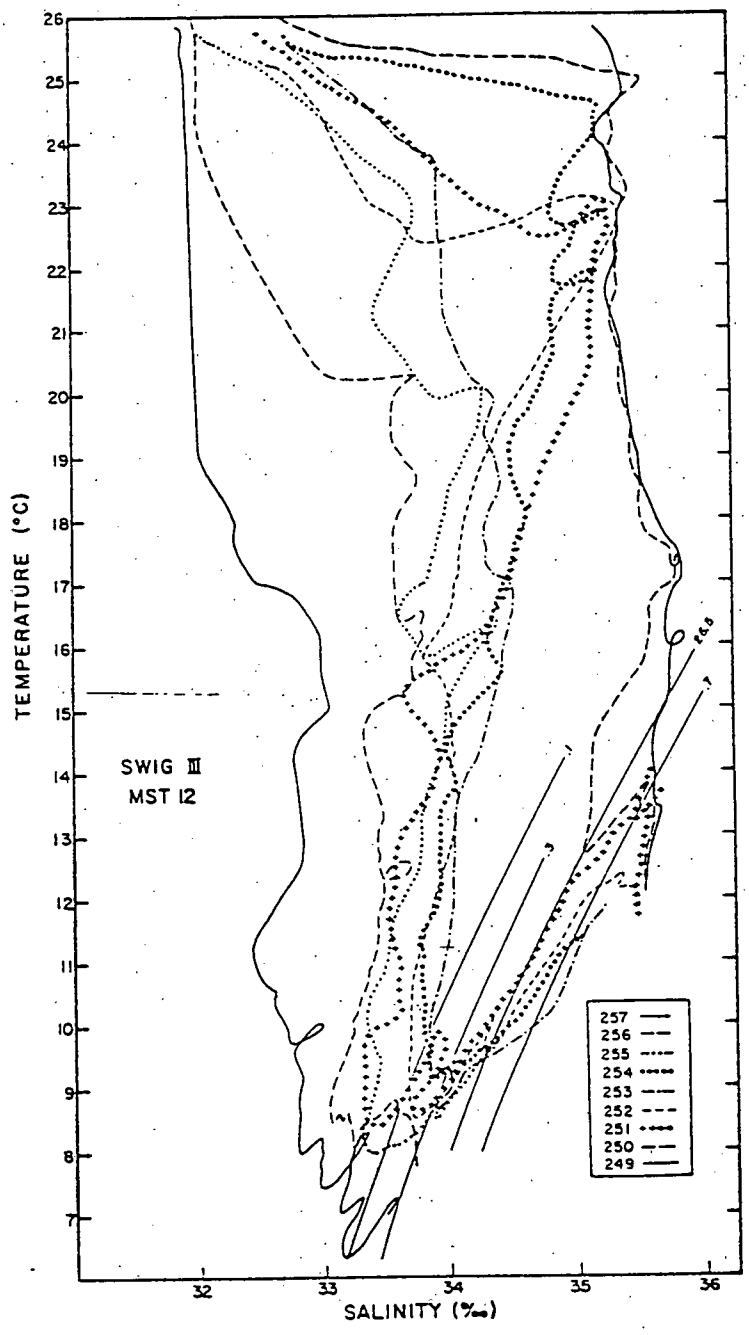
TEMPERATURE (°C)
SALINITY (‰)
SWIG III
MST 12
257
256
255
254
253
252
251
250
249

Fig. 4.1-23

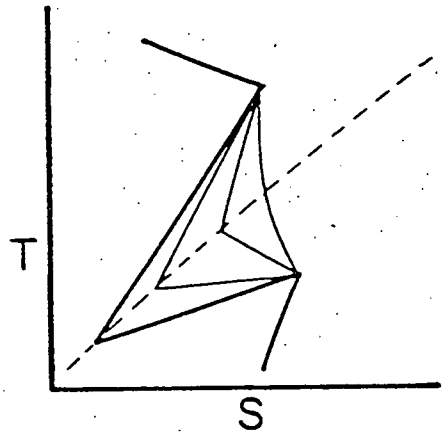

Fig. 4.1-24

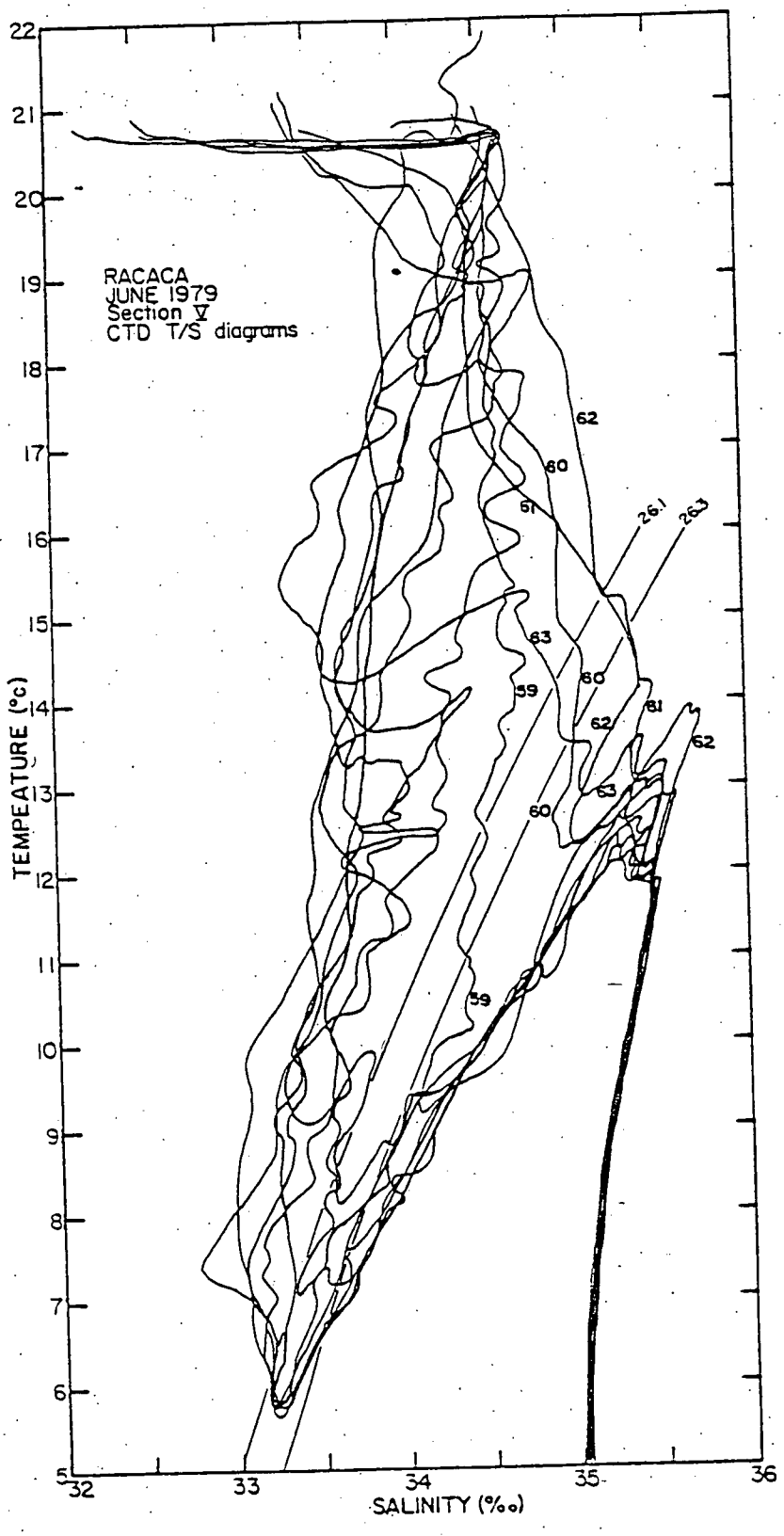
RACACA
JUNE 1979
Section V
CTD T/S diagrams
TEMPEATURE (°c)
SALINITY (‰)
22
21
20
19
18
17
16
15
14
13
12
11
10
9
8
7
6
5
32
33
34
35
36
62
60
61
26.1
26.3
63
59
60
61
62
62
63
60
59

Fig. 4.1-25

parcel of water may or may not be attached to its slope water source, but the advection (or large scale turbulence) which drives it onto the shelf dominates the small scale isopycnal turbulence that mixes it into the shelf water.

The frontal boundary remains remarkably sharp throughout the summer. In August 1979 there was a 5°C gradient over 1 km (see Fig. 4.1-26). From Okubo's scaling (1971) this implies a local lateral diffusivity coefficient, K_L, of approximately $5 \times 10^3 cm^2/s$. With this value of K_L approximately 40 days are required to spread an infinitely sharp frontal boundary to a width of 1 km.

Between May and August 1979, the mean temperature of the cold pool increased by 2°C. Assuming that this is the result of lateral isopycnal mixing through the frontal boundary yields a K_L of 4×10^4 cm^2/s. This relatively low value of K_L is consistent with both the net flux of heat into the cold pool and the sharpness of the frontal boundary.

It may be inappropriate to model the mixing over the shelf in the cold pool as a simple turbulent diffusive process. Oceanic forcing strains the frontal boundary into a highly convoluted surface. The resulting intrusions of shelf and slope water can be sheared into detached parcels that subsequently mix away at a very slow rate. Thus we often find small pockets of slope water imbedded in otherwise well mixed shelf water. Because of the remnants of these slope water parcels, the gradients across the cold pool are not monotonic, as

illustrated in Fig. 4.1-26. There are pockets of colder water as the cold pool warms throughout the summer.

The extreme case of this process is calving of the cold pool. Such a process removes cold pool water from the shelf without altering the T-S properties of the remaining water. Thus it is more difficult to estimate the importance and persistence of this process since direct observation is required. No calving was observed during the RACACA cruise. There does not exist enough hydrographic data over the shelf and slope for all seasons to establish the statistics of calving size and frequency necessary to estimate the removal of shelf water by this process.

Slope water intrusions onto the shelf occur via layer (2) and (4) (in Fig. 4.1-14) or by large cross-shelf displacements of the frontal boundary of layer (3). In the late summer the structure of the cold pool as it is finally breaking up should help to distinguish the relative importance of these three processes.

D. Pycnocline Salinity Maximum

A pronounced maximum in salinity (S-max), associated with the upper part of the seasonal pycnocline in the summer-autumn seasons, is consistently observed over the outer shelf of the Middle Atlantic Bight. This pycnocline S-max is very clear in the KNORR, August 1977, section off Long Island (fig. 4.1-27), and its T-S characteristics are almost identical with those of the slope water regime (see letter (B) of the August 77 T-S

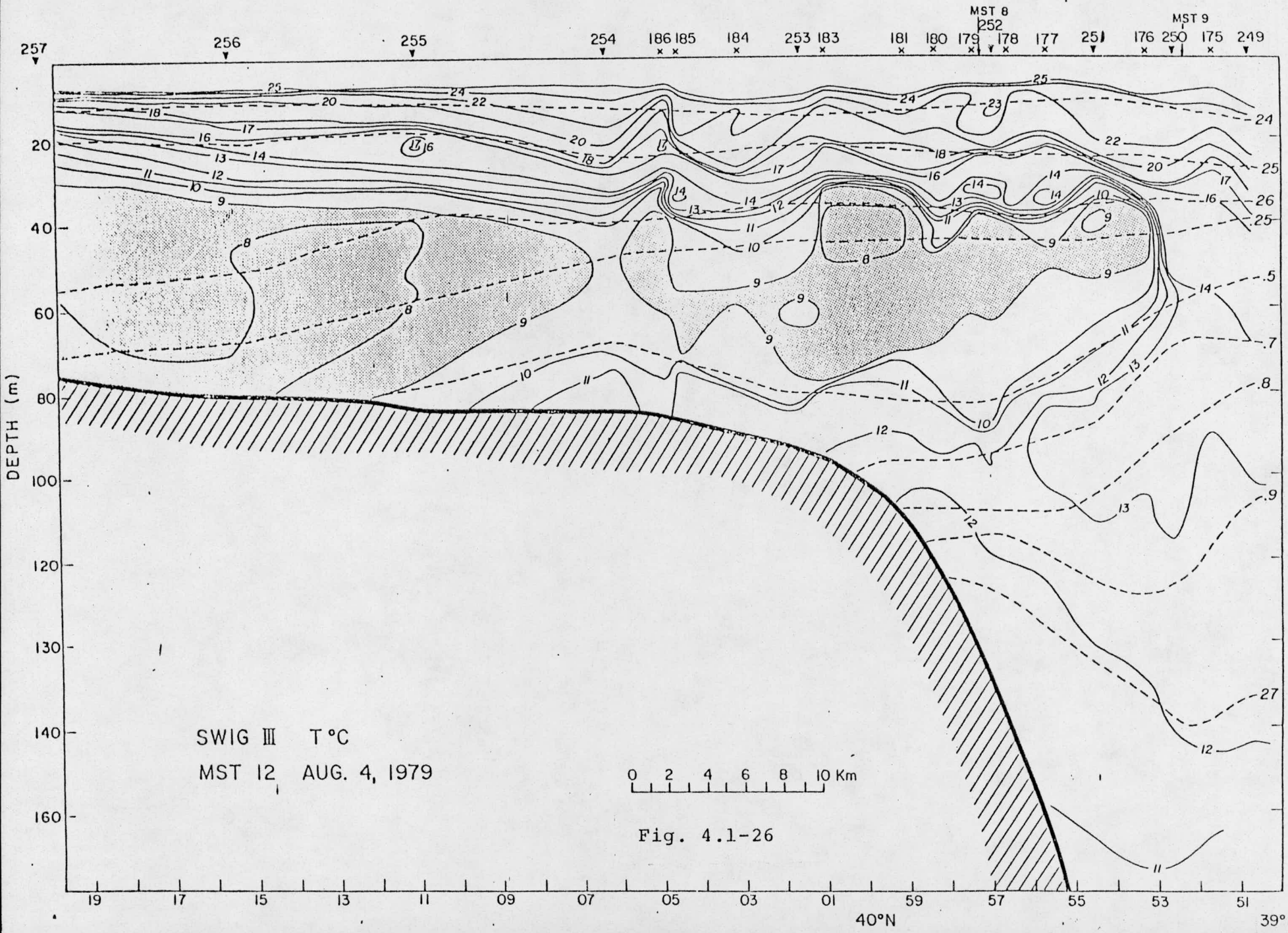
MST 8
MST 9
257
256
255
254
186 185
184
253 183
181
180
179
252
178
177
251
176
250
175
249
DEPTH (m)
20
40
60
80
100
120
130
140
160
SWIG III T °C
MST 12 AUG. 4, 1979
0 2 4 6 8 10 Km
19
17
15
13
11
09
07
05
03
01
59
57
55
53
51
40°N
39°N

Fig. 4.1-26

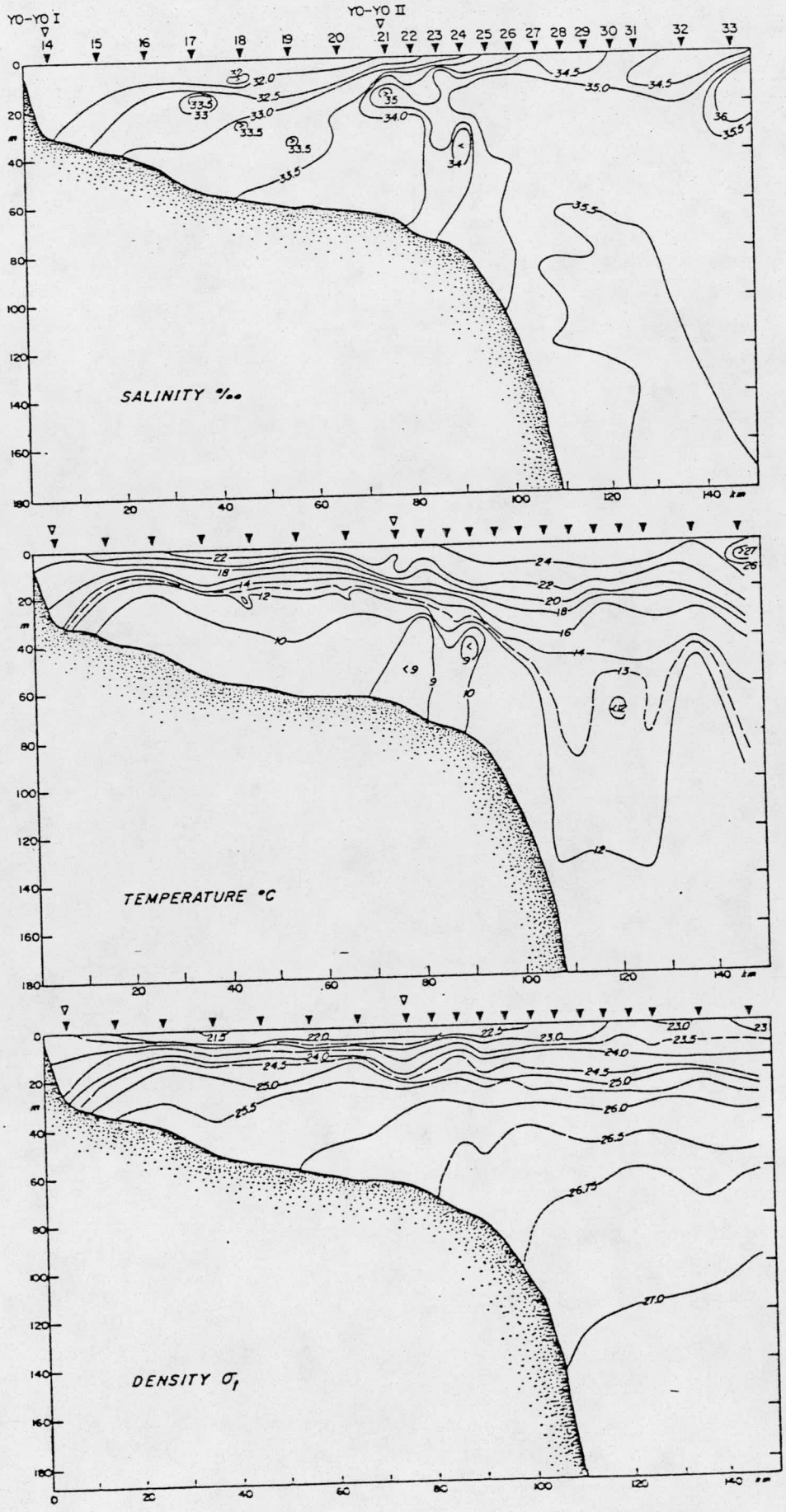
YO-YO I
YO-YO II
14 15 16 17 18 19 20 21 22 23 24 25 26 27 28 29 30 31 32 33
SALINITY ‰
TEMPERATURE °C
DENSITY σ_t
m
km

Fig. 4.1-27

diagram, Fig. 4.1-12a). It is induced by a nearly isopycnal transfer of slope water to the outer shelf, possible only in the stratified seasons when isopycnals are continuous across the shelf/slope front.

A conceptual model of the cross-shelf advective-mixing pattern associated with the S-max (represented in Fig. 4.1-28) is explained in detail in the reprint of the publication (Gordon and Aikman, 1980) in the appendix. It is concluded that the slope to shelf salt flux required to produce and maintain this seasonal intrusion may supply about one half of the salt required to balance the annual river input into the shelf water of the Middle Atlantic Bight.

E. Warm Core Eddies

Warm core eddies, rings of Sargasso water encapsulated by a Gulf Stream meander, are prominant features of the slope water from Nova Scotia to Hatteras. There has been considerable research on their role in cross-shelf exchange (Morgan and Bishop, 1977) and coastal dynamics and Rossby wave radiation (P. Smith, personal communication). A warm core eddy was crossed during the 1979 RACACA cruise (see section I). We describe here an eddy observed during the July 1975 CONRAD cruise.

The eddy core was winter cooled and was distinguished by being located to the right of Iselin's NACW line in a T-S diagram (see Fig. 4.1-29). The position of the eddy, denoted

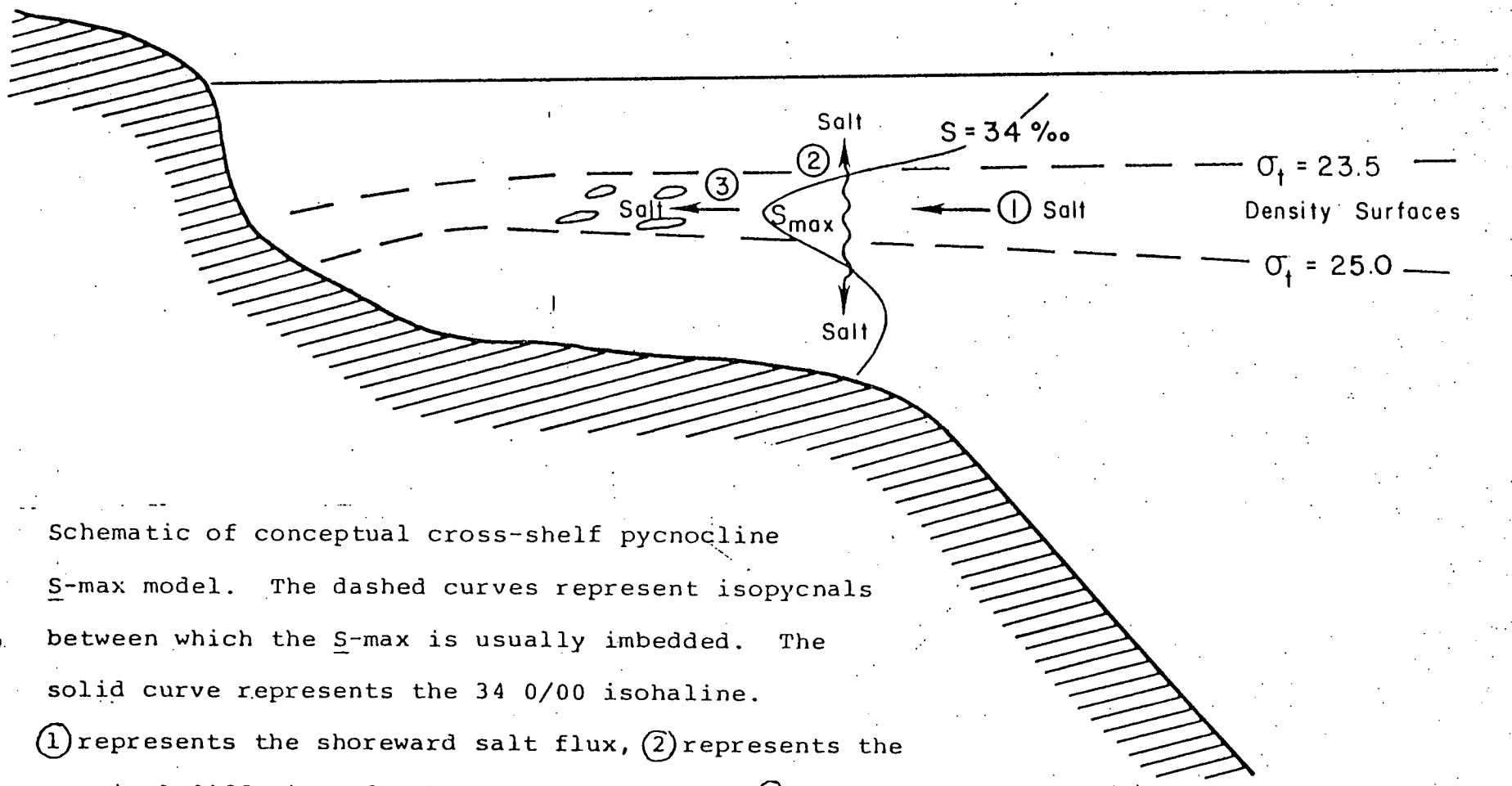

Schematic of conceptual cross-shelf pycnocline S-max model. The dashed curves represent isopycnals between which the S-max is usually imbedded. The solid curve represents the 34 0/00 isohaline. ① represents the shoreward salt flux, ② represents the vertical diffusion of salt out of the S-max, ③ represents the growth rate of excess salt of the pycnocline S-max.

Fig. 4.1-28

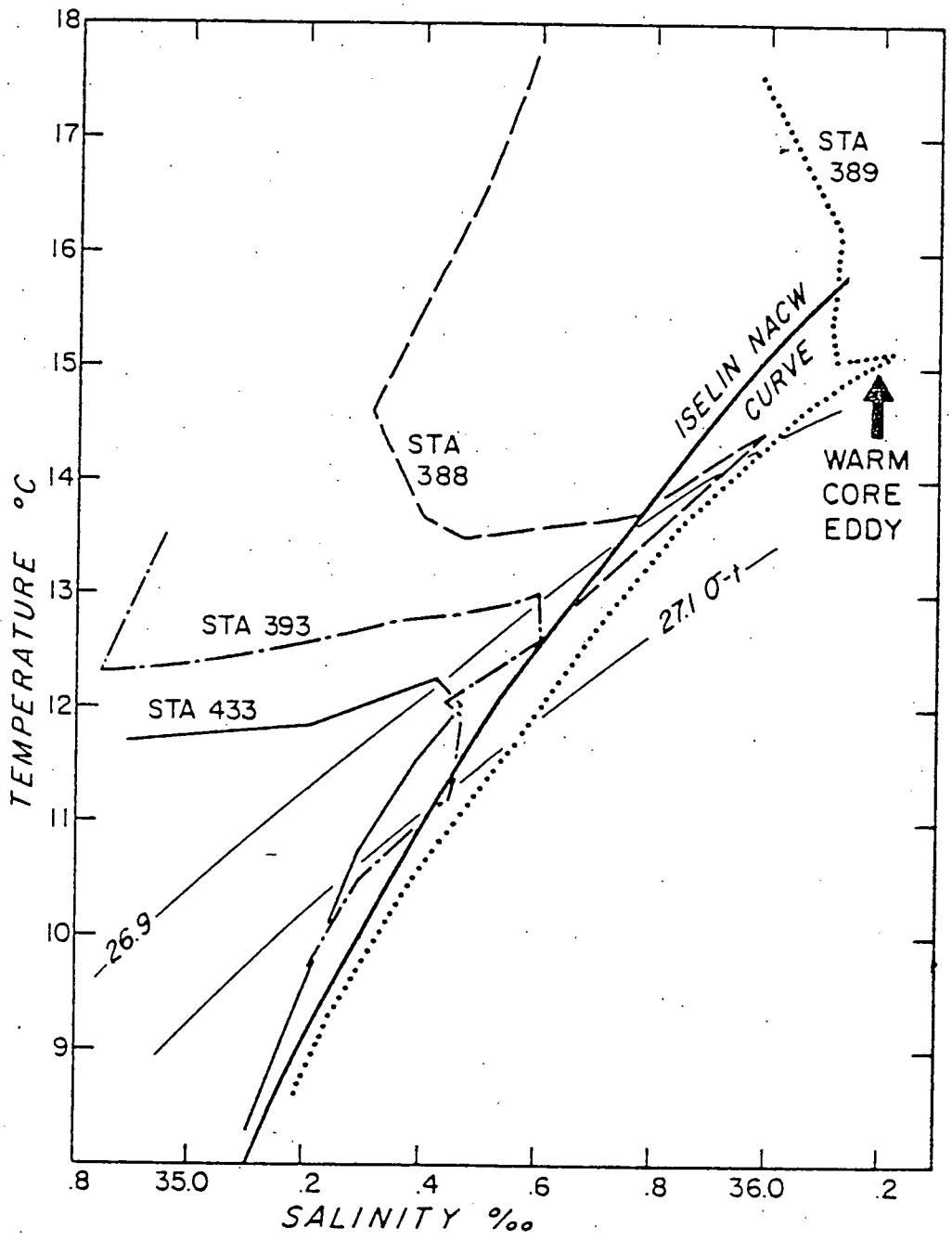
18
17
16
15
14
13
12
11
10
9
TEMPERATURE °C
STA 389
ISELIN NACW CURVE
STA 388
WARM CORE EDDY
STA 393
27.1 σ-t
STA 433
26.9
.8
35.0
.2
.4
.6
.8
36.0
.2
SALINITY ‰

Fig. 4.1-29

by the topography of the 15° isotherm shown in Fig. 4.1-30, coincides with that shown on the NAVOCEANO Frontal Analysis maps and has a diameter of approximately 100 km centered near station 384. A temperature section from the center to the shelf (Fig. 4.1-31a)shows the deep mixed core of the eddy with isotherms rising steeply up the slope. Temperature sections derived from other cruises when eddies were not present show roughly horizontal isotherms over the slope, with negligible seasonal fluctuations below 150 m. Using this average thermal structure we calculated the thermal anomalies shown in Fig. 4.1-32. The maximum anomaly of 8°C at 400 m depth is comparable to the anomaly structure of cyclonic rings (Hagan et al., 1978). However, along the slope upward isotherm displacements of 40-70 m produce temperature anomalies of -1 to +2°C. These displacements which are greatest where the eddy intersects the slope, are most likely upslope Ekman veering in a bottom boundary layer and not just internal wave distortion. It does, however, seem curious that this boundary effect extends 150 m or more above the shelf floor. A model of the bottom boundary layer by Weatherly and Martin (1978) for an interior flow of 0.15 m s^{-1} shows a distinct bottom layer with thickness of 9 m for a stratified water column with N_o=1.25 x $10^{-2}s^{-1}$, but a more ambiguous layer 50-70 m thick for an unstratified water column, i.e. N_o=4 x $10^{-3}s^{-1}$, but the interior flow is larger. Saunders (1971) has measured currents

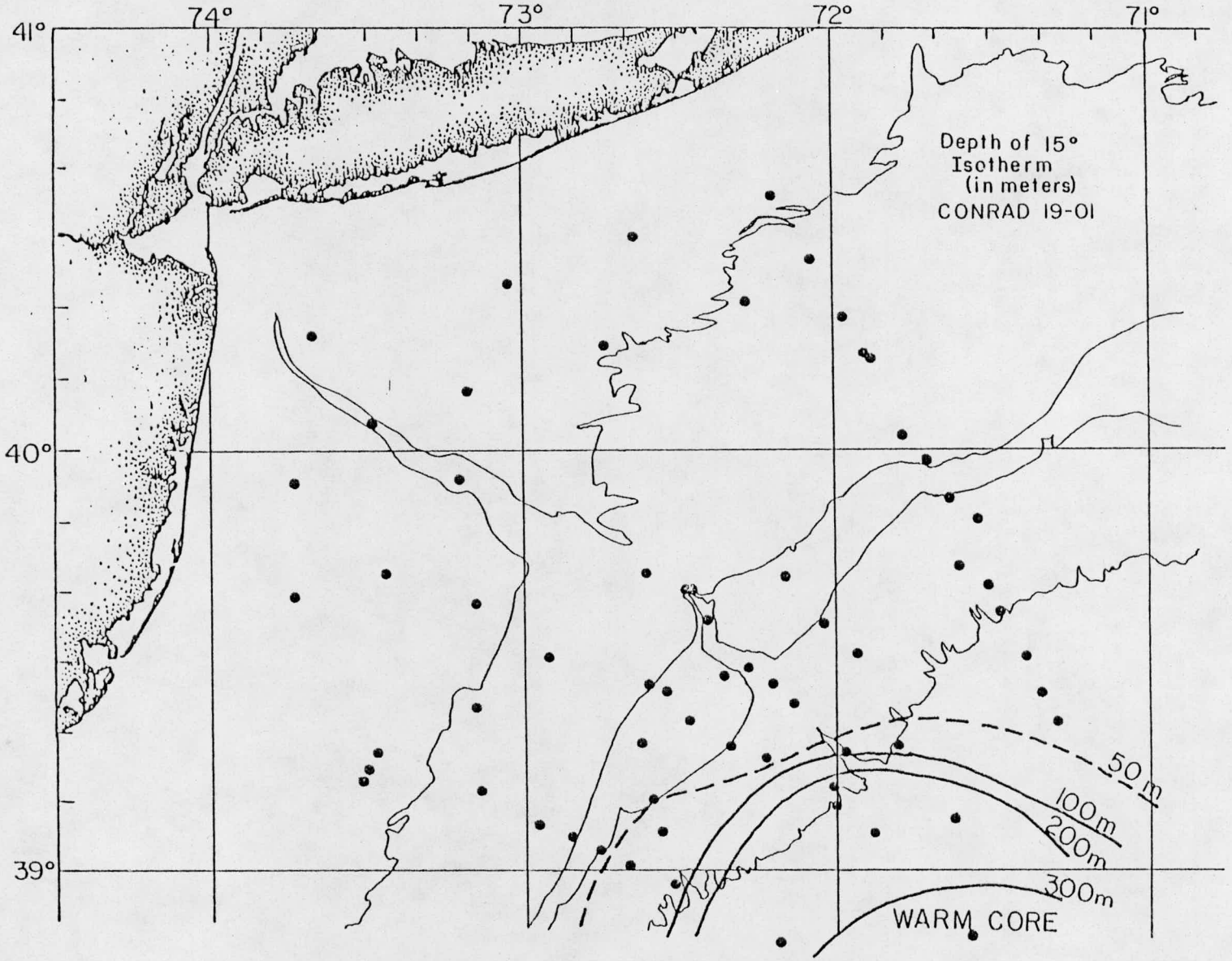
74°
73°
72°
71°
41°
40°
39°
Depth of 15°
Isotherm
(in meters)
CONRAD 19-01
50 m
100m
200m
300m
WARM CORE

Fig. 4.1-30

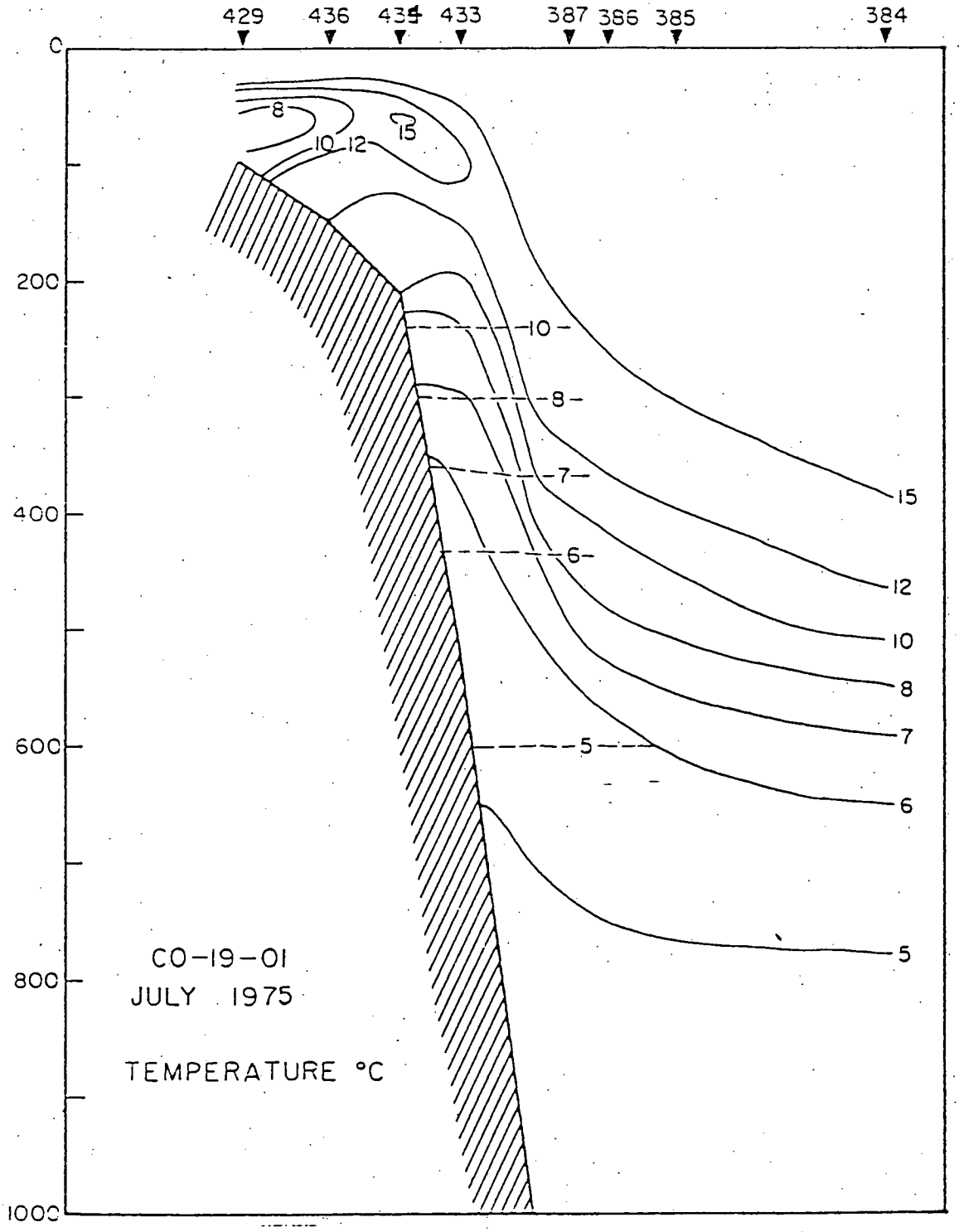

Temp. section through warm core eddy.

Fig. 4.1-31a

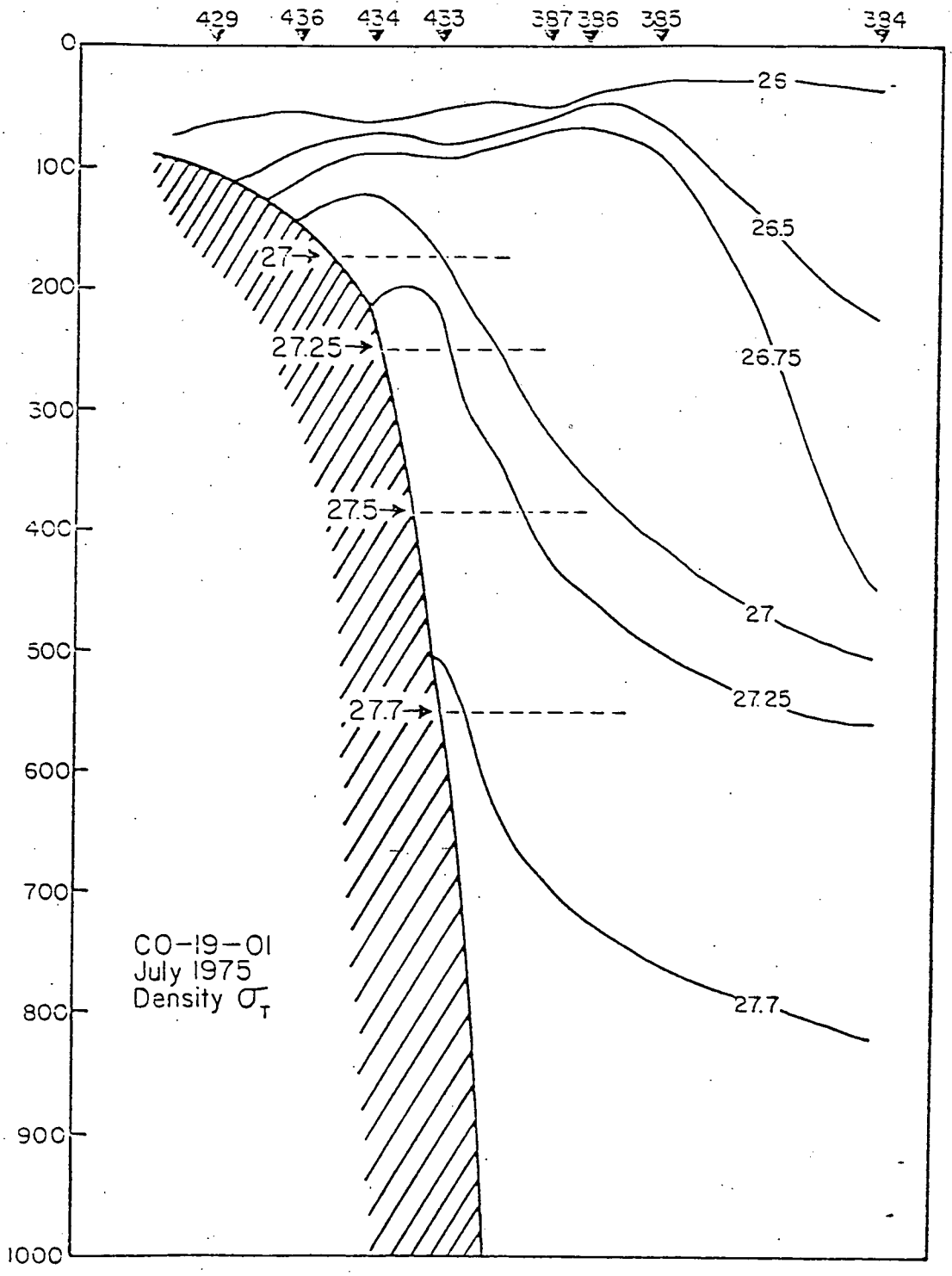

Density section through warm core eddy.

Fig. 4.1-31b

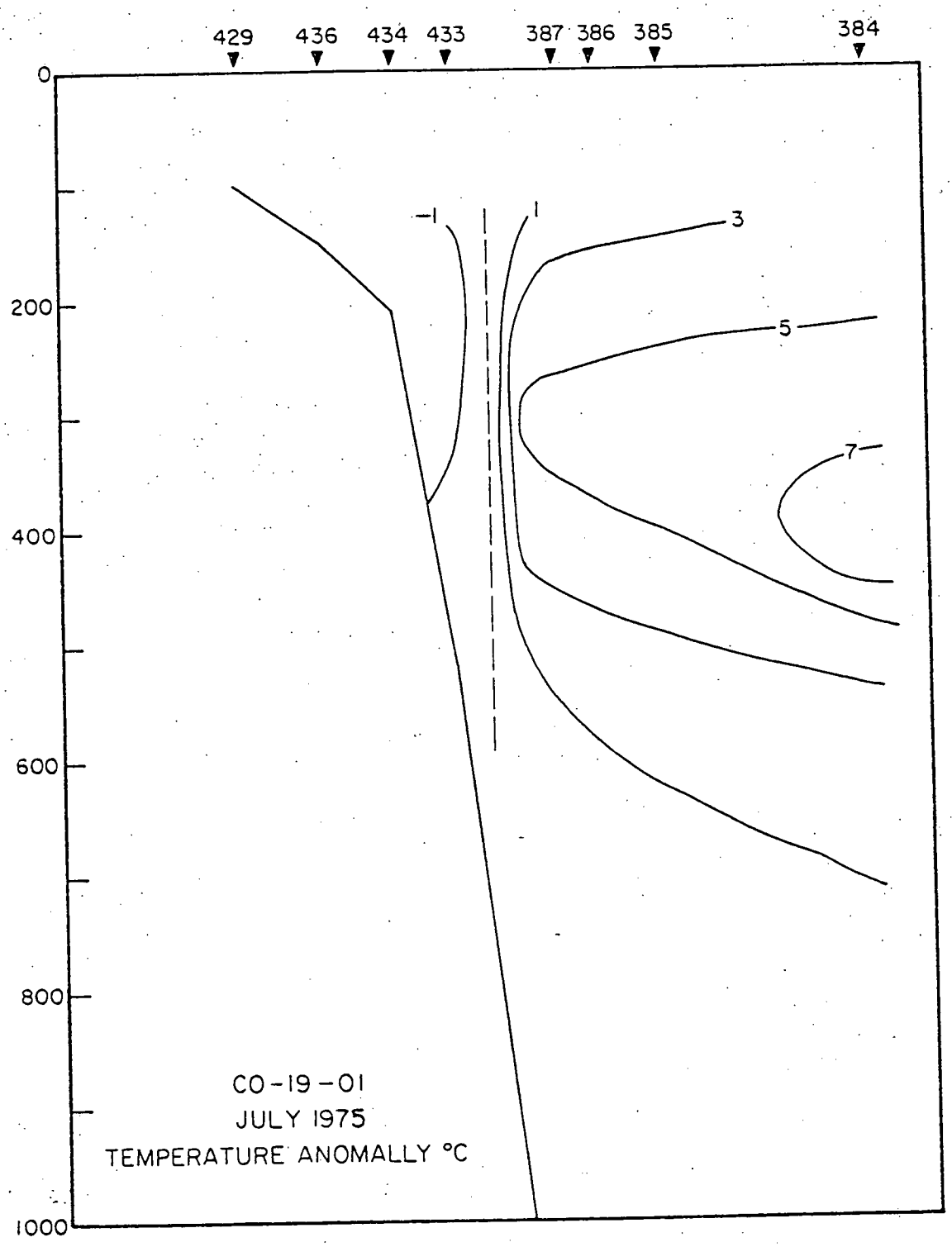
429
436
434
433
387
386
385
384
0
200
400
600
800
1000
-1
1
3
5
7
CO-19-01
JULY 1975
TEMPERATURE ANOMALLY °C

Fig. 4.1-32

.40 - .70 $m \cdot s^{-1}$ in a warm core eddy. If currents of this magnitude can penetrate the slope region then bottom boundary layers greater than 100 m are possible. However, the temperature profile over the slope, e.g. Sta. 433 (Fig. 4.1-30, does not show a well mixed region at the bottom.

It is also possible that up slope displacement is simply the conversion of kinetic to potential energy. Equating the two and neglecting friction we have $1/2\ \rho v^2 = \Delta\rho g h$ where v is the water velocity, h the vertical displacement, g the gravitational acceleration and $\Delta\rho$ the difference between the densities of the intruding and displaced water (Fig. 4.1-31b). Solving for h we have:

$$h = \frac{v^2\ \rho}{2g\ \Delta\rho}$$

For $\frac{\Delta\rho}{\rho} = .5 \times 10^{-3}$ and v = 50 cm/s we get h = 25 m. Thus velocities that have been measured in a warm core ring could lead to up slope intrusions comparable to our observations.

Our primary interest in these warm core eddies is to determine their role in heat and salt exchange onto the shelf. Because of the apparent upslope flow the temperature on the floor at the shelf-slope break will drop when a warm core eddy is incident on the slope. The S-max also moves upslope, distorting the base of the shelf-slope front. The salinity of the shelf water is so variable that it is impossible with our limited data set to determine whether this results in a net flux of salt onto the shelf.

The primary decay mechanism of Gulf Stream rings is thought to be isopycnal exchange from the core to the surrounding water (Lambert, 1974; Cheney and Richardson, 1976). Such processes are evident in the T-S diagram shown in Fig.4.1-29. Normally shelf water mixes with slope water on or slightly fresher than the NACW curve at 100 m depth. The T-S plot for Sta. 388 crosses the NACW line on the ρ=26.9 σ_t surface which passes into the eddy core (Sta. 389). The 27.0 σ_t density surface which normally is horizontal over the slope and intercepts the shelf between 120-175 m now dips down to 400-500 m in the eddy core. Thus the shelf waters can communicate isopycnally with a much larger volume of warm saline water.

The role of these warm core eddies in the salt balance in the shelf waters is uncertain. To balance the fresh water input onto the shelf requires approximately 2000 km^3/y of 35°/$_{oo}$ slope water (Wright, 1976; Gordon, 1977, abstract at 1977 Mid-Atlantic Bight Workshop). An equivalent amount of salt is derived from 1940 km^3/y of 36°/$_{oo}$ warm core eddy water. The upper 200 m of an eddy with a 50 km radius has a volume of 1560 km^3. Since there is an average of at least 3 eddies incident on the slope per year, they alone, if their water is mixed onto the shelf, could easily modify the salt balance.

We observe intrusions of shelf and slope water off and onto the shelf at the perimeter of the eddy similar to but smaller in magnitude to those reported by Morgan and Bishop (1977).

The data does not permit an accurate estimate of flux rates. We expect that warm core eddies are more effective at extracting shelf water off the shelf by entrainment than driving slope water onto the shelf, since the turbulent kinetic energy is greater in the eddy than on the shelf and the salinity maximum at 1000 m is below the more energetic currents near the surface of the eddy. The degree to which these intrusions are mixed to produce a net exchange of salt onto the shelf has yet to be evaluated. Given the infrequency of warm core eddies and the fluctuation of salinity on the shelf, one can only speculate on the relative importance of eddy induced shelf-slope water exchanges compared to isopycnal mixing that persists at the shelf-slope front throughout the year.

F. Temperature-Oxygen Relation

During most of the DOE cruises samples for oxygen concentration determinations were obtained. The T/O_2 relation for October 1974, July 1975, January 1976, August 1977, is given in Figure 4.1-33a,b,c.

Two points are now developed: (1) the migration of the T/O_2 portion of the shelf remnant winter water toward lower oxygen during the stratified period; and (2) the occurrence of a super-saturated layer in the summer thermocline, strongest at near 12°-16°C in July 1975 and above 16°C in August 1977.

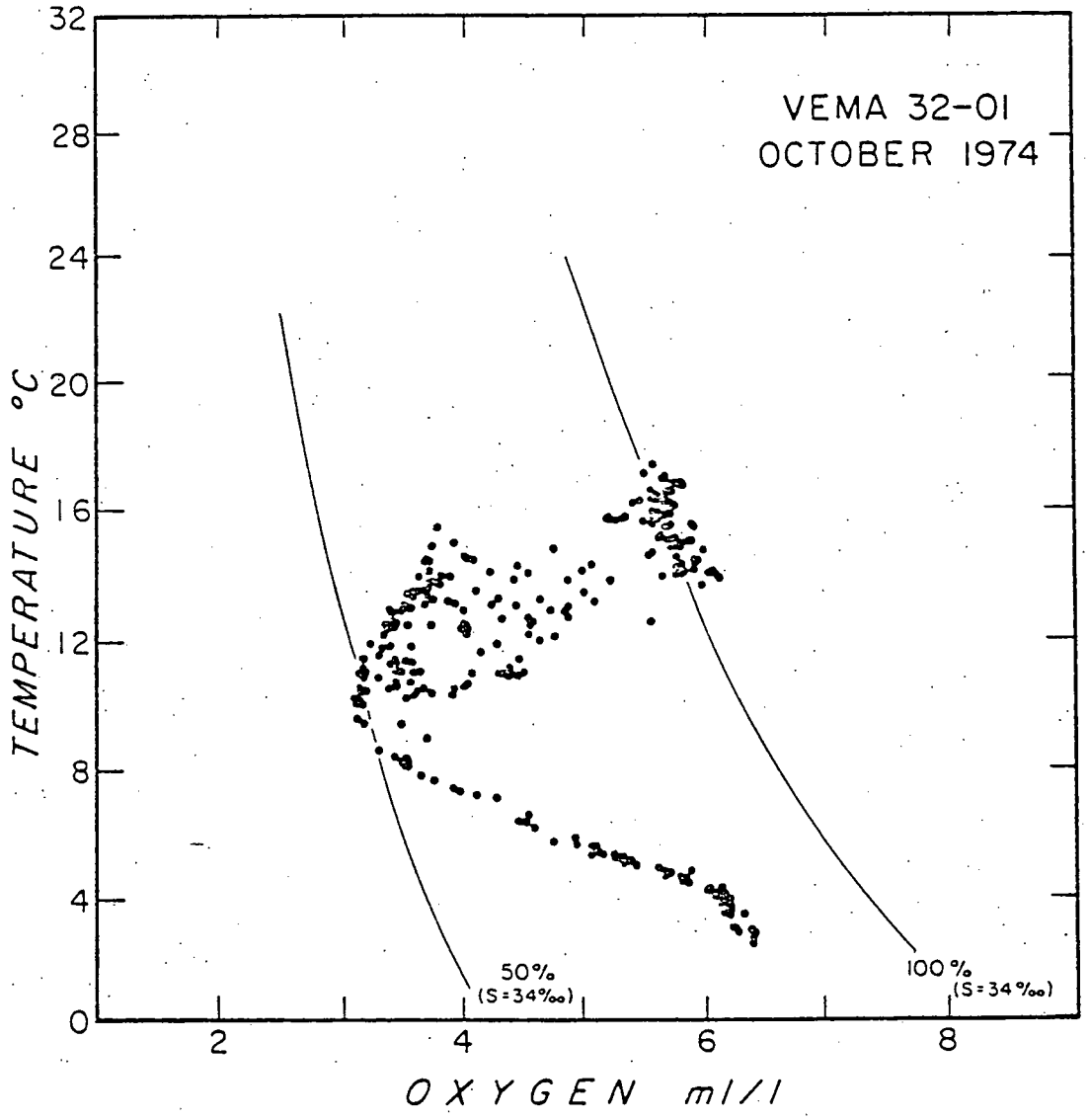
VEMA 32-01
OCTOBER 1974
TEMPERATURE °C
OXYGEN ml/l
50%
(S=34‰)
100%
(S=34‰)
0
4
8
12
16
20
24
28
32
2
4
6
8

Fig. 4.1-33a

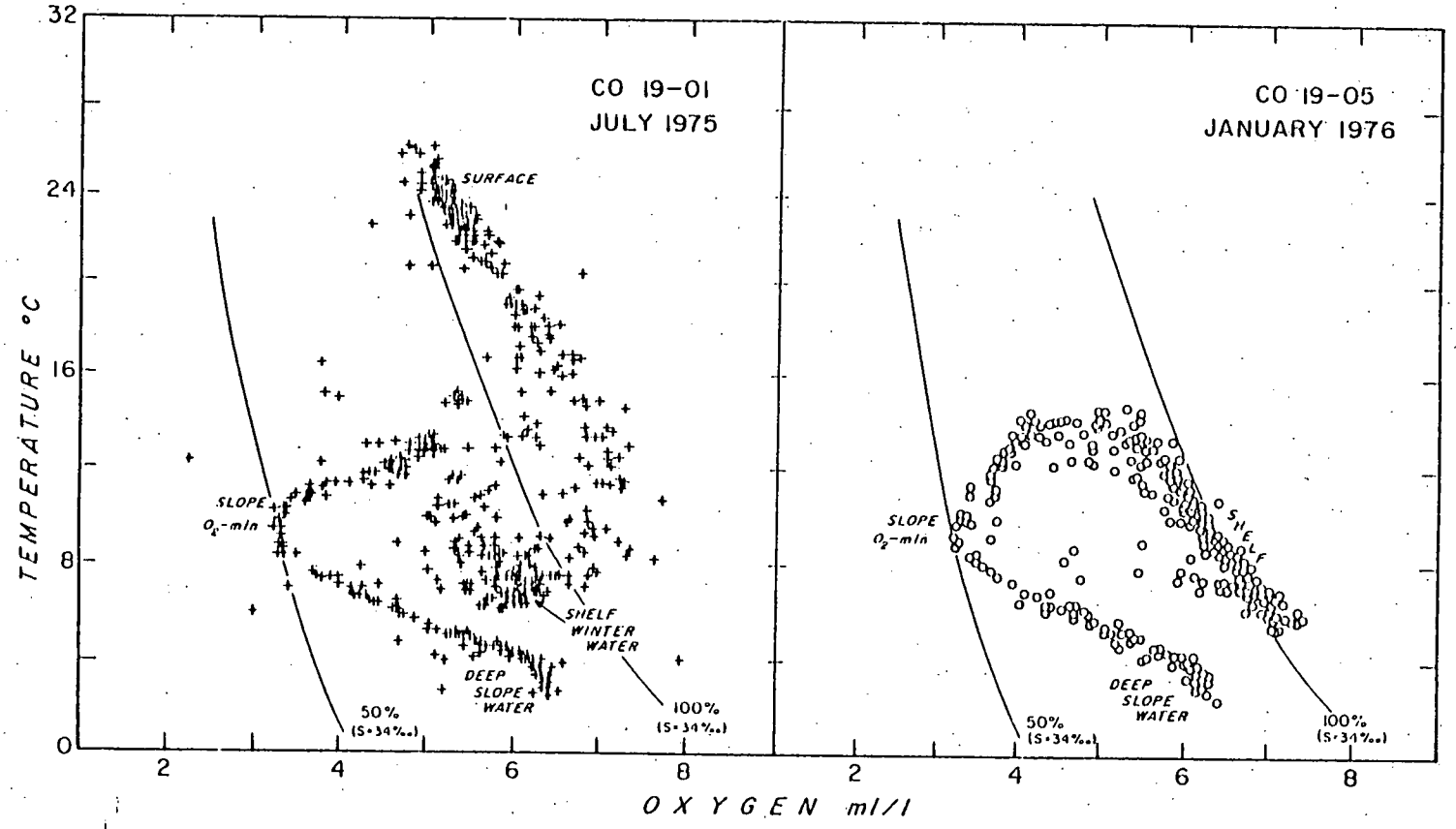
CO 19-01
JULY 1975
CO 19-05
JANUARY 1976
SURFACE
SLOPE
O_2-min
SHELF
WINTER
WATER
DEEP
SLOPE
WATER
50%
(S=34‰)
100%
(S=34‰)
TEMPERATURE °C
OXYGEN ml/l
0
8
16
24
32
2
4
6
8

Fig. 4.1-33b

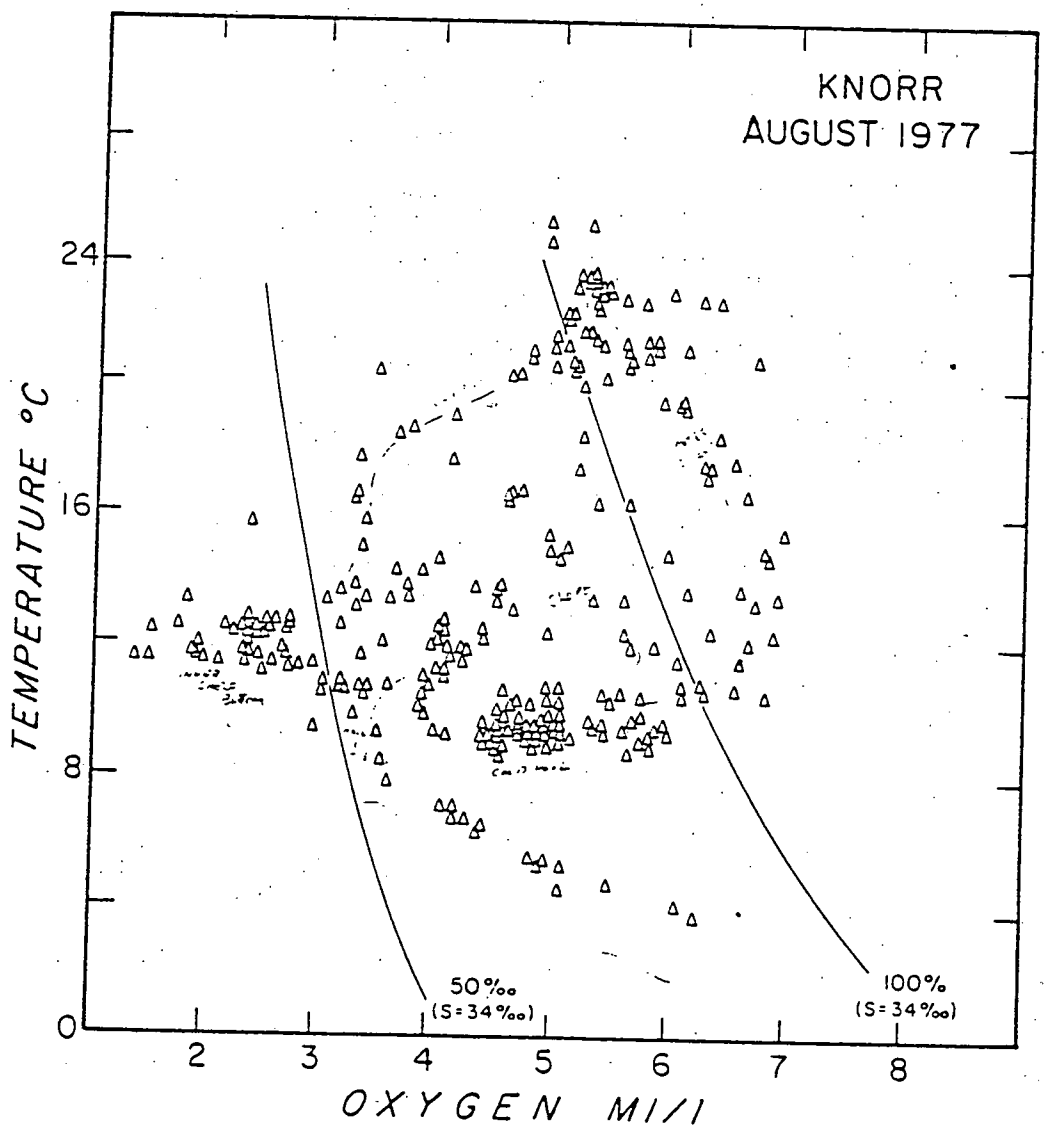
KNORR
AUGUST 1977
TEMPERATURE °C
24
16
8
0
2
3
4
5
6
7
8
OXYGEN M//l
50‰
(S=34‰)
100%
(S=34‰)

Fig. 4.1-33c

(1) The oxygen of the bottom water on the middle shelf in January 1976 is at the saturation level of about 7 ml/l. In July 1975 it is near 7 ml/l, 5 ml/l in August 1977, and in October 1974 it is near 4 ml/l. Assuming the decrease in bottom water oxygen begins with initiation of stratification in late March, an average oxygen decrease of 0.5 ml/l-month (April 1 to September 30) is suggested.

Since oxygen is introduced into the bottom water of the middle shelf by vertical diffusion and isopycnal exchange, the observed bottom water decrease is less than the consumption rate due to oxidation of bottom organisms. Hence, the actual oxygen utilization in the bottom layer of the middle shelf is in excess of 0.5 ml/l·month.

The oxygen of the bottom water over the inner shelf, sampled in August 1977, is significantly below the middle shelf bottom water oxygen (about 3 ml/l less). A decrease of about 1 ml/l·month for the inner shelf is suggested (April to August). Higher degree of oxygen utilization on the inner shelf is the probable cause. Again, vertical diffusion oxygen input to the inner shelf bottom water indicates that the actual oxygen utilization in the inner shelf bottom waters is greater than 1 ml/l·month.

(2) The supersaturation in the summer thermocline amounts to 115 to 120% of full saturation. An example of oxygen versus depth, displaying the thermocline O_2-max, is given in figure 4.1-34. The O_2-max is believed induced by a chlorophyll

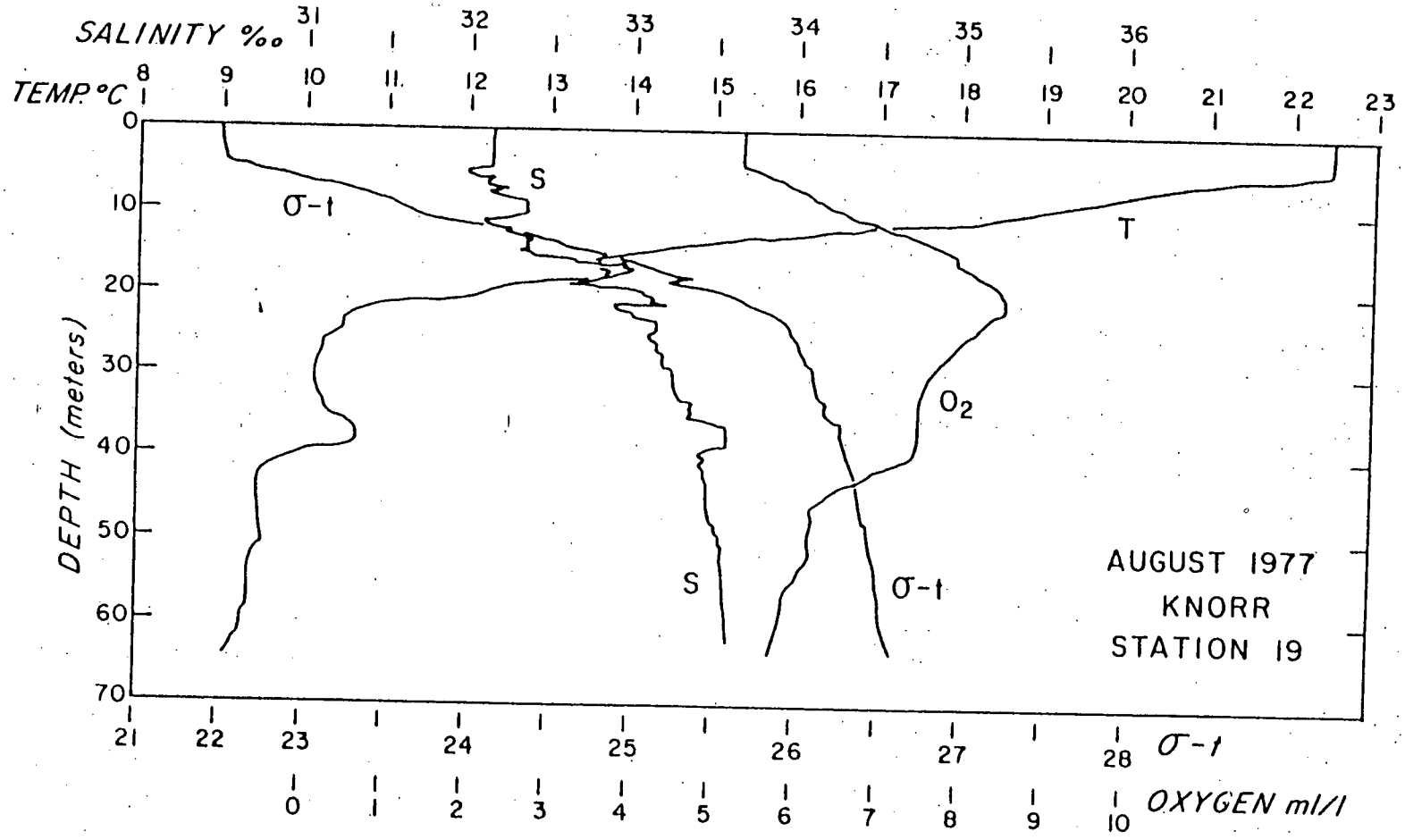
SALINITY ‰
TEMP. °C
DEPTH (meters)
σ-t
S
T
O2
S
σ-t
AUGUST 1977
KNORR
STATION 19
σ-t
OXYGEN ml/l

Fig. 4.1-34

maximum within the shallow shelf thermocline. The high increase of stability restricts the vertical outflux of dissolved oxygen produced by photosynthesis. The stability of the seasonal pycnocline chlorophyll maximum in the face of tidal induced turbulence can be determined using the formulation of Pingree et al., 1978.

$$E = \log_{10} \frac{C_D \frac{4}{3\pi} U_o^3}{h}$$

where U_o is the mean tidal current, h is the water depth and C_D is the drag coefficient (taken as 2.5×10^{-3} by Pingree et al). For the northwest European shelf Pingree et al (1978) show that the chlorophyll maximum is persistent when E lies between -1 and -2.

The typical U_o are 8 to 20 cm/sec for the inner shelf (Hansen, 1977). Using 10 cm/sec, E=-2.7; using 20 cm/sec E=-1.8. Hence a chlorophyll maximum is expected in the New York Bight (assuming the same E range applies to the New York Bight).

The appropriate E range is dependent on the vertical density gradients, which in conjunction with the local K_z provide the nutrients.

G. Estimates of K_z

Analysis of the physical and biological data sets have been combined to study the effective vertical eddy coefficient, K_z, under stratified conditions during the summer. A preprint of the paper (Malone, Houghton and Gordon, 1980), which has been submitted for publication, is included in the Appendix.

Calculations were based on the heat flux from the cold pool (assumed to be vertical), the diffusion of oxygen from the O_2 max layer (see previous section), and the flux of nutrients into the euphotic zone to balance primary productivity. Oxygen and nutrient data were taken from the stations shown in Fig. 4.1-35. Historical data (Coltan et al., 1968) and sections from the two 1977 cruises (Fig. 4.1-36) were used for the heat flux calculation. The resulting values of K_z (see tables 4.1-1 and 2) plotted as a function of the stratification $E = \frac{\Delta\sigma_\tau}{\Delta z}$ and compared with other results from the literature are shown in Fig. 4.1-37. We find that roughly $K_z \propto E^{-1}$ which is expected for oceanic and coastal regimes. It is remarkable that these independent calculations give comparable results. A calculation of K_z from the excess radon profile near the base of the pycnocline give similar results.

The large scatter in the K_z vs E plot could be the result of two effects: 1. differences in the turbulent velocity shear and 2. inclination of density surfaces such that isopycnal mixing has a vertical component. It was shown that given observed slopes in the density surfaces and realistic values of the lateral diffusion coefficient process (2) could make a significant contribution to K_z.

The agreement of K_z value from the heat flux calculation with that of the oxygen and nutrient calculation may be

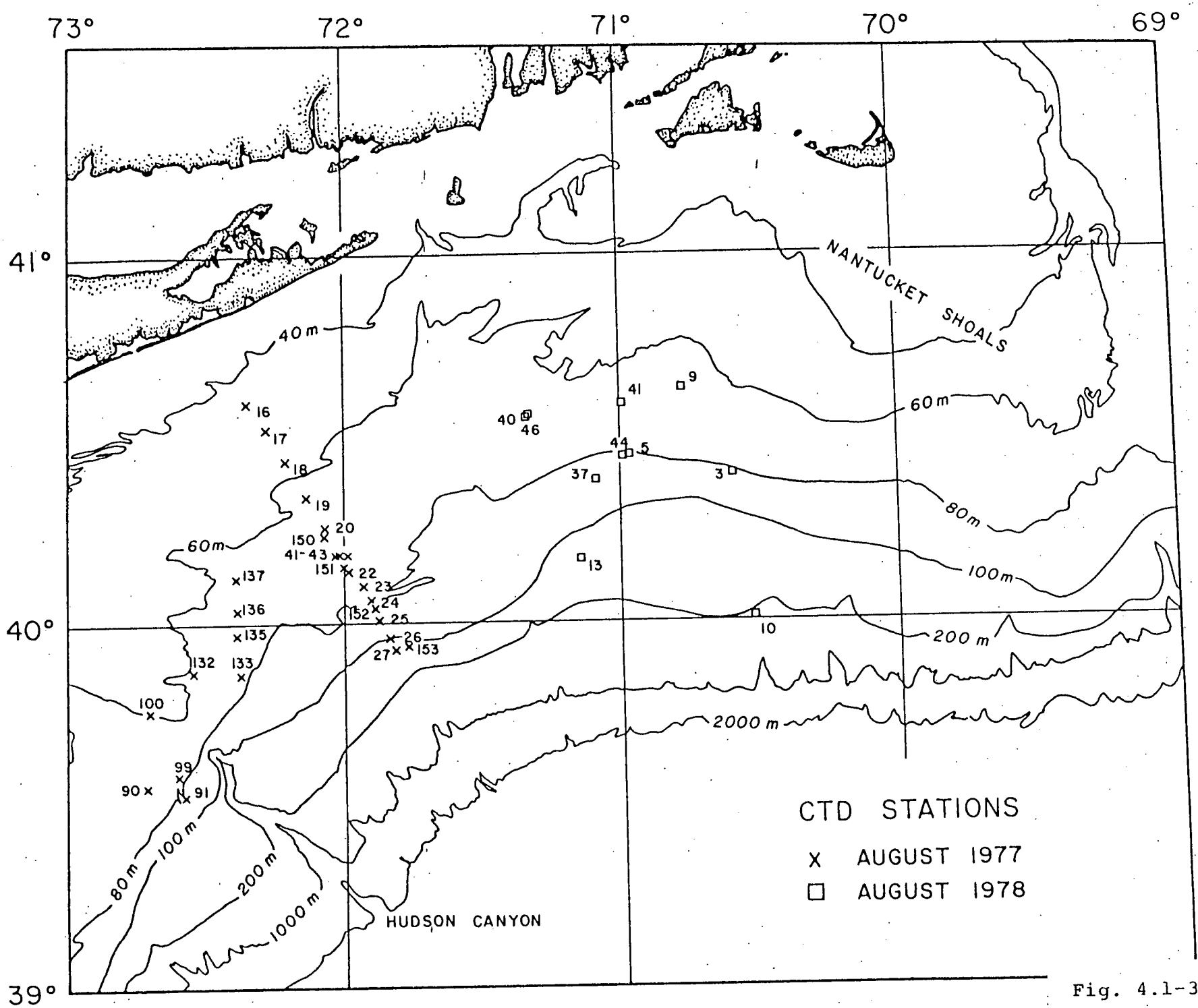
73°
72°
71°
70°
69°
41°
40°
39°
NANTUCKET SHOALS
40 m
60 m
80 m
100 m
200 m
2000 m
1000 m
HUDSON CANYON
CTD STATIONS
X AUGUST 1977
□ AUGUST 1978

Fig. 4.1-35

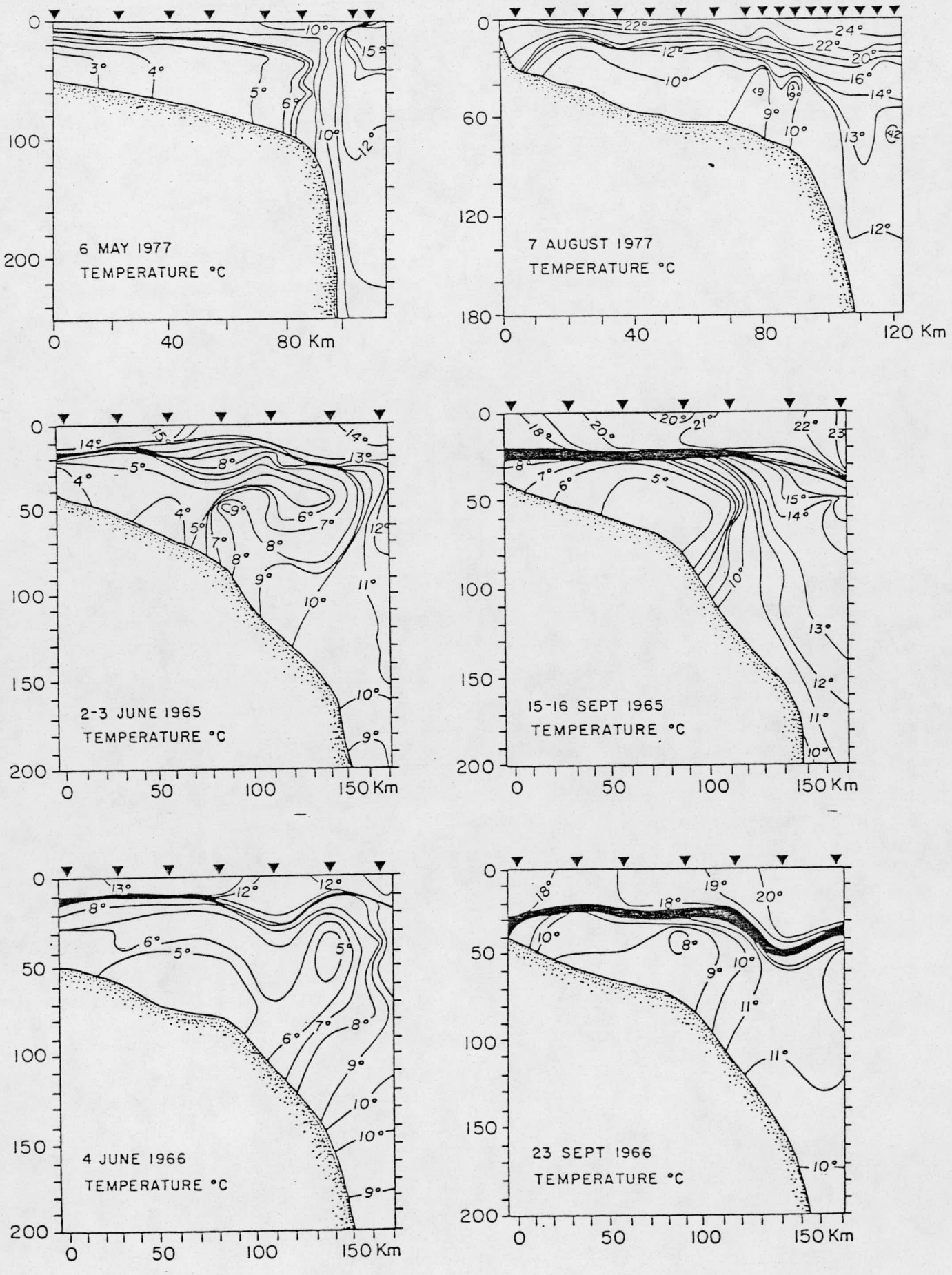
6 MAY 1977
TEMPERATURE °C
7 AUGUST 1977
TEMPERATURE °C
2-3 JUNE 1965
TEMPERATURE °C
15-16 SEPT 1965
TEMPERATURE °C
4 JUNE 1966
TEMPERATURE °C
23 SEPT 1966
TEMPERATURE °C
DEPTH (m)
0
40
80
120
150
50
100
200
60
180
Km

Fig. 4.1-36

Table 1. Estimates of coefficients of vertical eddy diffusion based on nitrate (K_{zn}) and oxygen (K_{zo}).

		$cm^2\ s^{-1}$				$cm^2\ s^{-1}$	
Date	Sta.	K_{zn}	K_{zo}	Date	Sta.	K_{zn}	K_{zo}
7 Aug 77	16		0.10	27 Aug 77	132	0.09[a]	
	17		0.30		133	0.08	
	18		0.24		135	0.43	
8 Aug 77	19	0.55	0.28		136	0.40	
	20		0.30	28 Aug 77	137	0.12	
	22	0.58			150	0.36	
	23[a]	0.06			151	0.12	
	24	0.05			152	0.11	
	25	0.05			153	0.06[a]	
	26	0.15		14 Aug 78	3	0.75[a]	0.52
	27	0.08			5	0.20	0.38
11 Aug 77	41	0.30		15 Aug 78	9[b]	0.45[a]	1.01
	42[a]	0.18		16 Aug 78	10	0.94[a]	1.11
	43	0.18		17 Aug 78	37	0.45[a]	0.59
22 Aug 77	90	0.78		18 Aug 78	40	0.65[a]	0.87
	91	0.60			41	0.27	0.37
23 Aug 77	99[a]	0.06					
	100	0.54					

[a]Stations at which primary productivity was measured.

[b]Omitted from correlation of K_{zn} on K_{zo}.

Table 2. Estimates of coefficients of vertical eddy diffusion based on heat (K_{zh}), nitrate (K_{zn}), and oxygen (K_{zo}); K_{zn} and K_{zo} are means calculated from data in Table 1.

Year	K_{zh}	K_{zn}	K_{zo}
1965	0.02	-	-
1966	0.25	-	-
1977	0.18	0.26	0.24
1978	-	0.57	0.64

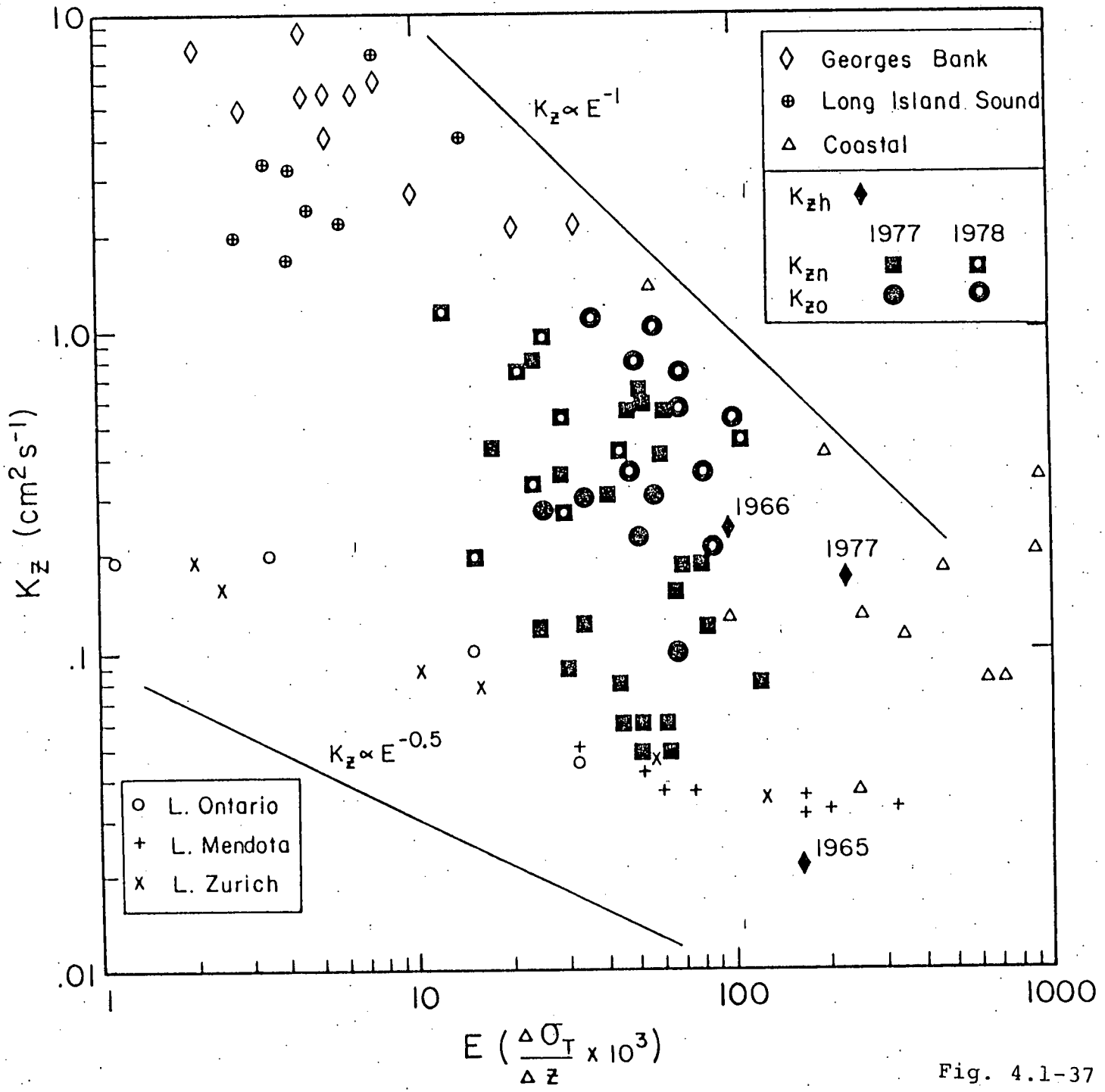
10
1.0
.1
.01
K_z (cm^{2}s^{-1})
1
10
100
1000
$E\left(\frac{\Delta\sigma_T}{\Delta z} \times 10^3\right)$
$K_z \propto E^{-1}$
$K_z \propto E^{-0.5}$
Georges Bank
Long Island Sound
Coastal
K_{zh}
1977
1978
K_{zn}
K_{zo}
1966
1977
1965
L. Ontario
L. Mendota
L. Zurich

Fig. 4.1-37

fortuitous for in Section C we noted that the cold pool as it warmed evolved primarily along an isopycnal, implying that heat fluxes laterally, not vertically. However there were exceptions to this suggesting that heat and salt exchange with the cold pool occurs by various processes whose relative importance change with the season and degree of stratification.

H. IMPORTANCE OF RIVER RUNOFF IN PYCNOCLINE DEVELOPMENT

The summer pycnocline over the shelf is shallower and more intense than that of the slope region. The August 1977 o-t section (Fig. 4.1-27) clearly shows this. The consequences of this seasonal development is a reversal in the winter period cross shelf-slope lateral density gradient in the mid depth range. The SWIG III (an NSF funded Physical Oceanography-Biology program for study of the shelf-slope front) section (Fig. 4.1-38) shows that in the 10-50 m range density decreases seaward, in contrast to the surface water and deeper water column, which are more similar to the winter condition of increasing density seaward.

The principle thermohaline signature related to the pycnocline change over the shelf is the presence of the cold pool. The mass of cold water induces a thick layer of decreased vertical density gradient in the deep water on the

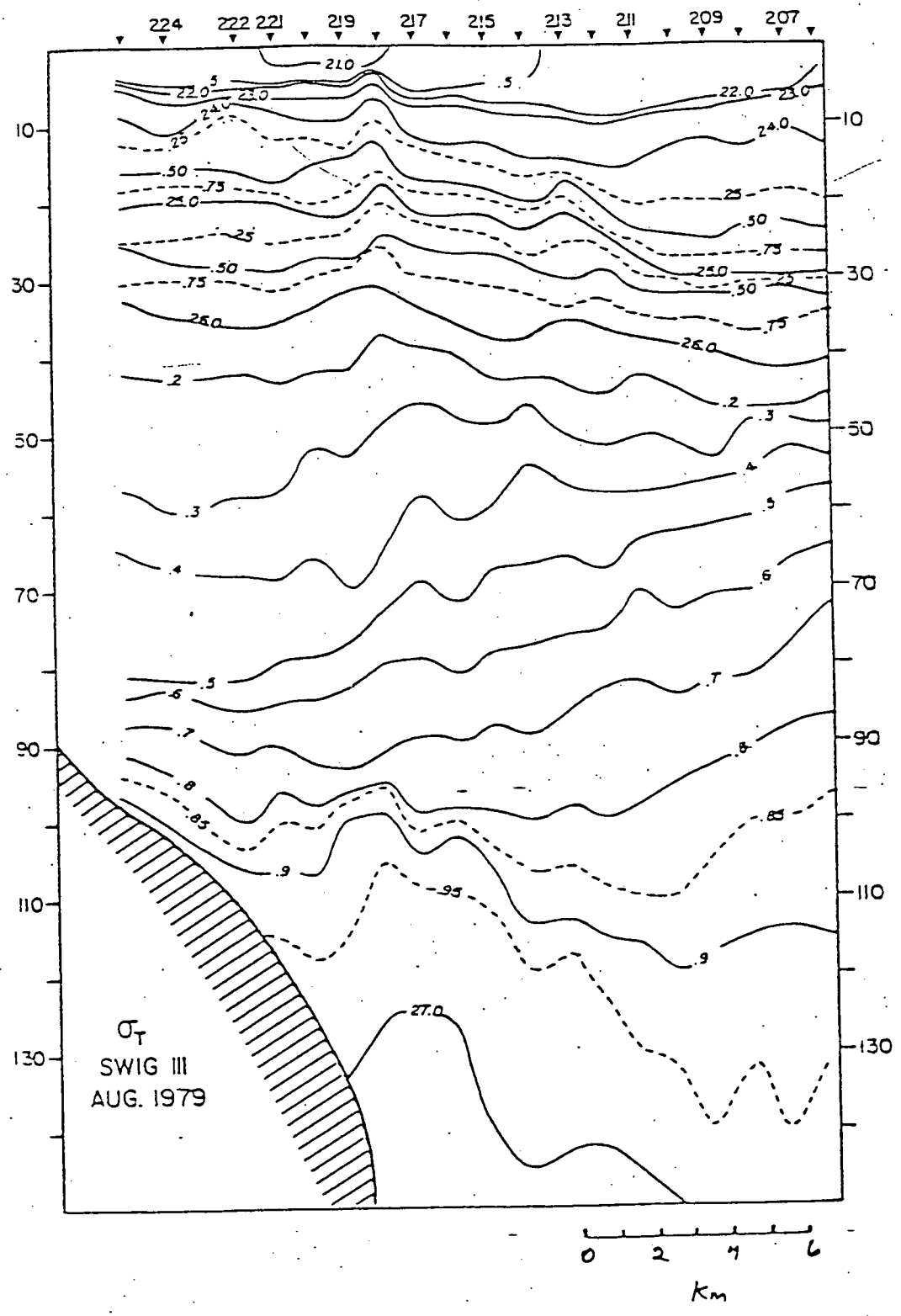
224
222
221
219
217
215
213
211
209
207
10
30
50
70
90
110
130
σ_T
SWIG III
AUG. 1979
0
2
4
6
km

Fig. 4.1-38

shelf. This has the effect of fanning out the slope isopycnal surfaces as they cross over to the shelf region.

A hypothesis is now presented which may explain the strong shallow shelf pycnocline. The hypothesis will be tested and expanded as research continues.

The difference between the shelf and slope pycnoclines may be a response to different thermohaline histories of the surface water. The development of a seasonal pycnocline depends on sea-air exchange of buoyancy and in the efficiency of downward mixing of the buoyant water. The surface waters of the shelf and slope probably have similar short wave radiational heating patterns and wind mixing. The major difference deals with fresh water input: while P-E may not be very different, continental runoff input does differ. The shelf region receives a spring time pulse of fresh water from the coastal boundary. The river water lowers the surface salinity, which spreads across the shelf. The slope region is not influenced by the river flow until later in the warm season.

The early spring haline stratification of the shelf surface water by the river water may have important water column effects. Assuming similar heat, water and momentum input across the sea-air interface, the early spring stability of the shelf water would have a positive feedback, since it would hinder downward mixing of the surface heating, relative to the slope condition. Thus the river water initiates a

rapidly developing thermocline and a very buoyant mixed layer. The remnant winter water or cold pool below the pycnocline is well protected from surface effects.

The slope region's seasonal pycnocline is mixed downward to a greater extent, since the surface heating is not confined to a initially stable layer. The wind more efficiently carries surface heating downward.

The river influence on the shelf would have a greater impact on confining the spring and summer heating to the immediate surface if it is already present at the start of the heating season. Since much of the runoff into the Middle Atlantic Bight is a response to snow melt early heating and runoff occur close to the same time (approximately April and May), but heavy spring rains or mid-winter thaw could induce a pre-heating season stability.

The impact of fresh water input on seasonal pycnocline development can be studied using one-dimensional models, with equal heating and momentum budgets of varied fresh water input. In this way the shelf water column stratification and slope stratification can be compared.

It is suspected that the early stratification of the shelf water has two important effects: 1. Protects the deep water from surface heating, thus allowing a large mass of winter remnant water to be preserved through the summer. The earlier and/or greater the river input, the earlier is the

cold pool isolated and hence colder and thicker. 2. The mismatch of the shelf and slope pycnocline induces the reversal of intermediate depth lateral density gradients.

The density gradient reversal may force a fold in the shelf-slope front and a slope water intrusion of slope water into the shelf pycnocline (Posmentier and Houghton, 1980), which may be a significant salt input to the shelf to compensate for river water (Gordon and Aikman, 1980). It is interesting to point out that if the river water stratification is responsible for the shallow intense shelf pycnocline, then it may actually force onto the shelf saline slope water which acts to compensate for the river water. An important question is: does the timing and amount of river water input induce changes in the pycnocline salinity maximum feature? Perhaps earlier and/or stronger haline stabilization leads to a greater mismatch of shelf and slope pycnoclines and a more intense pycnocline salinity-maximum. Thus the more river water the greater the compensation by slope water transfer to the shelf.

I. RACACA Cruise

INTRODUCTION - In June 1979 we took a series of seven combined CTD and XBT cross-shelf transects extending alongshore southward from a line off Barnegat, New Jersey to just south of Cape Hatteras, and extending seaward from just inside the foot of the shelf-slope front (~ the 80 m isobath) to at least

2000 m on the continental slope (Fig. 4.1-1b). The motivation behind this field work was to look at the benthic density structure and processes on the continental slope that could be related to the radon-deficient zone usually observed somewhere between 200 and 2000 m along the slope, and to investigate the long-shore variation in slope water thermohaline characteristics with the intent that it would lead to information on shelf-slope exchange.

OBSERVATIONS -

The quasi-synoptic nature of this cruise provided a look at the three-dimensional picture of the outer shelf and slope water early summer stratification, including the shelf/slope front and the seaward extent of the cold pool. Fig. 4.1-39 shows the spacial structure of the cold pool as defined by the 8°C isotherm viewed from above, offshore and the south (the dashed lines are bottom profiles). By transect VI this feature is no longer evident as the Gulf Stream impinges right up to the shelf break. Relative to the isobaths, the cold pool extends out into much deeper water in transect V then elsewhere, but keep in mind that the bottom slope is simply steeper there. What is remarkable is that the cold pool, despite slight warming to the south ($\sim$1°C between sections I and V), maintains an almost constant density (σ_t = 26.2) from north to south. Enough salt is somehow incorporated into it to balance the heating effect.

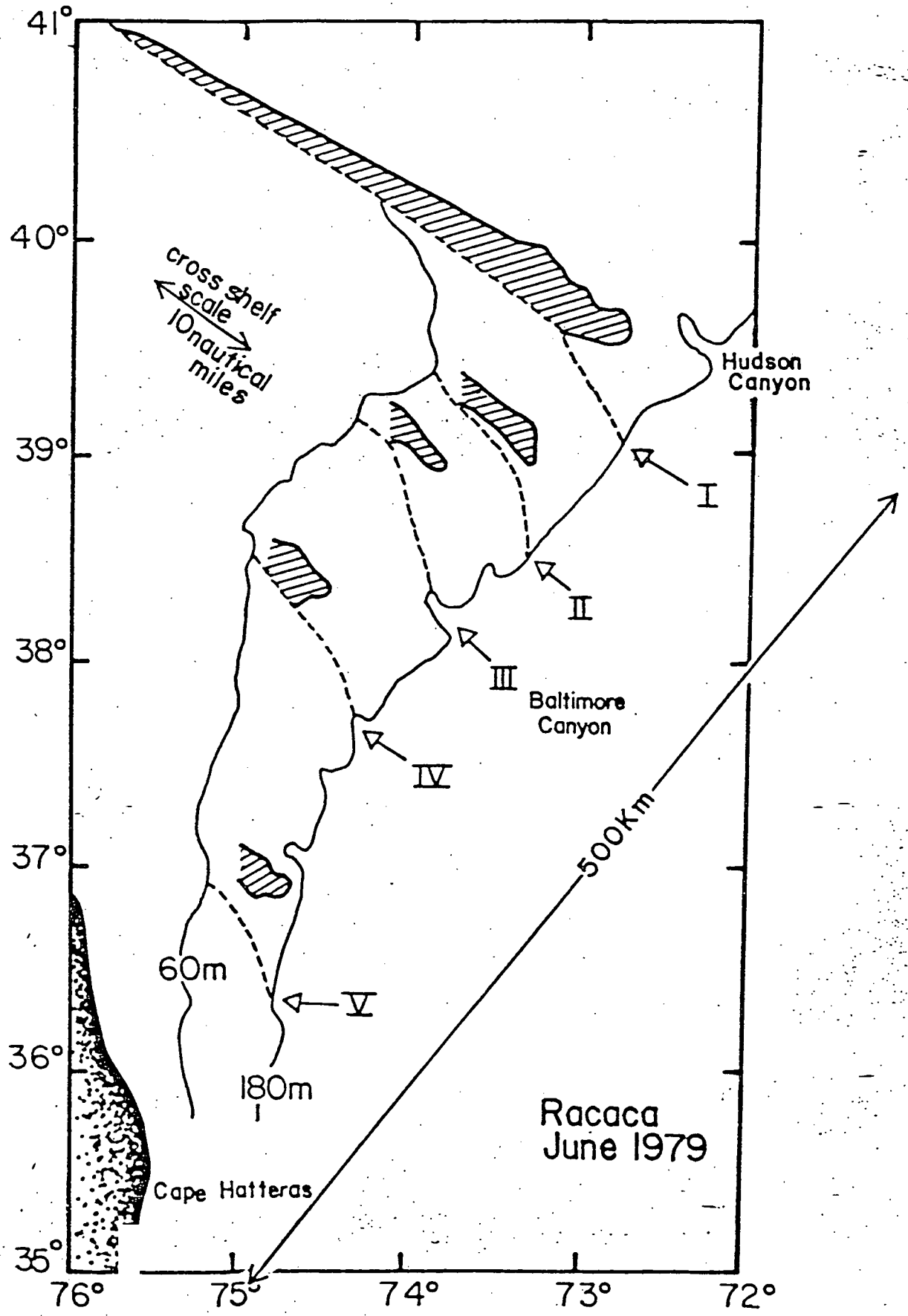
41°
40°
39°
38°
37°
36°
35°
76°
75°
74°
73°
72°
cross shelf scale 10nautical miles
Hudson Canyon
I
II
III
Baltimore Canyon
IV
V
500Km
60m
180m
Racaca June 1979
Cape Hatteras

Fig. 4.1-39

I. Warm Core Eddy

A remnant (possibly winter cooled) warm core eddy was traversed in section I (Figs. 4.1-40a,b,c). Any surface expression of this feature was not apparent in the seasonally warmed slope water nor in the routinely published EOFA charts for this region at this time. However, a stricter and more careful interpretation of the enhanced satellite IR images shows that Eddy 79-A most likely is the feature we observed (J.L. Chamberlain - personal communication). It is impossible from our data alone, to determine where in it's cross section we traversed the eddy (though most likely on its southern extent), nor to estimate a diameter because of this, but we do observe a temperature anomaly of 3°C at 350 m as well as isotherm displacements of from 50 m (15° isotherm) to 100 m (14° isotherm). Our primary interest in these eddies is with their role as inducers of exchange of water across the shelf break. Many have observed eddies such as this entraining shelf water well out into slope regions as well as depositing some slope water onto the shelf. Most of these observations have been surface observations. In July of 1975 we encountered another warm core eddy in approximately the same area (CO 19-01 cruise). In both instances isopycnals were observed to slope dramatically upward near the bottom as the shelf is approached from offshore (see Fig. 4.1-31b). This apparent shelfward 'pumping' of deeper slope water could possibly be as paramount (the equivalent volumetrically) as the more commonly observed

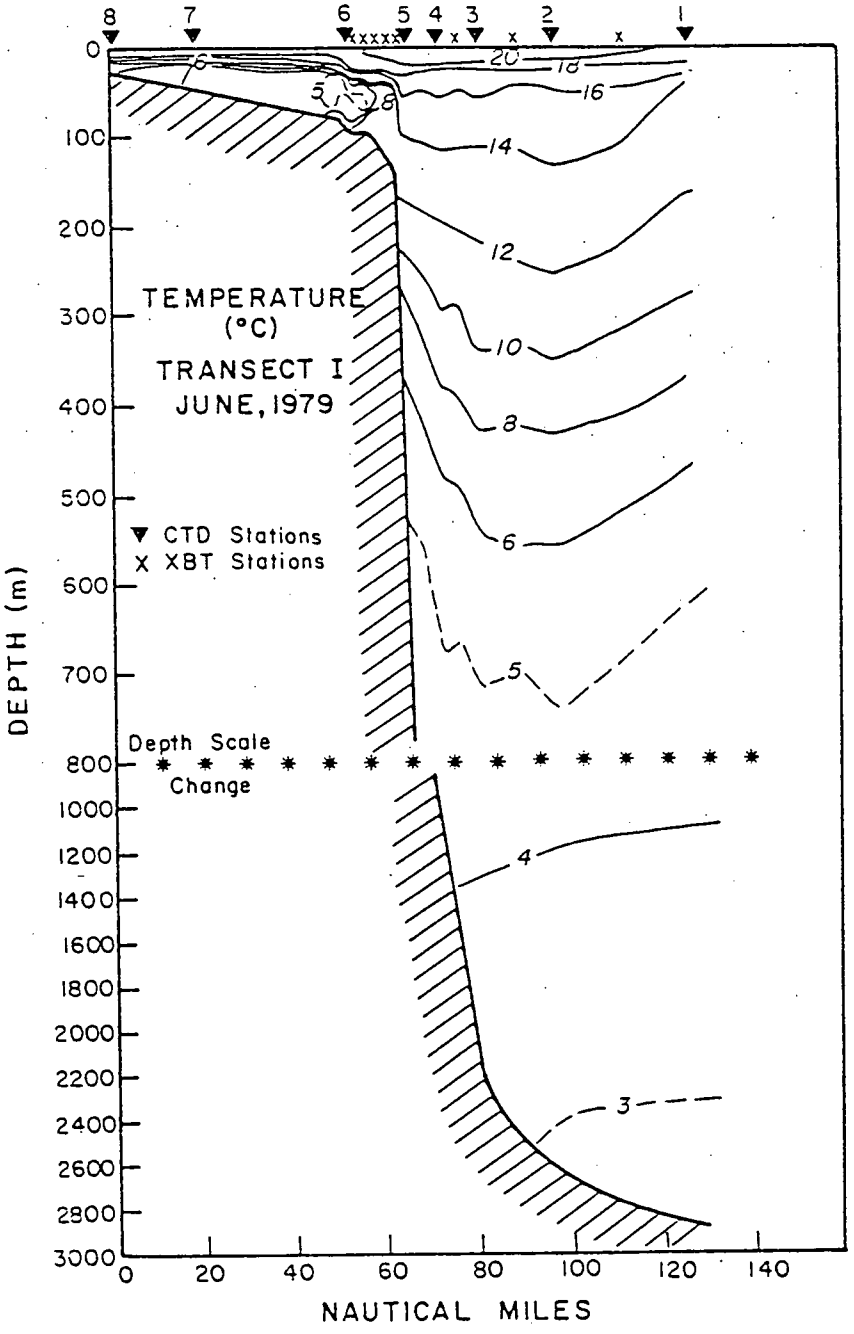
8
7
6
5
4
3
2
1
0
100
200
300
400
500
600
700
800
1000
1200
1400
1600
1800
2000
2200
2400
2600
2800
3000
20
18
16
14
12
10
8
6
5
4
3
TEMPERATURE
(°C)
TRANSECT I
JUNE, 1979
▼ CTD Stations
X XBT Stations
Depth Scale
Change
DEPTH (m)
0
20
40
60
80
100
120
140
NAUTICAL MILES

Fig. 4.1-40a

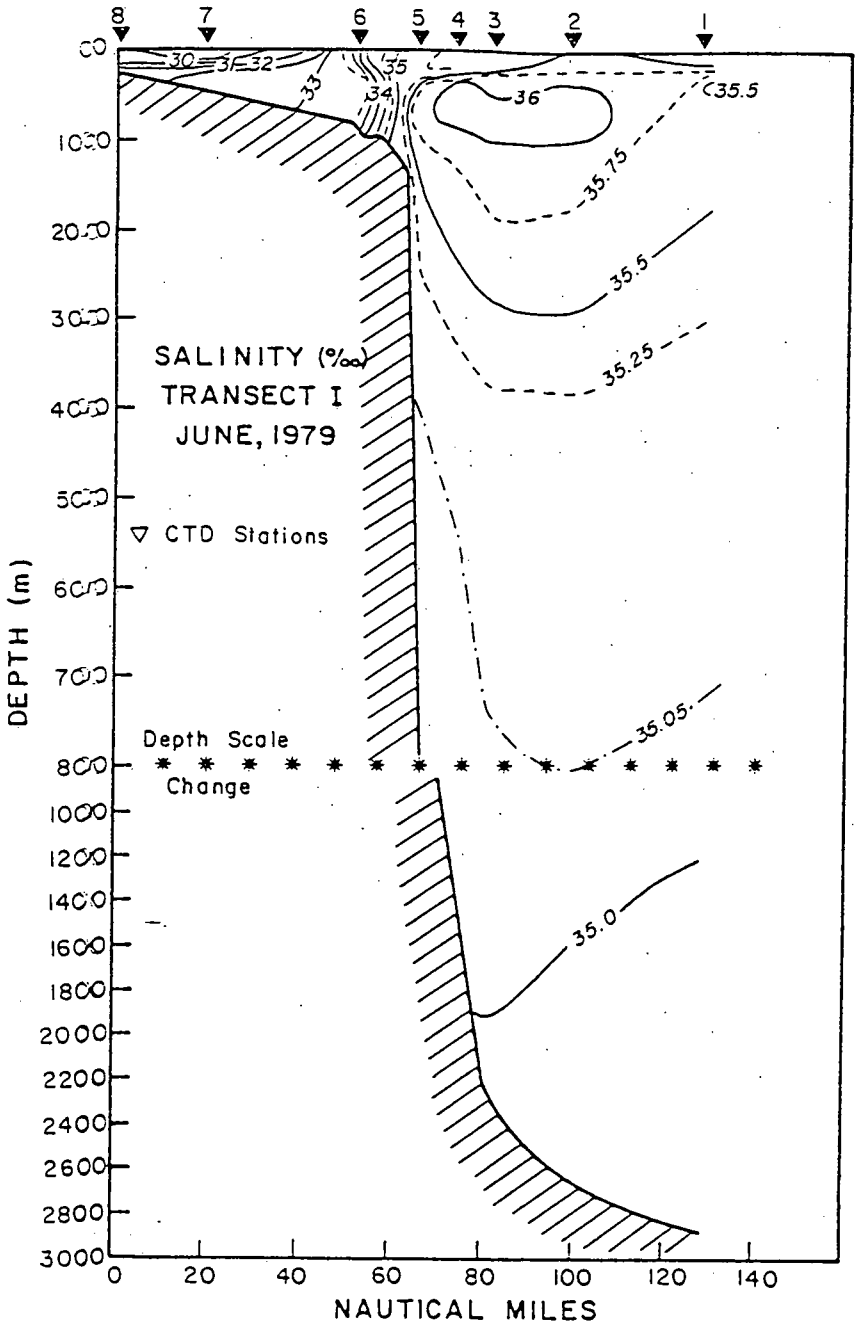
8
7
6
5
4
3
2
1
30
31
32
33
34
35
36
35.5
35.75
35.5
35.25
35.05
35.0
SALINITY (‰)
TRANSECT I
JUNE, 1979
▽ CTD Stations
Depth Scale
Change
DEPTH (m)
0
1000
2000
3000
4000
5000
6000
7000
8000
1000
1200
1400
1600
1800
2000
2200
2400
2600
2800
3000
0
20
40
60
80
100
120
140
NAUTICAL MILES

Fig. 4.1-40b

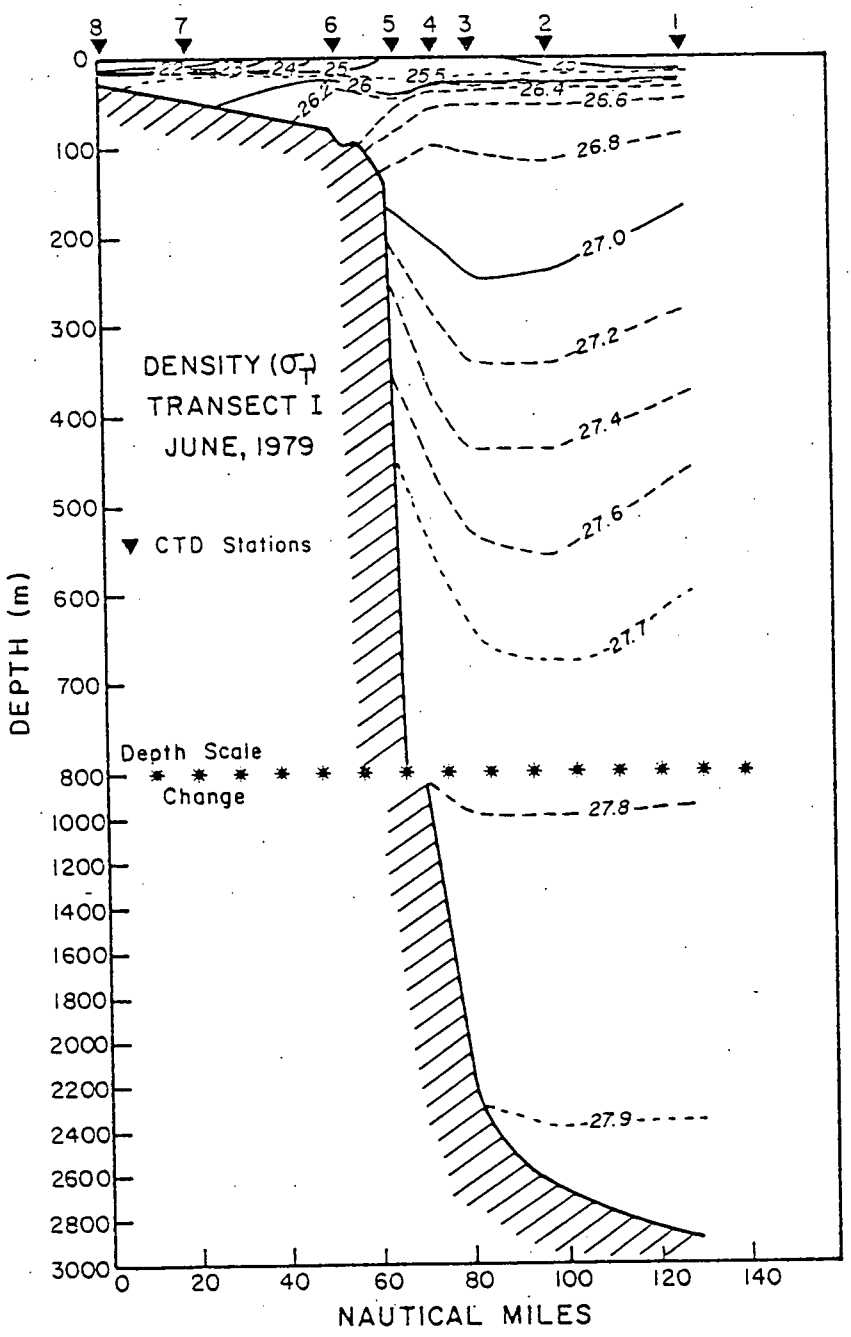
8
7
6
5
4
3
2
1
0
100
200
300
400
500
600
700
800
1000
1200
1400
1600
1800
2000
2200
2400
2600
2800
3000
DEPTH (m)
DENSITY (σ_T)
TRANSECT I
JUNE, 1979
▼ CTD Stations
Depth Scale
Change
25.5
26.4
26.6
26.8
27.0
27.2
27.4
27.6
27.7
27.8
27.9
0
20
40
60
80
100
120
140
NAUTICAL MILES

Fig. 4.1-40c

offshore surface entrainment of shelf water associated with such eddies. Estimates of the shoreward forcing of water and slope water properties by this warm core eddy process are not possible now.

II. Calving

We had expected to encounter detached parcels of shelf water in the slope region at this time of year (Wright, 1976), but none were evident. Even in regions of prominent bottom relief, i.e. the Baltimore Canyon, when the calving process is thought to be most active (Mooers, et al. 1979), calving was not observed. Perhaps our sample spacing was not dense enough, but this seems unlikely. If our data set is not anomalous, then it is possible that previous estimates of the amount of shelf water being deposited in slope regions through calving has been overestimated (see Wright, 1976; Cresswell, 1967).

III. Longshore Variations

A variety of approaches will be used to look at alongshore variations in the thermohaline properties of the slope water and the outer shelf water.

One such approach was to look at the mean slope-to-shelf temperature and salinity differences within 0.2 σ_t density intervals, and how these mean differences vary from the north to the south in the Middle Atlantic Bight (MAB). Ignoring seasonal and interannual variations for the moment, the amount of fresh water emptying into the MAB increases, proceeding south-

ward from the Hudson River to Cape Hatteras, with the Delaware and Chesapeake Bays contributing progressively larger volumes of river water (65% of fresh water flow into the MAB occurs south of 39°N). This, coupled with the mean southwesterly drift, which would act to transport river outflow to the south, leads one to expect a greater concentration of river water on the shelf in the southern portions of the Bight. On the slope side of the shelf-slope front one might look for the mean temperature and salinity to increase to the south where the Gulf Stream is closer to the shelf. Coupling these two expectations, one could expect the mean slope-shelf temperature and salinity differences to increase to the south, quite the opposite of what is seen (Fig. 4.1-41a and b). Except for the very lightest surface water (σ_τ > 25) and Section II above the density of the cold pool (σ_τ = 26.2), the mean slope-shelf temperature and salinity differences diminish from south of Section I to just north of Cape Hatteras. The greatest differences are found at a density of σ_τ = 26.2, the consistent alongshore density of the cold pool between Sections I to V.

Ketchum and Keen, 1955, find a decrease in the average content of river (fresh) water in the direction of the mean alongshelf flow to the southwest, despite the addition of river water along its course, and conclude that the cross-shelf transport of fresh water must exceed the alongshelf transport. Wright and Parker, 1976, also examine the latitudinal, as well as seasonal, volumetric changes within 1 0/00 salinity inter-

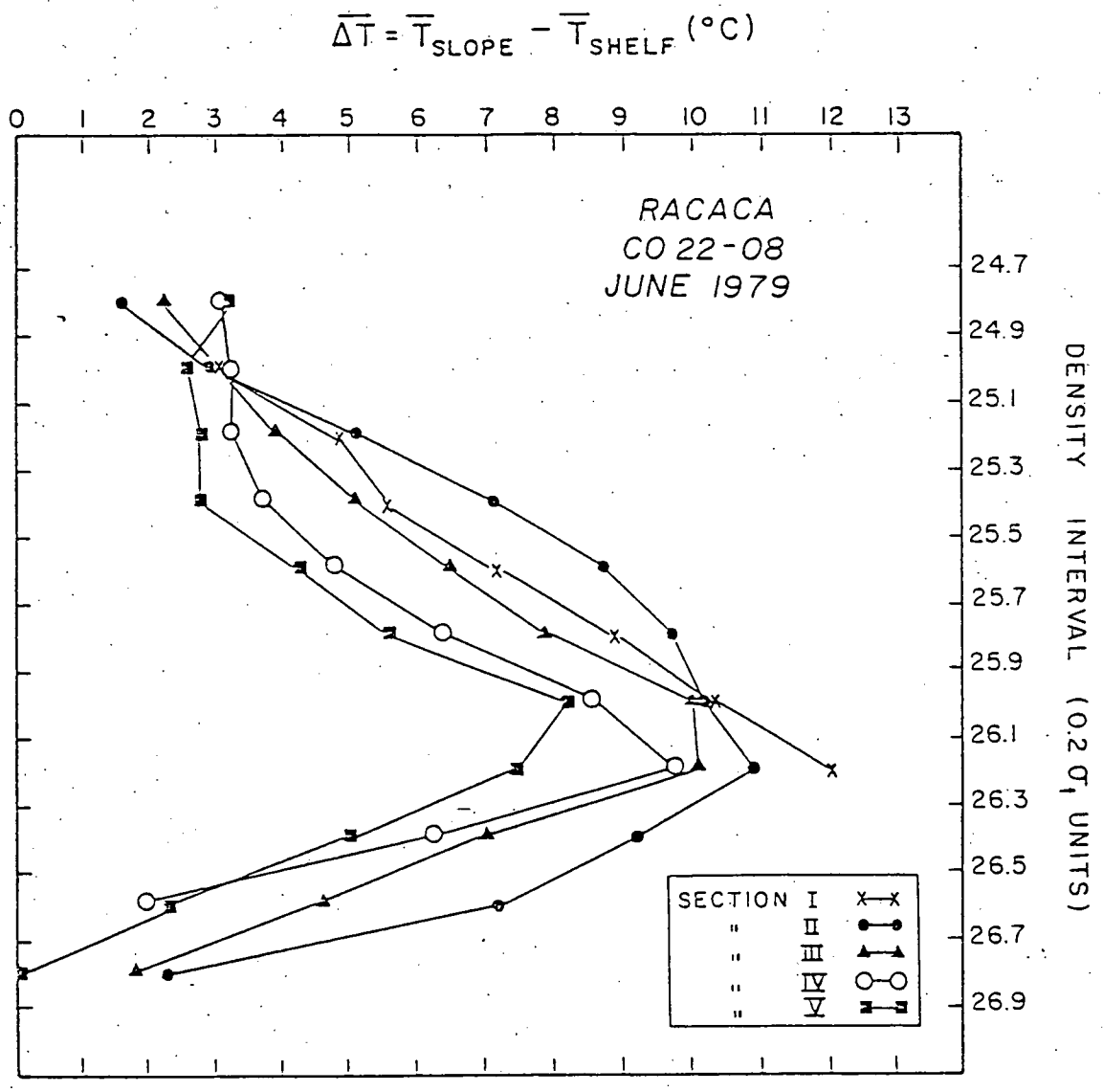
$\overline{\Delta T} = \overline{T}_{SLOPE} - \overline{T}_{SHELF}$ (°C)
0 1 2 3 4 5 6 7 8 9 10 11 12 13
RACACA
CO 22-08
JUNE 1979
24.7
24.9
25.1
25.3
25.5
25.7
25.9
26.1
26.3
26.5
26.7
26.9
DENSITY INTERVAL (0.2 σ_t UNITS)
SECTION I
II
III
IV
V

Fig. 4.1-41a

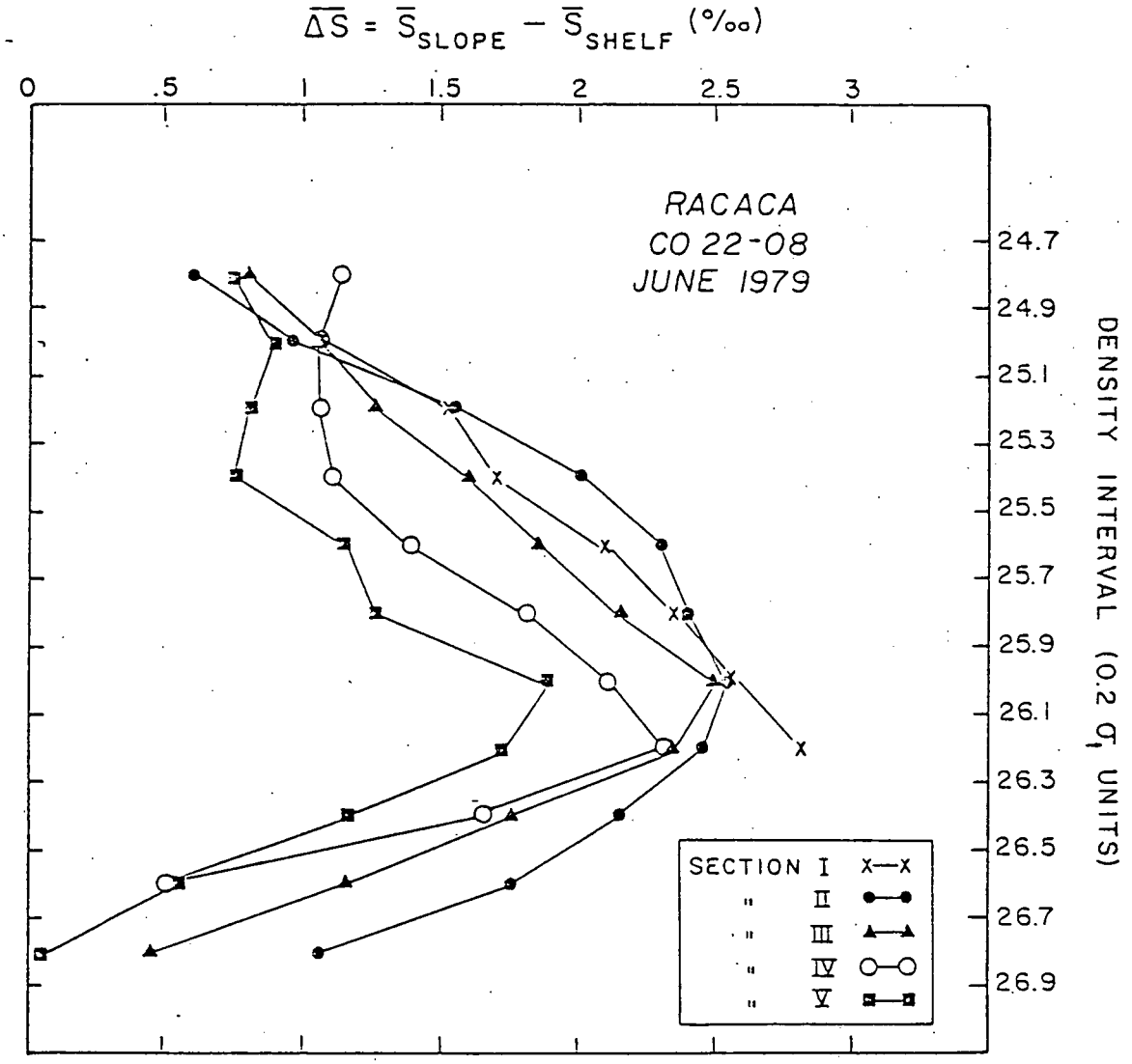
$\overline{\Delta S} = \overline{S}_{SLOPE} - \overline{S}_{SHELF}$ (‰)
0
.5
1
1.5
2
2.5
3
RACACA
CO 22-08
JUNE 1979
24.7
24.9
25.1
25.3
25.5
25.7
25.9
26.1
26.3
26.5
26.7
26.9
DENSITY INTERVAL (0.2 σ_t UNITS)
SECTION I x—x
" II
" III
" IV
" V

Fig. 4.1-41b

vals (see Fig. 4 of their paper). While they observe both a uniform alongshore summertime increase in fresh water (S = 30-32 0/00) content and a corresponding decrease in the more saline (S> 35 0/00) shelf edge water, they find the intermediate salinity (32-34 0/00) water volume increasing to the south and the saltier (34-35 0/00) water volume decreasing to the south. Both these sets of observations are consistent with ours.

Three possibilities seem capable of explaining the diminishing summertime slope-shelf thermohaline differences to the south in the Middle Atlantic Bight.

1. If shelf and inner slope waters both exhibit a net longshore flow to the southwest (Beardsley & Flagg, 1976, cannot confirm the 10 cm/sec. geostrophic shear predicted to occur across the shelf-slope front on the basis of the observed mean density field), then these waters could have upwards of 180 days (net longshore flow of 4 km/day) in which to exchange properties in their traverse from the Great South Channel to Cape Hatteras (800 km).

2. Entrainment of shelf water at the slope water-Gulf Stream boundary north of Cape Hatteras has been observed on numerous occasions (Kupferman & Garfield, 1977; Fisher, 1972; Ford et al., 1952). Estimates of the transport of shelf water by these freshened sur-

face and subsurface bands indicate they could carry a significant fraction of the shelf water passing through the Middle Atlantic Bight. This process could contribute to our observations, both by diluting slope water properties shoreward of the Gulf Stream north of Cape Hatteras, and by serving as a vehicle for the discharge of shelf water as the continental shelf narrows to Cape Hatteras. [There's the likelihood that we observed part of such a subsurface shelf water filament at 100 m depth of Transect VI (Fig. 4.1-1b) just north of Cape Hatteras.]

3. Perhaps it is the simple result of more vigorous mixing between shelf and slope waters to the south.

Given the diminishing slope-shelf water T/S differences to the south, we thought it useful to look at the alongshore variations in both the slope water and shelf water thermohaline characteristics, to see at whose expense (slope water or shelf water) the difference was shrinking. Figures 4.1-42a and b and 4.1-43a and b summarize this approach, wherein the mean temperatures and salinities of each transect, within 0.2 σ_t density intervals, are normalized to transect I for both the slope waters and the waters of the outer shelf. Of course warm core eddy 79-A was present in transect I, and this does complicate the picture, but it nevertheless is valid to compare the other transects to this one, and thus to one another.

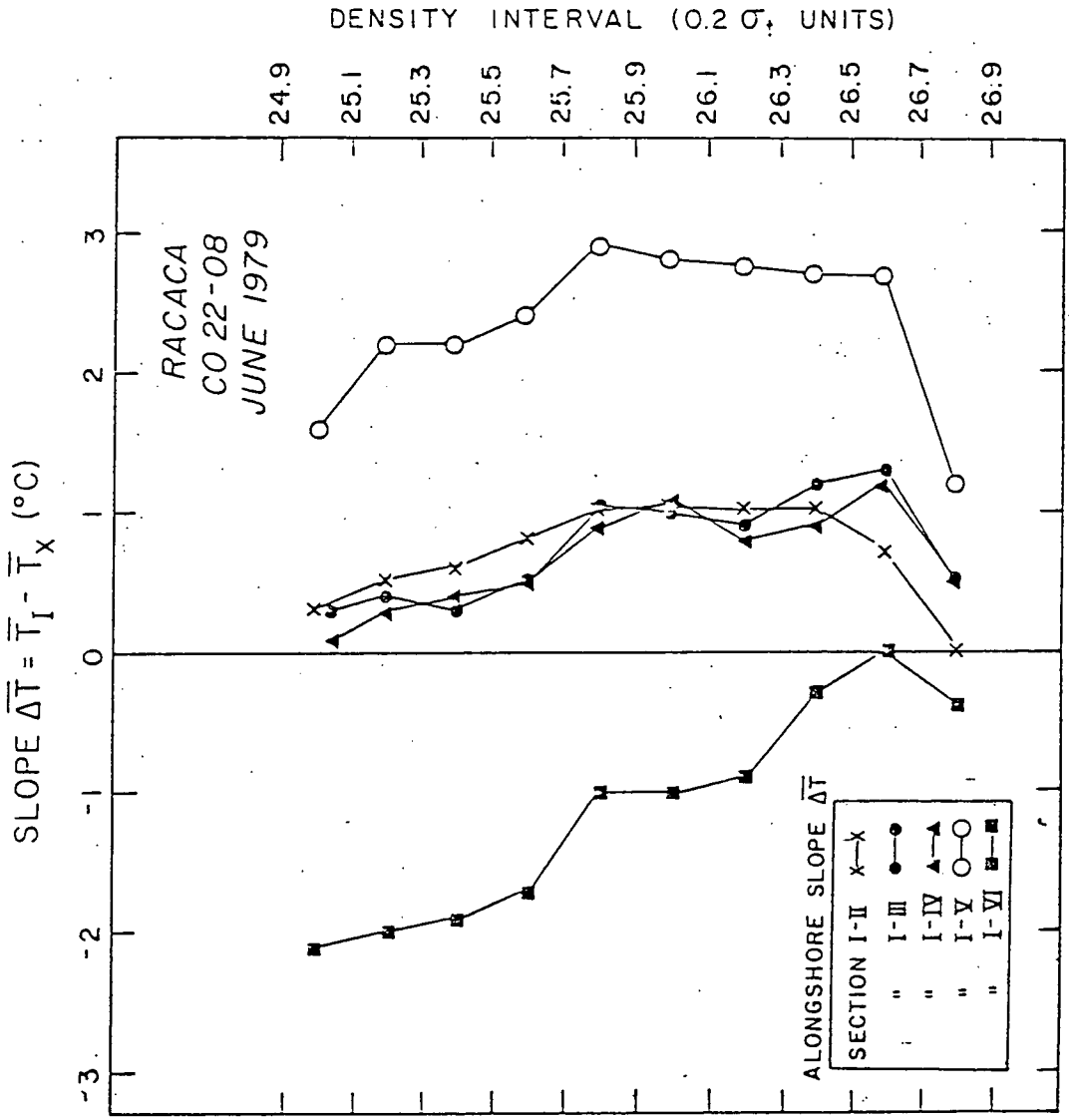
DENSITY INTERVAL (0.2 σt UNITS)
24.9
25.1
25.3
25.5
25.7
25.9
26.1
26.3
26.5
26.7
26.9
RACACA
CO 22-08
JUNE 1979
SLOPE ΔT = T̄I - T̄X (°C)
3
2
1
0
-1
-2
-3
ALONGSHORE SLOPE ΔT
SECTION I-II
I-III
I-IV
I-V
I-VI

Fig. 4.1-42a

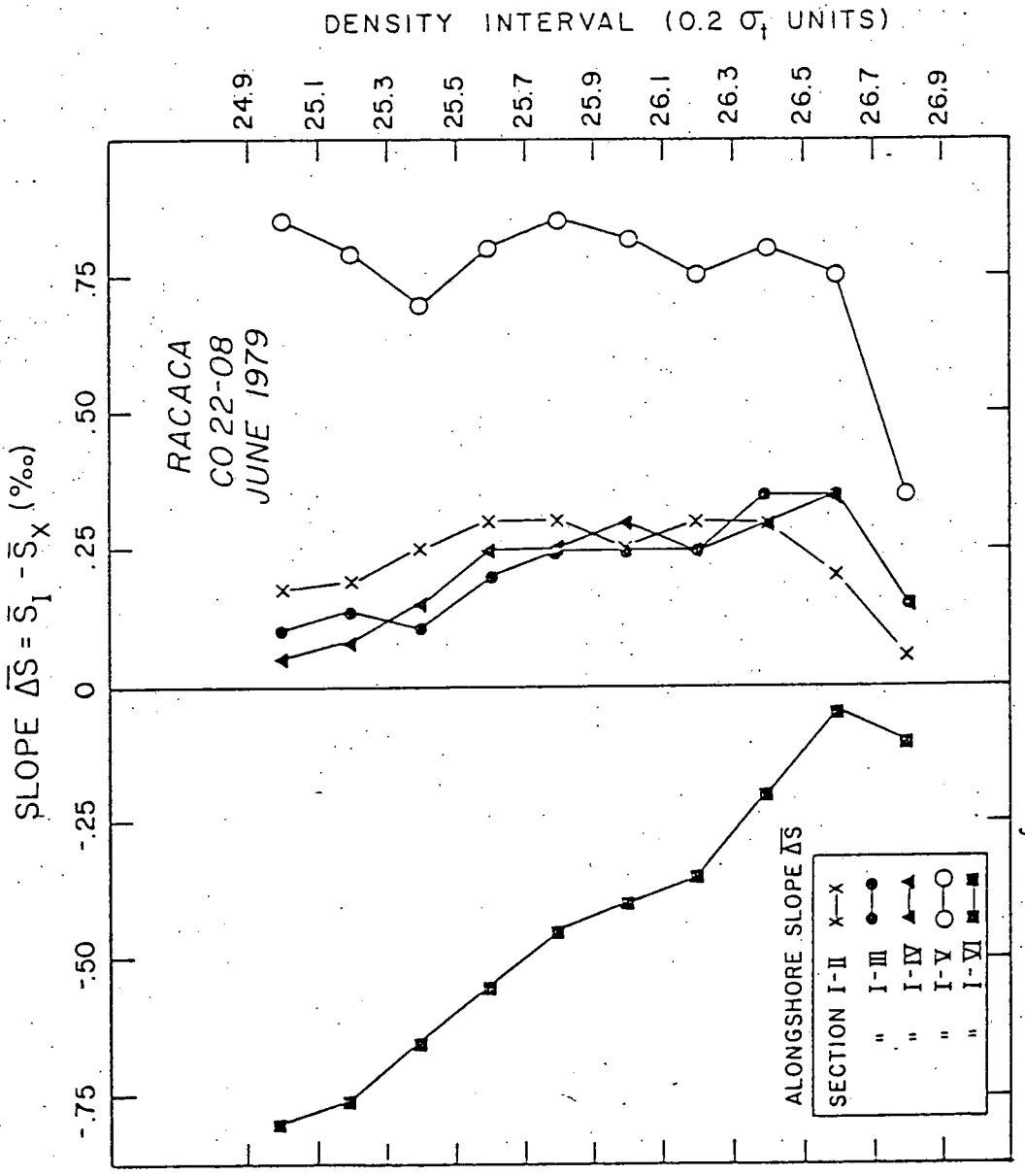
DENSITY INTERVAL (0.2 σ_t UNITS)
24.9
25.1
25.3
25.5
25.7
25.9
26.1
26.3
26.5
26.7
26.9
SLOPE $\overline{\Delta S} = \overline{S}_I - \overline{S}_X$ (‰)
.75
.50
.25
0
-.25
-.50
-.75
RACACA
CO 22-08
JUNE 1979
ALONGSHORE SLOPE $\overline{\Delta S}$
SECTION I-II X—X
" I-III ●—●
" I-IV ▲—▲
" I-V ○—○
" I-VI ■—■

Fig. 4.1-42b

The interpretation of these figures is rather straightforward for the alongshore slope water variations, but less clear for the more complex stratification over the outer shelf. In discussing these figures, the temperature and salinity differences vary consistently in relation to one another (warmer corresponding to saltier and cooler corresponding to fresher), so only temperature differences will be referred to for simplification.

1. Slope water alongshore variations: (Fig. 4.1-32a & b)

Sections II, III and IV are about equally cooler than I and exhibit little change over a short distance. In section V the apparent effect of one or more of possibilities (1) - (3) above (i.e. increased outflow from Chesapeake Bay getting across the shelf and mixing into the slope water column) can be seen in the dramatic cooling throughout the slope water column. Section VI slope water is dominated by the Gulf Stream right up to the shelf break.

2. Outer Shelf Water alongshore variations: (Figs. 4.1-33a & b)

At the very surface and within the mixed layer ($\sigma_t > 25$), II is warmer than I, most likely due to the dynamic effects of onshore forcing of slope water by eddy 79-A to the north. III and IV are cooler to the south probably due to river outflow. Section V is puzzling at the very surface because it is the warmest surface water north of VI, yet within

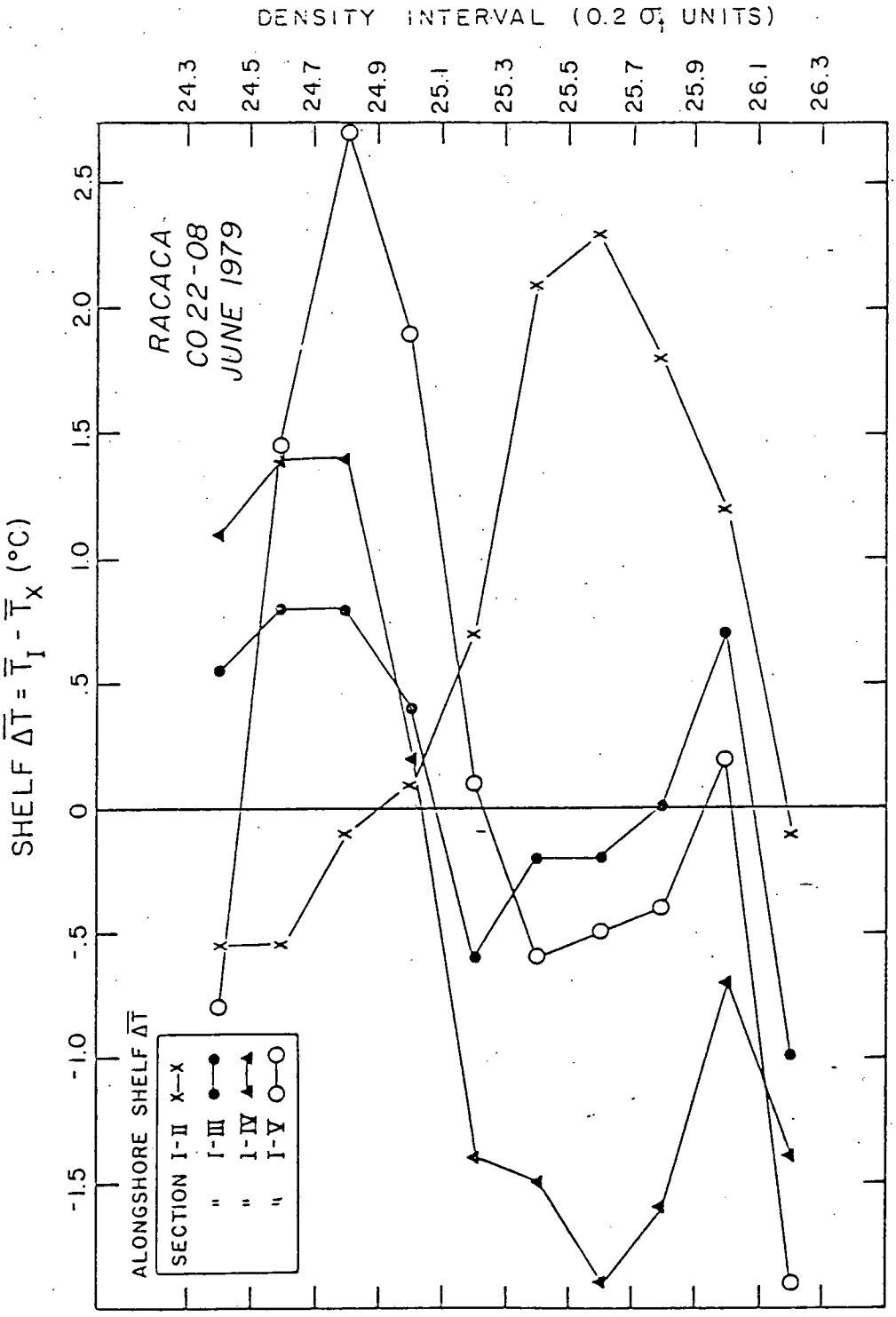
DENSITY INTERVAL (0.2 σ_t UNITS)
24.3
24.5
24.7
24.9
25.1
25.3
25.5
25.7
25.9
26.1
26.3
RACACA
CO 22-08
JUNE 1979
SHELF $\overline{\Delta T} = \overline{T}_I - \overline{T}_X$ (°C)
2.5
2.0
1.5
1.0
.5
0
-.5
-1.0
-1.5
ALONGSHORE SHELF $\overline{\Delta T}$
SECTION I-II x—x
" I-III
" I-IV
" I-V

Fig. 4.1-43b

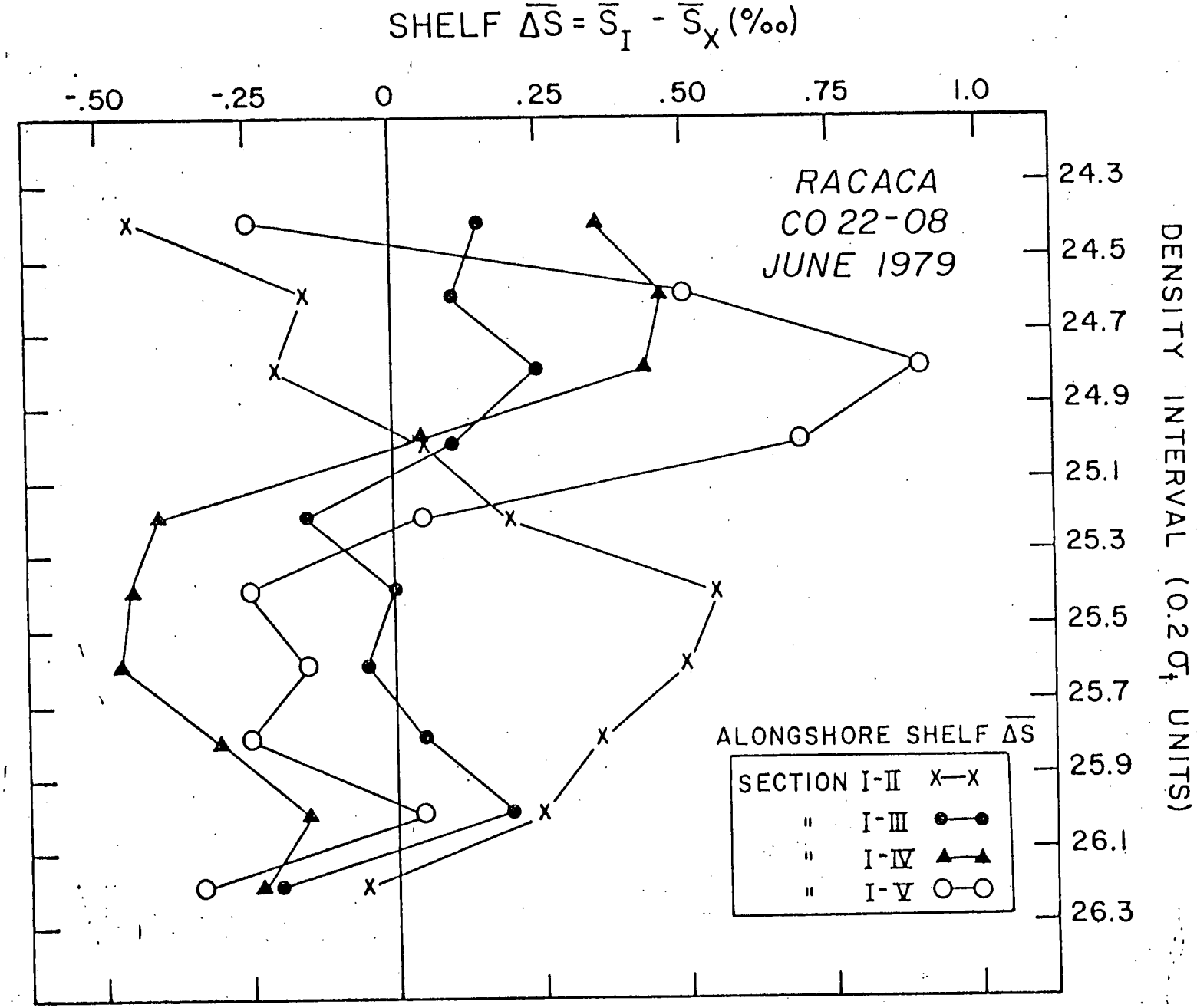
SHELF $\overline{\Delta S} = \overline{S}_I - \overline{S}_X$ (‰)
-.50
-.25
0
.25
.50
.75
1.0
RACACA
CO 22-08
JUNE 1979
24.3
24.5
24.7
24.9
25.1
25.3
25.5
25.7
25.9
26.1
26.3
DENSITY INTERVAL (0.2 σ_t UNITS)
ALONGSHORE SHELF $\overline{\Delta S}$
SECTION I-II X—X
= I-III
= I-IV
= I-V

Fig. 4.1-43a

the mixed layer it is expectedly the coolest water over the outer shelf. Within the pynocline (σ_τ between 25 and 26) section II is significantly cooler than I, yet sections III, IV and V become warmer, but not in a consistent alongshore progression. The warming is understandable in terms of isopycnal exchange and the differences observed to the south, but section II is puzzling. At the density of the cold pool (σ_τ = 26.2) the outer shelf gets steadily warmer (and saltier) to the south, while maintaining that consistent density.

Additionally, we are in the process of examining any alongshore variations that may exist in the deeper slope water below the main salinity maximum, which represents the seasonal extent of atmospheric penetration. This slope water is a mixture of components of Scotian shelf and slope water, NACW, Labrador Sea intermediate water, Mediterranean outflow water as well as NADW components.

IV. Low Radon Zone

One of the primary motivations behind this cruise was to examine the benthic hydrographic structure along the slope in the regions of the radon deficient zone (see the Geochemistry section on the low radon zone) with an eye towards evaluating the processes responsible for this phenomenon. While it is generally accepted that the lack of excess radon must result from rapid mixing of the radon away from the boundary layer, there is no concensus as to how the excess radon is transferred out of the boundary layer to where larger scale isopycnal

events (mixing) can take over. The RACACA CTD data is being closely examined to see: a: if any relationships exist between specific features of the T/S structure (i.e. the salinity minimum of the Labrador Intermediate water near 1000 m) and the low radon zone; and b: what the details of the vertical and horizontal density field look like and how they might relate to several proposed processes.

One possible mechanism involves the generation of internal tidal waves at certain locations along the continental slope where the bottom topography is thought to be more conducive to efficient generation through interaction with the surface tide (see the 1978 report and proposal). It is thought that enhanced mixing due to internal waves generated along the slope at places where the bottom slope is critical could be related to the radon minimum. A consideration of bottom profiles between the Hudson Canyon and Hatteras suggested we might expect the deeper parts of the radon minimum zone to be less apparent to the south, however the results of the RACACA survey do not corroborate this (see the Geochemistry section on the RACACA results).

A second potential mechanism involves variations in the vertical density gradient, possibly driven by internal waves or tides, that could result in an effective pumping of water in and out of the boundary layer. A time series of the vertical temperature gradient above the radon minimum zone is

essential to evaluating this time dependent mechanism, so we must await the recovery of our mooring in October 1980 (see the section 4.1.4 on Fieldwork - 1980.

A third possible explanation being evaluated with the use of the RACACA data is that zones of convergences and/or divergences (i.e. upwelling or downwelling) may exist in the bottom boundary layer due to an Ekman-type veering and that this could account for zones of low radon. While our analysis is still embryonic, it is possible that a vertical shear of the geostrophic current (a thermal wind shear) can be induced in the bottom boundary layer due to a horizontally non-homogeneous density field. For example, Fig. 4.1-44 pictures the density field (σ_T) over the slope of transect II with the low radon zone shown to be centered at about 1200 m, but being rather vague in the up or down-slope extent of this zone (see the Geochemistry section on the low radon zone). Horizontal gradients in the density field as well as tilting of the isopycnals near the bottom, as suggested by this figure, may be indicative of this process, but we are still tentative for several reasons: 1) inaccuracies in the dynamic method of computing relative currents (the geostrophic shear) in shallow areas and over a sloping bottom; 2) the dearth of current meter observations near the bottom over the slope in areas where we've observed the radon deficiency; and 3) doubts as to whether we have the data and resolution in the data to satisfactorily evaluate this possibility.

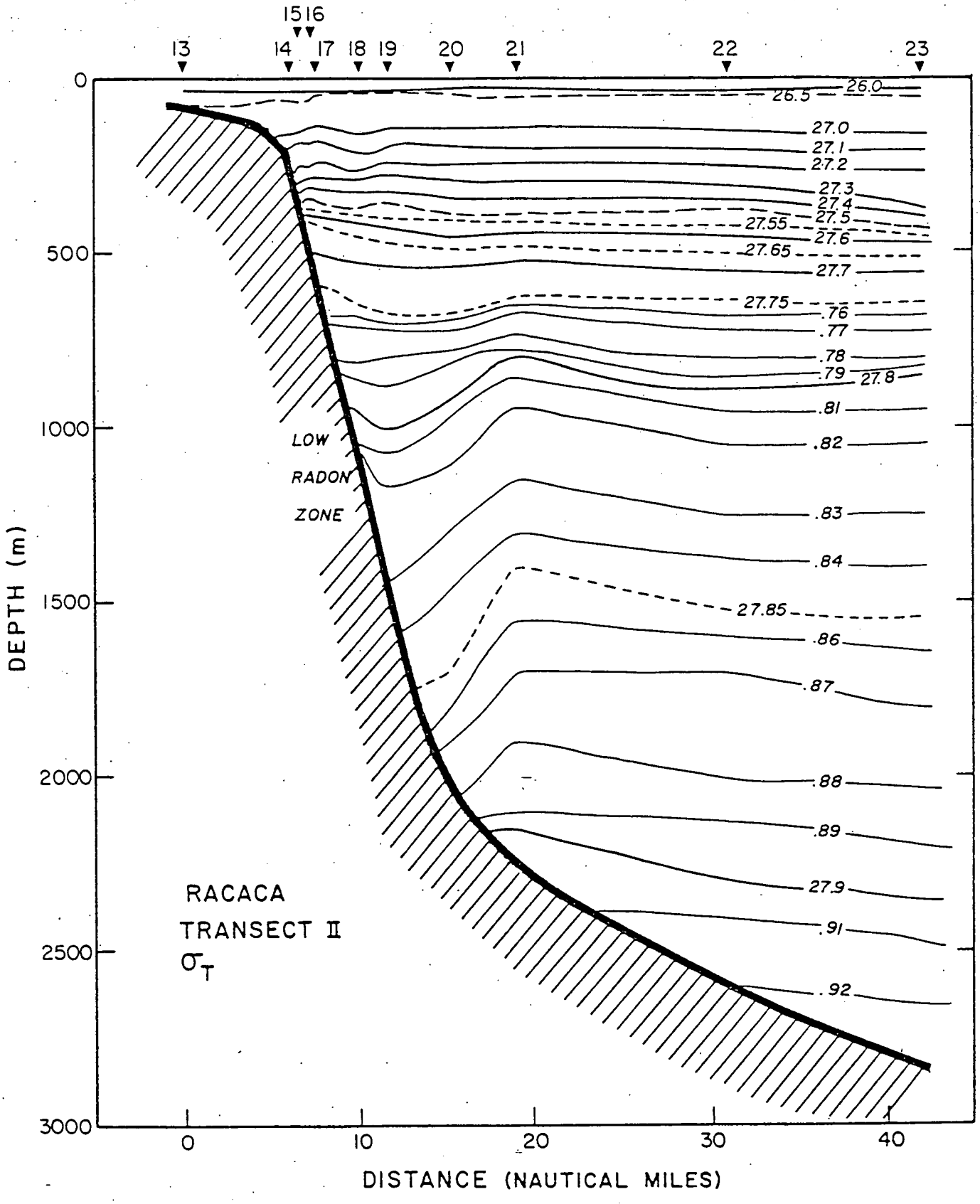
15 16
13
14
17
18
19
20
21
22
23
0
500
1000
1500
2000
2500
3000
DEPTH (m)
26.0
26.5
27.0
27.1
27.2
27.3
27.4
27.5
27.55
27.6
27.65
27.7
27.75
.76
.77
.78
.79
27.8
.81
.82
.83
.84
27.85
.86
.87
.88
.89
27.9
.91
.92
LOW
RADON
ZONE
RACACA
TRANSECT II
σ_T
0
10
20
30
40
DISTANCE (NAUTICAL MILES)

Fig. 4.1-44

4.1.4 FIELD WORK - 1980

On July 30, 1980 we deployed a mooring containing a 100 meter thermistor string and a current meter in roughly the same spot as last year (near the 1000 m isobath just South of the Hudson Canyon), to investigate the hypothesized pumping mechanism which may be responsible for the observed radon minimum band over the continental slope. This pumping mechanism involves the effective forcing of water in and out of the bottom boundary layer along the slope. Water can be driven along isopycnal layers by the differential motion of isopycnals, associated with variations in the vertical density gradient, and most likely driven by low frequency internal waves or internal tides.

Our mooring's thermistor chain will produce a temperature time series at 10 meter intervals from 100 to 200 m above the bottom. This should be good for detecting variations in the vertical density gradient, as a single valued T-S relation exist in the slope water below the depth of seasonal penetration of the atmosphere or shelf water influence (approximately 150 m and the 27 σ_t surface). Upon recovery, in late October, 1980, we plan a 25 hour CTD yo-yo time series (a diurnal tidal cycle) at the site of the mooring, to establish a relationship between temperature and density, to calibrate the thermistors, and to see how well the thermistor records compare to vertical density gradient variations in other parts of the water column.

Above the thermistor string, at the top of the mooring, we deployed a single Aanderaa RCM-4 current meter, which will give us an idea of the mean (and variations about the mean) flow above the bottom boundary layer.

At the time of last year's proposal it was reported that our thermistor chain mooring, deployed for fifty days from June 16th through August 5th, 1979, had been recovered and that the data was being processed. Unfortunately, the instrument failed due to a 'manufactured' hairline crack in the 'water tight' mouthpiece, allowing water to short out the connecting plug between the Aanderaa thermistor string and the Aanderaa TR-1 temperature profile recorder, and resulted in no useful data. Aanderaa accepted complete responsibility (little compensation for the lack of data) and has repaired the instrument.

References (Section 4.1)

BEARDSLEY, R.C., and C.N. FLAGG (1976) The water structure, mean currents, and shelf-water/slope-water front on the New England continental shelf. Mem. Soc. Roy. Sci. Liege, 6(X): 209-225.

BEARDSLEY, R.C., W.C. BOICOURT, and D.V. HANSEN (1976) Physical oceanography of the Middle Atlantic Bight. Middle Atlantic Continental Shelf and the New York Bight, Am. Soc. Limnol. & Oceanogr., Special Symposia, 2 [M.G. Gross, Ed.], 20-34.

BOICOURT, W.C., and P.W. HACKER (1976) Circulation of the Atlantic continental shelf of the United States, Cape May to Cape Hatteras. Mem. Soc. Roy. Sci. Liege, 6(X): 187-200.

BUMPUS, D.F. (1973) A description of the circulation of the continental shelf of the east coast of the United States. Prog. Oceanogr., 6: 111-157.

BUNKER, A.F., and L.V. WORTHINGTON (1976) Energy exchange charts of the North Atlantic Ocean. Bull. Am. Meteorol. Soc., 57: 670-678.

CHENEY, R.E., and P.L. RICHARDSON (1976) Observed decay of a cyclonic Gulf Stream ring. D.S.R., 23: 143-155.

CHUANG, W.-S., D.-P. WANG, and W.C. BOICOURT (1979) Low frequency current variability on the southern Mid-Atlantic Bight. Preprint submitted to J.P.O.

COLTON, J.B., R.R. MAREK, S. NICKERSON, and R.F. STODDARD (1968) Physical, chemical, and biological observations on the continental shelf, Nova Scotia to Long Island, 1964-66. U.S. Dept. Interior, F.W.S. Data Dept., 23, Washington, D.C.

CRESWELL, G.H. (1967) Quasi-synoptic monthly hydrography of the transition region between coastal and slope water south of Cape Cod, Mass. W.H.O.I. Ref. No. 67-35 (Unpublished manuscript).

CSANADY, G.T. (1973) Turbulent diffusion in the environment. Geophys. Astrophys. Monogr. 3, 248 pp.

FISHER, Alvan, Jr. (1972) Entrainment of shelf water by the Gulf Stream northeast of Cape Hatteras. J. Geophys. Res., 77 (18): 3248-3255.

FORD, W.L., J.R. Longard and R.E. Banks (1952) On the nature, occurrence and origin of cold, low salinity water along the edge of the Gulf Stream. J. Mar. Res., 11 (3): 281-293.

GORDON, A.L. and F. Aikman III (1980) The Middle Atlantic Bight pycnocline salinity maximum. Limnol. Oceanogr. (in press).

GORDON, A.L., A.F. AMOS, and R.D. GERARD (1976) New York Bight water stratification - October 1974. Middle Atlantic Continental Shelf and the New York Bight, Am. Soc. Limnol. & Oceanogr., Special Symposia, 2 [M.G. Gross, Ed.], 45-57.

HAGAN, D.E., D.B. OLSON, J.E. SCHMITZ, and A.C. VASTANO (1978) A comparison of cyclonic ring structures in the northern Sargasso Sea. J.P.O. 8: 997-1008.

HALLIWELL, G.R., Jr., and C.N.K. Mooers (1979) The space-time structure and variability of the shelf water-slope water and Gulf Stream surface temperature fronts and associated warm core eddies. J. Geophys. Res., 84: 7707-7725.

HANSEN, D.V. (1977) Circulation. MESA New York Bight Atlas Monograph 3, 23 pp. N.Y. Sea Grant Inst., Albany, N.Y.

HOPKINS, T.S., and N. GARFIELD III (1979) Gulf of Maine Intermediate Water. J. Mar. Res., 37: 103-139.

JOYCE, T.M., W. ZENK, and J.M. TOOLE (1978) The anatomy of the Antarctic polar front in the Drake Passage. J.G.R., 83: 6093-6113.

KETCHUM, B.H., and N. CORWIN (1964) The persistence of "winter" water on the continental shelf south of Long Island, New York. Limnol. & Oceanogr., 9: 467-475.

KETCHUM, B.H., and D.J. KEEN (1955) The accumulation of river water over the continental shelf between Cape Cod and Chesapeake Bay. D.S.R., Suppl. to 3, 346-357.

KUPFERMAN, S.L. and N. Garfield (1977) Transport of low salinity water at the slope water-Gulf Stream boundary. J. Geophys. Res., 82 (24): 3481-3486.

LAMBERT, R.B. (1974) Small-scale dissolved oxygen variations and circulation in the Sargasso Sea. D.S.R., 21: 529-546.

McLELLAN, H.J. (1957) On the distinctness and origin of the slope water off the Scotian shelf and easterly flow south of the Grand Banks. J. Fish. Res. Bd. Can., 14: 213-239.

MALONE, T.C. (1976) Phytoplankton productivity in the apex of the New York Bight: Environmental regulation of productivity/chlorophyll a. Middle Atlantic Continental Shelf and the New York Bight, Am. Soc. Limnol. & Oceanogr., Special Symposia, 2 [M.G. Gross, Ed.], 260-272.

MAYER, D.A., D.W. HANSEN, and D.A. ORTMAN (1979) Long-term current and temperature observations on the Middle Atlantic shelf. J.G.R., 84: 1776-1792.

MOOERS, C.N.K., R.W. Gorvine, and W.W. Martin (1979) Summertime synoptic variability of the Middle Atlantic shelf water/ slope water front. J. Geophys. Res., 84: 4837-4854.

MORGAN, C.W. and J.M. Bishop (1977) An example of Gulf Stream eddy-induced water exchange in the Mid-Atlantic Bight. J. Phys. Oceanogr., 7: 472-479.

OKUBO, Akira (1971) Oceanic diffusion diagrams. D.S.R., 18: 789-802.

PINGREE, R.D., P.M. HOLLIGAN, and G.T. MARDELL (1978) The effects of vertical stability on phytoplankton distributions in the summer on the northwest European shelf. D.S.R., 25: 1011-1028.

POSMENTIER, E.S., and R.W. Houghton (1980) Springtime evolution of the shelf break front. (submitted to J.G.R.)

SAUNDERS, P.M. (1971) Anti-cyclonic eddies formed from shoreward meanders of the Gulf Stream. D.S.R., 18: 1207-1219.

SMITH, P.C. (1978) Low frequency fluxes of momentum, heat, salt, and nutrients at the edge of the Scotian Shelf. J.G.R., 83: 4079-4096.

STERN, M.E. (1967) Lateral mixing of water masses. D.S.R., 14: 747-753.

VOORHIS, A.D., D.C. WEBB, and R.C. MILLARD (1976) Current structure and mixing in the shelf/slope water front south of New England. J.G.R., 81, 3695-3708.

WALSH, J.J., et al., preprint, Wind events and food chain dynamics within the New York Bight.

WEATHERLY, G.L., and P.J. MARTIN (1978) On the structure and dynamics of the oceanic bottom boundary layer. J.P.O., 8: 557-570.

WRIGHT, W.R. (1976) The limits of coastal water south of Cape Cod, 1941 to 1972. J. Mar. Res., 34: 1-14.

WRIGHT, W.R., and C.E. Parker (1976) A volumetric temperature/salinity census for the Middle Atlantic Bight. Limnol. Oceanogr. 21 (4): 563-571.

WUNSCH, C. (1968) On the propagation of internal waves up a slope. D.S.R., 15, 251-258.

WUNSCH, C., F.S. HOTCHKISS, and R.C. MILLARD (preprint) Dynamics of deep water canyons.

4.2 Oxygen Isotopes as Tracers of Water Mass Origins and Mixing on the Continental Shelf

The oxygen isotopic composition of precipitation is primarily regulated by the temperature difference between the source region)region of evaporation) and the region of precipitation. As a result the $H_2{}^{16}O$ molecule is progressively enriched in meteoric water with increasing latitude. The broad latitudinal range of the Middle Atlantic Bight, and the coastal geometry, and the substantial local fresh water contribution to the shelf waters provide a unique opportunity to use this sensitive water mass tracer.

During this past funding year we have completed the development and testing of a high precision CO_2 equilibration system for oxygen-18 analysis of seawater. We are now calibrated to the international O-18 standards and the system is fully operational at a precision of XX ± 0.05 °/oo $\delta^{18}O$. We are nearing the end of the first stage of the isotope program which is to define the isotopic end members of the system. This step permits us to empirically determine which mixing process can be resolved by this method.

4.2.1 Recent results

$^{18}O/^{16}O$ ratio measurements isotopically delineate five water types or end members which define the Middle Atlantic Bight system (figure 4.2-1). (1) Gulf Stream water at 36.302 °/oo salinity and 1.09 °/oo $\delta^{18}O$. (2) High latitude meteoric water at -21.97 °/oo $\delta^{18}O$. (3) Scotian Shelf meteoric water at -14.50 °/oo $\delta^{18}O$. (4) Middle Atlantic Bight meteoric water at -11.23 °/oo $\delta^{18}O$. (5) South Atlantic Bight meteoric water at -3.92 °/oo $\delta^{18}O$.

The Scotian Shelf transect ranges in salinity from 30.73 °/oo to 35.705 °/oo. Waters with salinities greater than 32.70 °/oo are pure Labrador Sea waters (figure 4.2-1). These samples are from deep casts at all 6 Scotian Shelf stations (Table 4.2-1). Station 6 is beyond the continental shelf. These data define a binary mixing line with Gulf Stream water at 36.302 °/oo salinity and 1.09 °/oo $\delta^{18}O$ with meteoric water at -21.97 °/oo $\delta^{18}O$. The slope ($d\delta^{18}O/d\delta$) of this line is precisely the same as the $d\delta^{18}O/d$ relationship due to evaporation-precipitation processes in high latitude surface waters (Craig and Gordon, 1965). Our value for the meteoric component (-21.97 °/oo $\delta^{18}O$) agrees with Tan and Strain's (1980) estimated value of -21.8 ± .80 °/oo $\delta^{18}O$ for the Labrador Sea south of Davis Strait, which is an area free of sea ice melt water.

Surface water (less than 50m) samples at stations 1, 2 and 3 with salinities less than 32.70 °/oo show mixing with local meteoric water with a mean composition of -14.50 °/oo $\delta^{18}O$.

Six samples from the Middle Atlantic Bight show binary mixing between pure Labrador Sea water at sample 294 (34.137 °/oo salinity; -0.26 °/oo $\delta^{18}O$; 19.8°C) on the outer continental shelf and meteoric water with a $\delta^{18}O$ composition of -11.23 °/oo. Sample 271(B1) is "cold pool" water (32.889 °/oo salinity; 5.845°C) and its departure from the Labrador Sea water mixing line results from an admixture of 3.66% local meteoric water with pure Labrador Sea water with a salinity of 34.137 °/oo and a $\delta^{18}O$ composition of -0.26 °/oo.

Two samples of slope water fall on a mixing line between Gulf Stream water and mid-Atlantic Bight water with an isotopic composition equal to

"cold pool" water but 0.325 °/oo fresher than cold pool water at station 271(B1).

Four Gulf Stream samples show good agreement. Samples 347 and 332 are definitely within the Gulf Stream and fall directly on the mixing line. Sample 345 is adjacent to the Cape Hatteras shelf and is slightly influenced by local meteoric water. Sample 346 is also near the Cape Hatteras shelf but appears to be isotopically depleted by 0.1 °/oo. This analysis needs to be triplicated.

The South Atlantic Bight mixing line is dashed on figure 4.2-1. The mean meteoric component for the South Atlantic Bight is estimated at -3.92 °/oo based on H/D measurements for the Roanoke River (-24 °/oo), Ogeechee River (-21 °/oo) and the Darien River (-19 °/oo) (Friedman et al., 1964). The relationship between δD and $\delta^{18}O$ relative to SMOW obeys the equation $\delta D = 8\delta^{18}O + 10$ (Craig 1961). The estimated South Atlantic Bight mixing line should be accurate because local runoff is the only significant source of fresh water.

4.2.2 Discussion

Cold Pool

IN the Middle Atlantic Bight the transition zone between cold shelf water and warmer, saltier slope water usually occurs as a sharp inclined front located near the shelf break in winter. During summer months these temperature and salinity gradients below the seasonal thermocline are maintained although the front is not as sharply defined. This "cold pool" is a continuous and persistent feature from Chesapeake to Georges Bank. Ketchum and Crowin (1964) assumed that the cold pool formed by winter mixing and remained stationary during the summer months.

Mooring data indicate that the cold pool moves southward at velocities equal to or exceeding the mean southward current of the surrounding warmer water (Beardsley et al., 1976). Beardsley et al. (1976) concluded that the cold pool found near Hatteras in August must have formed by winter cooling near Cape Cod or possibly in the Gulf of Main. Citing Sutcliffe's (1976) evidence that fluctuations in the tranport of the St. Lawrence system can be traced down the Scotian shelf and into the Gulf of Main, Beardsley et al., suggested a freshwater pathway from the St. Lawrence to Cape Hatteras.

Pure Labrador Sea water (sample #294) at 34.137 °/oo salinity with a $\delta^{18}O$ composition -0.26 °/oo is present at the outer continental shelf. This water mixed with 3.66% local meteoric water at -11.23 °/oo $\delta^{18}O$ apparently produces cold pool water (i.e., sample #271B1) with a salinity of 32.889 °/oo and a $\delta^{18}O$ composition of -0.75 °/oo (t = 5.845°C).

Two samples of slope water (#325, #312) near the shelf/slope break are approximately an even mixture of Gulf Stream water and "cold pool" water. In principal, slope water can probably be defined on an ^{18}O-salinity plot by the 3-component system: Gulf Stream, local meteoric, and Labrador Sea meteoric water.

Once a first order isotopic description of Middle Atlantic Bight circulation patterns and rates are completed on a seasonal scale, our ability to predict circulation details or events from upstream isotopic measurements may become a reality. Oxygen isotope ratios and salinity measurements offer the first conservative tracer-pair suitable for detailed descriptive physical oceanography of the Middle Atlantic Bight region. Full application of this tracer can only be accomplished through a

Table 4.2-1. Oxygen isotope sample data.

CSS Dawson; Bedford Institute; J.M. Bewers, Oct. 1975

Scotian Shelf Samples						
LDGO #	Station #	Sample #	Depth(m)	Lat./Long.	$\delta^{18}O$ (raw) SMOW	Salinity
4918	1	751800	1	44°24.2'N 63°26.1'W	-1.78	31.113
4984	1	751801	25	44°24.2'N 63°26.1'W	-1.67	31.590
4920/4985	1	751802	80	44°24.2'N 63°26.1'W	-1.20	32.713
4922	2	751810	20	44°15.6'N 63°18.6'W	-2.00	30.736
4986	2	751811	75	44°15.6'N 63°18.6'W	-1.19	32.725
4987	2	751812	100	44.15.6'N 63°18.6'W	-0.86	33.209
5057/5088	3	751826	118	43°53'N 62°52.8'W	-0.03	34.542
5058	3	751825	52	43°53'N 62°52.8'W	-1.20	32.490
5059	3	751828	216	43°53'N 62°52.8'W	0.29	35.003
5060	5	751853	90	43°11'N 62°7'W	-0.52	33.775
5061/5089	6	751861	100	42°51'N 61°44'W	0.69	35.705

Table 4.2-1. Oxygen isotope sample data (continued)

Mid-Atlantic Bight/Gulf Stream RACACA: June 1979

Scotian LDGO #	Shelf Station #	Samples Sample #	Depth(m)	Lat./Long.	(raw) SMOW	Salinity
4552	270		1	39°31.5'N 73°56.9'W	-1.43	30.296
4553	271B11		1	39°23.5'N 73°33.1'W	-1.61	30.212
4554	271B1		deep	39°23.5'N 73°33.1'W	-0.75	32.889
4555	294		1	38°19.3'N 73°50.0'W	-0.26	34.137
4540	301		1	37°40.5'N 74°22.6'W	-0.52	33.238
4539	312		1	36°37.6'N 74°11.6'W	0.30	34.792
4538	314		1	36°37.6'N 74°49.1'W	-0.88	31.944
4537	325		1	36°18.8'N 74°02.8'W	0.30	34.578
4441/4536	329		1	35°24.7'N 75°08.6'W	-1.02	30.835
4442	332		1	35°18.8'N 74°58.8'W	1.15	36.379
4443	345		1	34°54.6'N 75°16.5'W	1.10	36.192
4444	346		1	34°52.0'N 75°23.4'W	1.01	36.335
4445	347		1	34°54.4'N 75°15.5'W	1.09	36.303

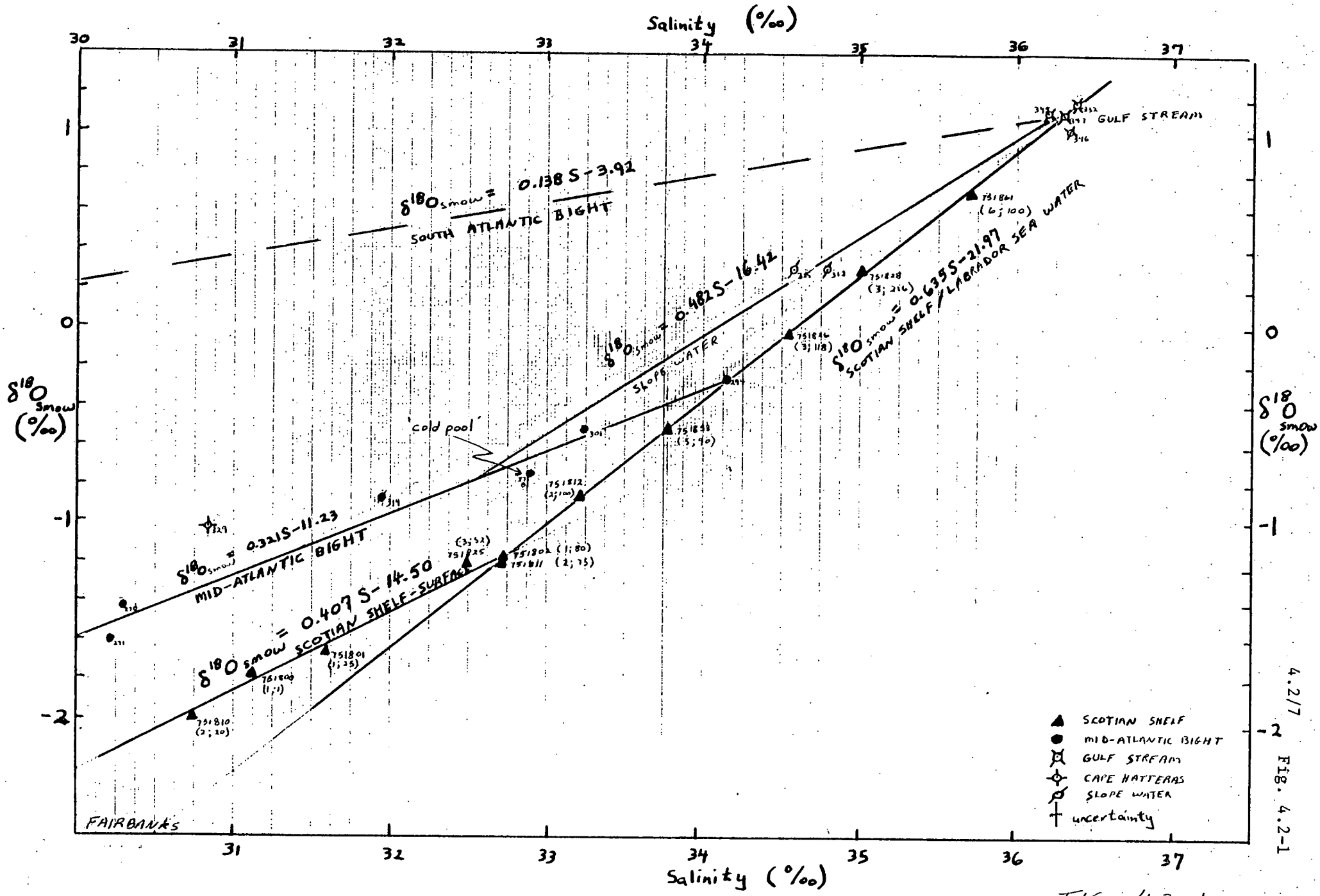

FIG. 4.2-1

4.2/7 Fig. 4.2-1

References Cited

Beardsley, R.C., W.C. Boicourt and D.V. Hansen. 1976. Physical oceanography of the middle Atlantic bight. Am. Soc. Limnol. Oceanogr. Spec. Symp. 2: 20-34.

Craig, H. 1961. Standards for reporting concentrations of deuterium and oxygen-18 in natural waters. Science 133: 1833-1834.

Craig, H. and L.I. Gordon. 1965. Deuterium and oxygen-18 variations in the ocean and the marine atmosphere. In: Stable Isotopes in Oceanographic Studies and Paleotemperatures. Spoleto Conference Proceedings, E. Tongiorgi, ed. Consiglio Nazionales delle Richerche, Pisa, 9-130.

Friedman, I., A.C. Redfield, B. Schoen, and J. Harris. 1964. The variation of the deuterium content of natural waters in the hydrologic cycle. Rev. Geophys. Space Phys. 2(1): 177-224.

Sutcliff, W.H., R. Loucks, and K. Drinkwater. 1976. Considerations of ocean circulation and fish production on the Scotian Shelf and in the Gulf of Maine, Pt. 1. Ocean circulation and physical oceanography. 33(1): 98-115.

Tan, F.C. and P.M. Strain. 1980. The distribution of sea ice meltwater in the eastern Canadian arctic. J. Geophys. Res. 85(C4): 1925-1932.

4.3 Tritium as a Tracer of Water Mass Origins on the Continental Shelf

Very similar to O-18 tracer, the tritium concentration of river waters flowing into the Atlantic Bight is also a function of latitude. Therefore tritium is another useful tracer for studying the processes of water mass mixing on the continental shelf.

The tritium data from the RACACA cruise (June 1979) are limited, however the tritium concentration vs. salinity plot (Fig. 4.3-1) shows consistent results as compared to oxygen isotope data (Fig. 4.2-1) i.e., the "cold pool" water is a mixture of inner shelf water, Gulf Stream water and high tritium northern water (probably originated from the Labrador Sea). In addition the surface slope water is a mixture of the "cold pool" water and the Gulf Stream water. Even though, the tritium analysis is more time consuming than oxygen isotope, we hope to analyze some more samples in conjunction with the oxygen isotope works.

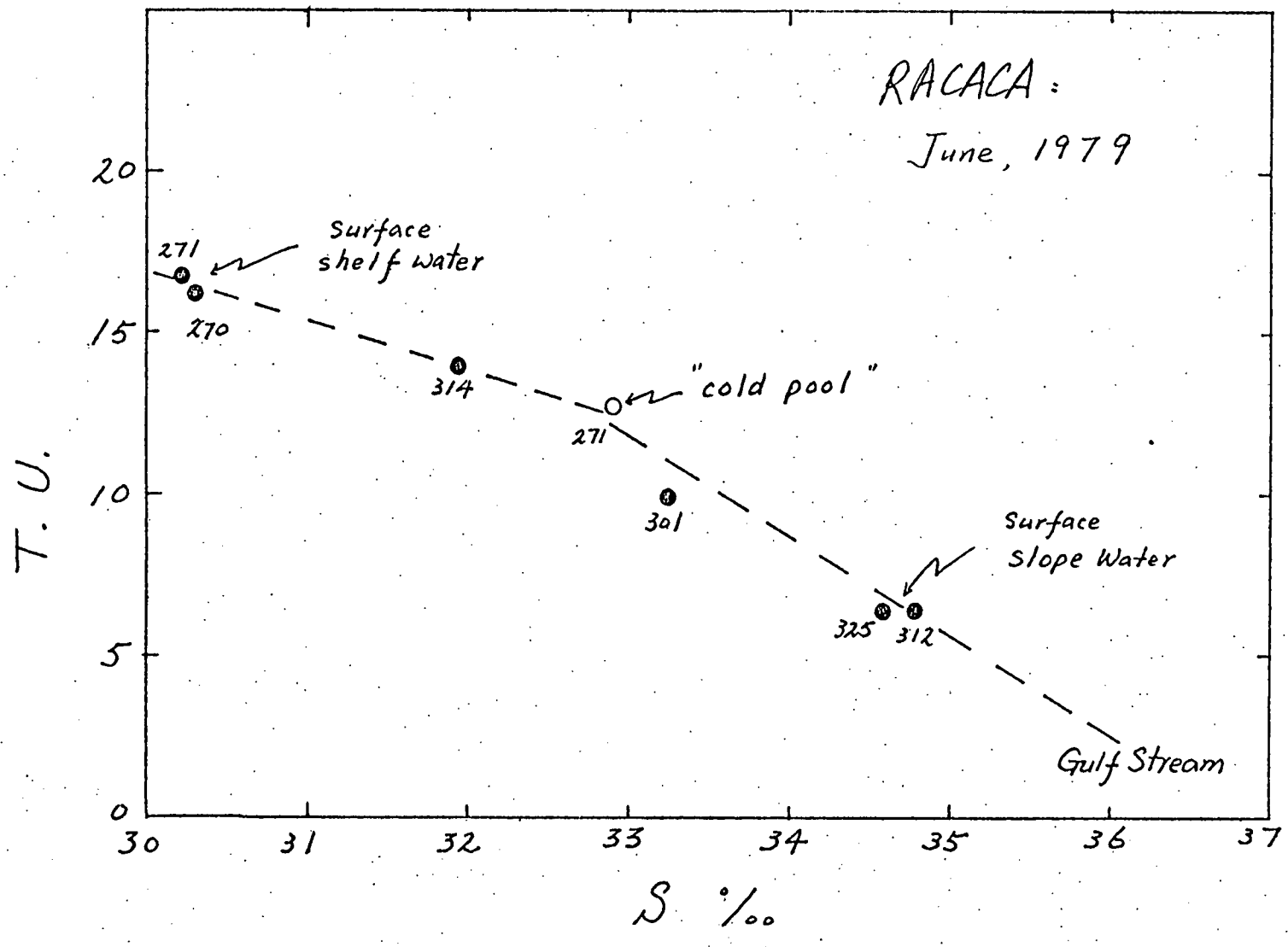

Fig. 4.3-1 The plot of tritium concentration (T.U.) vs. salinity in the New York Bight during the RACACA cruise (June 1979).

4.4 Radon-222 as a Tracer of Water Motions and Mixing

4.4.1 Introduction

Radon-222 (^{222}Rn) is a radioactive noble gas with a half-life of 3.8 days. It's properties of chemical inertness and a short radioactive half-life make it suitable for studies of water motions that occur on time scales of about one week. Although radon is produced throughout the water column by the decay of dissolved ^{226}Ra, the major source of ^{222}Rn in shallow water and in near-bottom water of the deep ocean is the sediments at the bottom in which the concentration of ^{226}Ra is much higher than in the overlying water. As a result of the strong concentration gradient of ^{222}Rn between the sediment and the overlying water, significant amounts of radon diffuse upward across the sediment water interface. It is this radon that enters the water column from the sediments (known as excess radon, i.e., in excess of that produced within the water column) that is useful in studies of both vertical and horizontal transport of dissolved substances within the overlying water.

Study of the vertical and horizontal distributions of dissolved ^{222}Rn in the waters of the New York Bight and the adjacent slope has been an important focus of the Lamont research effort supported by this contract. Six areal surveys of the radon distribution in the Bight covering all four seasons have been conducted. On four of these cruises extensive sampling of the near-bottom waters of the adjacent continental slope was also performed. In addition to these surveys another cruise focused on the area referred to here as the "Mud Hole" (a large area of fine-grained sediment south of Rhode Island and Martha's Vineyard, figure 4.4-1) in order to examine the time variability of vertical profiles of ^{222}Rn.

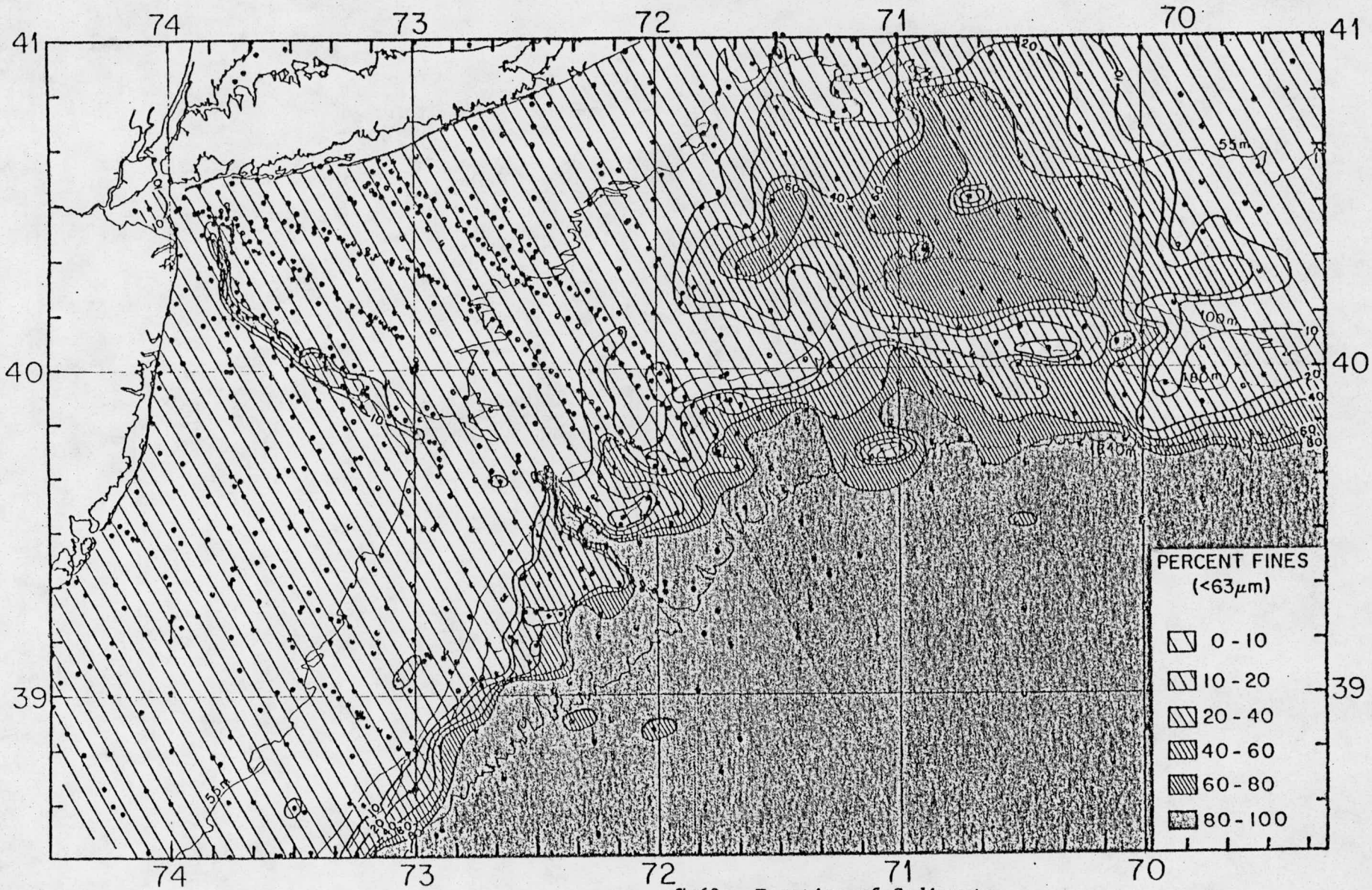

%<63μ Fraction of Sediments

("Mudhole" is fine-grained area north of 40°N between about 70°-72°W.)

Fig. 4.4-1

On the most recent cruise, the waters of the continental slope from the New York Bight to Cape Hatteras (Fig. 4.1.1a) were sampled in order to determine the extent and possible causes of the low radon zone observed in all of our previous cruises on the slope (see section 4.4.5). All water column measurements of ^{222}Rn were accompained by measurements of hydrographic properties and the concentrations of suspended particles. Sediment samples were also collected on all cruises in order to determine the distribution of radon production in sediments and to gain some understanding of the flux rate of radon out of the sediments.

The results of this work are being incorporated in a Ph.S. thesis currently being written by Steve Carson and in two papers one concerning the shelf distribution and the other concerning the slope. Much of this work has been discussed in previous annual reports. In this report we will summarize all of our results as presented in the above mentioned thesis and papers with emphasis on recent findings.

4.4.2 Source Function of Radon-222 from Sediments.

In order to understand the distribution of excess ^{222}Rn in the waters of the shelf and slope one requires a knowledge of the distribution of the sediment source function of radon. The bulk of our effort in this direction has been to collect surface grabs and cores to be used in measurements of the production of radon that enters the pore waters and can diffuse from there into the overlying water. (Diffusible radon is produced by radium that is on or near grain surfaces. Radon produced deep within sediment grains cannot diffuse out of the grain lattice before decaying.)

The other more recent part of our effort to define the source function has involved the collection of cores which are sampled on shipboard at discrete intervals down the core in order to measure the distribution of *in situ* pore-water radon. The samples are later measured in the lab for production of diffusible radon, i.e., the equilibrium pore-water radon concentration with no radon loss, as well as other radioisotopes (see Sec. 3.1). The *in situ* radon concentration in the upper part of the core should be less than the concentration of diffusible radon due to loss of radon from the sediment to the overlying water. The difference between the two sets of measurements integrated down the core should give a measure of the total loss (flux) of radon from the sediment to the overlying water.

4.4.2.1 Radon Source Function on the Shelf.

The most important feature of the distribution of diffusible radon production in the sediments of New York Bight area is that radon production is strongly correlated with grain size in most parts of the Bight. Much of the shelf sediment of the Bight has less than 3% < 63μm sediment and most of these sands show radon productions of .02 to .06 dpm/mgm (dry weight)(figures 4.4-1 and 2). The exception to this is found to the southwest of the Hudson Shelf Channel and will be discussed later.

The sediments of both the Hudson Shelf Channel and the Mudhole, however, contain high concentrations of < 63μm sediments. When radon production is plotted versus the percentage < 63 μm sediments in these areas a strong linear correlation is found. This correlation can be easily explained from the fact that the grain surface area per unit weight increases with increasing percentage of fine grained sediment and that clays in the fine grained portion of the sediment have exchange sites to which radium can be adsorbed.

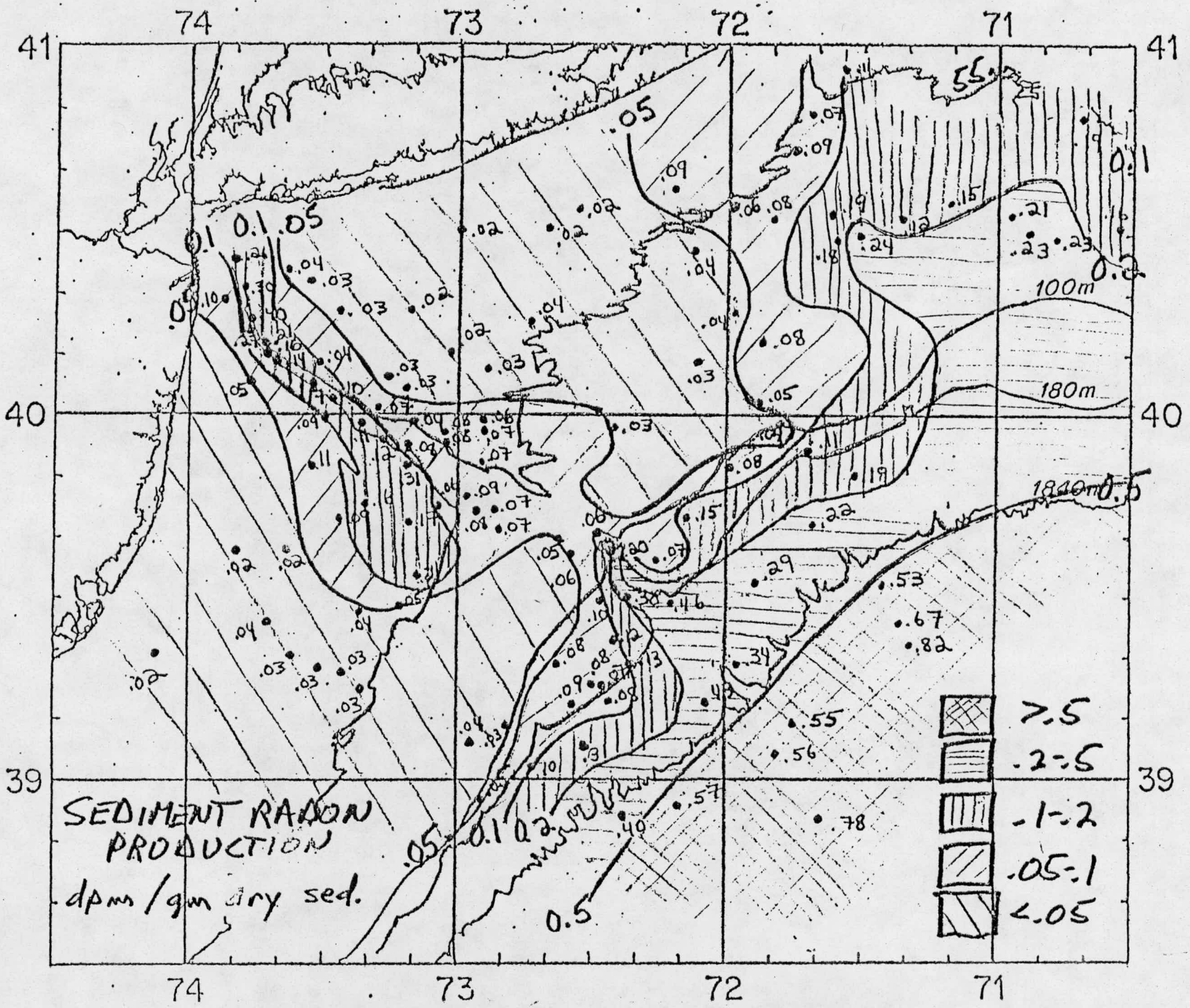
74
73
72
71
41
40
39
100m
180m
SEDIMENT RADON PRODUCTION
dpm/gm dry sed.
>.5
.2-.5
.1-.2
.05-.1
<.05

4.4/6 Fig. 4.4-2

As can be seen in figure 4.4-3 the sediments of the Channel have a correlation between production and grain size that is different from the correlation in the Mudhole. The former correlation has a much steeper slope. This indicates that the fine grained end member of the mixing curve formed by sediments in the Channel has higher concentrations of surface radium, i.e., higher radon production, than the fine grained sediments of the Mudhole (.48 dpm/g vs. .26 dpm/g). The reasons for this difference in the fine grained end members are currently under investigation. Samples from the two areas have been fractionated into sizes < 2μ, 2-63μ and > 63μ. Radon production analyses of these fractions are being performed at the present time.

As mentioned above the one exception to the general relationship between radon production and percentage < 63μm sediment is in an area of sandy sediment (< 3% finer than 63 μm) in a region southwest of the Hudson Shelf Channel (referred to as the "anomalous sands") (figures 4.4-1 and 2). Radon production in the sediments of this area ranges from .06 to .31 dpm/g. The extent of the area is at least 40 km in the direction parallel to the axis of the Channel (southeast) and ~ 35 Km in the direction perpendicular to the Channel axis (Fig. 4.4-2).

Experiments designed to determine the source of the high radon production in these sands are underway. So far results have shown that, surprisingly, most of the radon is coming from the > 63μm fraction of these sediments. In order to narrow down the range of possible minerals that may be contributing to the high production, two samples from the "anomalous" sandy area, i.e., high-production sands, and one from a "normal" sandy area, i.e., low-production sands, have been separated with a Franz isostatic magnetic separator. In the process six fractions were

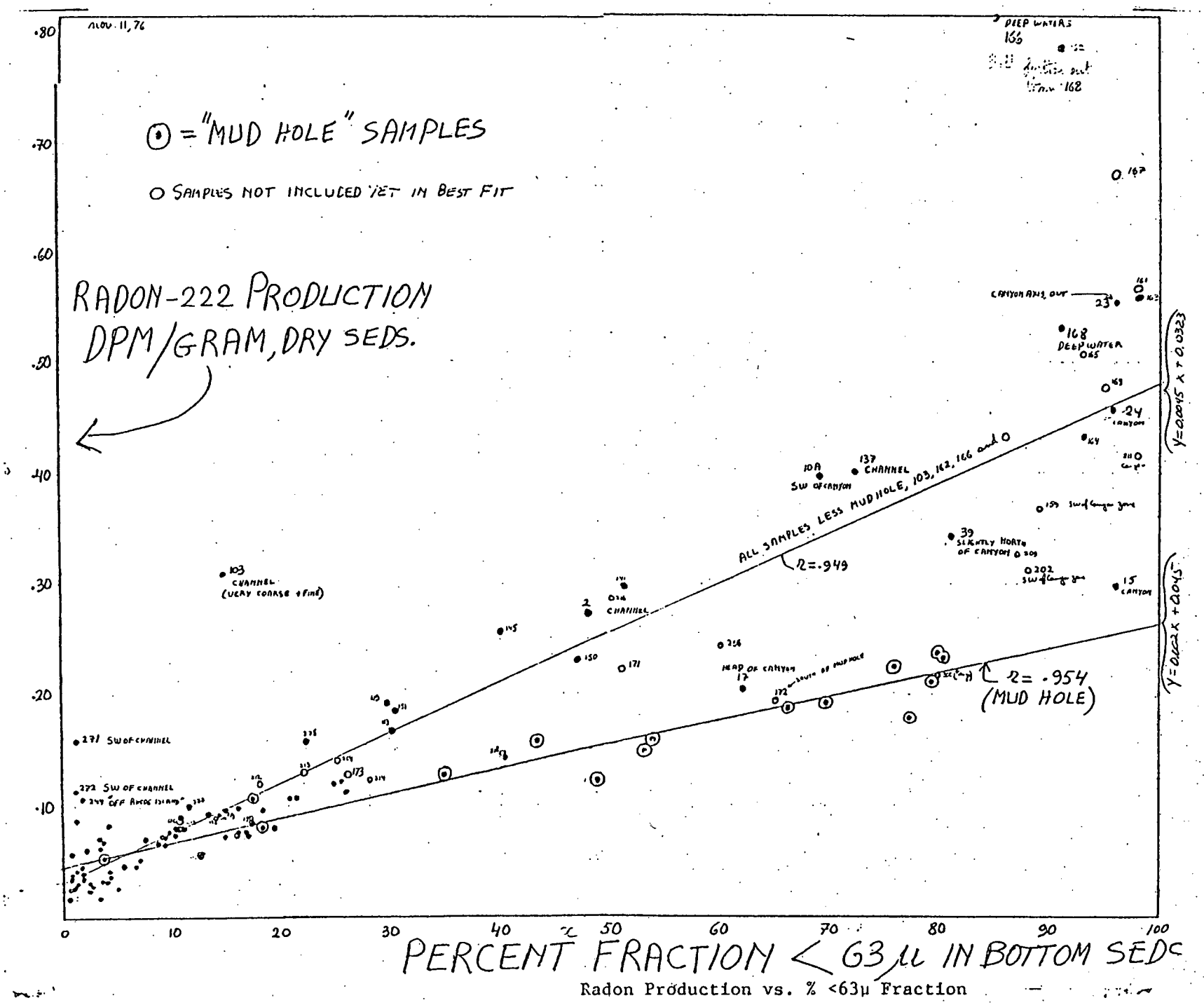

Radon Production vs. % <63μ Fraction

4.4/8

Fig. 4-4-3

produced: 4 with varying degrees of operationally-defined magnetic behavior; one that is operationally non-magnetic and one that is too large for the separator (> 1.19 mm). The fractions are presently being analyzed for radon production. Preliminary resuslts from one of the anomalous sands indicates that about half of the total production comes from the > 1.19 mm fraction and about one quarter of the total comes from the two least-magnetic fractions. When final results from this and the other samples are completed mineralogical analysis of important fractions will be carried out to identify the minerals responsible for this anomalously high radon production.

4.4.2.2 Radon Source Function on the Slope

Analysis for radon production of sediments collected during the RACACA cruise of June, 1979 was completed during this contract year. The results of these analysis, which are from parts of the slope south of the New York Bight, have been combined with analysis of samples collected from the slope adjacent to the Bight to demonstrate that the radon production is strongly correlated with the depth from which the samples is taken (Fig. 4.4-4). This can be understood from the geochemical source of much of the ^{226}Ra in deep sea sediments. The ^{234}U dissolved in ocean water decays to ^{230}Th which has a very short residence time compared to its half life and which is removed from the water by particles that settle to the ocean floor. In the sediments ^{230}Th decays to ^{226}Ra which in turn produces a large portion of the diffusible ^{222}Rn. Sediment from deeper parts of the slope can be expected to show higher production rates than sediments from shallower parts because there is a thicker water column overlying the deeper sediments from which ^{230}Th can be stripped. Thus there

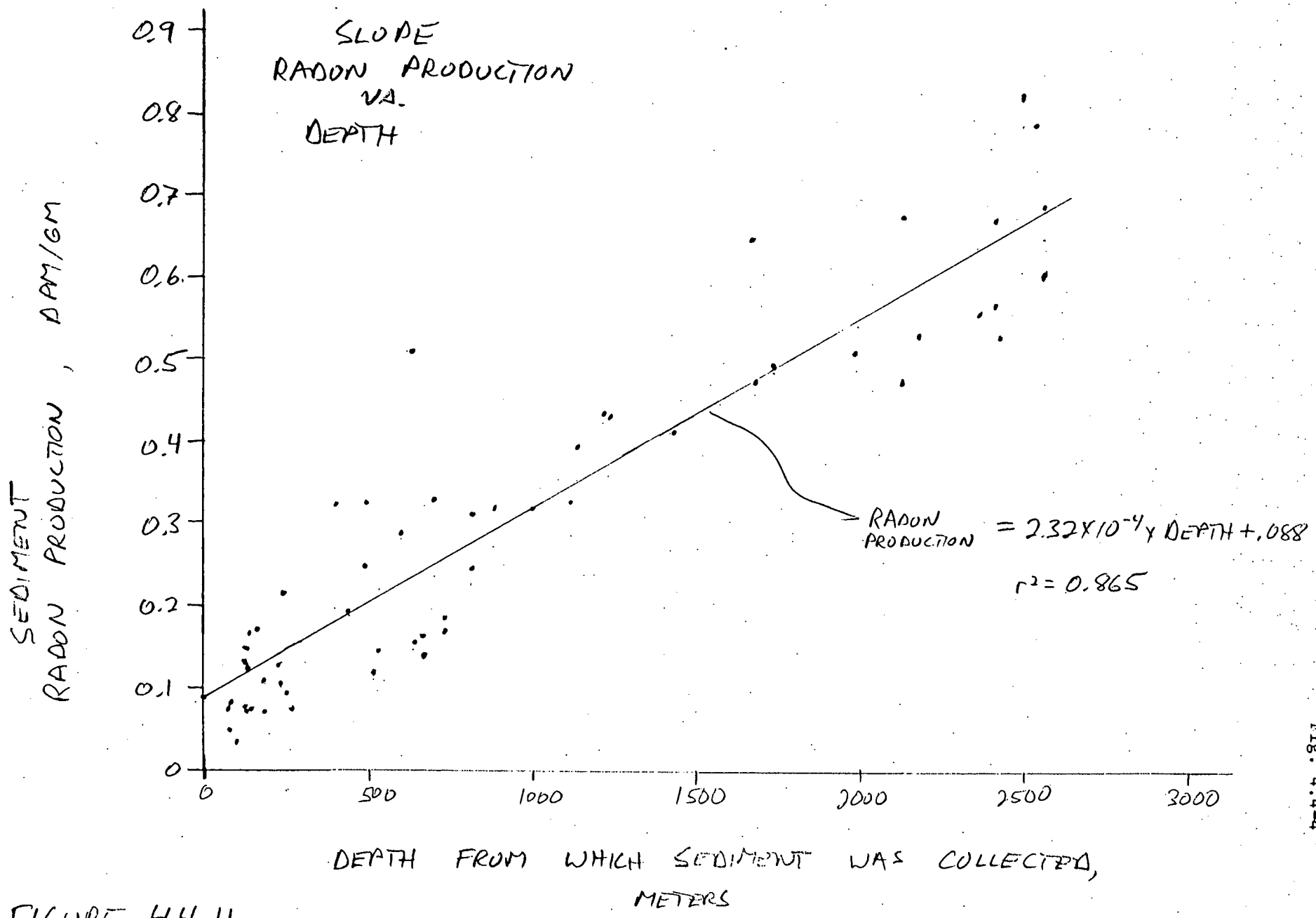

FIGURE 4.4-4

4.4/10
Fig. 4.4-4

are higher accumulations of ^{230}Th in the deeper sediments than the shallower sediments and higher resultant surface ^{226}Ra concentrations (Fig. 4.4-4).

In order, however, for there to be a linear relationship between radon production and depth in such a process it would be necessary for sedimentation rate to be the same at all depths. Otherwise the ^{230}Th stripped from the water column by particles raining down on the sediments would be more diluted in areas of higher sedimentation rate. If, for example, the sedimentation rate decreased with depth the data of Fig. 4.4-4 would fall on a curve that is concave upward, i.e., greater dilution of less thorium at shallow depths and less dilution of more thorium in the deep slope. The fact that the data fall on a straight line may be indicative of a constant sedimentation rate (at least for the lower slope) if the hypothesis explaining the depth distribution of radon production is correct. As discussed below, other factors beside just depth are responsible for control of the radon production of sediments on the upper slope.

Figure 4.4-5 shows the relationship between production of radon in slope sediments to the percentage of fine grained sediments. The two lines drawn in figure 4.4-5 are the correlations established from the shelf sediments in the Channel (upper line) and the Mudhole (lower line). None of the slope sediment data shown in figure 4.4-5 were used in determining the two lines shown. It can be seen that sediments on the slope with less than 90% of the < 63μm fraction fall within the envelope of the two lines established for the shelf sediments. Most of the sediments containing greater than 90% fines were collected from depths greater than 700m. Many of these fall outside of the envelope established on the basis of shelf sediments. This is probably due to the predominance of the depth effect mentioned earlier, such that the deeper samples have higher

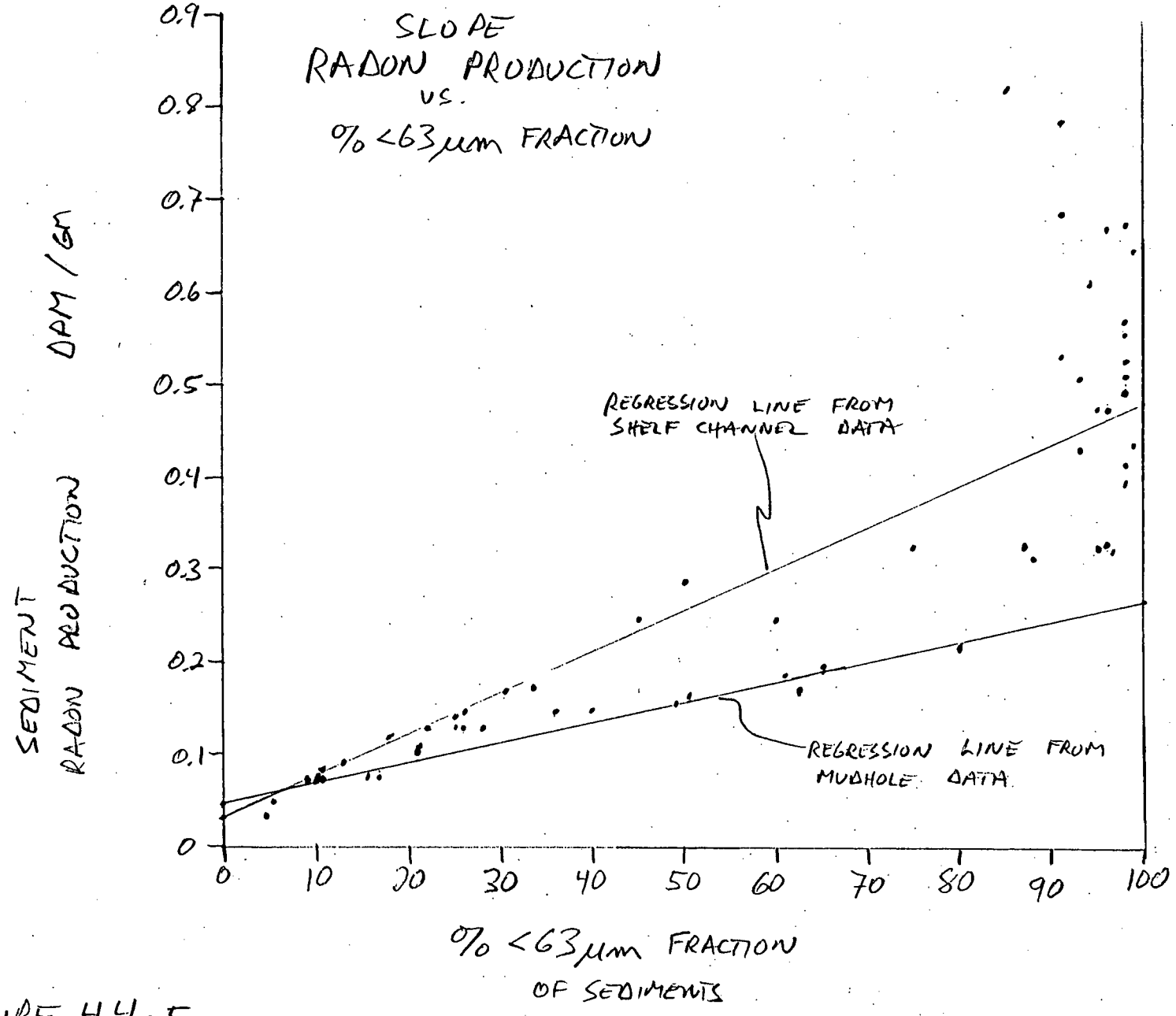

FIGURE 4.4-5

Fig. 4.4-5
4.4/12

concentrations of surface radium than would be expected on the basis of grain size alone.

It is not at all clear at this point why the sediments collected from less than 700m water depth should show a correlation with depth that is consistent with the deeper sediments while, at the same time, exhibiting a grain size relationship that falls within the envelope determined from shelf sediments. One extreme way in which this would be possible is if the depth effect is somehow unimportant in the upper 700m of the slope and if the fine-grained sediments of that region are composed of a combination of two end members. One end member would be similar to the fine grained sediments of the Hudson Shelf Channel while the other would be similar to fine grained sediments of the Mudhole. In such a case the radon production of the upper slope sediments would be controlled by the proportions in which the two fine grained end members and the > 63 μm fraction were mixed.

Such a situation could occur if the sedimentation rate of the upper slope were significantly greater than that on the lower slope. A high sedimentation rate on the upper slope would significantly dilute the thorium added from the water column. As a result the surface radium of the originally deposited sediment would overwhelm the contribution from the thorium raining down from the overlying water.

If the above explanation were correct then the fact that the sediments of the upper slope fall along the production versus depth line shown in Fig. 4.4-4 would be compleltely fortuitous. The stations shallower than about 700m depth have been considered separately from those deeper than 700m in order to compare how well the linear regression of each group compares with the regression line determined from all the samples together. The linear regression between radon production and depth shown in

Fig. 4.4-4 is actually determined largely by the deeper sediments. When the sediments deeper than 700m are considered alone, the linear regression is given by:

$$RP = 2.29 \times 10^{-4} \times D + .092 \quad r^2 = .792$$

where RP = radon production in dpm/g and D = depth in meters. This compares well to the regression for all the samples as shown in Fig. 4.4-4 of:

$$RP = 2.32 \times 10^{-4} \times D + .088 \quad r^2 = .865.$$

When the stations shallower than 700m depth are considered separately, the regression gives:

$$RP = 3.73 \times 10^{-4} \times D + .051 \quad r^2 = .500$$

The correlation coefficient for the shallower stations alone is much less significant and the slope of the regression line is steeper than for either all the stations together or for the deeper stations taken separately. This steeper slope would be indicative of a lower, rather than a higher sedimentation rate as posited earlier. The slope of this regression is not very significant, however, as indicated by the low correlation coefficient. This low value for r^2 is the result of scatter produced by the grain size effect.

These results do not indicate strongly whether or not the depth effect is very important in the sediments of the upper slope. If it is assumed, however, that sedimentation rate is constant down the slope and therefore that the depth effect is linear down the slope, then it can be seen whether a relationship between grain size and radon production still holds on the upper slope. This was done by calculating the contribution to surface radium due to depth as determined by the linear regression fit to all points and subtracting this depth-related concentration from the

total production of each sample. These depth-corrected surface radium values are plotted versus < 63μm sediment figure 4.4-6. As indicated in the figure the points can be grouped according to grain size and depth characteristics. The samples from <500m depth containing < 50% of < 63μm sediment all fall along a line that has the following equation:

$$RP = 3.17 \times 10^{3} \times \% < 63\mu m + .0055 \quad r^2 = .826$$

This would give an end-member, fine-grained value for radon production of .32 dpm/g and an end member > 63μ sediment value of ~ .005 dpm/g. This compares with a regression fit to the uncorrected data shown in figure 4.4-5 of:

$$RP = 2.84 \times 10^{-3} \times \% < 63\mu m + .049 \quad r^2 = .892$$

The latter gives a value of .33 dpm/g for the end-member radon production from the < 63μ fraction and .05 dpm/g for production from the > 63μm fraction. If all stations with approximately less than 50% < 63μm fractions are considered it can be seen that most of the samples from ~ 500 - 700m water depth fall much lower than the trend established from the stations shallower than 500m. If the relationship established from the samples from < 500m is invalid, then these could be explained by "recent" movement of coarse grained sediment down slope. Such movement would result in over-correction for depth causing the points to fall below the line calculated for stations < 500m depth. Since samples with such low percentages of < 63μm sediment are generally found on the upper slope, such an hypothesis is not unreasonable.

The four samples from shallower than 500m with > 50% < 63μ sediments show a very different trend. They fall along a line given by;

$$RP = 4.76 \times 10^{3} \times \% < 63\mu - .216 \quad r^2 = .980.$$

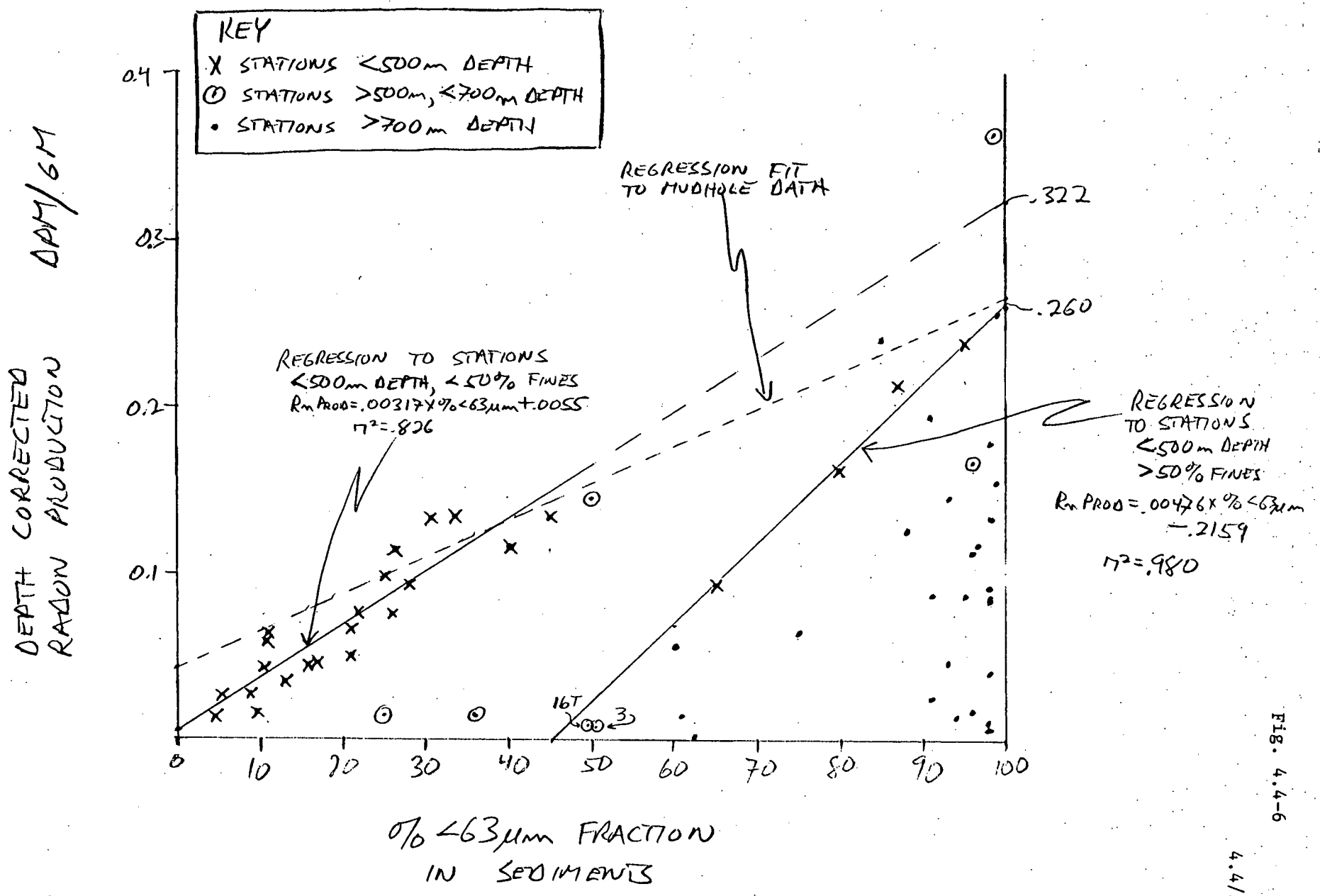

FIGURE 4.4-6 DEPTH CORRECTED RADON PRODUCTION IN SEDIMENTS VS % <63μm FRACTION

Fig. 4.4-6

4.4/16

Thus a radon production of zero is indicated at 45% < 63μ sediments. If this group is extended to encompass stations of the same grain size characteristics down to 700m depth (an addition of two more stations 16T and 3) the line becomes:

$$RP = 5.08 \times 10^{-3} \times \% < 63\mu m - .243 \quad r^2 = .993$$

giving zero radon production at 46% < 63μ and a production of .26 dpm/100gm for 100% < 63μ sediment. It is not clear whether these two < 700m points should be considered part of this group or part of the group discussed in the previous paragraph.

Such results could be explained by a large influx of <63μm sediment that contains very little surface radium to these sites. This would have the multiple effects of 1) increasing the % of < 63μ relative to other stations at similar depths; 2) lowering the radon production of the fine grained end member and 3) diluting the thorium from the overlying water column. The third effect weould result in an error in depth correction used in producing figure 4.4-6. All three effects would offset the values of radon production toward lower values at a given sediment grain-size composition. This is consistent with figure 4.4.-6. It is hard to conceive, however, how a higher influx of low-radium sediments to a few stations would result in such a good correlation for those stations.

Most of the points in figure 4.4.-6 fall below the line produced from the Mudhole sediments which is the lower of the two shelf lines. Thus if the depth effect is important throughout the slope, then the fact that many points from stations shallower than 800m fall within the envelope of the two shelf sediment lines when uncorrected for depth (figure 4.4-5) could be fortituous. If, however, the slope sediments from < 50% fines can be considered together, then the end-member, fine grained production

of .33 dpm/g falls between the end members on the shelf (in the Channel and in the Mudhole).

As can be seen from figure 4.4-6 the samples from deeper than 700m show considerable scatter in radon production values after correction for depth. This may be the result of varying sedimentation rates at different stations.

One final comparison between the sediments of the upper slope and those of the lower slope that can be made is that of the relative values of the radon production of the initial, or "continental" < 63 μm fraction, (i.e., the fine fraction) without the effect of depth-related thorium. As discussed above, the value for the upper slope appears to lie between .26 and .48 dpm/g with a value of .33 dpm/g most likely. If the regression for sediments deeper than 700m is extrapolated to zero water depth (Fig. 4.4-4), then a value of .09 dpm/g for these mostly fine grained sediments is indicated. If the samples deeper than 700m are normalized to 100% of < 63μm sediments, then a linear regression indicates a value of about .14 dpm/g at zero water depth. In either case the fine grained sediments of the lower slope appear to have a lower initial surface radium content than those of the upper slope.

It is clear from the above discussion that many questions about the details of slope sediment radon production remain to be resolved and many hypotheses can be tested. Some things that can be done with the samples on hand include determination of organic content, performing leaching experiments and comparison of sedimentation rates calculated from the regression line and water column ^{234}U content with the rates determined from cores already collected. Other questions concerning the differences between the upper slope and lower slope could be resolved by coring that is proposed for the coming contract year. Such questions include the

relative sedimentation rates, the possibilities of slumping of coarse-grained sediments down slope and the possible influx of low-radium content fine grained material on parts of the upper slope.

Although many questions remain unresolved, the established relationship between radon production in slope sediments and depth is important in itself to the interpretation of the low radon zone as discussed in section 4.4.5 of this report. It also places constraints on the origins of slope sediments of general interest to the problem of the ultimate or penultimate repository of pollutants.

4.4.3 Horizontal Distribution of Dissolved ^{222}Rn on the Shelf.

The distribution of dissolved ^{222}Rn has been measured on the shelf on 6 cruises covering the four seasons. In all cruises the same general pattern of distribution has been observed. As discussed in previous reports the distribution of excess radon is strongly related to the distribution of sediment production. High water column concentrations are associated with high production areas such as the Mudhole, the Hudson Shelf Channel and the anomalous sandy area to the southwest of the Channel. The pattern is then distorted by advection which produces tongues of high radon water over areas of low production.

Stations in the Mudhole were occupied on only two cruises and not much detail is known about the radon distribution in that area. One cruise was in January 1976 during relatively well-mixed conditions with a slight benthic pycnocline (see section 4.4.4 for detailed discussion of vertical distributions). One line of stations was occupied eastward through the Mudhole. The stations in the Mudhole had standing crops higher than stations occupied over low production areas in the same cruise (Fig. 4.4-7).

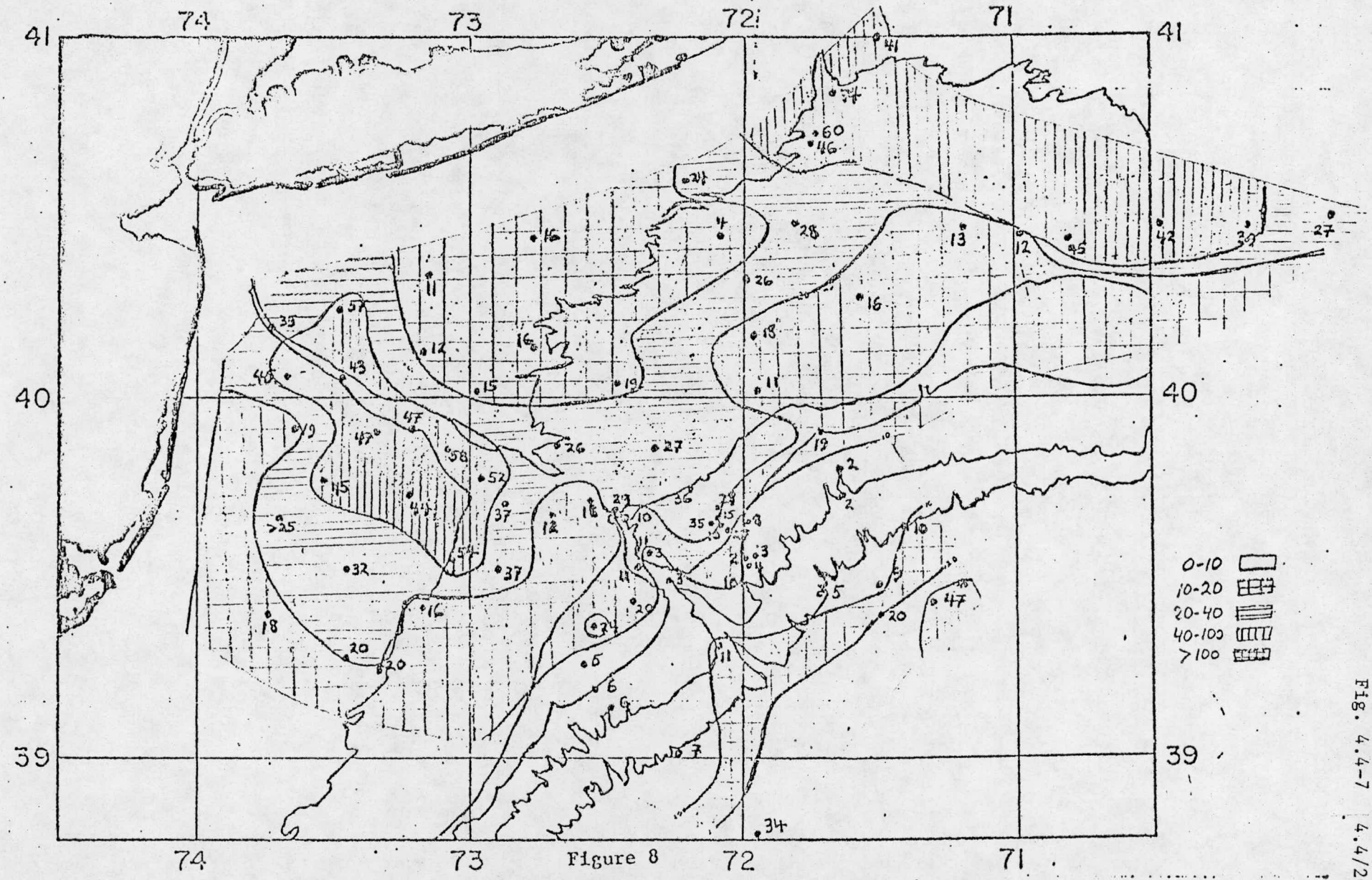

Figure 8

Radon-222 standing crop integrated up to 30 meters above bottom, January 1976, New York Bight.

Fig. 4.4-7 | 4.4/20

The second cruise to sample the Mudhole area focused exclusively on that area and occurred in August of 1978. It was designed, in part, to test the time variability of radon profiles. Again significantly higher standing crops were found in the Mudhole area on this cruise in comparison to lower production areas samples on previous summer cruises. Unfortunately, a great deal of variability in radon distribution and in hydrographic properties was observed. The Mudhole is in a slightly deeper part of the shelf and appears to be subject to intrusions of water from the slope and other parts of the shelf. Thus any attempts to model horizontal or vertical distributions in the area are not useful during such hydrographically-complicated conditions.

Another area that appears to be somewhat variable and thus difficult to interpret quantitatively is found off the eastern part of Long Island between the Mudhole and the Hudson Shelf Channel. A transect of stations extending southeastward from eastern Long Island has been occupied on three cruises: January, 1976; May, 1977 and July, 1975. In all cases complex intertonging of high-and low-radon waters was indicated both by the radon and by the hydrography (see figures 4.4-7 to 9 for radon distributions). High radon waters probably come from the Mudhole or areas to the north that have not been extensively sampled such as along Long Island or in Rhode Island Sound. Stations occupied to the northeast of the transect in January 1976 showed high standing crops. A tongue of high radon water appears to be coming from the northeast in July, 1975 (Fig. 4.4-8).

Seasonal trends along this transect show considerable variability. High radon tongues appear to be persistent features but variable in location, i.e., they are always encountered but not in the same place and intensity. Without detailed hydrographic and radon surveys to the east

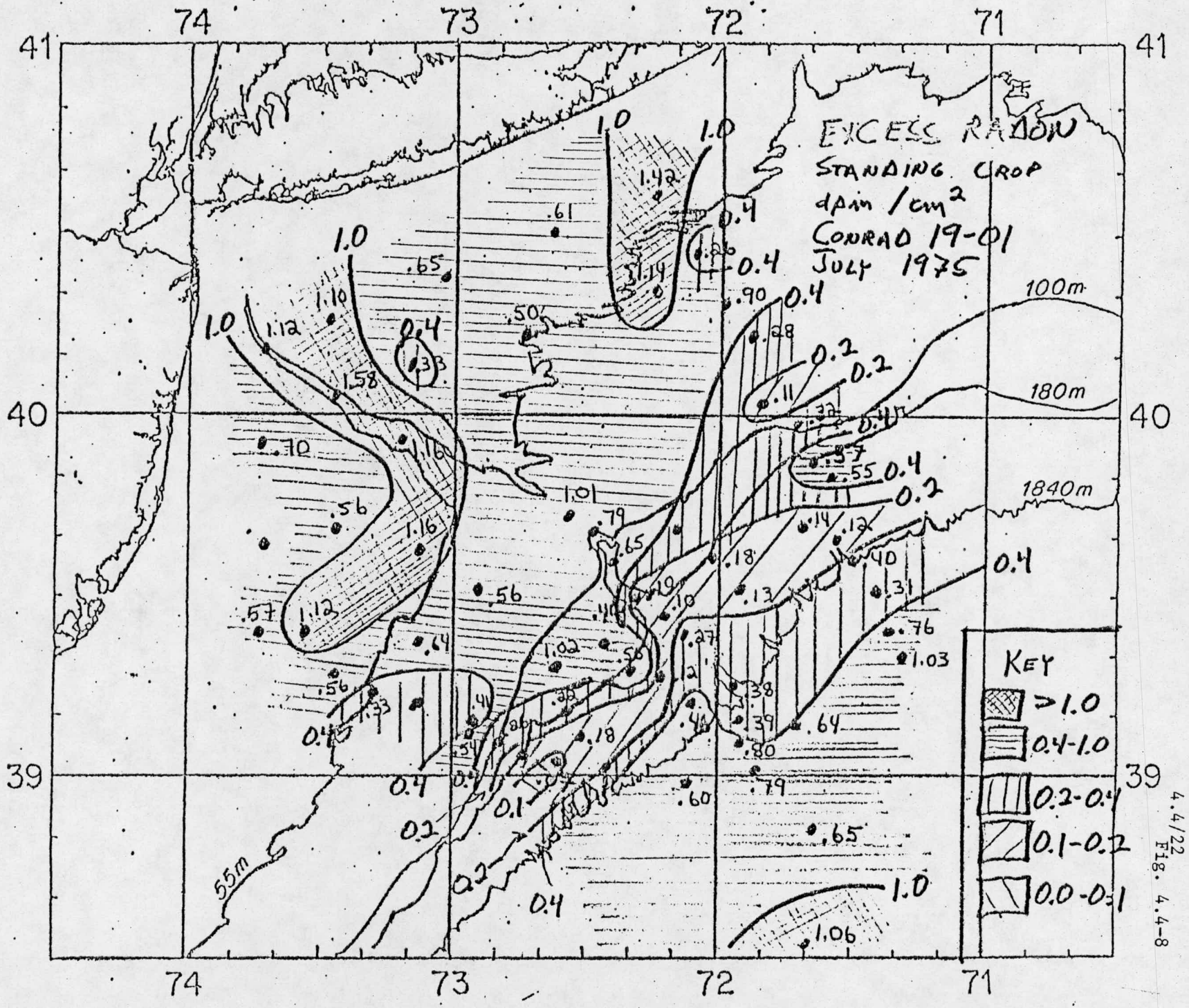
EXCESS RADON
STANDING CROP
dpm / cm²
CONRAD 19-01
JULY 1975
74
73
72
71
41
40
39
100m
180m
1840m
55m
KEY
>1.0
0.4-1.0
0.2-0.4
0.1-0.2
0.0-0.1

4.4/22
Fig. 4.4-8

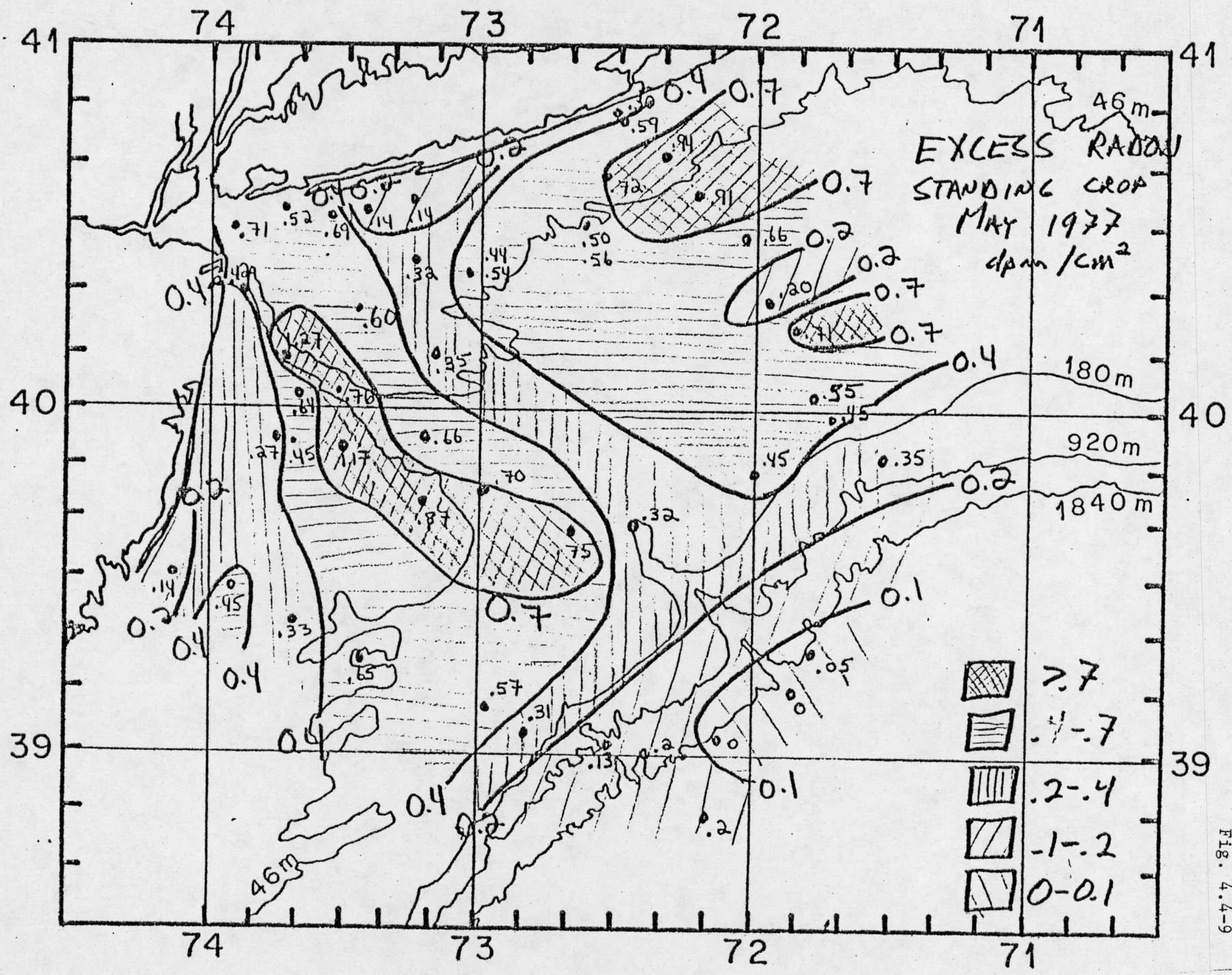
74
73
72
71
41
40
39
46m
180m
920m
1840m
EXCESS RADON
STANDING CROP
MAY 1977
dpm/cm²
≥.7
.4-.7
.2-.4
.1-.2
0-0.1

4.4/23
Fig. 4.4-9

and more detailed coverage of radon production to the northeast it is impossible to make any quantitative statements about the radon distribution in the area. Both radon and hydrography seem to indicate that the flow off eastern Long Island is not uniform but rather appears jet-like, with narrow bands of water travelling at different speeds and perhaps from different source areas.

The most seasonally-uniform area that has been observed is in the area of the Hudson Shelf Channel. Whereas much of the shelf in the Mudhole area and to the south of Long Island is deeper than 55m, the area near the Channel has a broader expanse of waters shallower than 55m. It is in this area that features appear to be more constant and thus can be adequately modelled. Also, detailed coverage of both water column radon and sediment production has been carried out on five cruises: two in the winter and early spring and three in the presence of a thermocline.

The main features of the horizontal distribution of excess radon near the Channel are high concentration and standing crops in the Channel itself and in a tongue of water generally extending to the southwest with lower standing crops in surrounding waters (Figs. 4.4-7 to -10). The interpretation of this distribution has gone through considerable evolution as our knowledge of the area has increased and as new approaches have been tried. Briefly, it was first thought that the main source of excess radon was the sediments of the Channel and that the tongue of high radon extending to the southwest had its source in the Channel from which it was advected. Further detailed sampling demonstrated the existence of the "anomalous" sandy area (see section 4.4.2) which is clearly an important local radon source. Examination of cross sections of radon concentrations and hydrography through the Channel indicate that the radon produced by

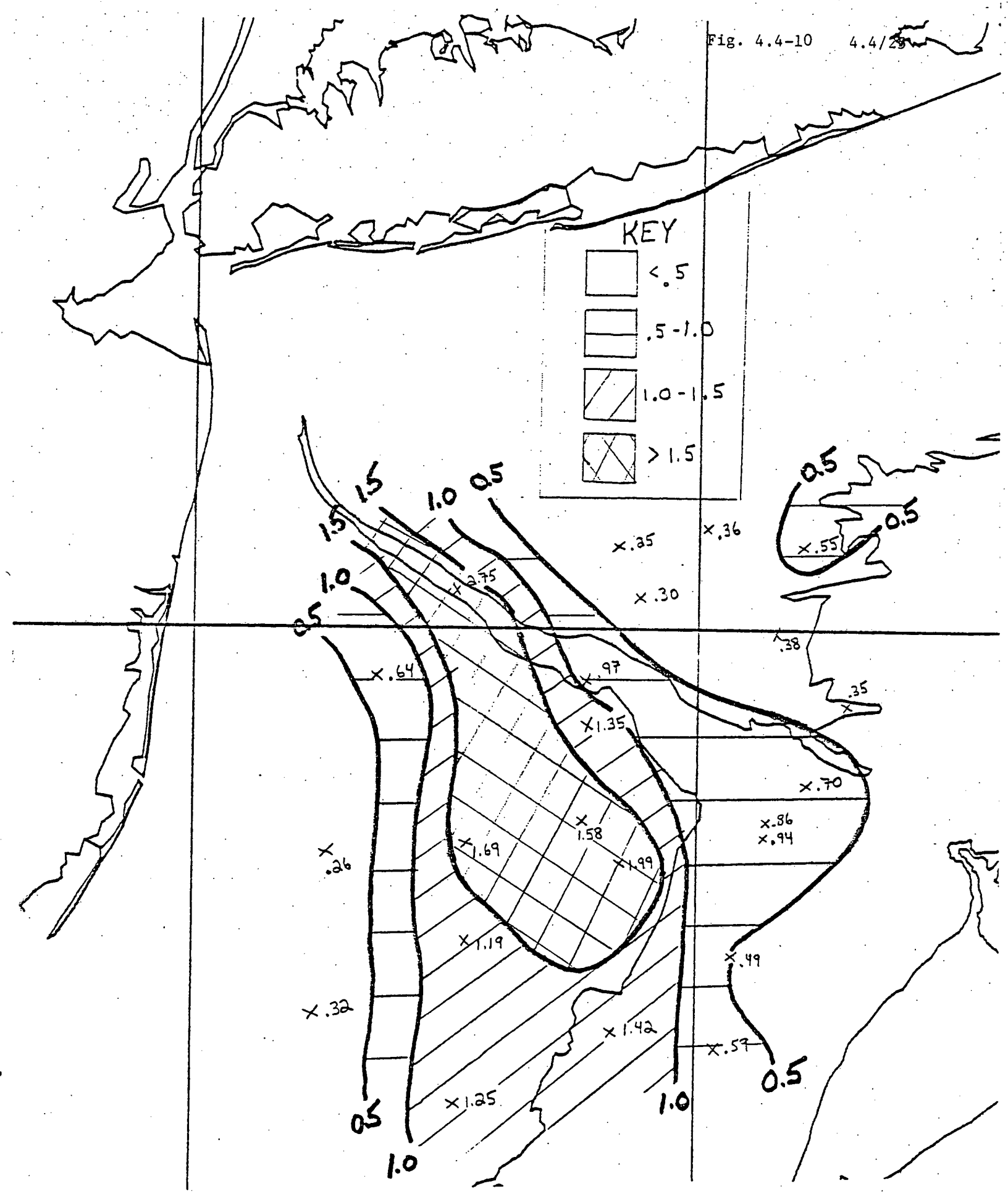

Radon-222 Standing Crops, September, 1977, Ch77-15, dpm/cm^2.

Channel sediments is largely trapped in the Channel. Current meter data indicating that flows in the Channel are mostly up and down the axis (Han, personal communication and in a paper submitted to Limnology and Oceanography) support this conclusion. Thus it appears that, except under conditions of extreme vertical mixing throughout the water column, the Channel sediments are probably not an important source of excess radon to waters adjacent to the Channel. The strong source in the region appears to be the anomalous sandy area and recent modelling has proceeded under that assumption.

4.4.3.1 Modelling of Horizontal Distributions

Previous modelling of the horizontal distributiotn of excess radon had been done with a simple three dimensional model developed by Nevil Milford of the University of Queensland, Australia. The model involved three dimensional diffusion into anistropic semi-infinite medium with a given vertical diffusion coefficient and a different (higher) horizontal diffusion coefficient. The source function was a grid of point sources spaced at ~ 5 km intervals, the strengths of which were based on the distribution of grain size and the relationship of production to grain size in most of the Bight and on direct measurements in the anomalous sandy area. The amount of radon that would diffuse from each grid point in a given radius about station locations to points at various depths about the station point was calculated. These results were summed vertically to produce standing crops. Since a map of production was used for the source function (rather than real fluxes) under the assumption that flux is proportional to production, the model calculations were normalized to the data by summing both the measured standing crops and the model

calculations for the whole area and determining the ratio of the two sums.

Model calculations were run only for the summer cruises when the presence of a thermocline assured trapping of all the excess radon. During the winter and early spring cruises excess radon was observed all the way to the surface, indicating probable loss to the atmosphere.

Model results had previously been displayed and compared by calculating the ratio of the model standing crop to the measured standing crop and plotting a map of these ratios. The optimum horizontal diffusion coefficient was selected on the basis of which one of those used in the calculation gave the most number of stations for which model results and measured standing crops matched to within 20%. This technique has proved confusing and inadequate. A more quantitative technique of selecting a diffusion coefficient by doing a least squares bit between the model results and measured standing crops showed little correlation indicating that a simple diffusion model is inadequate for the area.

It has recently proved useful to examine standing crop data and compare model results by plotting them one dimensionally along axis perpendicular to or parallel to the Channel axis rather than by using maps. This simpler approach has shown many important features that will be illustrated with the data from cruise CH77-15 (September, 1977; Fig. 4.4-10). This cruise was the most detailed in the area and is thus best for modelling purposes.

By first plotting all of the data on an axis perpendicular to the Channel axis it could be seen that the data could be classifed in three geographically distinct groups (Fig. 4.4-11 and -12). The first group lies shoreward of a line that runs perpendicular to the Channel through the most shoreward extent of the anomalous sands. The second group lies seaward of that line and shoreward of about the 55m isobath. The third

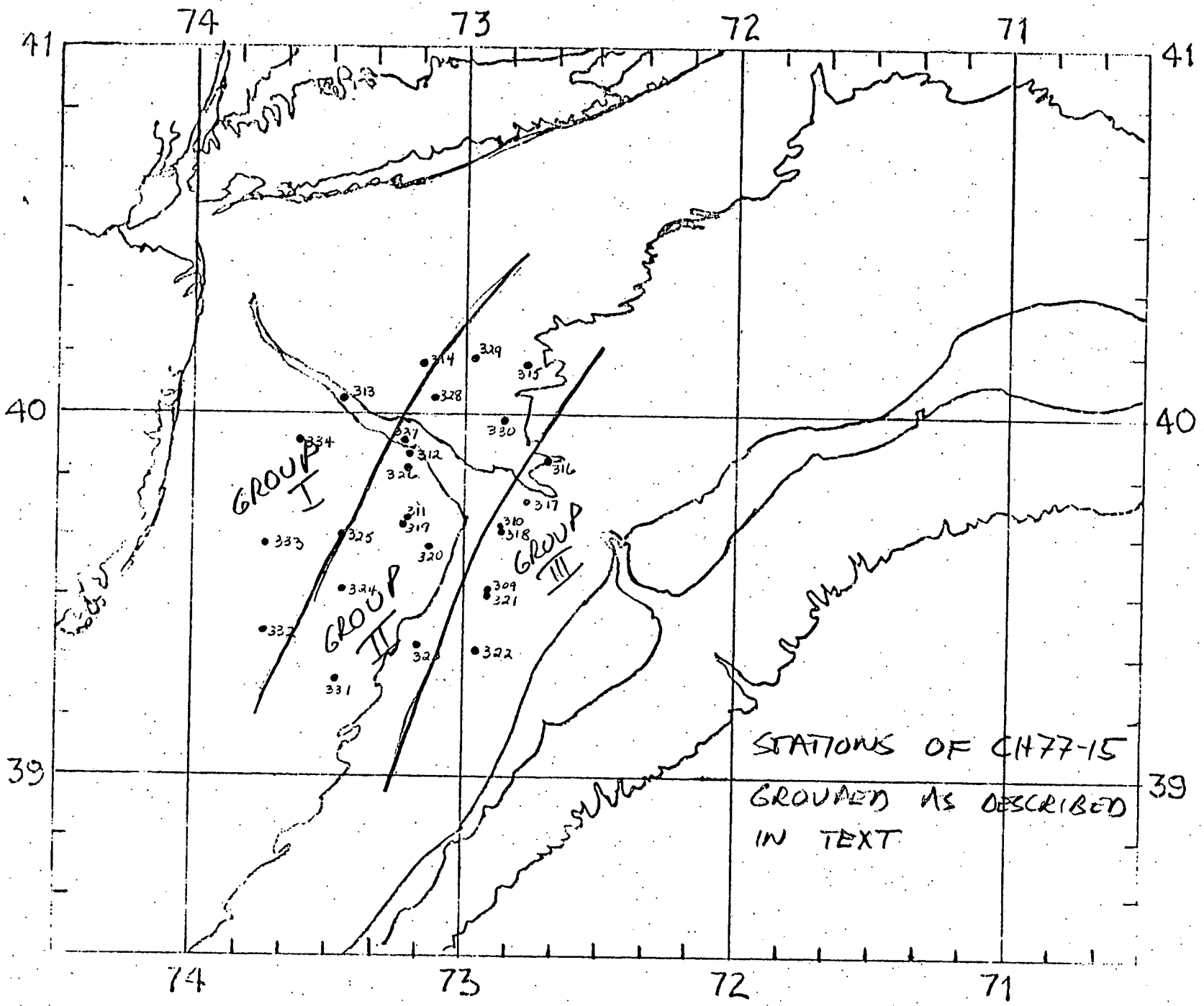

FIGURE 4.4-11

CH 77-15

4.4/28
Fig. 4.4-11

FIGURE 4.4-12
CH77-15 SEPT. 1977
EXCESS RADON STANDING CROPS
VS. DISTANCE FROM CHANNEL

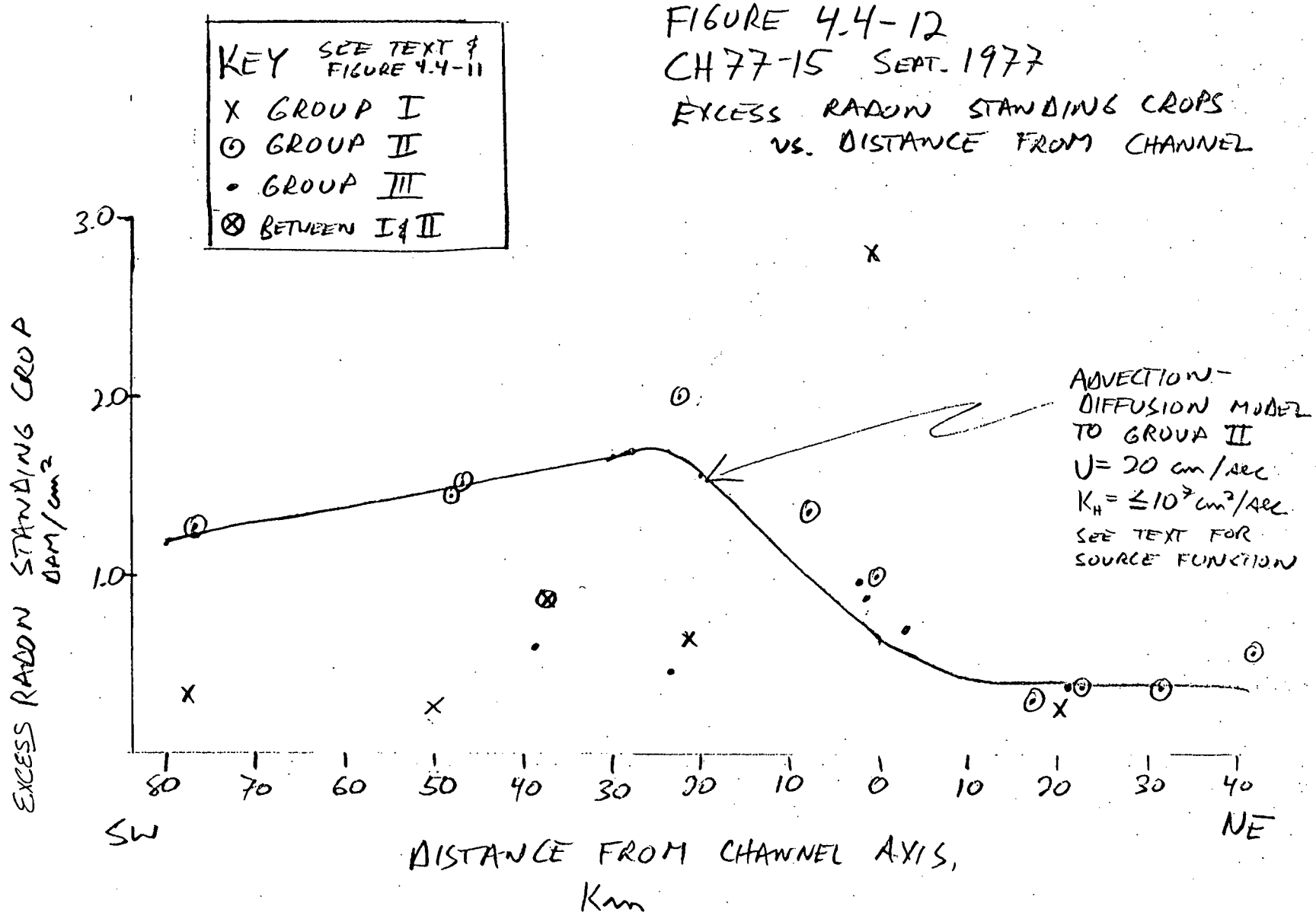

4.4/29 Fig. 4.4-12

FIGURE 4.4-12

group lies seaward of about the 55m isobath.

The first group shows high standing crops in the Channel and low standing crops on either side. This is to be expected from the distribution of production which is also high in the Channel and low to either side. The high water column concentrations are largely trapped within the Channel as discussed previously.

The second group shows high concentrations over the anomalous area and to the southwest. Concentrations are lower over the Channel and very low to the northeast. This pattern is indicative of advection to the southwest over the anomalous sands.

The third group shows relatively constant standing crops of low to moderate magnitude.

The only group of data that can be meaningfully modelled is the second group since it is the only one that shows the influence of a stong source without bathymetric trapping. It is clear from the distribution of standing crops in this group that advection is very important and that the simple diffusion model would be inadequate to describe the data.

Before examining the results of an advection-diffusion model for the second group of stations it is useful to compare the distribution of standing crops between the different groups along axes parallel to the Channel axis. It can be seen in figure 4.4-13 that the highest concentrations southwest of the Channel are confined to the group 2 region both over the anomalous sands and to the southwest. This indicates relatively low cross shelf eddy diffusion and low cross-shelf advection. Comparison of the diffusion model calculations on the same axis show that the cross shelf diffusion coefficient is certainly no higher than 10^6 cm^2/sec and probably is of the order of 10^5 cm^2/sec or less within the limits of the

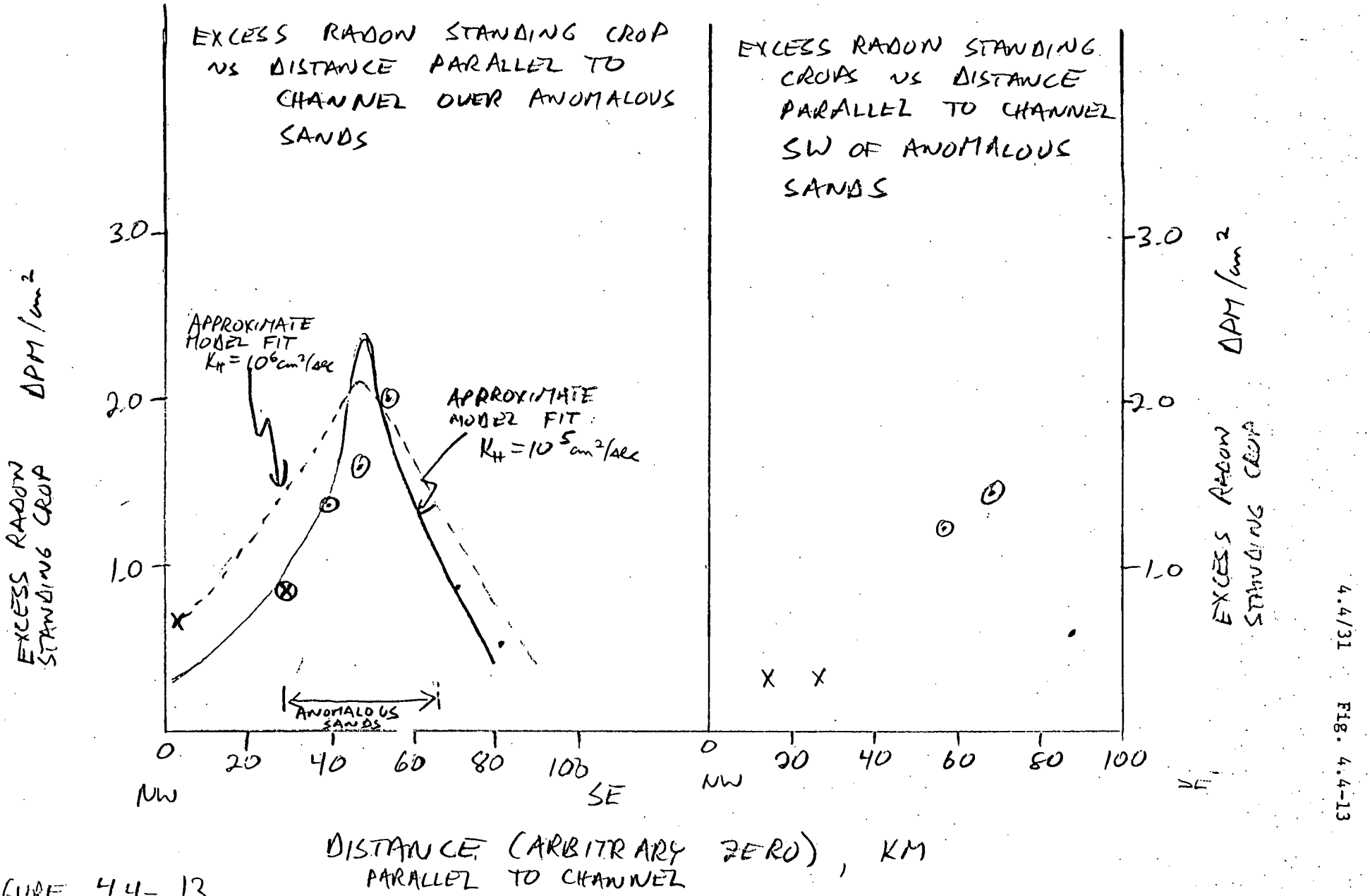

FIGURE 4.4-13

4.4/31 Fig. 4.4-13

data. (Because of the size of the source region and the spacing of stations the radon method is not sensitive to diffusion coefficients less than 10^5 cm^2/sec.) Thus it is clear that the standing crops in group 2 can be adequately modelled with a one dimensional advection diffusion model with advection to the southwest.

This was done by using a standard one-dimensional advection-diffusion-decay model expressed in the equation:

$$\frac{\partial C}{\partial t} = K_H \frac{\partial^2 C}{\partial x^2} - \frac{\partial C}{\partial x} - \lambda C$$

where C is concentration, K_H is horizontal eddy diffusion coefficient, U is horizontal velocity and λ is the decay coefficient of radon. Since no time-dependent data are available we must assume steady state. Under steady state conditions the solution to this equation about a point source is:

$$C = Co \exp \left[Ux/\partial K_H \left(1 \pm \sqrt{1 + 4\lambda K_H/U^2}\right)\right]$$

where C_o is the concentration at the point source. The exponent with the positive sign refers to values of $x < 0$ (upstream of the point source) and the negative sign to $x > 0$ (downstream). (Solution from O'Connor "Estuarine Analysis" in textbook Mathematical Modelling of Natural Systems from a course given at Manhattan College.) The value of C_o can only be determined with knowledge of the input of radon from sediments. Since the input is only known on a relative scale a normalization procedure was used as discussed below.

The model was applied by calculating the distribution of excess radon about point sources spaced at 5 km intervals and then summing over the whole region. The relative strengths of the point sources were chosen as a schematic representation of the distribution of radon production in the group 2 area. Point sources northeast of the Channel axis were set at 4 or 5 dpm/g. Point sources at 5, 10, 15, 20 and 25 km southwest of the Channel were considered the strongest sources of the anomalous region and given values of 20 dpm/g. The points in the Channel axis and at 30 km southwest of the axis were considered transitional and given values of 10 dpm/g greater than 30 km to the southwest were set at 3 to 4 dpm/g.

After calculating the distributions about all the point sources and summing, the model results were normalized by setting the standing crop of the furthest upstream station to a value of .4 dpm/cm^2 and using the ratio of the model upstream value to .4 dpm/cm^2 to convert all other model values to standing crops. It was found from examination of the group 2 plots of standing crop vs. distance from Channel that the station northeast of the Channel (upstream) had standing crops generally near to .4 dpm/cm^2.

The most detailed coverage of the group 2 area was performed on the cruise CH77-15 in September, 1977. The shape of the radon distribution around the anomalous area can be matched with a current velocity of about 20 cm/sec. The magnitudes of the standing crops are not fit by the model if a direct proportionality between the flux of radon from the sediments and the production of the radon in the sediments is assumed. The observed standing crops are approached by the model calculations only if the ratio of flux to production in the anomalous sands is three times that in the normal sands Fig. 4.4-4. This could be the case if the anomalous sands

were the site of higher biological activity than the normal sands. Such activity could enhance fluxes by increased sediment mixing and pumping of pore waters.

The data from May, 1979 and July, 1975 are much sparser with only one or two stations above the anomalous sands, one or two upstream and one downstream in both cruises. The May data are indicative of a current of about 10 cm/sec and a "flux:production" ratio that is the same in anomalous sands as in the normal sands. The July data suggest a current of 20 cm/sec and a flux:production ratio about 2 to 2 1/2 times greater in the anomalous sands than in the normal sands. The apparent seasonal progression of flux:production ratios is consistent with an explanation of biological activity enhancing fluxes in the anomalous sands, since such activity would likely increase from spring to summer to early fall.

Currents for the three cruises were calculated from wind velocities at Kennedy Airport on the basis of a correlation determined by Greg Han of AOML (personal communication). The calculated six day average currents in the bottom waters near the anomalous sands were dominated by the southwestward component, but showed magnitudes that were 1/3 to 2/3 of those suggested by the advection-diffusion model. Also the September, 1977 cruise was the one on which drogues were launched in order to determine current velocities on the cruise. Although the drogues failed shortly after launching due to manufacturer defects, some worked for up to two days and the apparent southwestward component of the mean current over those brief periods was 5 to 15 cm/sec in contrast to the 20 cm/sec suggested by the radon data.

A possible explanation for these discrepancies would be the existence of high production sediments to the southwest of the known anomalous sands. We have not observed such sediments but our coverage in that area has not been very dense. However, grab samples from stations at which high radon standing crops were observed showed low production.

4.4.4 Vertical Distribution of ^{222}Rn

As discussed in previous annual reports the vertical distribution of ^{222}Rn is largely controlled by hydrographic properties of the water column. Under relatively well-mixed conditions excess radon is mixed all the way to the surface. Under stratified conditions the pycnocline acts as a barrier to vertical mixing and excess radon is trapped below. In this section the general characteristics of the vertical distribution for each season will first be described followed by a discussion of the vertical modelling that has been applied to some data sets.

4.4.4.1 Seasonal description of Vertical Thermocline

Winter - January, 1976.

The vertical profiles of ^{222}Rn from the cruise RC19-05, which took place in January, 1976, can be broken into four groups according to the vertical distributions of radon, temperature, salinity and density. These groups also tend to fall into four distinct geographic regions. In the waters of the New York Bight itself (as distinguished from waters east of Long Island) most of the stations occupied shoreward of the 55m isobath showed well-mixed conditions for all properties (T, S, σ_t and ^{222}Rn). In some cases the radon concentrations were randomly variable vertically. This would suggest that over short time scales (of the order of a few hours) the water column may not be well mixed and thus could show vertical patchiness in properties that have short time constants for growth or decay. Over a longer time scale that would be reflected in the distribution of conservative properties, however, the water column is well mixed as indicated by the vertical constancy of T, S and σ_t even where radon is variable. The radon variability could be the result of parcels of water a few meters thick that were well mixed within

themselves but did not mix rapidly with adjacent parcels (e.g., individual eddy cells) that spent time near the surface (where radon would be lost) or near the bottom (where radon would be gained) before being moved by a large scale mixing process downward or upward into the middle of the water column. If this were the case such parcels would have to maintain their integrity at the surface or the bottom for about three to six hours in order to achieve the observed variability in the vertical radon distribution.

The second group of stations includes a few in waters shallower than the 55m and many deeper than 55m in the New York Bight. These show gradual increases in temperature and salinity with depth. The radon concentrations at these stations also show slight increases with depth as would be expected if vertical mixing were inhibited by water column stratification.

The third group was found above the Mudhole and also include stations to the northwest of the Mudhole and a few stations in the New York Bight waters deeper than 55m. In this group the temperature and salinity were well mixed or showed gradual increases with depth down to about 10 meters above bottom (MAB). At about 10 meters above bottom there were dramatic increases in temperature, salinity and density with a fairly well mixed layer below. The radon profiles also shwed will mixed distributions down to about 10 MAB at which point there was also an abrupt increase in radon concentration (usually observed only in the bottom-most sample).

The final group includes only two stations east of the mudhole where the temperature and salinity decrease near the bottom but where the density is vertically constant. At one station the radon was constant and at the other the radon increased with depth.

Spring - Late March 1977

The cruise K77-02 (March-April 1, 1977) occurred during a period of apparent transition from well-mixed winter conditions to the stratification of the summer. The vertical radon distribution did not always bear an obvious relationship to the vertical distribution of hydrographic properties. About 1/3 of the stations showed variations in radon that could reasonably correspond with vertical density changes (i.e., well mixed radon where density is constant, decreases in radon with distance above bottom where stratification was observed). About 1/6 of the stations showed radon distributions that were not inconsistent with hydrography, but, because of the sparseness of the data, it cannot absolutely be said that the two sets of data agree. The remainder of the stations (about 1/2) showed radon distributions that were clearly inconsistent with the observed hydrography (i.e., constant radon through stratified regions or strong gradients of radon in well mixed waters). This cruise obviously took place during a very complicated transitional period during which steady state could not be assumed. Time variability at some stations that were reoccupied during this cruise was very great.

Late Spring - Summer - Early Fall (Stratified conditions) May 1977, July 1975, September 1977, October 1974.

On all four of the cruises CH77-01 (May 1977), RC19-01 (July 1975), CH77-15 (September 1977) and V32-01 (October 1974) stratified conditions were obsserved. The vertical radon distribution in the Bight waters was consistently found to correspond to the hydrographic properties. Radon in the bottom mixed layer was relatively well mixed or showed smooth increases toward the bottom. It was not unusual to find maxima or minima

within the bottom mixed layer indicating some patchiness in mixing over short time scales as discussed in regard to the well mixed vertical stations. In this case patchiness in vertical radon distribution would result from parcels of water maintaining their integrity near the bottom for a few hours during which time they would gain radon before being mixed upward as a unit or from longer term isolation of parcels from mixing with adjacent parcels during which time some excess radon could decay. In areas of strong enough horizontal gradients intrusions of high or low radon water from adjacent regions could also cause patchiness.

Abrupt decreases in radon concentrations above the bottom mixed layer were usually associated with stratification: either the bottom of the thermocline or (at some of the deeper stations) weaker stratification below the thermocline. Since the thermocline deepened from late spring through early fall and since the standing crops generally increased during the same period, the gradients in radon concentration at the top of the bottom mixed layer increased through the stratified period.

4.4.4.2 Modelling of Vertical Distributions

Winter

The only modelling that has been done on the winter data has been on the stations of the New York Bight shallower than 55m that showed vertically constant properties. For these stations a constant vertical eddy diffusion coefficient and steady state conditions can reasonably be assumed. The model solved for a vertical distribution of radon controlled solely by vertical diffusion and decay. The bottom boundary condition was a designated concentration as estimated from the profile being modelled. The upper boundary condition was loss of radon to the atmosphere based on

a stagnant film model for gas exchange where the controlling parameters that had to be input were the ratio of molecular diffusion of radon to film thickness and the atmospheric concentration of radon. The film thickness was calculated for different assumed concentrations of atmospheric radon by assuming that the amount of radon lost to the atmosphere from a given station corresponded to the difference between the standing crop at that station in May 1977 (when there was no loss to the atmosphere) and the standing crop in January 1976.

The calculated vertical diffusion coefficients for the well mixed stations place a lower limit of 100 cm^2/sec on the vertical diffusion coefficient of the Bight waters shallower than 55m. Since the relatively constant radon profiles could be matched within the error of the data by an infinite vertical diffusion coefficient, only a lower limit can be reasonably calculated.

Spring

Obviously the data collected on K77-02 (late March 1977) cannot be modelled because the assumption of steady state is inappropriate and there is no time variability data. It does seem, however, that a study of the radon at a few stations over the period of thermocline formation could provide useful insights into the changes in the turbulent structure during that transitional period. The fact that the vertical distribution of radon does not match well with the hydrography at half the stations may be indicative of complexities in turbulence that cannot be observed with temperature and salinity.

Late Spring - Summer - Early Fall

Modelling of data collected under stratified conditions was discussed in detail in last year's report. Briefly, because most profiles showed similar characteristics of a bottom mixed layer overlain by an abrupt decrease in radon, the data from each station was normalized to the average bottom layer concentration and all of the stations were grouped together. A two layer model with a different constant vertical eddy diffusion coefficient in each layer was applied to the data. Since the lower layer often showed variability as discussud in the previous section it was not possible to assign a good value for the vertical diffusion coefficient to that layer. In May, 1977 the data from all stations that showed the same characteristic shape fell within the range of 0.05 to 0.5 cm^2/sec for the vertical diffusion coefficient of the upper layer. If only the stations at which the top of the mixed layer corresponded with the bottom of the thermoclinewere considered, the range was narrowed to 0.05 to 0.3 cm^2/sec. The July 1975 upper layer data fell within the range 0.05 to 0.5 cm^2/sec. Thus the vertical diffusion coefficient at the base of the thermocline lies in the range 0.05 to 0.5 cm^2/sec. This range would be an upper limit for the most stratified part of the thermocline because the abrupt radon decrease occurs at the bottom of the thermocline and because data from profiles in which the radon decrease occurs at weaker stratification below the thermocline also falls within the range 0.05 - 0.5 cm^2/sec.

4.4.5 The Low Radon Zone

Work involving the characterization and description of the low radon zone that has occurred during this contract year has included more detailed description of the source function (see section 4.4.2), the measurement of ^{226}Ra in samples collected on the RACACA cruise and the use of these data in further defining the low radon zone.

The "low radon zone" is the name we have given to a region of the continental slope extending from the shelf-slope break to about 2000m depth in which excess radon concentrations and standing crops have been found to be much lower than those expected from the radon production of the underlying sediments - indeed, lower than observed anywhere else in the world oceans, deep or shallow. The zone is generally centered at about 1000m depth where concentrations of excess radon are as low as 0 dpm/100ℓ. Concentrations and standing crops increase both upslope and downslope from there. This zone has been observed on the slope adjacent to the New York Bight on four cruises in different seasons, and has also been observed at individual stations on the slope south of the Mudhole and south of Nova Scotia. Last year on the RACACA cruise in June radon measurements were made along seven cross-shelf transects extending from the southern extent of the New York Bight to just south of Cape Hatteras (Fig. 4.4-14). As discussed in last year's report the low radon zone was found to extend along the whole Mid-Atlantic Slope and is obviously an important feature of the mixing characteristics of slope and interior water.

The radium analyses have been completed on 15 samples and is underway on another 20 (nearly complete for most of those). Preliminary results had indicated that the radium was fairly constant at about 9.7 dpm/100ℓ down to about 1100m depth and increased with depth below that to about 12 dpm/100ℓ at 2800m depth. While this still appears to be approximately true for the two transects from which radium was first measured (Transects I and V), recent results from other transects indicate that the radium distribution is more complex. While some idea of the distribution can be determined from the data, it will be necessary to measure many more samples to get a complete picture. An accurate knowledge of the radium concentrations is necessary to the calculation of radon standing crops.

Fig. 4.4-14

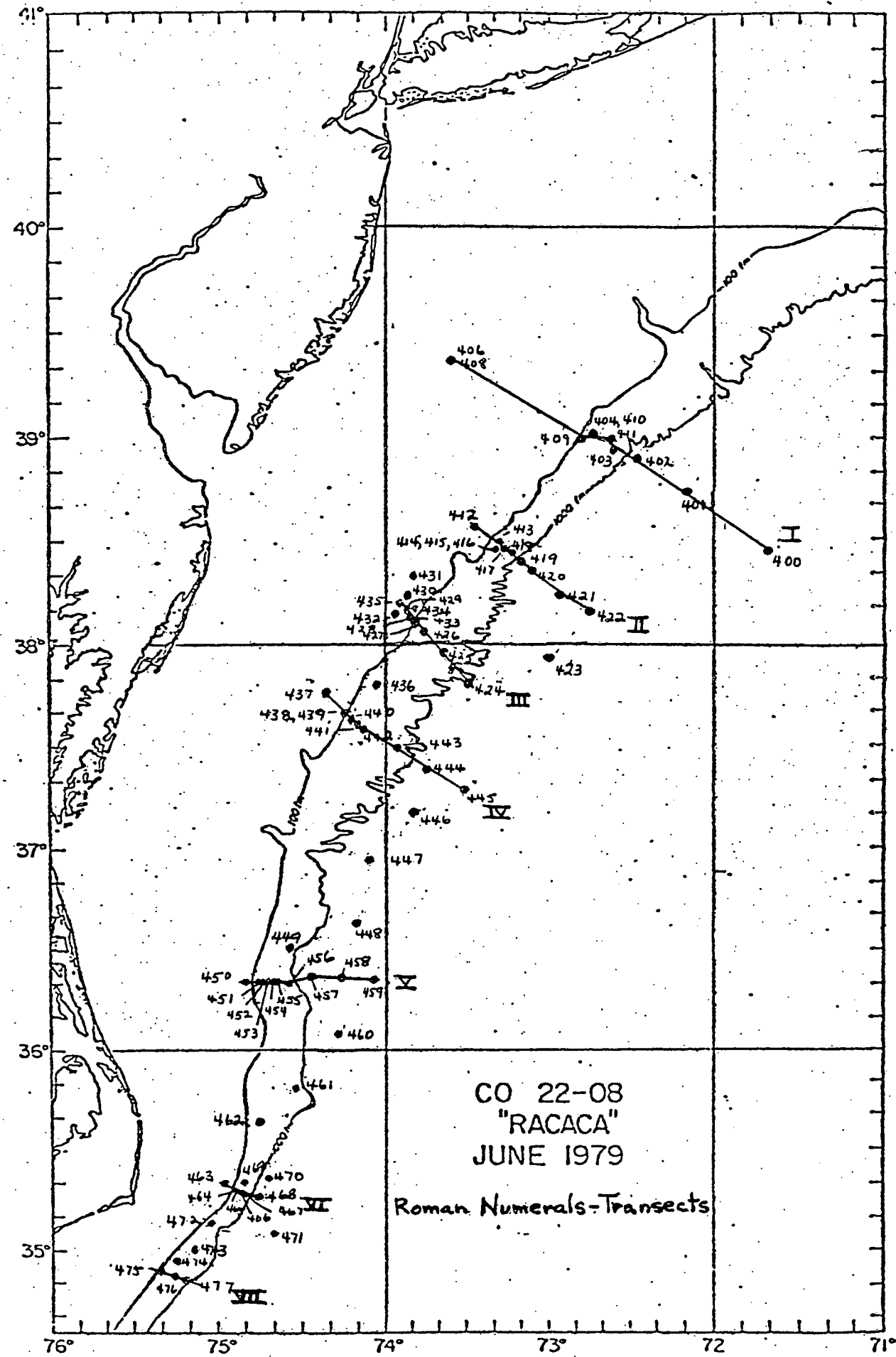
41°
40°
39°
38°
37°
36°
35°
76°
75°
74°
73°
72
71°
100 m
406
408
404, 410
409
403
402
401
400
I
412
413
414, 415, 416
417
419
420
421
422
II
431
430
429
435
434
432
433
426
423
424
III
437
436
438, 439
441
443
444
445
IV
446
447
448
449
456
458
450
451
455
457
459
V
452
454
453
460
461
462
463
470
464
468
VI
472
466
467
471
473
474
475
476
477
VII
CO 22-08
"RACACA"
JUNE 1979
Roman Numerals - Transects

The depth distribution of dissolved ^{226}Ra determined from transects I and V were used to correct the RACACA standing crops that had been previously calculated on the basis of an assumed dissolved ^{226}Ra value of 10 dpm/100ℓ at all stations. The depth distribution of radon production in the sediments discussed in section 4.4.2b (Fig. 4.4-4) was then incorporated by calculating the ratio between the standing crop and the calculated sediment production for each station. The values of standing crop, calculated production, and ratio of standing crop to production is shown for each station of transects I and II in figures 4.4-15 and 4.4-16, respectively. Transect locations are shown in figure 4.4-14. The errors on the standing crop:production ratios are based on assumed errors of ±0.05 dpm/gm on the production values and ±0.1 dpm/cm^2 on the standing crop values.

Under the assumption that the depth distribution of radon production in sediments reflects the depth distribution of the flux of radon out of the sediments, it can be seen that combining production results with standing crops gives a somewhat different picture of the low-radon zone than that seen from examining the standing crops alone. Relatively high ratios (>1) are generally observed on the upper 400-500m of the slope. Ratios > are not seen at greater depths anywhere along the slope. If the flux of radon out of the sediments is considered proportional to the radon production in sediments at all depths, then the low radon zone clearly extends from at least 400m depth to depths greater than our deepest stations at 2500-2900m.

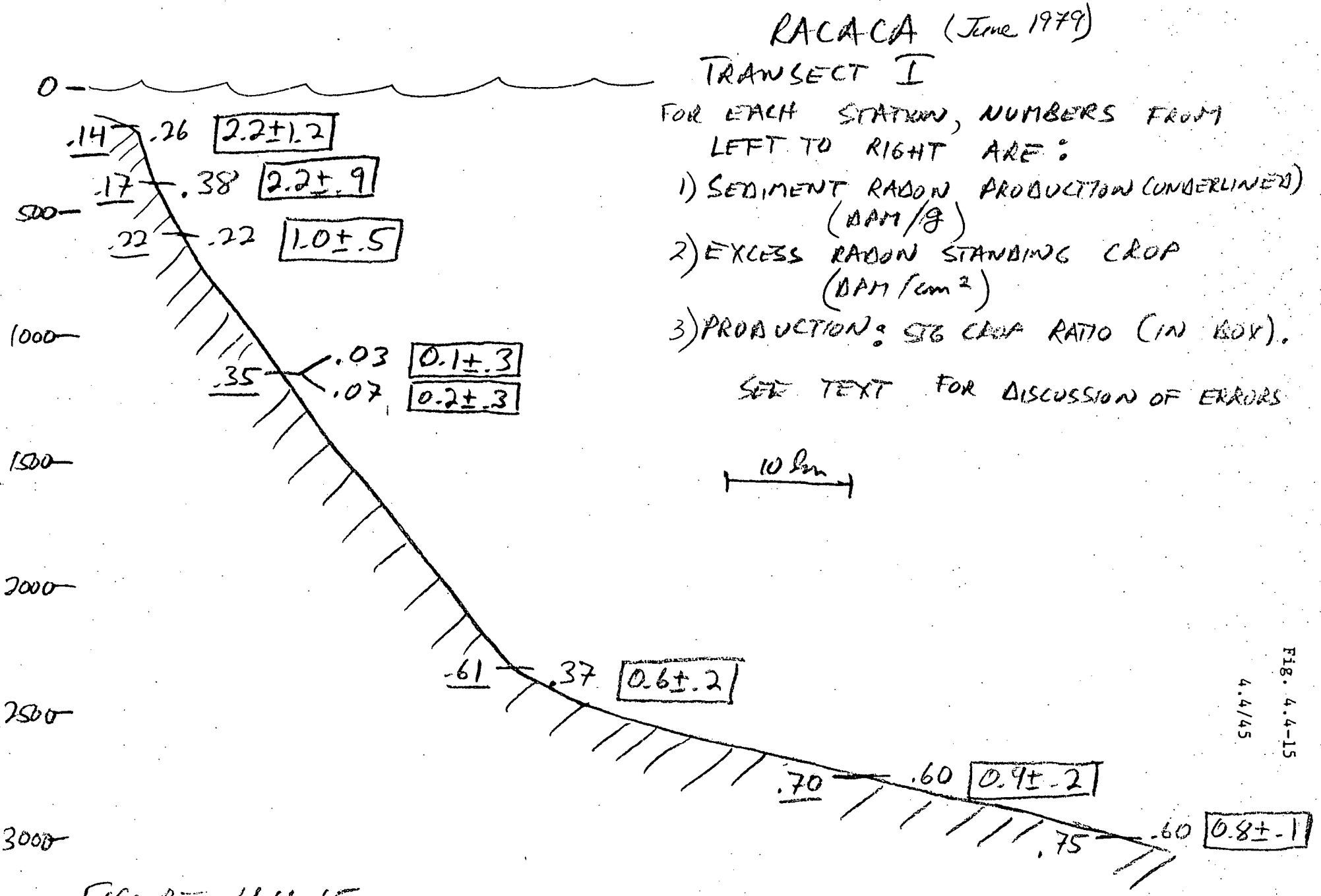

FIGURE 4.4-15

Fig. 4.4-15
4.4/45

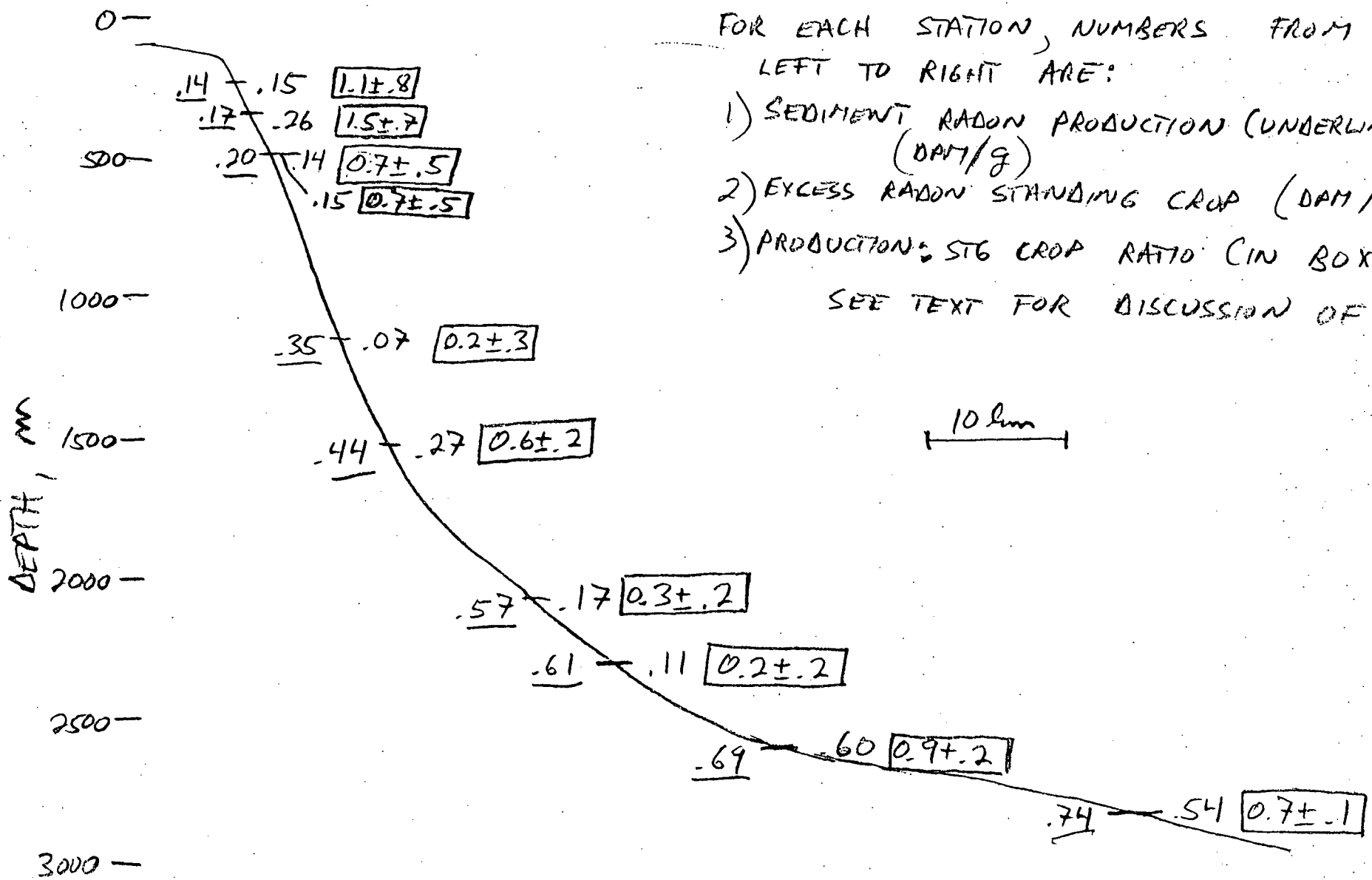

FIGURE 4.4-16

4.4/46

Fig. 4.4-16

Although a proportionality between radon productionin the sediment and flux out of the sediment is the only assumption for which we have enough data at present, several factors may well cause deviation from this proportionality. Two obvious possibilities are the nature of the sediment, i.e., grain size and lance porosity, and the nature and intensity of biological activity. As indicated in section 4.4.2b, the upper slope has a higher percentage of coarse grained sediments than the middle and lower slope. Thirty four camera stations were taken on the RACACA cruise with a view to discerning something of the nature and intensity of biological activity as well as direct indications of current activity in the surface sediment. Dr. Barbara Hecker, a benthic biologist in the L-DGO Marine Biology Group, has made a preliminary investigation of our bottom photos. As expected, she finds wide variation in the suite of benthos and in their apparent intensity of working the sediments as a function of depth on the slope. From what one can see in photographs, however, it is not obvious that one might appeal to one or another group of benthos to account for variability in radon flux, aside from a generally greater intensity of biological activity toward the upper slope.

One must therefore consider that the upper slope standing crop:production ratios are not the limiting ratios, but that they are higher because of higher flux to production ratios. In that case the ratios of .7-.9 observed at the deepest stations may be limiting. Comparison with ratios from other areas of the North Atlantic has not proved helpful since they seem top vary considerably with location. Studies of radon distributions in cores already collected and those proposed for next year should help in determining whether or not flux:production ratios are different on the upper and lower slope.

In either case, it can be seen that the lowest ratios are observed at the same depths as the lowest standing crops. Thus the "strongest" part of the low radon zone is formed over the same depth range with both ways of examining the data. The low radon zone appears more variable and complex when considering standing crop:production ratios than when examining standing crops alone. The error on the ratios are substantial, however, so it is uncertain how significant the variability is. The importance of this new calculation has not yet been fully assessed and will be dependent on the new dissolved ^{226}Ra measurements that are being and will be performed. Nonetheless, the low-radon zone is still found to be a significant feature on the slope. An understanding of the causes of this feature is essential to an understanding of transport of dissolved (and possibly suspended material in and away from the slope waters. A discussion of possible mechanisms that could be the cause of the low-radon zone is presented in section 4.1.3-I-IV (pp. 4.1/107-109).

4.4.6 Summary of Utility of Radon in Continental Shelf-Slope Studies

The primary use of radon as a tracer in the shallow waters of the continental shelf is as a tool for understanding vertical mixing processes. Under the relatively steady state well-mixed conditions of the winter radon distributions can be used to quantify mixing in whole water column. During summer stratified conditions radon can be used to place limits thermocline mixing rates. These vertical mixing parameters from both extreme seasons are necessary to the understanding of vertical distributions of other substances and as inputs to more complicated hydrodynamic models.

Although not possible from the data at hand, it appears that measurements of of vertical distributions of radon during transition periods between well-mixed and stratifed conditions could aid in understanding the evolution of vertical turbulent structure and the development of the thermocline. A time series of data at a few stations during this period in an area of known source strength distribution would be necessary.

In cases in which detailed knowledge of radon production and standing crops are available some quantification of horizontal diffusion and advection is possible. More understanding of actual fluxes and more comparison with other techniques of current measurement are necessary in order to completely assess the usefulness of radon in this connection. Since the radon method is not sensitive to horizontal diffusion coefficients less than 10^5 cm^2/sec and since it reflects only average currents over a few days, the radon method does not seem to be an important addition to techniques for quantifying horizontal currents and mixing. Radon can, however, be useful as a tracer in complicated areas in which tongues of water from different source areas interleave provided sufficiently detailed knowledge of sources and signficant hydrographic backup are available.

On the continental slope the analysis of radon has provided an indicator of a potentially important phenomenon that, so far, has not been observed through any other tracers or conventional hydrographic technique. The low-radon zone is a region in which mixing characteristics appear to be unique, though the processes involved are not yet understood. It is clearly a region which needs further study in order to understand the apparent mixing of slope water (with its shelf-derived burden of dissolved and suspended pollutants) with water of the interior ocean.

As a result of attempts to determine the distribution of radon sources some interesting features of the radium distribution in sediments have been observed which help place constraints on the origins of the sediments.

5.0 Field Work

A reduction in the budget proposed for this year's support precluded a major cruise, but we have mounted two field efforts we thought sufficiently important at this time. The first is a mooring in the low-radon zone of the continental slope and the second is an effort to obtain box core samples of sediment from the shelf and upper slope where we now lack any samples.

The mooring is primarily a repeat of the one attempted last summer in which a thermistor chain and sediment traps were deployed for about seven weeks on the continental slope in the zone of radon deficiency. The objective was to measure vertical differential displacement of isotherms as an indication of a possible tidal pumping mechanism for mixing the radon tracer away from the boundary and into the interior slope water (see section 4.1.3, I. RACACA cruise, IV Low Radon Zone). This effort failed due to a manufacturer's defect in the thermistor chain. On 29 July 1980 we redeployed the repaired thermistor chain at essentially the same location (38°58.82'N 072°31.52'W) in 1235M water along with an Aanderaa current meter and 18 sediment traps. Two of the traps are the same 12 inch diameter traps used on last years mooring (the results of which are reported in section 2.3). In addition 16 miniature traps (3 in. diameter) were deployed in an experiment to test the effectiveness of several of the poisons used in sediment trap work. This experiment is being done in conjunction with Dr. Hugh Ducklow who has joined the LDGO Marine Biology group since last year and who will be participating the coming year's work.

Despite the now-widespread use of sediment traps to obtain samples (and to presumably to measure fluxes) of suspended particulate matter, the question of whether or not to poison traps in order to prevent bacterial decomposition of organic matter, and, if poisoned, which poison to use, has not been addressed in a coherent manner. We have taken advantage of the arrival of Hugh Ducklow and the deployment of the thermistor chain/current meter mooring to compare the effects of three poisons (mercuric chloride, formalin and sodium azide) against the use of no poison. The two 12 inch traps were poisoned as were those deployed and recovered last year with sodium azide.

The mooring was deployed from RV CAPE HENLOPEN on 29 July 1980 and we are tentatively scheduled for several days of CAPE HENLOPEN time in early November to recover the mooring. In addition to deploying the mooring, we tried our Soutar-type box corer now mounted in a frame and obtained two cores in six attempts. Dr. Jeanne Stepien took a number of zooplankton tows and hydrocasts were made to calibrate water temperature at the beginning of the thermistor chain record. On the recovery cruise in November maximum use of the ship time will be made to obtain additional hydrocasts, box cores, and zooplankton samples.

The second field effort this year is a piggy-back collaboration effort with Dr. G. Rowe of Brookhaven National Laboratory. The DOE-supported BNL group has a cruise in the New York Bight on R/V KNORR at this writing. They have provided us with one berth to allow a technician to participate in the box coring that Rowe plans on this leg. Our technician will be sampling box cores from a number of shelf/slope locations for radon flux (by the radon deficiency method) and to obtain samples for anthropogenic and natural radionuclide analysis.